



The
University
Of
Sheffield.

**Gas Permeability of Gas Diffusion Media Used in Polymer
Electrolyte Fuel Cells**

By:

Olutomisin Manase Orogbemi

A thesis submitted in partial fulfilment of the requirements for the
degree of Doctor of Philosophy

The University of Sheffield
Faculty of Engineering
Department of Mechanical Engineering

January, 2017

The candidate confirms that the work submitted is his/her own, except where work which has formed part of jointly-authored publications has been included. The contribution of the candidate and the other authors to this work has been explicitly indicated below. The candidate confirms that appropriate credit has been given within the thesis where reference has been made to the work of others.

The work in **Chapter 4** of the thesis has appeared in publication as follows:

O. M. Orogbemi, D. B. Ingham, M. S. Ismail, K. J. Hughes, L. Ma, M. Pourkashanian, Through-plane gas permeability of gas diffusion layers and microporous layer: effects of carbon loading and sintering, Journal of the Energy Institute, (2016).

The other authors were my supervisors who acted in an advisory role and gave suggestions regarding the research direction and analysis methods.

The work in **Chapter 5** of the thesis has appeared in publication as follows:

O. M. Orogbemi, D. B. Ingham, M.S. Ismail, K. J. Hughes, L. Ma, M. Pourkashanian, The effects of the composition of microporous layers on the permeability of gas diffusion layers used in polymer electrolyte fuel cells, International Journal of Hydrogen Energy, 41 (2016). pp. 21345-21351.

The contributions of other authors were my supervisors who acted in an advisory role and give suggestions regarding the research direction and analysis methods.

This copy has been supplied on the understanding that it is copyright material and that no quotation from the thesis may be published without proper acknowledgement.

The right of Olutomisin Manase OROGBEMI to be identified as Author of this work has been asserted by him in accordance with the Copyright, Designs and Patents Act 1988.

© 2017 The University of Sheffield and Olutomisin Manase OROGBEMI

Abstract

The awareness of global climate change by emissions of greenhouse gases from fossil fuel combustion is widely known by current society. Polymer Electrolyte Fuel cell (PEFC) technology has been a very promising clean technology with high efficiency that has been used in a wide range of portable, automotive and stationary applications. The fuel cell research has been developing very rapidly and successfully in the last few years. However, some issues remain largely unresolved, namely water management and high cost of the PEFC component. One of the efficient and cost-effective ways to improve the design of the PEFC and consequently resolve the above mentioned issues is through modelling. However, the built PEFC models need to be fed with accurate transport coefficients to enhance their productivity. One of the most important transport coefficients is the gas permeability of the PEFC porous media which highly affects the convective flow.

Therefore, in this thesis, thorough experimental studies have been conducted to investigate the gas permeability of gas diffusion media used in PEFCs. The focus has been on the effects of the following on the gas permeability of the gas diffusion layers (GDLs): (i) type of carbon black used in the microporous layers (MPL) attached to the GDL, (ii) carbon and polytetrafluoroethylene (PTFE) loading, and (iii) the thickness of the MPL.

Further, a novel method has been proposed to estimate the penetration of the MPL into the carbon substrate (i.e. the GDL before being coated with the MPL ink). Also, the effect of sintering on the gas permeability of the MPL has been investigated for the first time.

Publications and conferences

Journal papers

1. **O. M. Orogbemi**, D. B. Ingham, M. S. Ismail, K. J. Hughes, L. Ma, M. Pourkashanian, Through-plane gas permeability of gas diffusion layers and microporous layer: effects of carbon loading and sintering, Journal of the Energy Institute, (2016), in press. **Chapter 4.**
2. **O. M. Orogbemi**, D. B. Ingham, M.S. Ismail, K. J. Hughes, L. Ma, M. Pourkashanian, The effects of the composition of microporous layers on the permeability of gas diffusion layers used in polymer electrolyte fuel cells, International Journal of Hydrogen Energy, 41 (2016) 21345-21351. **Chapter 5.**
3. **O. M. Orogbemi**, D. B. Ingham, M. S. Ismail, K. J. Hughes, L. Ma, M. Pourkashanian, On the gas permeability of the microporous layer used in the polymer electrolyte fuel cells. **Chapter 6.** In preparation for submission to Journal of the Energy Institute.

Conferences

1. Gas permeability of gas diffusion layers: effects of carbon loading and sintering'. Hydrogen Fuel Cell SUPERGEN Conference in the UK, University of Birmingham (December 12-14, 2014). Oral Paper: <http://h2fcsupergen.com> (**Chapter 4**).
2. On the through-plane gas permeability of non-coated and coated gas diffusion layers'. Hydrogen Fuel Cell SUPERGEN Conference in the UK, University

of Birmingham (December 12-14, 2013). Poster Presentation.
<http://h2fcsupergen.com> (**Chapter 4 and 6**).

3. The effects of the microporous layers composition on the permeability of gas diffusion layers'. EFC15-239, 2015 Naples Italy. (Proceedings of European Fuel Cell Conference, December 14-19, 2015). (**Chapter 5**).

4. The effects of microporous layer composition on the permeability of PEM fuel cell porous gas media. Energy PhD Event, University of Sheffield: Opportunity for networking and future careers (20th September, 2015). Poster Presentation. (**Chapter 5**).

Acknowledgements

First and foremost, my deep appreciations and gratitude go to the Almighty God for providing me the blessings to start the doctoral programme with good success to complete it.

I am highly indebted to my supervisors and I would like to express my sincere appreciations to them all, namely: Professor Mohamed Pourkashanian, Professor Derek B. Ingham, Dr Kevin J Hughes and Professor Lin Ma, for their tremendous support, help and advice. Their comprehensive guidance has helped me handle hurdles of life during this work, successfully complete my thesis, and advice on my career research development.

Also, I am thankful to Dr Mohammed. S. Ismail for his continuous support both in kind and in deed, and the comprehensive advice during my doctoral training. I have been fortunate to have all these wonderful people as my supervisors. They were always there to support, guide and advise me throughout the different stages of my doctoral training stages.

I appreciate the technical assistance that I have received from Mr Paul Crosby and Mr Dmitry Govonikhim in the Energy 2050 group at the University of Sheffield together with Mr Gurdev Bhogal at the University of Leeds. I could complete all the experimental work in this thesis through their technical help and assistance.

Special thanks to Ven. Dr Ernest and Mrs Eunice Anyacho. Their comprehensive guidance and support are highly appreciated.

I would like to highly acknowledge the Management of Federal College of Education, Obudu and the Federal Republic of Nigeria Government for their financial support.

Also, I wish to acknowledge with thanks all form of support and assistance I received from Mrs Magdalene. O. Adie, Mrs Monica Iroegbu and all other staff of the Federal College of Education, Obudu, Nigeria, for their tremendous support and help.

I highly appreciate the assistance that I received from all my family, for their support and for their unconditional love they have shown to me. I am extremely grateful to my wife (Dolapo) and children (David, Eniola, Favour and Toluwalase), my mother (Martha Mese-Orogbemi), and my sisters (Mrs. Orowole, Mrs. Abiodun and Mrs. Abigail) and brothers (Pastor Ajodun, Barrister Samuel, Engr. Manasseh, Engr. Sunday and Mr Emmanuel).

This work is dedicated to my late brother Asetolorun Orogbemi who wished to see me a doctor and my late Pa Igbane Ezekiel Orogbemi who sacrificed his life for me to achieve this dream with dignity.

Table of Contents

Abstract	iv
Publications and conferences	v
Acknowledgements	vii
Table of Contents	ix
List of Tables	xii
List of Figures	xiv
Nomenclature	xix
Chapter 1 Introduction	1
1.1 Research motivation and objectives.....	5
1.2 Research scope and limitations	6
1.3 Structure of the thesis	7
Chapter 2 Literature Review	9
2.1 Renewable energy	10
2.2 Renewable energy sources.....	11
2.3 Fuel cells.....	12
2.3.1 Fuel Cell Technology.....	14
2.3.2 Polymer electrolyte membrane fuel cells	15
2.4 PEM fuel cell efficiencies and issues	19
2.4.1 Water management	20
2.4.2 Gas transport.....	24
2.5 Materials used in the gas diffusion media.....	25
2.6 Gas permeability of the gas diffusion layer.....	29
2.7 Gas permeability of the microporous layer	31
2.8 Effect of the microporous layer sintering	35
2.9 Effect of the microporous layer composition	37
2.10 Microporous layer penetration	39
2.11 Limitations in Knowledge	41
2.12 Contribution of this thesis on PEM fuel cells	43
2.13 Summary	44
Chapter 3 Techniques used to Investigate Gas permeability of Porous Media	46
3.1 Materials	48

3.2 Methods	51
3.2.1 Microporous layer preparation process	51
3.2.2 Gas diffusion layer preparation process	59
3.2.4 Sintering setup	65
3.2.5 Calibration of the flow meter	66
3.2.6 Gas permeability setup	71
3.3. Data analysis.....	74
3.3.1 Darcy's law.....	75
3.3.2 MPL thickness and gas permeability	75
3.3.3 MPL penetration and gas permeability	76
3.4. Uncertainty and error analysis.....	80
3.5. Summary	105
Chapter 4 The effects of Carbon black as the material used for the Microporous Layer of Gas Diffusion Media	106
4.1 Through-plane gas permeability of the carbon substrate.....	108
4.2 Through-plane gas permeability of MPL-coated GDLs.....	109
4.2.1 Effects of carbon loading	111
4.2.2 Effects of carbon black type.....	116
4.3 Effects of sintering	119
4.4 Through-plane gas permeability of MPLs	123
4.5 Conclusions	126
Chapter 5 The Effects of the Composition of the Microporous Layer on the Through-plane Gas Permeability of the Gas Diffusion Media	128
5.1 PTFE loading in the MPL.....	130
5.1.1 Effects of the carbon black loading	134
5.1.2 Effects of the carbon black types	139
5.2 Effect of sintering.....	142
5.3 Through-plane gas permeability of MPLs	144
5.4 Conclusions	154
Chapter 6 An Estimation of the Microporous Layer Thickness	156
6.1. MPL with penetration	159
6.1.1 MPL thickness with penetration	164
6.1.2 MPL gas permeability with penetration.....	167
6.2 MPL without penetration.....	169
6.2.1 MPL gas permeability	170

6.2.2 MPL penetration into the carbon substrate	180
6.3 Conclusions	186
Chapter 7 Conclusions and Possible Future Work	188
7.1 Contribution to Knowledge	188
7.2 Conclusions	190
7.3 Possible future work	193
Bibliography	196
Appendix A	
Calculations of the compositions loadings for MPL ink preparation	213
Appendix B	
Estimation value for MPL-coated GDLs thickness with Ketjenblack and Vulcan carbon black loading	222
Appendix C	
Estimation values for carbon-PTFE loaded onto GDL samples	232
Appendix D	
The Measurement of Error Bars of 95% Confidence Interval for Gas Permeability of MPL-coated GDLs with Ketjenblack and Vulcan carbon blacks	242

List of Tables

Table 2.1. Electrolyte types and the characteristics of fuel cells.	18
Table 3.1. Manufacturer's physical properties of the SGL 10 BA carbon paper substrate.	49
Table 3.2. The manufacturer's physical properties of carbon black materials (AkzoNoble, the Netherlands datasheets) and (Cabot Corporation, USA datasheets).	50
Table 3.3. The carbon black and PTFE dispersion loadings measured by weight (mg) for the preparation of the MPL ink.	56
Table 3.4. The carbon black and PTFE mixture required per sample by weight (mg).	57
Table 3.5. Amount of MPL slurry coating on the top of one-side of the carbon substrate sample surfaces.	58
Table 3.6. The estimation of the amount of Carbon-PTFE coated on one-side of the GDL sample surface by weight.	64
Table 3.7. The experimental data for voltage signal used for the calibration curve flow rate.	69
Table 3.8. Experimental data for data the flow meter calibration of a litre/minute flow meter.	70
Table 5.1. The through-plane gas permeability of the MPL with Ketjenblack and Vulcan carbon black.	133
Table 6.1. Measured thickness values for the microporous layers of Ketjenblack and Vulcan carbon blacks.	162
Table 6.2. List of the parameters values estimated for the two types of MPLs with no penetration.	171
Table 6.3. A comparison of the MPL visible thickness and penetration of the two carbon types for the different carbon loadings in the MPL.	182

Table 6.4. A comparison of the MPL total thickness and the GDL total thickness after the coating of two different carbon types for various carbon loadings in the MPL..... 185

List of Figures

Figure 2.1. A simple fuel cell.....	13
Figure 2.2. A typical polymer electrolyte fuel cell (Barbir, 2013).	16
Figure 2.3. A typical MEA (Barbir, 2013).....	20
Figure 2.4. A schematic of a dual-layer GDL for PEFCs (Park et al. 2006).	23
Figure 3.1. Schematic of the general technical experimental approach used in this thesis.....	47
Figure 3.2. Schematic of a typical porous gas diffusion layers in a PEM fuel cell.....	48
Figure 3.3. Photographs of the preparation of microporous layer ink procedures and steps for (a) carbon black powders loading by weight, (b) PTFE loading by weight, and (c) past-like material mixture of microporous layer slurry.	54
Figure 3.4. Photograph of the preparation of homogeneous suspension of MPL ink using an Ultrasonic bath.....	55
Figure 3.5. Photograph of set of carbon substrates made circular with a 2.50 cm diameter before coating.....	59
Figure 3.6. Photograph of the measured thickness technique for the carbon substrate sample before and after the coating MPL ink on the GDL on one side surface.....	60
Figure 3.7. Photographs of the SEMs facilities used to measure the thickness, surfaces and cross-sectional micrographs of the carbon substrate samples before and after coating with MPL, of (a) MA15SEM (EVOZEISS, 80 mm ²) at University of Leeds, and (b) JEOL JSM-6010LA at University of Sheffield.....	61
Figure 3.8. Photographs of the measured GDL sample by mass weight (a) before coating, and (b) after coating.	63
Figure 3.9. Photograph of a set of samples after coating and heat treated at temperature 80 °C of the heated plate.	65
Figure 3.10. Photograph of the furnace used for the heat-treatment of the GDL samples.....	66
Figure 3.11. Photograph of the calibration setup for the flow meter.	67
Figure 3.12. The calibration curve for a 10 litre per minute mass flow meter for the calculation of pressure drop for the flow across the samples.	69
Figure 3.13. The experimental setup of the through-plane gas permeability of the tested GDL samples.	72
Figure 3.14. Schematic diagram of the experimental setup.....	73
Figure 3.15. Schematic representation of a method for estimating the MPL penetration into a porous carbon substrate.....	79

Figure 3.16. Amount MPL slurry coating on the top of one-side of the carbon substrate sample surfaces.	81
Figure 3.17. The estimation of the amount of Carbon black type-PTFE loading in the MPL coated on one-side of the GDL sample surface by weight and measurement error bars of 95 % conf. int.	86
Figure 3.18. The measurement error bars of 95% confidence interval for pressure gradient of MPL-coated GDLs with Vulcan for each of 6 tested samples of 20 wt.% PTFE.....	91
Figure 3.19. The measurement error bars of 95% confidence interval for pressure gradient as a function of velocity of flowing gas across MPL-coated GDLs with Ketjenblack and Vulcan carbon blacks of 20 wt.% PTFE.	96
Figure 3.20. The measurement error bars of 95% confidence interval for gas permeability of MPL-coated GDLs as a function of carbon loading in the MPL with (a) Ketjenblack and (b) Vulcan carbon blacks with 20 wt.% PTFE.	97
Figure 3.21. The measurement error bars of 95% confidence interval for gas permeability of MPL-coated GDLs as a function of PTFE loading in the MPL with Ketjenblack and Vulcan carbon blacks.....	102
Figure 3.22. The measurement error bars of 95% confidence interval for MPL thickness as a function of carbon loading in the MPL with (a) Ketjenblack and (b) Vulcan carbon blacks.	103
Figure 3.23. The measurement error bars of 95% confidence interval for gas permeability of MPL as a function of carbon loading in the MPL with Ketjenblack and Vulcan carbon blacks.....	104
Figure 4.1. A typical SEM image for the surface area of a SGL 10BA carbon substrate.	109
Figure 4.2. Measured pressure gradient as a function of the gas velocity for a SGL 10BA sample. The solid line represents the linear pressure gradient-velocity curve.	110
Figure 4.3. Typical SEM image for the surface area of the MPL-coated GDL sample, (a) MPL-coated GDL with Ketjenblack carbon black, and (b) MPL-coated GDL with Vulcan carbon black.	112
Figure 4.4. Measured pressure gradient as a function of the nitrogen gas velocity for the MPL-coated carbon substrates with various carbon loadings in the MPL for 20 wt.% PTFE, and before and after, coating the GDL with MPL using Ketjenblack carbon black.....	113
Figure 4.5. Measured pressure gradient as a function of the nitrogen gas velocity for the MPL-coated carbon substrates with various carbon loadings in the MPL of 20 wt.% PTFE, and before and after, coating the GDL with MPL using Vulcan XC-72R carbon black.....	113
Figure 4.6. Thickness of the carbon substrate before and after coating.....	115

Figure 4.7. Through-plane gas permeability of the MPL-coated GDLs with various amounts of carbon loading in the MPL with 20 wt.% PTFE.	115
Figure 4.8. MPL-coated GDL thickness as a function carbon loading in the MPLs. Two different carbon types, Kejenblack carbon black and Vulcan XC 72R carbon black.	117
Figure 4.9. Through-plane gas permeability as a function of carbon loading of coated GDLs for different carbon black type loadings in the MPL, (a) Kejenblack carbon black and (b) Vulcan XC 72R carbon black.	118
Figure 4.10. Through-plane gas permeability of MPL-coated GDLs before and after sintering as a function of carbon loading in the MPL, for comparison of the effects of sintering on the MPLs coated on GDLs with 20 wt.% PTFE.	120
Figure 4.11. SEM images for the MPL with 1.5 mg/cm ² Ketjenblack of 20 wt.% PTFE carbon loading (a) before sintering, and (b) after sintering.	121
Figure 4.12. SEMs images for the MPL with 1.5 mg/cm ² Vulcan of 20 wt.% PTFE carbon loadings (a) before sintering, and (b) after sintering.	122
Figure 4.0.13. MPL thickness as a function of carbon loading in the MPL for (a) Ketjenblack carbon black and (b) Vulcan carbon black as materials for the MPLs.	125
Figure 4.14. A typical SEM cross-sectional micrograph of an MPL-coated GDL for MPL with Ketjenblack carbon black.	125
Figure 4.15. Through-plane gas permeability of the MPL as a function of carbon black loading in the MPL with two different carbon blacks (a) Ketjenblack carbon black and (b) Vulcan carbon black.	126
Figure 5.1. Measured pressure gradient as a function of the nitrogen gas velocity for the MPL-coated carbon substrates with different PTFE loadings in the MPL for 0.5 mg/cm ² Ketjenblack carbon black.	132
Figure 5.2. Measured pressure gradient as a function of the nitrogen gas velocity for the MPL-coated carbon substrates with different PTFE loadings in the MPL of 0.5 mg/cm ² Vulcan carbon black.	132
Figure 5.3. Through-plane gas permeability as a function of carbon loading in the MPL (a) Ketjenblack and (b) Vulcan.	136
Figure 5.4. SEMs of cross-sectional images of the coated GDLs with Ketjenblack carbon black loadings of (a) 0.5 mg/cm ² , the MPL thickness (i = 121, ii = 79, iii = 99, iv = 79, v = 64, and vi = 74) μm. (b) 1.0 mg/cm ² , the MPL thickness (i = 116, ii = 106, iii = 96, iv = 100 and v = 84) μm. (c) 1.5 mg/cm ² , the MPL thickness (i = 138, ii = 117, iii = 152, iv = 166, v = 145) μm. (d) 2.0 mg/cm ² , the MPL thickness (i = 168, ii = 142, iii = 126, iv = 137, v = 158) μm.	137
Figure 5.5. SEM image for the surface of the MPL with Ketjenblack of 0.5 mg/cm ² and 20 wt.% PTFE.	138

Figure 5.6. SEM for the surface of the MPL with Vulcan XC-72R of 0.5 mg/cm ² and 20 wt.% PTFE.....	138
Figure 5.7. The through-plane gas permeability of the MPL-coated GDLs as a function of the PTFE loading for various carbon loadings, (a) gas permeability of MPL-coated GDLs with Ketjenblack carbon black, and (b) gas permeability of MPL-coated GDLs with Vulcan carbon black.	141
Figure 5.8. Through-plane gas permeability of MPL-coated GDLs before and after sintering as a function of PTFE loading in the MPL, for comparison of the effects of sintering on the MPLs coated on the GDLs with different PTFE (wt.%) consist of 1.5 mg/cm ²	143
Figure 5.9. (a)-(b) The curves representing the gas permeability of the MPL as a function of PTFE loading for various Ketjenblack EC-300JD and Vulcan XC-72R carbon black, and (c) - (d) the curves after excluding the 0.5 mg/cm ² carbon loading curve from (a)-(b).	147
Figure 5.10. SEMs images for the surfaces of the MPL with PTFE loadings ranging from 0 to 50 wt. % PTFE, and 2.0 mg/cm ² of Ketjenblack and Vulcan carbon black.....	153
Figure 6.1. Through-plane gas permeability of the MPL as a function of the MPL visible thickness of (a) Ketjenblack carbon black, and (b) Vulcan carbon black, as the materials of the MPLs.	161
Figure 6.2. Gas permeability of the MPL as a function of the carbon black loading in the MPL, for a comparison of the (a) Ketjenblack carbon black, and (b) Vulcan carbon black, as the materials of the MPLs.....	162
Figure 6.3. A schematic diagram for the cross-section of the MPL-coated GDL and the penetration of the MPL into the carbon substrate.	163
Figure 6.4. The MPL-coated GDL thickness as a function of carbon loading and carbon type utilised as materials in the MPL (a) Ketjenblack, (b) Vulcan and (c) comparison of MPLs thicknesses.....	166
Figure 6.5. Comparison of the MPL visible thickness as a function of the carbon loading and carbon type utilised as materials in the MPL.	168
Figure 6.6. SEM cross-sectional image view for the membrane filter after coating with MPL.	170
Figure 6.7. SEMs of (a) a coated membrane filter with 0.5 mg/cm ² cross-sectional image of Ketjenblack EC-300JD carbon black, and (b) a coated membrane with 0.5 mg/cm ² cross-sectional image of Vulcan XC-72R carbon black.	172
Figure 6.8. The MPL visible thickness without penetration as a function of the carbon loading in the MPL.	173
Figure 6.9. Through-plane gas permeability of MPL without penetration as a function of the carbon loading for the Ketjenblack and Vulcan carbon blacks.	173

Figure 6.10. SEMs images for the surfaces of the MPL with various Ketjenblack and Vulcan carbon black loadings of 20 wt.% PTFE.....	179
Figure 6.11. Comparison of the MPL penetration thickness of the carbon loading and carbon type.	181
Figure 6.12. The SEMs cross-sectional images for the visible MPL thickness and the penetration of the coated GDLs with carbon black.....	184

Nomenclature

Roman letters

g	acceleration due to gravity, m/s^2
h	height of the porous medium in terms of its thickness, μm
k	permeability, m^2
k_{mpl}	permeability coefficient of the microporous layer, m^2
k_{sub}	permeability of non-coated microporous layer, m^2
k_{gdl}	permeability of coated gas diffusion layer, m^2
L_{gdl}	thickness of the coated gas diffusion layer, μm
L_{mpl}	thickness of the microporous layer, μm
L_{sub}	thickness of the non-coated gas diffusion layer, μm
L	thickness of porous medium, μm
p	pressure, Pa
P_{rm}	room pressure, Pa
Q	volume of flow rate, m^3/s
R	Universal gas constant, $J/(mol.K)$
R_{tot}	air resistance value for coating materials, N
R_{mpl}	resistance value for microporous layer, N
R_{sub}	resistance value for material before coating, N
r	radius of the porous medium, m
t	time, s
T_{rm}	room temperature, K
v	velocity vector, m/s
wt	weight of a sample, mg

Greek characters

μ	fluid viscosity of air flow, Pa.s
ρ	density, kg/m^3
φ	potential for solid or electrolyte phase
π	Pi
∇	math symbol for gradient
Δwt	weight difference of a sample, mg

Abbreviations

AFC	Alkaline fuel cell
CL	Catalyst layer
DMFC	Direct methanol fuel cell
GDL	Gas diffusion layer
GDM	Gas diffusion media
MPL	Microporous layer
MEA	Membrane electrode assembly
MCFC	Molten carbonate fuel cell
PEMFC	Polymer electrolyte membrane fuel cell
PEFC	Polymer electrolyte fuel cell
PAFC	Phosphoric acid fuel cell
PTFE	Polytetrafluoroethylene
SEM	Scanning electron microscope
SOFC	Solid oxide fuel cell

Chapter 1

Introduction

Energy is one of the most fundamental parts of human living and plays an important role in our society. Basically, we use energy to do work, light our cities, power our vehicles, planes and rockets, warm our foods, homes, play music and power machinery in factories. In fact, civilization and development would come to an end without energy. Energy comes from many different natural sources such as wind, sun, water, fossils, animals, plants and the Earth, Philibert (2007) and Mattick et al. (2010). However, people were learning how to use many of these different energy sources and types of energy that they produce before and after the industrial revolution, Barge et al. (2014).

Also, the energy sources are classified into three major groups: nuclear power, fossil fuels and alternative energy, Ladislav (2011). Each energy source is a system which makes energy in a certain way, for instance nuclear power is a form of energy which arises from a reaction between atomic nuclei. This form of energy comes mainly from nuclear fission. Fossil fuels include oil, natural gas and coal. When the fossil fuel has been burnt, energy is generated and used as a source of heat to make steam from water, and this is used for driving a turbine. This turbine makes electricity with the assistance of a generator, Williams (2006)

Clearly, the traditional burning of fossil fuels, such as coal, to create power is effective, but very damaging to the environment since it releases harmful greenhouse gases, such as carbon dioxide (CO₂), methane, nitrogen oxides, hydrofluorocarbons, perfluorocarbons, particulate emissions, and other pollutant that contribute to global warming and climate change, Hoffmann (2012). To control these environmental

challenges, there is a need to employ the endless sources of alternative (renewable) energy that are available in mother nature. Moreover, renewable energy has been referred to as the various forms of energy that are produced by means of other than the traditional burning of fossil fuels, Appleby (1992), and the advantage is that the Energy sources are endless and do not produce any pollution (Ladislaw, 2011; Williams, 2006 and Merewether, 2003).

However, to understand how renewable energy use can assist in the preservation of the delicate ecological balance of the planet, and help conserve the non-renewable energy sources, such as fossil fuels, it is important to know what types of alternative energy are connected to eliminating or minimising the emission of conventional pollution (Clean Energy, 1999) and Kulikovsky et al. (1999). Currently, the trend has been towards the use of renewable sources for energy, such as biofuel, hydropower and fuel cells (Hoffmann, 2012). Fuel cells are promising technology for use as an alternative energy source in our World today, Barge et al. (2014).

A fuel cell is referred to as a device that can directly convert chemical energy into electrical energy by continually feeding it with fuel, such as hydrogen gas (Figure 2.1). The fuel cell is used to address the problems associated with the use of fossil fuels, such as global warming and the greenhouse effect. There are a variety of fuel cells that have been developed and they are identified by their composition of their electrolyte, which could be either an alkaline solution, phosphoric acid, a molten carbonate, a solid metal, or solid polymer membrane, Barbir (2013). The applications and use of these different electrolytes depend on the applications on which the fuel cell systems are required. In general, hydrogen is the fuel used in most fuel cell systems and it can be extracted by several procedures from many hydrogen-carriers, including water, gasoline natural gas,

and alcohols, Lister and Mclean (2004), Barbire, (2013) and Barge et al. (2014). Fuel cells are classified into different types, according to the electrolyte employed. There are six popular types of fuel cells that have been identified by scientists, Koido et al. (2008) and Lin et al. (2004), namely: solid oxide, molten carbonate, alkaline, direct methanol, phosphoric acid and solid polymer fuel cells, Jena and Gupta (1999) and Belkhiri et al. (2011). However, each of these fuel cells types operate slightly differently, Singh et al. (1999).

Fuel cell technology is creating a suitable and energy secure hydrogen-driven economy through the widespread use of fuel cells. The fuel cell innovation holds the potential to provide major environmental, energy, and economic benefits that advance critical national environmental goals (Jena and Gupta, 1999). In the current energy producing technologies, fuel cells offer the most promising technologies for delivering clean and efficient power for automotive, industrial, residential and consumer applications (Lister and Mclean, 2004; and Jena and Gupta, 1999).

Fuel cells are promising technology for use as a source of heat and electricity in buildings and an electrical power source for vehicles. Clearly, this has determined the goals for research and development of the electric driven system, and presently the design, fabrication and manufacture of the fuel cell systems require much more innovation to make a much larger impact on the future energy conversion markets, Maiyalagan and Pasupathi (2010). Fuel cell technology is most certainly innovative and has an advantage over generation using conventional fossil fuels.

Some potential future roles of fuel cells are introduced in this thesis in the order of the fuel cell development and hydrogen production from renewable resources. There are many significant technical factors, such as durability and cost, that need to be overcome

for fuel cell technology advancement. Therefore, breakthroughs are required to reduce or eliminate these barriers. In particular, the effects of such gas flow structure, for example, pressure drop and gas permeability and electrode structures, and new material development require significant improvements in a fuel cell performance, Ismail et al. (2010).

Further, on the role of fuel cells being a clean energy technology to improve the economy, protect the environment from the emissions of CO₂ and pollution by fossil fuels in a more sustainable and renewable energy future, the literature has revealed that the fuel cell future development directions are three fold: applications in portable, stationary power generation and transport; fuel in use – in the most recent technology advancement; and technology – by pinpointing major challenges in different types of fuel cell technologies. For example, in the future development of the polymer electrolyte fuel cell (PEFC) technology (Haile, 2003; Lister and Mclean, 2004; Ismail et al. 2010).

Further, future development and implementation of PEFC technology depends on the upward trend in a carbon constraint economy, i.e. climate change imperatives into full cost accounting and sustainability by rapidly gaining momentum in a world where a shift towards a low carbon economy, and this is limited by the dwindling fossil fuel reserves, climate change and the improvement in hydrogen energy infrastructure, Hoffmann (2012) and Carrette et al. (2000). In addition, due to the PEFC high efficiencies and low emission, Carrette et al. (2001), attention is required for the knowledge-generating activities to enable improvements in the understanding of PEFC operation principles and the engineering of PEFC technology.

The polymer electrolyte fuel cell is an energy conversion device, and theoretically it has the capability of generating electrical energy for as long as the fuel (hydrogen) and

oxidant (oxygen) are supplied to the porous media, i.e. electrodes (see Chapter 2, Figure 2.2). In reality, there are many significant hurdles to overcome, and if possible to eliminate, on the primary components of fuel cells that limits or influences the practical operating life time conditions of the fuel cells, Wang et al. (2011).

However, various interrelated and complex phenomena occur during the fuel cell operation, including mass or heat transfer, electrochemical reactions, and ionic or electronic transport, which govern the PEFC operation. The prime importance is to improve the design of polymer electrolyte membrane (PEM) fuel cells and the understanding of the transport reactant gas and its limitations.

1.1 Research motivation and objectives

Firstly, the thesis is motivated mainly by the significant hurdles associated with the primary components of the MEA (membrane electrode assembly), namely the porous gas diffusion media (gas diffusion layer, microporous layer and catalyst layer) that influence the effectiveness of the performance of PEM fuel cells. Also, some challenges occur during the full operation of the PEFC system, such as water flooding and reactant gases transport, thus limiting the efficiency performance of the fuel cell. Clearly, there is a need to understand the characteristics of the physical properties of the porous gas diffusion media used in the PEFCs. For example, the effect of the MPL (microporous layer) compositions, and the performance of these porous gas diffusion media in the design of PEM fuel cells.

Secondly, in order to ensure the presence of a sufficient amount of the reacting gases for the reaction in the catalyst layers, the porous gas diffusion media, especially the gas diffusion layer (GDL) and MPL must demonstrate high transport properties, and gas

permeability is one of the transport properties that signals how effective is the convective transport. Thus, there is a need to understand the effect of the gas permeability phenomena process in the porous materials used in the design of PEM fuel cells.

Therefore, the aim of the thesis is to determine the gas permeability of the porous media in the PEM fuel cells. Also, the accurate prediction of the gas diffusion media, by studying the effects of flowing gas pressure across gas diffusion media in PEM fuel cells.

To summarise, the objectives of this thesis are as follows:

- to experimentally determine the through-plane gas permeability of porous media in PEM fuel cells,
- to investigate the effects of the compositions of the MPL and sintering on the gas permeability of the GDLs
- to experimentally measure and analyse the microporous layer penetration into the porous carbon substrate.

1.2 Research scope and limitations

In many applications, the performance of the PEFCs is influenced by the in-plane and through-plane permeability of the components of the MEA. However, in this thesis, only the through-plane gas permeability of the porous gas diffusion layers as a gas transport property of the components of the MEA is covered.

The scope of this thesis is mainly the experimental measurements, estimations and investigations of the porous media materials permeability properties of the components of the MEA in PEFC, namely the GDL and the MPL. The purpose of the experimental investigation is to accurately input the gas permeability values of the porous gas diffusion layers in the modelled fuel cell. However, in this thesis, the in-plane gas permeability

properties of the porous gas diffusion layers is not taken into account during the experimental study and the numerical investigation. Also, the tested materials (samples) are experimentally investigated by determining and predicting the effectiveness and efficiencies of the materials in an operational fuel cell system is uncovered in the thesis.

1.3 Structure of the thesis

This thesis is divided into 7 chapters. The introductory chapter describes the general basic energy background and the fundamental information on the energy sources and renewable sources. The fuel cell of interest is, the polymer electrolyte membrane (PEM) fuel cell. The chapter has been concluded by pinpointing the motivation, the objectives, scope and limitations of the thesis, and the thesis structure.

In **Chapter 2**, a comprehensive critical literature review of the porous gas diffusion media, used in PEM fuel cell is explored and gaps have been highlighted. Clearly, the gas diffusion layer and the microporous layer have significant effects on PEM fuel cell performance, and the most common technical issues of the porous gas diffusion media are described in the this chapter. In Sections 2.6, 2.7 and 2.8, the attempts to estimate the gas permeability of the porous media has been described. The focus was on reviewing the areas that have been investigated in the thesis which are the effects of the following on the through-plane gas permeability of the GDL: carbon black loading and carbon black type, sintering and MPL composition.

Chapter 3 discusses the techniques and methodology used in this thesis to investigate the gas permeability of the porous media. Additionally, an analysis has been added to show the limitations of the method.

In **Chapter 4**, the effect of the carbon black loading and carbon black type as materials used in the MPLs, and sintering on the through-plane gas permeability of MPL coated GDLs is investigated.

In **Chapter 5**, the effect of composition of microporous layer on the through-plane gas permeability of the gas diffusion layer is investigated.

In **Chapter 6**, the effects of the microporous layer penetration into the porous carbon substrate on the through-plane gas permeability of the microporous layer coated gas diffusion layers is investigated. The chapter addresses the effect of the microporous layer thickness on the gas permeability both with or without penetration.

Finally, **Chapter 7**, concludes the thesis by giving a summary account of the main findings and discusses possible future work.

Chapter 2

Literature Review

Energy comes from many different natural sources such as wind, sun, water, fossil fuels, animals, plants and the Earth. Communities have been using energy for a long time from the use of the sun, wood, gravity, wind and tidal, Boyle et al. (2012). We use energy in all aspects of our lives, and without energy, civilisation and development as we know it would end.

The energy sources produce forms of energy related to their sources, for example, wind energy is a form of energy generated from the wind, Taylor (2012), solar energy from the sun, biomass energy is energy produced from plants (Boyle et al., 2013; Morris and Scurlock, 2012). Also, other forms of energy, such as hydro power and wave energy are generated from water and oceans. However, people have been learning how to use many of these different energy sources, and types of energy they produce before and after the industrial revolution, and even today (California Energy Commission, 2012; The NEED Project, 2016).

The energy sources harnessed through technologies from the power of sun, wood, water, radioactive materials and wind are classified into three groups: nuclear power, fossil fuels and renewable energy. However, each of the energy sources are a system which makes energy in a certain way. For instance, nuclear power is a form of energy which arises from a reaction between atomic nuclei. This form of energy comes mainly from nuclear fission. Fossil fuels include oil, natural gas and coal. When the fossil fuel is burnt, energy is generated and used as a source of heat to make steam from water, and this is used for the operation of a turbine to make electricity with the assistance of a generator, Williams (2001). In the case of renewable energy, the energy source in the case of sun, wind or

water is endless and does not produce any pollution (Boyle et al., 2012). Clearly, all these forms of renewable energy could be used for generating electrical energy.

2.1 Renewable energy

Fuels are any material that can potentially store energy in forms that can be practicably released and used as another form of energy, such as heat energy. The concept initially applied only to those materials storing energy in the form of chemical energy that could be released through combustion, and also applied to other sources of heat energy (for example nuclear energy). The heat energy released by many fuels is harnessed into mechanical energy through an engine. Fuels are contrasted with other methods of storing potential energy, such as those that directly release mechanical or electrical energy, Boyle (2012).

The combustion of wood or sticks was the first to be used as fuel. The fossil fuels were rapidly adopted during the industrial revolution and this was because they were more concentrated and flexible than traditional energy sources. The traditional burning of fossil fuels, such as coal to create power is effective, but very damaging to the environment, as it releases harmful greenhouse gases, such as carbon dioxide (CO₂), that contributes to global warming and climate change. To control these environmental challenges, there is a need to employ the sustainable sources of renewable energy that exist. These have the advantage of having no greenhouse gas emissions if based on solar, wind or water power, or much reduced if biomass based.

The aim of eliminating or minimising the use of conventional fossil fuel as energy sources to produce electrical power, in general, has been a main concern of energy technologies, that is, interdisciplinary engineering science for the future of energy sustainability (Ismail

et al., 2011 and Boyle, 2012). Conventional energy technology produces large amounts of electrical power but results in conventional pollution-emissions that affect everyone, Ryan (2009). However, many other forms of non-conventional energy sources, i.e. renewable energy sources can also produce electricity by harnessing natural processes, e.g. sunlight and wind.

Presently, renewable energy technology is receiving more attention because of the awareness of global warming and energy intensity. In addition, many types of renewable energy resources, namely wind and solar energy, are continuously being replenished and will never run out, Taylor (2012). Most of the renewable energy resources come either from the sun or other natural resources on the Earth. However, the greatest number of renewable sources of energy are directly or indirectly derived from the sun or solar energy.

2.2 Renewable energy sources

The renewable energy sources, namely wind, solar, hydropower, biomass, and geothermal, provide clean alternative energy when they are compared to fossil fuels, for example coal and oil. Among the renewable energy sources, hydrogen can be generated with an enormous potential as a fuel (Barbir, 2013), and the most common element on Earth, for instance, water is two-thirds hydrogen.

Further, hydrogen is an energy carrier and it is one of the emerging renewable energy resources, for example, it can be used as the fuel in the fuel cells. The hydrogen can be produced from three production processes, (i) as a component extracted from natural gas, (ii) transformation of natural gas into hydrogen through a reforming process, and (iii) electrolysis of water, that is, using energy already transformed to electricity, Sørensen

(2004). Hydrogen fuel cells systems potential and opportunities have been identified as being one of the greatest advantages over other energy conversion technologies, O'Hayre et al. (2006). However, the most critical challenge is developing new strategies to improve the energy efficiency in the generation of electrical power with zero-emission and the least environmental damage. This is the greatest impact that fuel cells have over both the conventional and non-conventional energy conversion technologies.

2.3 Fuel cells

The fuel cell is a renewable energy system (source) for the future. A fuel cell is a device that converts chemical energy into electrical energy when continuously feed with fuel, namely hydrogen. The general purpose of a fuel cell is to generate electricity through an alternative energy fuel (i.e. hydrogen) from a non-polluting electrochemical process. The fuel cell is used to address the problems associated with the use of fossil fuels, such as global warming and the greenhouse effect. However, there are a very large variety of fuel cells that have been developed.

Fuel cells are not like primary batteries and conventional combustion systems, see Figure 2.1. A comparison of energy densities offered by the fuel cell are higher than those of battery energy densities and they are rechargeable by refuelling, and batteries are recharged only by plugging them into an electrical outlet or if not, Sin et al. (2013). Compared to conventional combustion systems, the electricity production through the chemical energy by the fuel cells is more efficient, O'Hayre et al. (2006).

Further, fuel cells are electrochemical devices that are made of thin, planar structures that consist of an anode, a cathode, catalysts and an intervening electrolyte, and they are attached to an electrical circuit, see Figure 2.1. Hydrogen is a fuel supplied to the anode

and oxygen (or air) to the cathode in most fuel cell systems. This results in the production of electricity, water and heat. However, fuel cells are comparatively efficient and reliable, have no moving parts, operate without hydrogen combustion, and are modular and scalable. The size and the shape of the fuel cell system is flexible and adaptable. In addition, they are virtually silent, relatively safe and do not pollute the environment, see Hoogers (2003) and O'Hayre et al. (2006). Among the renewable energy technologies, the fuel cell technology requires special attention, mainly on the advanced material development for the improved component performance, Sin et al. (2013).

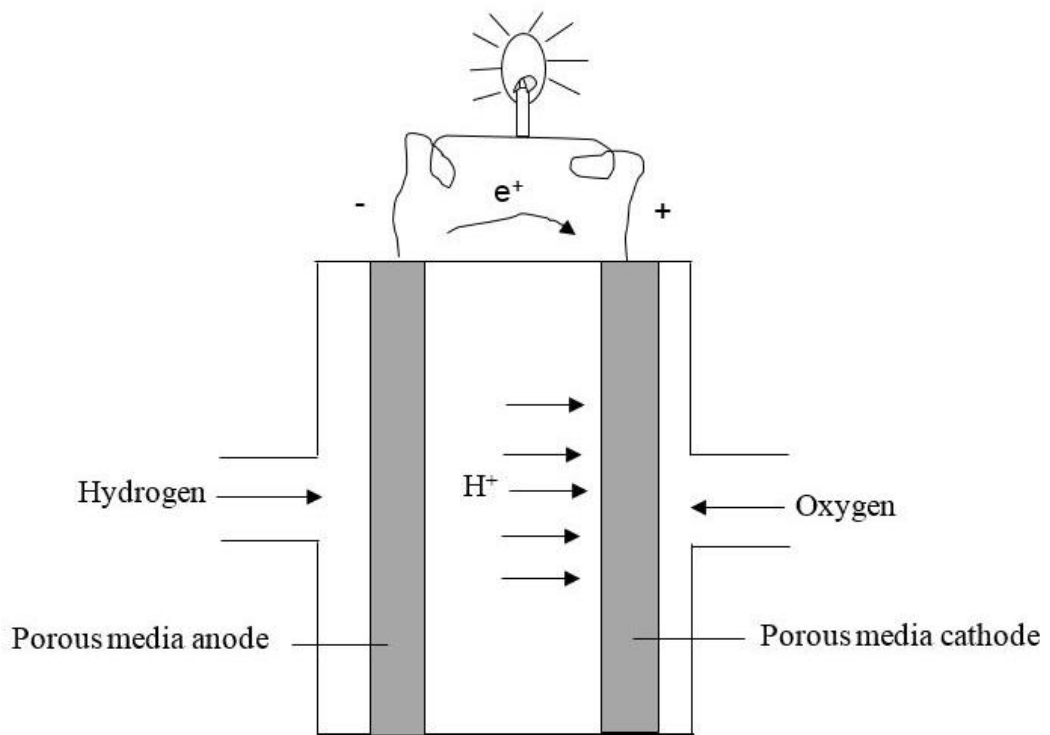


Figure 2.1. A simple fuel cell.

2.3.1 Fuel Cell Technology

The fuel cell technology is receiving great attention in order to address the use and consumption of natural energy resources. However, there are a variety of fuel cells that have been developed. In recent years, scientists and engineers have refined technologies that are relevant to the fuel cell types and generally there are six main types of commercial fuel cells on the market, Sin et al. (2013).

A fuel cell is identified by the composition of its electrolyte, which defines the chemical reactions that occur in the cell during the operational process, see Table 2.1. Table 2.1 presents a classification of the fuel cell types, the kind of electrolytes required, operating temperatures, performance of the fuel cell efficiency, the catalyst used, the advantages and the disadvantages and the main applications, as discussed in the literature, see Sin et al. (2013), Barbir (2013), O'Hayre et al. (2006) and Hoogers (2003).

In recent years, scientists and engineers have refined technologies that are relevant to the different fuel cell types. Clearly, the electrolyte to be used depends on the application. For portable and automotive application (e.g. smart phone and vehicles), the electrolyte is normally a solid polymer membrane. In stationary power plants, the phosphoric acid, molten carbonates, or metal oxides could be used as an electrolyte in the fuel cell employed. In general, hydrogen is the fuel used in most fuel cell systems, and this can be extracted by several procedures from many hydrogen-containing substance: water, gasoline, natural gas and alcohols, Merewether (2003) and Hoogers (2003).

As mentioned earlier, fuel cells are categorised into six types, based on the electrolyte employed. The five common types of fuel cell electrolyte are as follows (Sin et al., 2013 and Kulikosky et al., 1999): solid oxide, molten carbonate, alkaline, phosphoric acid and solid polymer electrolyte membrane. The common fuel cells are therefore named as:

alkaline fuel cells (AFCs), phosphoric acid fuel cells (PAFCs), molten carbonate fuel cells (MCFCs), solid oxide fuel cells (SOFCs), direct methanol fuel cells (DMFCs) and polymer electrolyte or proton exchange membrane (PEM) fuel cells. Furthermore, AFC, PEM fuel cells, DMFC and PAFC operate at low- and intermediate-temperatures and the two other fuel cells, namely MCFC and SOFC, are high-temperature fuel cells and operate at a temperature range of 600 – 1000 °C, see Table 2.1 (Carrette et al., 2001).

2.3.2 Polymer electrolyte membrane fuel cells

The future development and implementation of polymer electrolyte or proton exchange membrane (PEM) fuel cell technology depends on the increasing pressures in a carbon constrained economy (Basu, 2013), limited by dwindling fossil fuel reserves, climate change and the improvement in hydrogen energy infrastructure (Hotza and Costa, 2008). Also, due to low emissions and the high efficiencies of the PEM fuel cells, attention is needed for the knowledge-generating activities to enable improvements in the understanding of the operation principles and the engineering of a typical low temperature PEM fuel cell system, Wang et al. (2008).

PEM fuel cells make use of hydrogen as the fuel which serves as the source of energy and oxygen (or air) as the oxidant, and clearly, hydrogen is not a readily available fuel (Barbir, 2013), see Figure 2.2. It has to be produced from sources of energy such as biogas, coal, natural gas, or by electrolysis of water. Use of these sources to generate hydrogen may significantly reduce the dependence on fossil fuels, Garland et al. (2012), this will have an impact on the control of the CO₂ emission and issues of national security, Barbir (2013) and Sørensen (2012). However, the operating principles are based on the electrochemical energy conversion by converting chemical energy of fuel (i.e. hydrogen)

directly into electrical energy, and unlike combustion systems that converts the chemical energy stored in a fuel into heat.

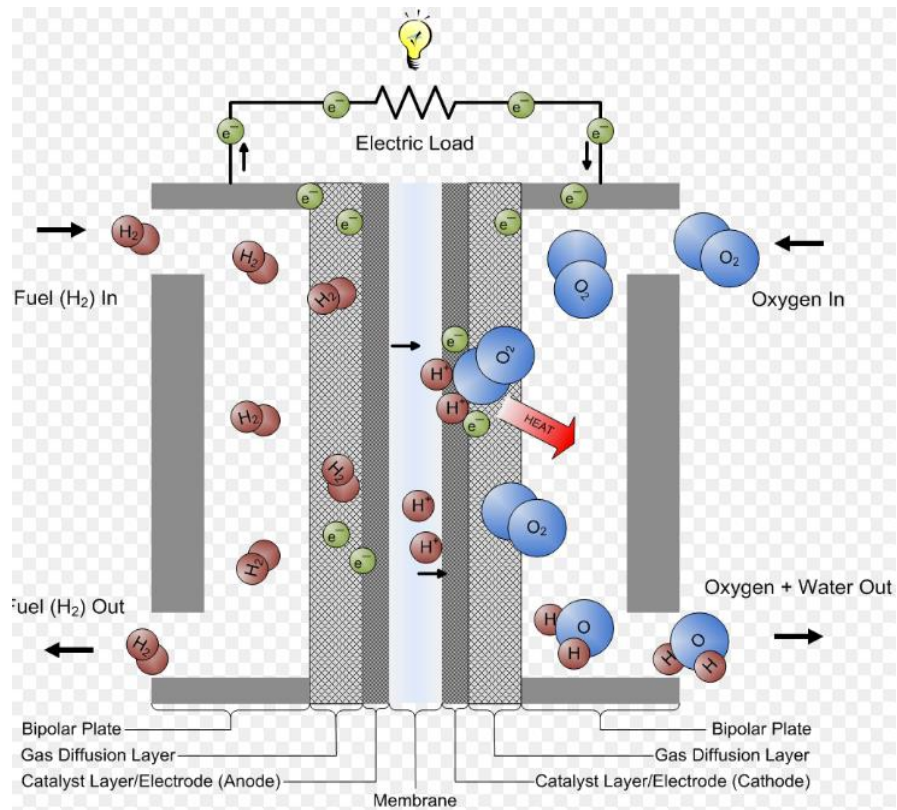
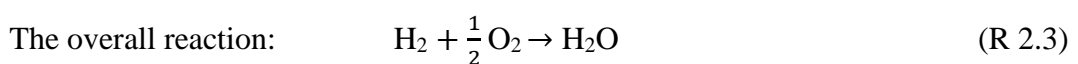
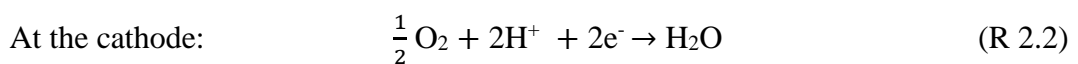
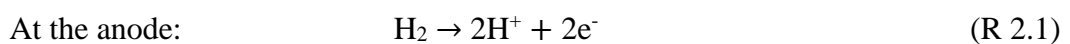


Figure 2.2. A typical polymer electrolyte fuel cell (Barbir, 2013).

In general, electrochemical reactions occur simultaneously on both sides of the membrane, and the hydrogen oxidation reaction splits into two electrochemical half reactions, Barbir (2013) and O’Hary et al. (2006). The basic reactions that occur are as follows:



The above electrochemical reactions describe the main processes in a typical PEM fuel cell in Figure 2.2. The reactions are thereby spatially separated. Electrons are transferred from the fuel, namely hydrogen, forced to flow through an external circuit from the anode side to the cathode side and this constitutes an electric current. Whilst the protons migrate through the electrolyte (membrane). Therefore, the charge transport performs useful work before the reaction can be completed.

In a typical PEM fuel cell, various interrelated and complex phenomena occur during the operation, namely mass or heat transfer, electrochemical reactions, ionic or electronic transport, and all of which govern the cell operation. Clearly, the operation conditions are known to influence the performance of PEM fuel cells, and are affected by many parameters, including, the MEA components construction and the design materials.

Table 2.1. Electrolyte types and the characteristics of fuel cells.

Fuel cell	Electrolyte	Retain material	Operating temperature	Efficiency (%)	Electrocatalyst	Advantages	Disadvantages	Application
Alkaline fuel cell (AFC)	Liquid KOH (immobilized)	Matrix of asbestos	35-50 wt.% concentration for low temperature (120 °C), 85 wt.% concentration for high temperature (250 °C)	50-70	Ni, Ag, metal oxide and noble metals	High efficiency	Intolerant to CO ₂ in impure fuel (H ₂) and oxidant (air), corrosion, expensive	Apollo space programme (Apollo)
Polymer electrolyte membrane (PEM) fuel cell	Perfluorosulfonated acid polymer	Thin proton conductive (< 50 μm) polymer membrane	50-100 °C	40-50	Typically platinum, CO, Pt-Ru alloy is used	High power density, low temperature	Intolerant to CO in impure fuel (H ₂), expensive	Small scale distributed stationary, power generator, vehicle and portable
Phosphoric acid fuel cell (PAFC)	Approx. 100 % concentrated Phosphoric acid, Liquid H ₃ PO ₄ (immobilized)	Matrix of SiC	150-220 °C	40-45	Platinum,	Tolerant to CO ₂ at a value of 20 % impure fuel (H ₂), commercial value	Lower power density, corrosion, Sulfur poisoning	Stationary use (stand-alone), combined heat and power
Molten carbonate fuel cell (MCFC)	A combination of alkali Li, Na, K carbonate (molten carbonate)	Ceramic matrix of LiAlO ₂	600-700 °C	50-60	Not required noble metal catalysts at high operating temperature, Nickel	High efficiency, commercial value	Electrolyte instability, corrosion, sulfur poisoning	Pre commercial or demonstration state for stationary generator, central, stand-alone, combined heat and power
Solid oxide fuel cell (SOFC)	Y ₂ O ₃ -stabilized ZrO ₂ (YSZ)	Ceramic (solid nonporous metal oxide)	800-1000 °C	50-60	Perovskites (ceramic)	High efficiency, direct fossil fuel	High temperature, thermal stress failure, coking and sulfur poisoning	Precommercial stage for stationary power generator, central, stand-alone, combined heat and power
Direct methanol fuel cell (DMFC)	Direct methanol	Polymer membrane	50-120 °C	25-40	Typically platinum, CO, Pt-Ru alloy is used	Using methanol as fuel, no reforming, High power density, Low temperature	Low efficiency, methanol cross, poisonous by-product	Vehicle, small portable

2.4 PEM fuel cell efficiencies and issues

A typical PEM fuel cell performance is linked to the efficiency of the power generation and the amount of fuel, namely hydrogen, required to generate the power. The performance of the PEM fuel cell depends on the operating conditions, namely pressure, temperature, reacting gases flow rates (namely, fuel and air) and humidity, Barbir (2013). However, PEM fuel cells are generally operated in the low temperatures range 50 to 80 °C, and at high temperature ranges of above 80 °C and less than 120 °C, Sin et al. (2013), Carrette et al. (2001) and O'Hayre (2006).

The efficiency of the PEM fuel cell performance is enhanced primarily by improving the water management and gas transport mechanisms that occur during the operational process. However, scientific and engineering breakthroughs are required to overcome barriers related to material developments.

Good performance is obtained, if the profiles for the water-saturation distribution are controlled in the porous material layers used in the design of the MEA components (see Figure 2.3), particularly in the two-phase flow regime of PEM fuel cells. The construction and properties of the porous materials is known to be influenced by many parameters depending on the materials. Also, the operating conditions affect the performance of PEM fuel cells. However, PEM fuel cell performance depends on proper water management during operation which relates to the construction of the MEAs, see Barbir (2013) and O'Hayre (2006).

In the water management with both application and performance of PEM fuel cells, tailoring the porous diffusion materials used as the gas diffusion media in Figure 2.4, there have been several approaches to improve water management in PEM fuel cells.

These approaches are associated with optimising the following: the content of the hydrophobic agent both the GDL and the MPL, various carbon loading and carbon type, e.g. PTFE and fluorinated ethylene propylene (FEP).

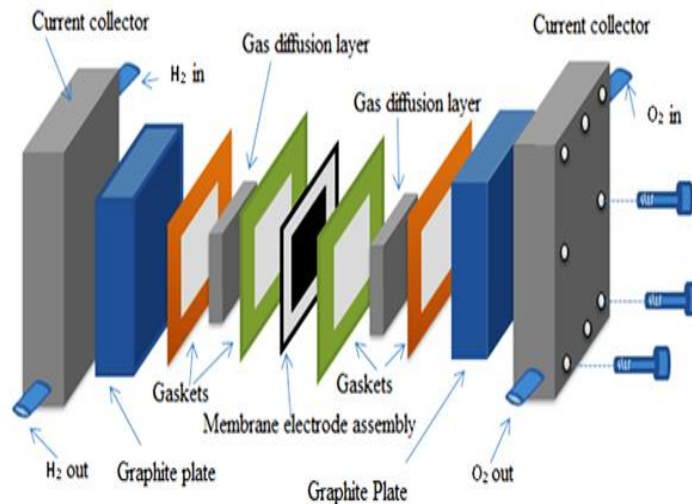


Figure 2.2. A typical MEA (Barbir, 2013).

2.4.1 Water management

The poor performance of fuel cells is often an issue as a result of poor water management, which reduces and blocks the gas pores in the catalyst layers and the porous gas diffusion media (i.e. GDLs and MPLs). The factors that influence the water content within the MEAs components are the hydrophobicity, hydrophilicity, and porosity and permeability properties of the porous gas diffusion layers (electrodes) under the specific operating conditions of the cells, Blanco and Wilkinson (2010).

To know the driving forces that are most dominant in the managing of the water transport for the performance of fuel cells, Park et al. (2004) investigated the design parameters of the gas diffusion layers (GDLs) and microporous layers (MPLs). They treated the gas

diffusion layers with different amounts of PTFE content and investigated the influence of the water management and the gas transportation. The hydrophobic coating facilitates the increase in the water and the air transport leads to an increase in the water contact angle which is between 1 and 20°. Further, for improving cell performance with the application of different hydrophobic agents, Lim and Wang (2004) studied the effects of the FEP (fluorinated ethylene propylene) in the carbon substrate (GDL) on the treated GDL without the microporous layer coating. They considered different amounts of FEP loadings on the GDL, and reported that at 10 wt.% the FEP impregnated into the carbon substrate sufficiently to coat the surfaces of the carbon fibres. Lim and Wang (2004) concluded that increasing the FEP content in the GDL only increases the thickness of the FEP coating layer, and there is no change in the surface hydrophobicity property of the treated GDL. In addition, Lim and Wang (2004) stated that better cell performance was obtained at 10 wt.% FEP. However, many studies in the literature have been more focused on the optimisation of the hydrophobicity and hydrophilicity property of the GDL for better water management and cell performance.

Through a thin film-agglomerate approach, Lin and Nguyen (2004) investigated the effect of water flooding in the gas diffusion layer and catalyst layer of the cathode on the overall performance of the PEM fuel cell. The results obtained indicate that more water flooding is observed at the catalyst layer than that of the porous gas diffusion layer, and they agreed that water is first formed in the catalyst layer. The porous layer has to be coated with the microporous layer for the purpose of controlling other operating parameters that affect the water generation and removal process, for example the RH (relative humidity) and operating temperature, relate to the performance of the porous media.

Further, Lin and Nguyen (2005) examined the effect of the thickness and wet-proof level (PTFE content) of the gas diffusion layers on the performance of a PEM fuel cell, and they have taken into account the carbon substrate coated and uncoated with microporous layers. The results obtained indicate that low current densities of the materials used exhibit common electrochemical behaviour. For example, some liquid water occurs when the GDL without coating materials are used, which does not affect the gas permeability of the GDLs, and the gas transport has been fast enough for an adequate supply of reactant gas flows with no significant loss being detected in the cells performance. For high current densities, loss of performance is also reported. Thus, more of the liquid water accumulation is observed at high current densities with non-coating GDL compared with the coated GDL that performs better. Also, the addition of high wet-proof material to the GDL (i.e. microporous layers with high PTFE content) has contributed to the improvement in the voltages and the pressure drops at the same current densities. A clear understanding of the gas flows, the liquid water and operating factors that affect the pressure drops of the porous gas diffusion layers has been also considered, which relate to the thickness of the coated GDLs. On the other hand, factors that influence the thickness property of the GDLs after coating have been considered, while further understanding of the effect has to be studied. However, the issue for controlling the cell performance as the current density increased beyond 1.1 A/m^2 , has been influenced by determining accurately the thickness and optimum microporous layer compositions of the gas diffusion media of the PEM fuel cells.

Furthermore, improving the water drainage in the channels and porous media for better cell performance, Wang et al. (2008) modelled two-phase flow in the PEM fuel cell channels by envisioning a structural and flow analogy between the channels and random porous media. Issues of the channels flooding, water trapping within the porous media of

the components of the MEA and other related parameter effects on the water drainage are addressed. They conclude that the liquid water builds up fast at the entrance region at full-humidification inlet conditions compared with what occurs elsewhere. In addition, the results obtained are to be validated against key factors that affect the saturation of the liquid water in the cell channels and the porous media in the PEM fuel cells. On the other hand, Mortazavi and Tajiri (2014) determined the dynamic behaviour of liquid water droplet and the detachment from the gas diffusion layer. Also, they reported that the other important dominant parameters, such as the surface adhesion force, drag force, capillary pressure and shape of the droplet strictly depends on the contact angle, which clearly affects the water management and the performance of the cells. However, the greatest challenges that have been addressed are in the improvement in the cells performance by targeting porous diffusion layers treatment and the coating properties, such as the water and gas transport properties in both the cases, see Mortazavi and Tajir (2014).

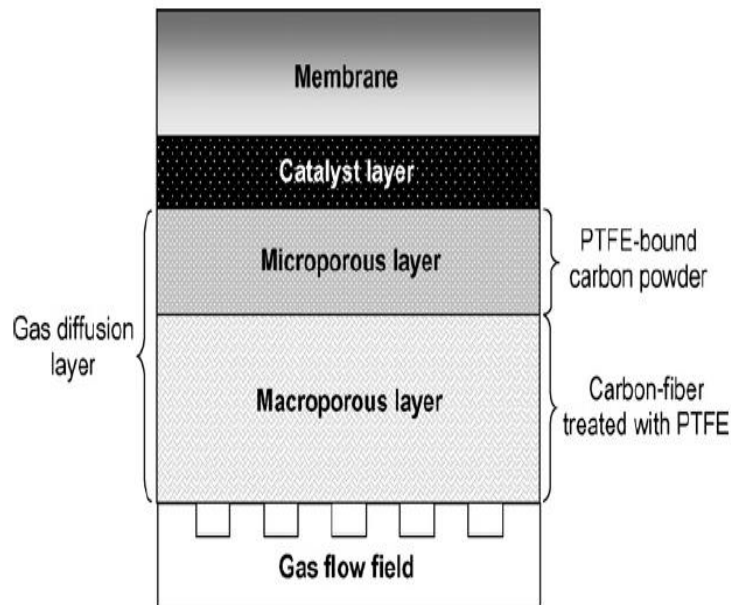


Figure 2.3. A schematic of a dual-layer GDL for PEMFCs (Park et al. 2006).

2.4.2 Gas transport

For improving the performance of PEM fuel cells, Jordan et al. (2000a) demonstrated the possibility of using electrode diffusion-layers made of two different carbon black materials, namely Vulcan XC-72 and Acetylene black, on the performance of different types of cells. Also, they studied the performance of the cells together with the optimum operating conditions of the cells. They explained that the gas diffusion can be improved, except the gas diffusion layer (for example, the diffusion layer made of Acetylene black) indirectly improves the diffusion by controlling the water formed (or product) in the cell. They concluded that the porosity of the carbon substrate used as a material in the porous gas diffusion layer could also affect the optimum water profile for the performance of the cells.

For an improvement in the overall gas diffusion layer characteristics for minimising the water management, Antolini et al. (2002) discussed that the cell performance is improved by increasing the polytetrafluoroethylene (PTFE) content material in the GDL. The impact of the carbon and PTFE as materials used have an influential impact on the cells performance, Jordan et al. (2000b) and Antolini et al. (2002). However, it is not clear in their investigations what is the gas transport mechanism within the porous gas diffusion layers for the efficiency of the cells performance.

Recently, on the mechanical properties of the GDLs with the application of good performance, Su et al. (2016) investigated the effect of the PTFE content on the GDL and the MPL on the electrode performance. They reported that varying the amount of PTFE content in the GDL does not have much effect compared with the PTFE loading in the MPL, which has a significant effect on the performance of the cell. Further, El-kharouf et al. (2012) characterised the GDLs for the PEM fuel cell performance, by considering

the GDL and MPL for the design and modelling of the MEA and the fuel cell stack. They concluded that the properties of the porous gas diffusion media are related, particularly in the substrate structure, PTFE and MPL loading, which is required for the development of the GDLs with higher performance for the cell performance.

Further, the characterisation of the transport properties in the porous gas diffusion media requires further attention, and the gas permeability is one of the features required in porous media for the reactant gases to have access to the catalyst layer, Zamora et al. (2015). Much work in the literature has been reported on the estimation of the transport properties in the gas diffusion layers, Gurau et al. (2007), Tamayol et al. (2012).

Gurau et al. (2007) measured the absolute permeability property of the GDLs, and estimated the in-plane and through-plane permeability values of the GDLs and MPLs. The gas permeability values of the GDLs is influenced by the presence of the MPL in the GDL, and similar results have been reported by Ismail et al. (2010), as the different PTFE loading in the MPL increases the permeability values of the GDLs. However, the reports from Gurau et al. (2007) and Ismail et al. (2010) have not been clarified and the conclusions that the characteristic gas transport properties of the porous media are relatively related has been claimed.

2.5 Materials used in the gas diffusion media

For materials development, many authors have investigated ways of improving the PEM fuel cells efficiency (Nguyen et al., 2015; Kim et al. 2013), in particular on the water management, and factors that affect the materials has to be targeted for the treatment of the porous gas diffusion media for the performance of the PEM fuel cells. However, the high efficiencies of the PEM fuel cells performance have been a greater issue, due to the

inherent non-uniformity, which has not been completely targeted, particularly on the transport properties, Nguyen et al. (2015).

The gas diffusion media generally consists of treated gas diffusion layers (GDLs) and with a coated thin layer, commonly known as microporous layers (MPLs). However, the GDL materials are treated and coated for the purpose of determining the hydrophobicity and hydrophilicity properties, Kim et al. (2013), and to avoid flooding accumulation and easy flow of the reactant gas flows within the PEM fuel cell (Zamel and Li, 2013; Barbir, 2013). In addition, the effect of the treatments of the porous GDL has been discussed in Section 2.4, particularly for the performance of the PEM fuel cells, and much more may be found in the literature, El-kharouf et al. (2012).

Further, the effect of coating the porous GDLs with the MPL made slurry have been considered in this section. The microporous layer is a layer that consists of two basic materials, namely carbon black particles (or powders) and hydrophobic agents, namely the PTFE and FEP, as made of a MPL slurry (ink). The MPL is simple in structure compared to the gas diffusion layer as described in the literature (Zamel and Li, 2013), and which can be used to evaluate the characteristic properties, El-kharouf et al. (2012).

The characterisation of the GDLs, as materials for the gas diffusion media, is an approach by coating the MPL ink onto one side of the carbon substrate surfaces. The addition of the MPL to the GDL is to enhance the performance of the MEA, for controlling the transport of the reactant gases (El-kharouf et al., 2012) and the management of the flow of the reactant gas product (liquid water formed) for the overall effective performance of the PEM fuel cells (Su et al., 2016).

The effects of the gas diffusion media have been presented by many authors on the different parameters that affect the performance of the PEM fuel cells. Chen and Chang

(2013) showed that the effects of the PTFE and carbon loading in the cathode MPL obtained the optimum cell performance due to the MPL composition at the cathode side for different operating conditions that were considered in their investigations. The optimum power density was obtained at the composition of the MPL with a carbon loading of 1.5 mg/cm^2 and 20 wt.% PTFE on effect of gas flow rate, and similar results were reported in Velayutham et al. (2008). Also, similar performances were obtained, as the effect of the different carbon loadings in the MPL with 20 wt.% PTFE content and the maximum power density were observed at a carbon loading of 1.5 mg/cm^2 . They explained that as the PTFE content and carbon loading in the MPL increases, the power density also increases. They have taken into account the effects of the various loadings of carbon black and the PTFE content in the MPL. However, it is unclear on the effects of the different carbon black types used in the materials of the MPL for the same operating conditions. The authors have not reported the effects of these factors on the other major parameters, such as the thicknesses and gas permeability of the gas diffusion media, and in this regard to have a better understanding of the operating conditions and the overall performance of the PEM fuel cell.

According to other reports, Lee et al. (2004) and Lin and Nguyen (2005), the effect of the gas diffusion electrode thickness on the PEM fuel cell performance was investigated. The best performance of the cells was obtained at intermediate carbon loadings in the gas diffusion electrode layers (Lee et al., 2004), and also, Lin and Nguyen (2005) reported that the gas diffusion media with thinner layers materials of the MPLs have been shown to have a better performance compared to the thicker layers. However, it is clear that an accurate thickness of the gas diffusion layer after coating with the microporous slurry still competes with the other properties, such as the gas permeability of the coated gas diffusion layers.

Further, Kim et al. (2013) studied the effect of the different carbon black powders as the material of the MPL composition on the performance of a high concentration methanol fuel cell. The PTFE content of the compositions was fixed at 25 wt.% in all the different types of carbon black particles used as the material in the MPL. The authors measured the thicknesses for all the MPLs of the different carbon types and those are estimated to be about 30 μm , which could have been attributed to the amount of the carbon loadings in the MPL and the type of the carbon substrate sheets (i.e. the GDLs) used and coated with the MPLs slurry of those carbon powders. In contrast, the gas permeability of those MPLs with different carbon powders are reported to be different, which could have been attributed to the characteristic properties of those carbon powders. Also, the variations in the gas permeability values of those MPLs can be as a result of the penetration of the MPLs slurry materials into the porous carbon substrates that affect an accurate estimation of the thickness of the MPLs, as described in Kitahara et al. (2010). However, they found that the carbon powders used as the materials for the MPLs have affected the electrical properties, namely the ohmic resistance of the MEA. In addition, the influence of the different MPLs with various carbon powder parameters, namely the carbon loading, carbon types and thickness have a significant impact on the performance of the MEAs and this can be ascribed to the effective performance of the PEM fuel cells.

Furthermore, Liu and Chang (2013) and Chen and Chang (2013) studied the effect of the microporous layer composition. They determined the optimum MPL composition at 1.0 and 1.5 mg/cm^2 of carbon loading. From these investigations, the performance of the cell has been obtained at 1.5 mg/cm^2 of carbon loading. As Liu and Chang (2013) reported, the performance of the cell begins to degrade after the carbon loading increases above 1.5 mg/cm^2 and a similar amount of carbon loading has been used to obtain the best performance by Chen and Chang (2013). In the case of the PTFE content in the MPL at

30 wt.% PTFE loading, a better performance was observed than that at 20 wt.% PTFE loading and the highest peak in the power densities was obtained at low RH (relatively humidity) in Chen and Chang (2013), and at 40 wt.% PTFE as it has been obtained by Liu and Chang (2013). It was concluded that the effect of the PTFE is significantly influenced by the performance of the MEA compared to the carbon loading in the MPL composition. In addition, the MPL material in the gas diffusion media significantly improves the transport of liquid water, particularly on the cathode side (Chen and Chang, 2013). However, further studies are required to investigate the relative effect of the PTFE content and carbon loading of the MPLs on the performance of the PEM fuel cells, Schweiss (2016).

2.6 Gas permeability of the gas diffusion layer

For influencing the physical parameters of the gas diffusion media (GDM), the thickness of the GDM has a direct effect on the transport properties of both the gas and water, namely the permeability, diffusion and electrical conductivity, El-kharaouf et al. (2012). The effect of the GDL and MPL thickness as the physical property of the GDM, has been attributed to the various amounts of the PTFE content and the carbon loadings in the GDL and MPL (Park et al., 2004; Lim and Wang, 2004). However, the thickness is an important property for the GDL materials. For the pressure drop of the gas flow through the porous media, this is related to factors such as the GDM thickness, as discussed by Lin and Nguyen (2005), and the GDLs with the highest thickness performs better compared with the GDLs of lesser thickness at high current densities. However, the different effects of the GDM thickness on the performance of the cells is traceable to the effect of the total GDM thickness on the through-plane gas permeability of the porous GDM.

Ong et al. (2008) detailed the effect of the MPL thickness on the gas permeability and the resistance of the GDL after coating. In their report, the resistance increases as the thickness of the MPL increases, but on the other hand, the gas permeability of the GDLs decreases with an increase in the MPL thickness. They concluded that the various amounts of the compositions of the MPL ratios are ascribed to the thickness of the GDLs. Moreover, the gas permeability of the gas diffusion media is affected mainly by the GDL thickness before and after the coating, porosity, pore size and pore distribution. For an effective permeability as a key parameter to be determined and tailored by adding MPL to the GDL, the GDL fibre structure affects the thickness of the GDM which apparently influences the gas flow direction through the porous media, Shou et al (2013). However, the influence of these parameters can be ascribed to the characteristic properties of the carbon black and the PTFE loadings as the materials of the MPLs and the GDLs.

Many researchers have studied the various amounts of PTFE and carbon loadings in the MPLs by considering the effect of different carbon types and PTFE loading on the thickness of the porous GDM through-plane gas permeability, Ismail et al.(2011), Tamyol et al. (2012) and Kim et al. (2013).

For the effect of the PTFE loading in the MPL, Ismail et al. (2011) experimentally measured the through-plane gas permeability of the GDL coated with MPLs of different loadings of PTFE. In addition, the estimated MPL thickness by adding GDL, and the same batch of the carbon paper has been investigated. They reported that the through-plane gas permeability of the MPL-coated GDLs increases as the amounts of the PTFE loading in the MPLs increases and this is in agreement with the literature, Ismail et al. (2010). While the carbon loading in the MPL decreases the through-plane gas permeability of the GDLs as the amount of the carbon loading increases at a constant

PTFE loading in the MPL, Tamyol et al. (2012) and Kim et al. (2013). However, the different effects of the MPLs added to the GDLs, on the gas permeability of the GDLs is more dependent on the thickness of the MPL and other affecting factors of the MPL, such as the pore size, porosity, etc., as detailed in Wilde et al. (2004) and Kim et al. (2013).

2.7 Gas permeability of the microporous layer

Further, the performance of PEM fuel cells are often controlled by the coating materials of the porous gas diffusion media with a wet-proof agent which is used to properly and adequately control the liquid water generated during the fuel cell operation. The effects of the various factors, such as the hydrophobicity content in the gas diffusion media have been investigated by many authors, in particular on the effect of the PTFE content in the gas diffusion layers (GDLs) and the microporous layers (MPLs).

The hydrophobic polymer-treated porous GDL is identified as playing a crucial role in the performance of PEM fuel cells and this relates to the treated-GDL performance. Also, the reactant gas transport and water management (such as the flooding) rely strongly on the degree of the hydrophobic characteristics property of the treated-GDL (Lin and Wang, 2004), the through-plane gas permeability (Ismail et al., 2010), and the electrochemical reactions at the anode and cathode sides, for using different quantities of hydrophobic agents, such as PTFE (Moreira et al., 2003). However, the content of the hydrophobic agent in the treated-GDL significantly affects the PEM fuel cells performance. Moreira et al. (2003) and Lim and Wang (2004) investigated the influence of the hydrophobic agents contents, namely the PTFE and FEP in the gas diffusion media of H₂/O₂ and H₂/air PEM fuel cells, respectively. The best results are from the power density obtained at 10

wt.% compared with the 30 wt.% (Lim and Wang, 2004), and for the current 30 wt.% obtained at a potential of 0.5 V, Moreira et al. (2003).

The effect of the different PTFE-carbon ratios in the electrodes has a great influence on the performance of the PEM fuel cells. Significantly higher current densities were observed between the different electrodes as the hydrophobic agent and the carbon ratio increases, Bayrakçeken et al. (2008). Also, the electrodes with the large volume pores have a better mass transport at higher current densities and this is due to the high PTFE content in either the GDL or the MPL, Su et al. (2016). The ohmic resistance increases as the PTFE-carbon content ratio increases, thus changing the PTFE content has an effect on the performance of the PEM fuel cell. The results of Bayrakçeken et al. (2008) and Su et al. (2016), show that lower PTFE content in the MPL exhibited lower electrical resistance and decreased the ohmic resistance, which also results in higher performance of the fuel cells.

On other hand, Velayutham et al. (2008) investigated the effect of the PTFE loading in the GDL and MPL on the gas diffusion electrodes of the performance of the PEM fuel cell. They observed that as the PTFE-carbon content increased in both the GDLs and MPLs, the internal resistance was increased, and also there was higher electrical resistance. This has led to lower performance of the PEM fuel cells. However, the hydrophobic and hydrophilic properties of both the GDL and MPL effects the performance of the PEM fuel cells. Clearly, the PTFE loading in both the GDL and MPL have to be finely matched. For example, the results showed that a good performance of the cell was observed at 23 wt.% PTFE loading for the GDLs. For the MPL, the best performance was obtained at 20 wt.% PTFE loading. As the PTFE content in the GDL (carbon substrate) was kept constant at 23 wt.% and varied, the PTFE loading in the MPL

varied between 10 and 32 wt.%. However, it was only the effect of the PTFE content in the gas diffusion electrodes that has been taken into account. None of the authors have investigated the significance of the effects of the carbon loading and the carbon types.

Tseng and Lo (2010) measured the microscale characteristic properties of the MPL and GDL in order to determine the effects of the GDL before and after adding the MPL on the cell performance. They showed that the pore sizes of the GDL are in the range 18 to 26 μm , and were reduced to be in the range 0.32 to 12 μm with the MPL and this is due to the pore sizes distribution effects and the capillary effects. Also, they reported that the best cell performance was obtained for the GDL with 20 wt.% PTFE, and the MPL with 40 wt.% PTFE exhibited the best performance. Generally, the microscale properties of the MPL and GDL contribute to the degree of the cell performance. For example, the small pores have a higher capillary action, supporting the removal of the liquid water formed easily, and decrease the gas permeability mass of the gas diffusion media. In contrast, large pores enhance better transport of the reactant gases and reduce the mass transport resistance. In addition, the thickness of the MPL showed a significant effect on the performance of the cell. The thickness of the MPL estimated are varied in the range 38, 84 and 136 μm , the pore diameter increased as the thickness increased as well as the gas permeability. Clearly, the effects of the thickness of the MPL, the PTFE loading in the GDL and the MPL on the PEM fuel cell performance have been investigated. It is clearly shown that the difference in the variation of the MPL thicknesses is due to the amount of the carbon loading in the MPL, and this factor has not been taken into account. Also the compositions of the MPL (that is, the PTFE content and the carbon loading) have not been thoroughly considered in the studies, Tseng and Lo (2010).

However, the materials used to construct the required gas diffusion electrodes have to be systematically tailored to target the appropriate characteristic properties of the materials. The illustrated literature reviews highlight that the following effects have not been thoroughly investigated: (i) carbon black loading and carbon black types, (ii) compositions of the microporous layer, that is, the PTFE contents and the carbon loadings relation, and (iii) an accurate estimation of the thickness of the MPL of the gas diffusion media for the PEM fuel cell performance. In addition, the basic role of the MPL is known to facilitate the management of the liquid water formed within the MEA in order to improve the overall performance of the PEM fuel cells. However, it is still unclear (lack of in-depth) on the influence of the MPL basic property, namely the thickness, has on the reactant gas transport of the gas diffusion media in order to control the water transport mechanism within the MEA.

For the effect of the MPLs on the gas permeability, the MPL performance characterisation depends on the GDL and CL (catalyst layer) properties, such as the pore size, as detailed in Zamel and Li (2013). The MPL consists of a combination of a powdery mixture of carbon black and emulsion of PTFE particles. The preparation requires a heat treatment at a temperatures of 120, 280 °C and finally to be sintered at 350 °C and for 1 hour, 30 minutes and 30 minutes, respectively, Rohendi et al. (2014) and Jordan et al. (2000b).

The MPL effects can only be determined by measuring the parameters that are under investigation before and after adding the MPL to the porous GDLs, followed by estimating the influencing factors, Zamel and Li (2013). Much work has been reported in the literature on the effect of the MPLs with composite carbon black as the materials added to the GDLs to characterise the porous gas diffusion media performance in the PEM fuel cell technology, Wang et al. (2006).

Recently, Zamora et al. (2015) analysed the MPLs characteristic properties with different materials. A comparison of the behaviour of the advanced carbon materials, namely Carbon Nanospheres, Ribbon Carbon Nanofibers, and Platelet Carbon Nanofibers, together with Vulcan XC-72 has been performed. The permeability of the materials varies with the gases utilized and the porous materials investigated, and they concluded that the permeability values of the different gases in the MPLs made with Carbon Nanospheres and Vulcan XC-72 materials are higher than in the other materials investigated. The surface compaction has been found to be the only factor that could have hindered the flow of the gases. However, the effects of the other influencing parameters of the MPLs, such as the thickness, sintering, and penetration of the MPLs into the porous GDLs, may be considered to be worthy of further analysis.

2.8 Effect of the microporous layer sintering

The Sintering is the process of altering the effect of the PTFE distribution within the diffusion layer via heat. The sintering time of the treated GDL and MPL-coated GDL is an influencing factor on the physical properties of the porous gas diffusion media, namely, the through plane conductivity, gas permeability and hydrophobicity, Bevers et al. (1996) and Rohendi et al. (2014). However, the aim of the sintering is to characterise the relevant performance of the treated or coated porous media. However, little work has discussed the effects of the sintering temperature and the timing of the sintering.

Bevers et al. (1996) characterised the performance of the treated gas diffusion layers, and examined the sintering temperature at which the GDL is treated with PTFE. They explained the approach of the sintering process as the treated GDLs being placed into the sintering oven at a temperature below 200 °C and followed by the oven heating to the

desired sintering temperature for the desired time. In this case, the sintering temperature and timing of the sintering for the samples with different PTFE contents is set at 20 minutes and at a temperature 390 °C and the sinter time for the treated GDL sample of the different sintering temperature at 15 minutes. The gas flow through the treated GDL samples before and after is discussed and this shows that the pressure drop of the treated GDL samples before sintering are higher than after the sintering are for the pressure drop of the gas flow against the samples with a different sintering temperature. On the other hand, the treated GDL samples that are sintered with different temperatures of constant 180 wt.% PTFE loading exhibit a higher resistance after sintering than the non-sintering counterpart (treated GDL samples). It is clearly shown that the influence of the sintering of the treated GDLs significantly changed with different timings of the temperature. For example, Bevers et al. (1996) sintered for 20 min at 390 °C, and treated the GDL containing 35 wt.% PTFE sintered at a temperature at 350 °C for 3 hours by Rohendi et al. (2014). However, Bevers et al (1996) have only measured and examined the GDLs treated with PTFE and considered the effect of 15 minutes for the sintering time of the samples at different sintering temperatures, and they have not taken into account the influence of different sintering times on the gas permeability of the treated and coated GDLs.

In investigating the parameters that affect the optimal performance of the fuel cell, Jordan et al. (2000a) observed the parameters of the GDL when these parameters are varied by examining the effect of the sintering on the performance of the gas diffusion layers with different carbon black types. The effect of sintering on the MPL-coated GDLs with different carbon types is discussed, and it is found that the sintering significantly affects the performance of the fuel cell, particularly at high current densities. In addition, the type of the carbon black material utilised in the preparation determines the effect of the

sintering on the MPL performance, for example, Jordan et al. (2000a) found that the fuel cell has the best performance with the sintered MPL-coated GDLs with Acetylene black carbon rather with the same carbon black material and non-sintered. However, the MPLs compositions (PTFE contents and carbon loadings) physical properties have to be considered relative to the influence of the sintering, which the authors have not taken into consideration in their studies.

Prior to the measurement and estimation of the gas diffusion media, the sintering of the treated and coated GDLs for the uniform distribution of the PTFE in the GDL and MPL is an influencing factor that effects the relevant performance of the gas diffusion media. However, the impact of the sintering and the temperature on the overall performance of the fuel cells requires further studies. Thus, the effect of the sintering on the through-plane gas permeability of the MPL-coated GDLs has been measured, estimated and investigated in this thesis.

2.9 Effect of the microporous layer composition

The components of the MPL, i.e. the carbon black and the hydrophobic agent, are factors that influences the optimisation of the content and the thickness of the MPL, and this relates to the gas permeability of the gas diffusion media used in PEM fuel cells. However, different carbon black types are utilised in the preparation of the MPLs with different physical characteristic properties, such as the surface morphology, electrical resistance, gas permeability, microstructure, etc., Han et al. (2006), Ong et al. (2008) and Kim et al. (2013).

Han et al. (2006) studied the fabrication and electrochemical performance of a carbon-filled gas diffusion layer (CFGDL) and analysed the results from the investigation. The

CFGDL is made of a carbon electrode (PE-74) backing filled with a combined mixture of carbon particles and PTFE. The significant effect of the carbon content in the MPLs on the fuel cell performance over the PTFE content is reported. They found that a large amount of carbon particles of 6 mg/cm² and 40 wt.% PTFE in the MPL have been considered, while the PTFE content may require to be considered for the agglomerate composition of the MPLs and the performance of the fuel cell.

The effect of the preparative parameters on the hydrophobic agent has been investigated by Ong et al. (2008), who examined the characteristics of the preparative parameters on the MPL, such as the PVDF (polyvinylidene fluoride) concentration and the type of PVDF solvent. The effect of the MPL thickness on the resistance and gas permeability of the prepared MPL indicated that the resistance increases as the thickness of the MPL increases. On the other hand, the gas permeability decreases from 1.35 to 0.83×10^{-4} mols⁻¹Pa⁻¹m⁻² with an increase in the MPL thickness from 41 to 112 μm. In contrast, Chang and Chen (2013) studied the PTFE loading in the MPL, which indicates that the PTFE loading in the MPLs plays an important factor in the performance of the fuel cells. Within the range of the studies, the effect of the different types of PVDF have been considered and the influence of the different carbon black types for the preparation has not been taken into account.

For the effects of the various carbon blacks in the MPLs compositions in the anode, Kim et al. (2013) discussed in detail the physical properties that the various carbon particles and the compositions exhibited on the performance of the fuel cells. With different carbon black types, the thicknesses of the MPLs are about 30 μm and this agrees with the MPL thickness range reported in the literature, Kitahara et al. (2010). In contrast, the gas

permeability values are significantly different for the MPL-coated GDLs with different types of carbon blacks.

2.10 Microporous layer penetration

The difficulty of direct measurements of the microporous layer thickness as a primary parameter has not been possible to enable accurate estimation of the gas permeability of the layer. Thus, the microporous layer is not a stand-alone layer in the fuel cell, and its influencing parameters cannot be measured and estimated without the presence of the porous gas diffusion layer as a support layer. The thickness of the GDL before and after coating are measured by Ismail et al. (2011) and Kitahara et al. (2010) and the thickness of the MPL is inferred by determining the difference between the thicknesses of the GDL and the MPL-coated GDL.

The MPL thickness is manually measured by using a micrometer and scientifically verified by employing a scientific analytical technique, namely the scanning electron microscope method (SEM), Ong et al. (2008). Ong et al. (2008) measured in particular the thickness of the MPL from the same batch of three different samples and estimated the mean value. The MPL thickness is measured by a micrometer and they showed the SEMs images for cross-sectional view of the MPL. The measurements of the thickness is based on the total thickness of the coated GDL samples, which has a direct effect on the estimation of the gas permeability of the MPL-coated GDL. However, measuring the actual thickness of the MPL and calculating the accurate gas permeability are challenging and have not been reported in any of the literature.

Efforts to characterise the gas transport properties in PEM fuel cells has been made by Gurau et al. (2007), who experimentally measured and estimated the through-plane and

in-plane viscous inertia permeability values of GDLs with and without MPL. They stated that, knowing the permeability values for the GDLs without and with MPLs, the permeability of the MPL can be determined, however, they assumed that the porous layers (MPL and GDL) are parallel to each other. However, Gurau et al. (2007) did not account for the thickness of the MPL material that has penetrated into the porous substrate.

Weber and Newman (2004) modelled a simple fuel cell to predict transport of protons in the polymer electrolyte membrane, with the assumption that the porous diffusion media are uniform and symmetric. Similar assumptions were made by Pharoah (2005) in investigating the effect of gas diffusion media (GDM) permeability and he employed a computational model to determine the relevance of the convective transport as a function of the GDM permeability. Pharoah held the thickness of the GDM constant at 250 μm , and found that the value of the permeability for a bare substrate (i.e. without MPL) is 10^{-11} m^2 and the GDL coated with the MPL spanning one or two orders of magnitude from 10^{-12} to 10^{-13} m^2 .

Numerically, there have been two efforts to date on utilising the agglomerate structure of the MPL as a thin layer in the modelling of fuel cells (Zamel and Li, 2013 and Gurau et al., 2007) and it is assumed that the thin layer (MPL) and its counter-part (porous GDL) are parallel to each other (Pharoah, 2005), assigned values to the thickness of the agglomerates structure of the MPL (Kithara et al., 2010). However, it has not been taken into account the effect of the penetration of the MPL material into the porous substrate on the total thickness of the MPL used in fuel cell models in the literature.

Accurately, measuring the thickness of the MPL has not been possible, but the penetration of the MPL material into the porous substrate is important and therefore should be taken into account, as discussed by Kitahara et al. (2010). They described an approach by

comparing the in-plane permeability obtained from the GDLs before and after coating the MPL. Both the gas and water permeability have been considered to estimate the penetration thickness. They found that the penetration thickness of the MPL into the substrate increases the cross-sectional area of the porous substrate by significantly enhancing the in-plane permeability. In addition, the SEM method has not been able to view the unique visualisation of the boundary between the visible MPL layer and the penetration. However, estimation of the MPL thickness has not paved a way to establish values of the MPL gas permeability, which can serve as an information guide for fuel cell models, to accurately predict the performance of the porous media in fuel cells, Zamel and Li (2013).

2.11 Limitations in Knowledge

Due to the increase in the global population and the social-economic development, it has been observed that there is a high demand for energy. The conventional energy resources based on fossil fuels used to generate the energy release harmful chemicals and greenhouse gas emissions. The use of fossil fuels has caused the degradation of both local and global environment, which has posed health hazards to all the inhabitants of the Earth due to the climate change. The energy demand, and the security of access to and the distribution of energy have created global awareness in order to control the climate change. However, several energy source technologies have been engaged in research to find possible solutions for controlling greenhouse gas emissions into the environment.

Among the many renewable energy sources and their technologies, fuel cells technology has been considered because of its high energy efficiency and minimal total emissions.

Providing the hydrogen is sourced renewably. Fuel cells are promising renewable energy sources and energy converters with which high energy efficiency is achievable.

Polymer electrolyte, or proton exchange membrane (PEM) fuel cells are a suitable technology which has gained momentum as a result of the attainable high power densities and their relative simplicity of use. Clearly, there is a need for improving the performance of the fuel cell systems components, namely the MEA. The great challenge that limits the effectivity and efficiency of fuel cells performance is in particular the water management, followed by the gas transport mechanism within the porous media in the fuel cells. A comprehensive review on the engineering of porous gas diffusion media (GDL and MPL) has been given in more detail in this chapter where the limitations and areas of possible further investigations have been highlighted. It is clear that the impact and role that the MPLs play on the overall performance of the PEM fuel cell is significant. Thus, more insight into the improvement of the gas distribution and water management in the PEM fuel cell is required. To do this, the accurate transport properties of the reactant gases are crucial, and in particular in the numerical simulations. However, the following limitations have been identified, investigated and discussed in this thesis:

- the effect of carbon black as a material used in the microporous layers on the characterisation properties of the porous gas diffusion layers gas permeability for the performance of the MEAs in fuel cells.
- the influence of the composition of microporous layers with in the porous gas diffusion layers on gas permeability of porous gas diffusion media in fuel cells.
- the effect of the influencing factors, namely the thickness of the microporous layer and the penetration of microporous layer materials into the porous carbon substrate on the gas permeability of the porous media and the microporous layers.

In general, the studies of these effects and their influence parameters on the through-plane gas permeability of the porous gas diffusion media gives us a better understanding and a comprehensive information guide, particularly for the use in numerical models of PEM fuel cells. Those effects have not been reported in the literature and these limitations have been identified and investigated in this thesis.

2.12 Contribution of this thesis on PEM fuel cells

A typical polymer electrolyte membrane (PEM) fuel cell is environmentally advantageous compared to the conventional energy-generation resources that the PEM fuel cell technology wants to replace. The cost, durability and efficiency goals for PEM fuel cells are the major technical issues to the PEM fuel cell technology, Barbir (2013). For a typical fuel cell to achieve these goals and overcome the challenges, the development of the fuel cell has to be based on accurate measurements, estimations and predictions of the parameters that influence the design of the fuel cell. In addition, knowledge of the materials, processes and material interactions is important to properly design and fabricate fuel cell stacks, Barbir (2013). However, fuel cell modelling plays an important and significant impact in the design of fuel cells.

For numerical simulation, there are several efforts to date that have been made to determine the accurate gas permeability and estimate the actual thickness of the microporous layer for the designing of the porous media used in the development of the fuel cell stack, Zamel et al. (2013). Finding the gas permeability of the porous gas diffusion media accurately enhances the predictive capability of the PEM fuel cell model, and also increases the efficiency and durability of the porous media used in PEM fuel cells.

However, this thesis addresses the issues of unknown properties and parameters that influence the structure of the microporous layers of a typical PEM fuel cell to attain its best efficiency and durability during the processes of designing, modelling, fabricating and diagnosing the fuel cell. Further, the gas permeability and thickness values that are necessary to enhance the agglomerate structure of the microporous layer which is redesigned based on the stochastic models of the PEM fuel cell have been accurately experimentally investigated and calculated.

The PEM fuel cells are composed of architectural components that are small, with microscopic changes that have a significant effect on the performance. In this thesis, the carbon black loadings and carbon types have been taken into account. The impact of the microscopic changes on the PEM fuel cell performance becomes more sensitive on the multiple roles of the porous media. For example, carbon black loadings and types, as the materials used in the microporous layer, are increased or decreased, then the impact on the passage of the reactant gases transport and water (or heat) removal predictions for PEM fuel cell modelling (numerical simulation and modelling), Zamel and Li (2013) and Wang et al. (2011), since this is another aspect of how cost, durability (lifetime) and high efficiency are intimately related, Barbir (2013), that this thesis greatly contributes to the development of PEM fuel cell technology.

2.13 Summary

This chapter has discussed the polymer electrolyte membrane (PEM) fuel cell as a renewable energy technology and reviewed the challenges that are hindering the achievement of the cost, durability and efficiency goals for the design and performance of the PEM fuel cells. The emphasis has been based on the major technical barriers that

affect the performance of the fuel cells under the operational conditions and material components. Thus, the common properties and parameters of the porous materials, namely the gas diffusion layers (GDLs) and microporous layers (MPLs) used as porous media in the construction and design of the MEA components have been considered and reviewed in this chapter.

The water management and reactant gases transport within the path in the porous media that have been the primary challenges for the high performance of the PEM fuel cells have been also discussed in more detail. Further, the effect of the influencing factors that affect the parameters and properties of the porous gas diffusion media (i.e. gas diffusion layer and microporous layer) are discussed, and this chapter has helped identify the knowledge gaps in the literature which have to be addressed in the thesis.

In addition, this chapter has helped formulate the direction of this thesis by reviewing the fundamental and frontier knowledge on the gas permeability as one of the primary properties and parameters of the microporous layers and gas diffusion layers, which has been referred to as the porous gas diffusion media in this thesis. The through-plane gas flow directions and the through-plane gas permeability of the porous gas diffusion media have been reviewed.

Also, the chapter has discussed the contribution of this thesis on the PEM fuel cells as another aspect of how efficiency, lifetime (durability) and cost goals of the PEM fuel cell can be numerically accurate during the construction and design of the fuel cell stack and diagnosis. This chapter has critically reviewed the gas permeability of gas diffusion media used in the polymer electrolyte, or the exchange membrane fuel cells and this will help to provide guidelines for the measurement and estimation techniques that will be discussed in the subsequent chapter.

Chapter 3

Techniques used to Investigate Gas permeability of Porous Media

The techniques used to investigate the through-plane gas permeability of porous gas diffusion media, namely the microporous layers (MPLs) and carbon substrates are explained in detail in this chapter.

In-house experimental techniques have been employed to investigate the gas permeability of the porous gas diffusion media. The techniques are classified into three forms, namely preparation of materials methods, measurements of the properties procedures and the evaluation of the effects of the gas transport properties that are investigated. Many authors have employed in-house methods to (i) prepare materials, (ii) measure associated physical factors, and (iii) characterise the transport properties of the gas diffusion media (Tseng and Lo, 2010; Wang et al., 2010; Ismail et al., 2011).

An experimental approach has been undertaken in this thesis. Figure 3.1 presents a schematic view of the methodologies employed to address the investigation of the gas permeability of the porous gas diffusion material. The porous materials are the porous gas diffusion layers, namely the carbon substrates and microporous layers.

The experimental investigation includes the measurement of characterisation properties of the gas diffusion layers and their effects on through-plane gas permeability of the porous gas diffusion media for PEFCs. The effects of the characteristic physical properties investigated include: (i) the thickness of the GDLs (before and after coating) and MPLs, (ii) the carbon loading and carbon types, (iii) sintering, (iv) MPL composition, and (v) MPL penetration.

However, the porous media consists of a two-layer structure (L_{tot}), namely the microporous layer (MPL, L_{mpl}) and the gas diffusion layer (GDL, L_{sub}), as shown in Figure 3.2. Figure 3.2 depicts a schematic of the typical investigated porous gas diffusion media used in a PEFC. The MPL is a thin layer added to one side surface of the carbon substrate and the porous substrate layer is the visible part of the carbon substrate after coating with the thin layer (i.e. the MPL).

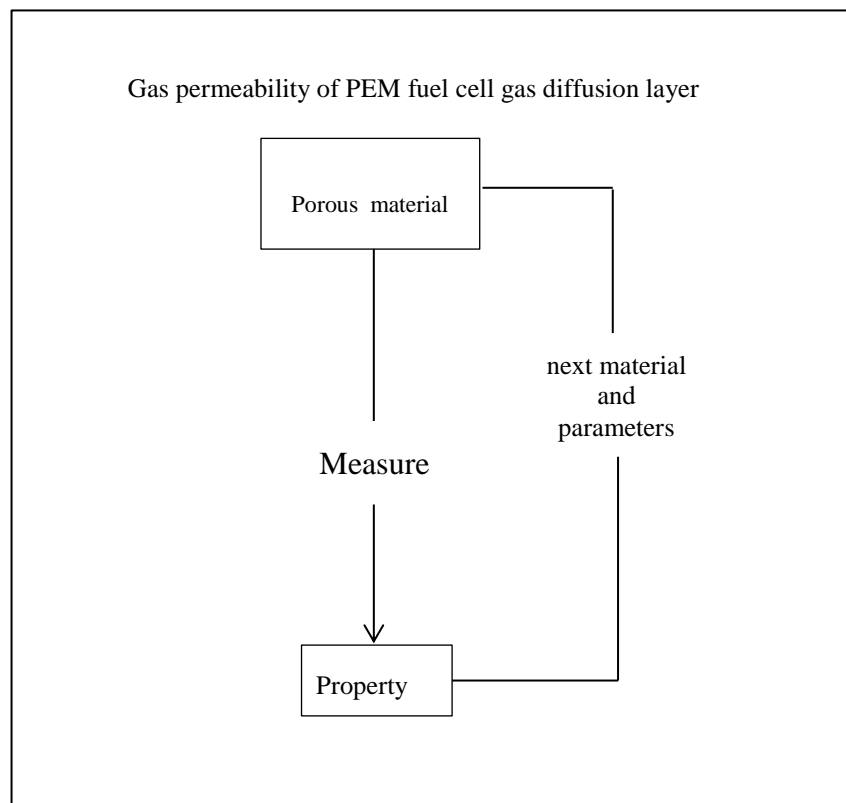


Figure 3.1. Schematic of the general technical experimental approach used in this thesis.

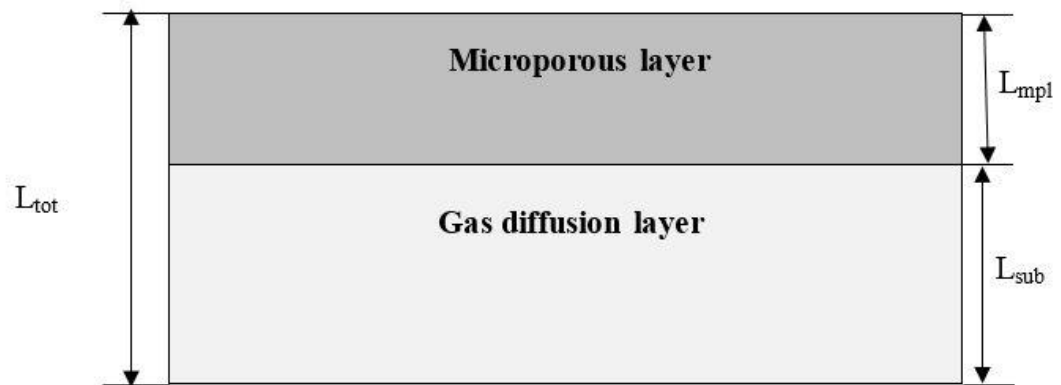


Figure 3.2. Schematic of a typical porous gas diffusion layers in a PEM fuel cell.

3.1 Materials

In this section, the main materials that have been used as the gas diffusion media materials are discussed in detail. The porous media with a two-layer structure was prepared. The SGL[®] 10BA carbon paper wet-proofed with 5wt% PTFE (polytetrafluoroethylene) content has been used as the porous substrate material for the gas diffusion layers (GDLs). All the samples were prepared from same batch of carbon paper sheets and the carbon sheets were provided by SGL Carbon GmbH, Meitingen, Germany. The carbon substrate is one of the most commonly used for gas diffusion layers (GDLs) in low temperature fuel cells. The substrate has about 88% porosity and 85 g/m² areal weight, as provided by the manufacturer in Table 3.1. However, Ismail et al. have calculated the porosity values of the GDLs using equation (18) in Ismail et al. (2011). Table 3.1 summarised the SGL[®] 10BA carbon substrate thickness, areal weight, porosity and PTFE content physical properties.

Further, to produce the porous media that allows negligible penetration of MPL material, a membrane filter, AAWP02500 (Merck Millipore, US), with a diameter of 25 mm, a thickness of 100 μm and pore size of 0.8 μm was selected as a candidate substrate.

Table 3.1. Manufacturer's physical properties of the SGL 10 BA carbon paper substrate.

Physical parameter	Reported value
Thickness	$380 \pm 60 \mu\text{m}$
Areal weight	$85 \pm 2 \text{ g m}^{-2}$
Porosity	0.88
PTFE loading	5 % by weight

However, one unique difference between the two substrates is that the carbon substrates were made of carbon fibre and the membrane filter is made of nitrocellulose membrane, Blanco and Wilkinson (2010).

Two different carbon black powders were used as materials to prepare the microporous layer, namely Ketjenblack EC-300J (AkzoNobel, the Netherlands) and Vulcan XC-72R (Cabot Corporation, USA). The carbon blacks have distinct characteristic physical properties as the materials used for the microporous layers applied to the surfaces of the porous carbon substrate. The physical properties, namely the pore volume, bulk density, surface area, particle diameter, pH and volatile content of these two carbon blacks are summarised in Table 3.2, as provided by the manufacturers. The differences in the MPLs prepared from the two different carbon powders are reported in the literature, in particular

the SEM (scanning electron microscope) of the surface of the MPLs, Yu et al. (2005), and gas permeability of the porous gas diffusion layers used in the PEFCs, respectively.

Table 3.2. The manufacturer's physical properties of carbon black materials (AkzoNoble, the Netherlands datasheets) and (Cabot Corporation, USA datasheets).

Properties	Ketjenblack EC-300J	Vulcan XC-72R
Pore volume (ml/100 g)	310-345	178
Apparent bulk density (kg/m ³)	125-145	20-380
Surface area (m ² /g)	950	254
Particle diameter (nm)	30	30
pH	9.0-10.5	2-11
Volatile (by weight % max.)	1.0	2-8

In addition, the preparation of the MPL also requires an hydrophobic agent as a bounding material for the carbon particles. The hydrophobic agent used was polytetrafluoroethylene (PTFE) with 60 wt.% aqueous dispersion emulsion, Sigma-Aldrich, UK. Also, isopropyl alcohol has been used as a dispersion agent, which is about 99.7 % concentration (Sigma-Aldrich, W292907-8KG-K, Germany). The following sections discuss in detail the methods employed in the preparation of the microporous layer ink, thus providing insight into the application of the MPL ink material on the surface of the samples (i.e. the GDLs).

3.2 Methods

In this thesis, a conventional method of wet-proof has been employed to a two-layer structure of the gas diffusion media. The method is a process of considering microporous layer ink on treated or untreated porous GDLs, and the mixture of the carbon particles and PTFE as materials for the MPL ink, see Yu et al. (2005) and Litster and McLean (2004).

3.2.1 Microporous layer preparation process

The process to prepare the microporous layer (MPL) ink prior to coating one-side of the porous carbon substrate sample surface is described as follows. The amounts of carbon black particles and the PTFE dispersion loadings in the MPLs were measured taking into account the calculations of the loading compositions, see Figure 3.3. The compositions of carbon black and the PTFE loadings in the MPLs (by weight) are of 50, 60, 70, 80 and 90 %, and 10, 20, 30, 40 and 50 wt. %, respectively. For simplicity, a composition of the MPL with 10 % of PTFE loading would require 90 % carbon black particles, and an MPL with 70 % carbon loading by weight requires 30 wt.% PTFE loading in the MPL ink.

For each set of preparations there were six carbon substrate samples which share the same compositions of the MPLs. The experimental calculations and analysis of the carbon black particles and the PTFE loadings that are required for preparing an MPL composition set are presented in more detail and discussed in Appendix A. All the calculated values of the compositions measurements (by weight) for the MPL preparation are summarised in Table 3.3.

Figure 3.3 shows photographs of the experimental procedures and the steps involved in measurement of the carbon loadings and the PTFE dispersion loadings prior to the

mechanical manual mixing of the mixture by using calibrated weight-Denver Instrument (Figure 3a-b). The calibration certificate for the scale is traceable to International prototype kilogram through NIST: National Institute of Standards and Technology (CE09-01-011, M, 24608827, Denver Instrument Germany). In Figure 3.3(a), the amount of the carbon black particles required in a composition of a MPL with 0.5 mg/cm^2 of 80 % (by weight) was measured, 46.20 mg. In Table 3.3, the actual estimated value for 0.5 mg/cm^2 of carbon black is 45.62 mg, and the slightly difference (± 0.58) has been taken into account in Section 3.4 and also for all other carbon loadings.

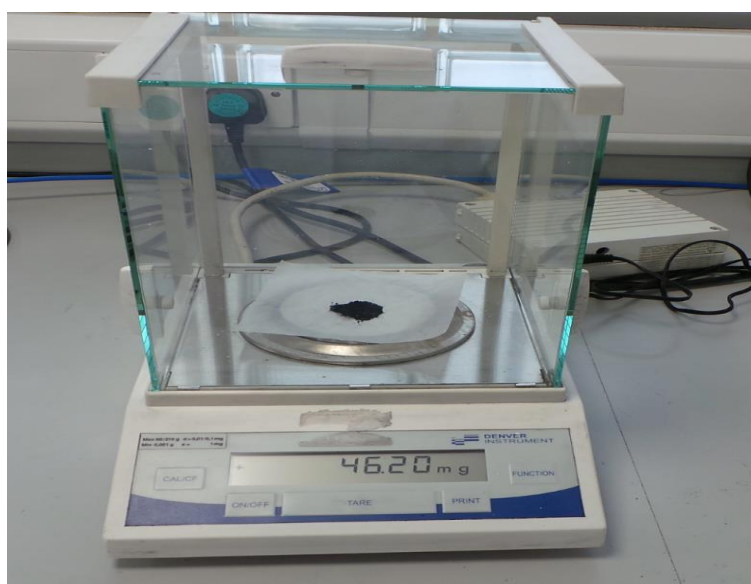
Similarly, the 20 wt.% PTFE loading was measured, 19.90 mg for 80 % carbon black particle loading in Figure 3.3(b). In Table 3.3, the estimated loading value for 20 wt.% PTFE of 0.5 mg/cm^2 is 18.22 mg, the difference in the experimental measurement value (± 1.68) has been taken into account in Section 3.4. In Figure 3.3(c), the paste-like material was formed by adding together the carbon particles and the PTFE solution in isopropyl alcohol solution (i.e. IPA) and were manually mixed. Figure 3.4 shows preparation of the MPL ink by adding more of IPA to the content of the mixture to form suspension homogenous MPL ink by using an Ultrasonic bath.

Generally, the preparation processes, procedures and steps of the MPL ink are summarised as follows: the carbon black loadings are considered in all the investigations to be 0.5, 1.0, 1.5, 2.0 and 2.5 mg/cm^2 , and these correspond to the compositions of the PTFE loadings range between 10, 20, 30, 40 and 50 wt.%, see Tables 3.3-3.5. The calculated and measured amounts of the carbon black particles and the PTFE dispersion were manually mixed in an alcohol solution (i.e. isopropyl alcohol, IPA) as a dispersion agent, until a paste-like material was formed. The paste-like material suspension was

homogenously mixed and stirred in an ultrasonic bath for a set period of 3 hour, see Figure 3.4.

The resulting formed homogenous suspension of the MPL slurry was applied to one of the surfaces of the carbon substrate samples and more detail is given in the next section.

In addition, the estimation of the analysis for the coating the actual amount of MPL to the carbon substrate is discussed in more detail in Section 3.2.3.



(a)



(b)



(c)

Figure 3.3. Photographs of the preparation of microporous layer ink procedures and steps for (a) carbon black powders loading by weight, (b) PTFE loading by weight, and (c) past-like material mixture of microporous layer slurry.



Figure 3.4. Photograph of the preparation of homogeneous suspension of MPL ink using an Ultrasonic bath.

Table 3.3. The carbon black and PTFE dispersion loadings measured by weight (mg) for the preparation of the MPL ink.

Carbon loading / mg cm⁻²	Carbon loading required / mg by weight	Carbon loading required per sample / mg cm⁻²	10 % PTFE loading required / mg by weight	20 % PTFE loading required / mg by weight	30 % PTFE loading required / mg by weight	40 % PTFE loading required / mg by weight	50 % PTFE loading required / mg by weight
0.5	45.62±0.31	2.54±0.16	8.10±0.07	18.22±0.15	31.23±0.07	48.59±0.06	72.88±0.06
1.0	91.24±0.5	5.08±0.92	16.20±0.93	36.44±0.09	62.46±0.06	97.18±0.08	145.76±0.99
1.5	136.86±0.52	7.62±0.13	24.30±0.13	54.66±0.25	93.69±1.23	145.77±0.24	218.64±0.18
2.0	182.48±0.36	10.16±0.14	32.40±1.37	72.88±0.29	124.92±0.12	194.36±0.54	291.52±0.42
2.5	228.10±0.81	12.70±0.26	40.50±0.24	91.10±0.6	156.15±0.50	242.95±0.99	364.40±0.61

Table 3.4. The carbon black and PTFE mixture required per sample by weight (mg).

Carbon loading / mg cm⁻²	10 wt.% PTFE mixture		20 wt.% PTFE mixture		30 wt.% PTFE mixture		40 wt.% PTFE mixture		50 wt.% PTFE mixture	
	PTFE loading required / mg	C + PTFE loading required / mg	PTFE loading required / mg	C + PTFE loading required / mg	PTFE loading required / mg	C + PTFE loading required / mg	PTFE loading required / mg	C + PTFE loading required / mg	PTFE loading required / mg	C + PTFE loading required / mg
0.5	0.28±0.05	2.82±0.38	0.64±0.17	3.18±0.73	1.09±0.11	3.63±0.31	1.69±0.78	4.23±0.32	2.54±0.18	5.08±0.30
1.0	0.56±0.04	5.64±0.30	1.28±0.12	6.36±0.49	2.18±0.23	7.26±0.65	3.38±0.30	8.46±0.62	5.08±0.52	10.16±0.87
1.5	0.84±0.08	8.46±0.67	1.92±0.63	9.54±2.66	3.27±0.49	10.89±1.39	5.07±0.57	12.69±1.20	7.62±0.32	15.24±0.53
2.0	1.12±0.13	11.28±1.13	2.56±0.55	12.72±2.31	4.36±0.55	14.52±1.54	6.76±0.26	16.92±0.54	10.16±0.85	20.32±1.43
2.5	1.40±0.15	14.10±1.30	3.20±0.60	15.90±2.54	5.45±0.91	18.15±2.56	8.45±2.61	21.15±5.52	12.70±2.04	25.40±3.45

Table 3.5. Amount of MPL slurry coating on the top of one-side of the carbon substrate sample surfaces.

Carbon loading / mg/cm²	Amount of MPL slurry coating per sample, $\frac{C + \text{PTFE}}{5.069}$ mg/cm²				
	10 wt.% PTFE	20 wt.% PTFE	30 wt.% PTFE	40 wt.% PTFE	50 wt.% PTFE
0.5	0.56±0.07	0.63±0.12	0.72±0.05	0.83±0.07	1.00±0.06
1.0	1.11±0.07	1.25±0.10	1.43±0.13	1.67±0.12	2.00±0.17
1.5	1.67±0.11	1.88±0.52	2.15±0.28	2.50±0.23	3.01±0.20
2.0	2.23±0.22	2.51±0.46	2.86±0.30	3.34±0.11	4.01±0.28
2.5	2.78±0.26	3.14±0.25	3.58±0.51	4.17±1.09	5.01±0.68

3.2.2 Gas diffusion layer preparation process

Prior to applying the MPL ink on one surface of the carbon substrate sample, the substrate sample was made circular with a 2.50 cm diameter, as shown in Figure 3.5. The thickness of the GDL sample was measured using a micrometre before and after coating the MPL ink using a micrometre, see Figure 3.6. The measurement technique employed, each sample was measured at 4 equal-spaced positions within it to provide a representative averaged valued of the thickness, see Appendix B. Also, the SEM (scanning electron microscope) technique was employed to confirm the thickness of the coated GDL samples by viewing the cross-sectional image of the coated sample. The micrograph of the cross-sectional images were used in estimating the thickness of the coated MPL which was required in calculating its gas permeability, as shown in Chapters 4, 5 and 6. The SEMs images were produced using MA15SEM (EVOZEISS, 80 mm²) and JEOL (JBM-BO10LA), see Figure 3.7.

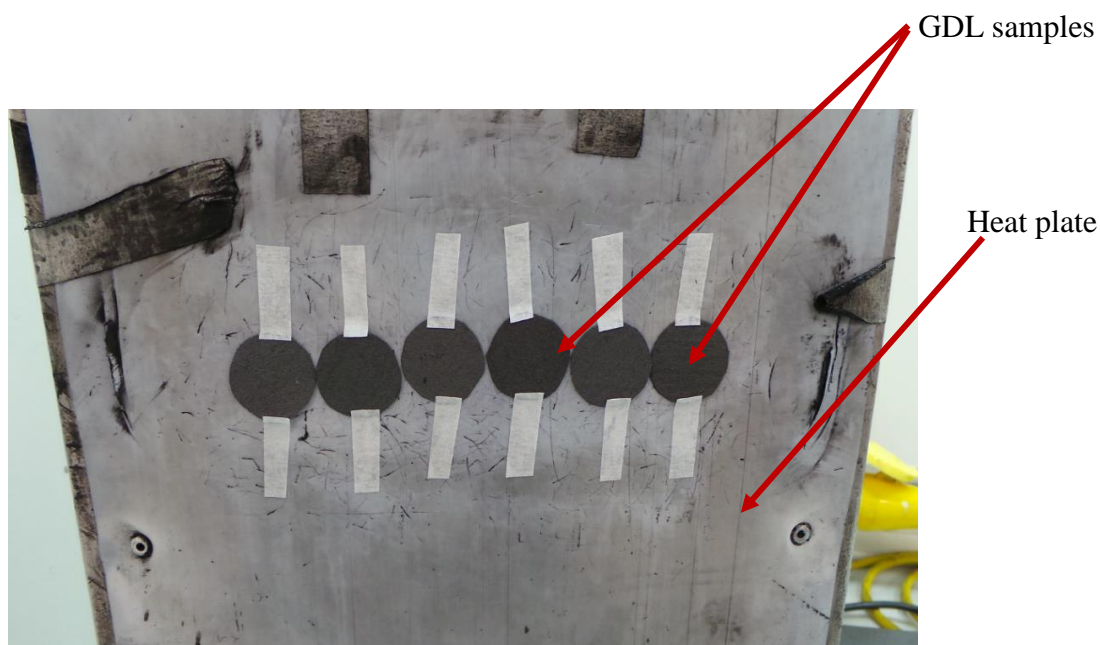


Figure 3.5. Photograph of set of carbon substrates made circular with a 2.50 cm diameter before coating.

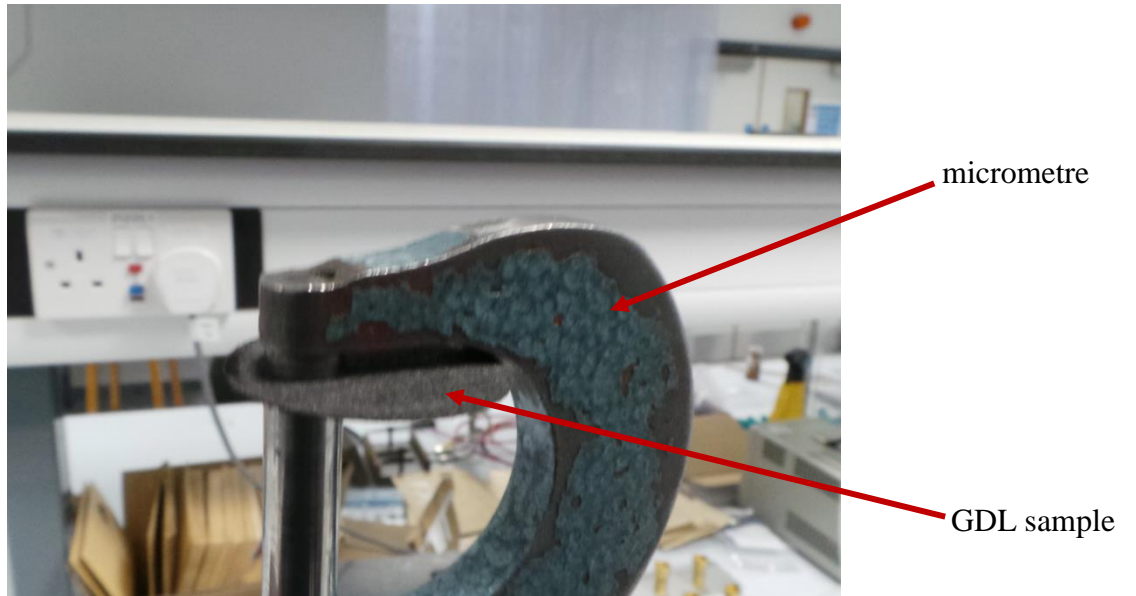
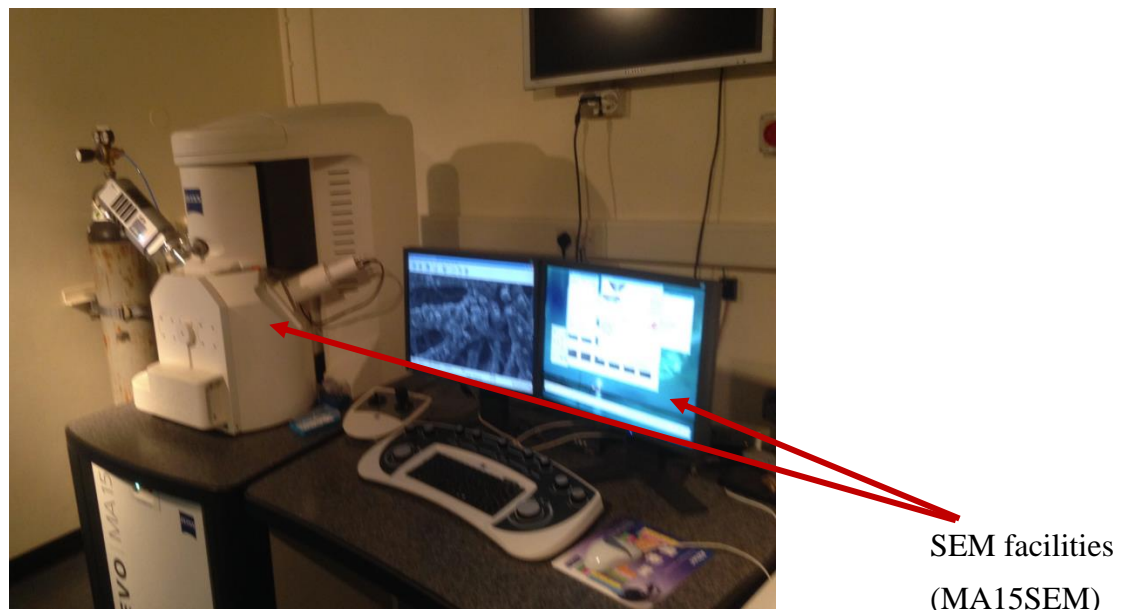
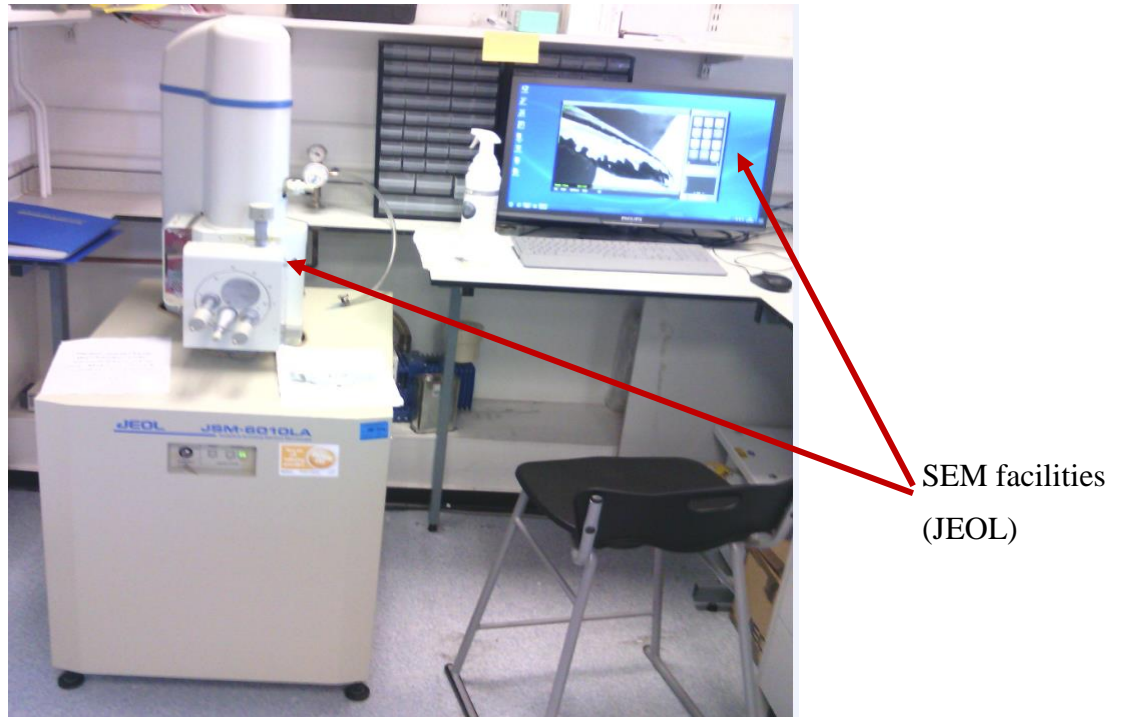


Figure 3.6. Photograph of the measured thickness technique for the carbon substrate sample before and after the coating MPL ink on the GDL on one side surface.



(a)



(b)

Figure 3.7. Photographs of the SEMs facilities used to measure the thickness, surfaces and cross-sectional micrographs of the carbon substrate samples before and after coating with MPL, of (a) MA15SEM (EVOZEISS, 80 mm²) at University of Leeds, and (b) JEOL JSM-6010LA at University of Sheffield.

The topography of tested samples' surfaces has been scanned through the SEs (Secondary electrons) of SEM type with distinct energy ranges used to detect the various signals, which depends on the information desired to obtain on morphology of the MPLs structures made of various carbon and PTFE loadings after coating on substrate, Robert and Dietmar (2012). The SEs is a process of In the next chapters, the signals of the SEs detectors are shown for both the cross-sectional and surfaces images of the GDLs before and after coating and sintering.

3.2.3 Microporous layer ink application process

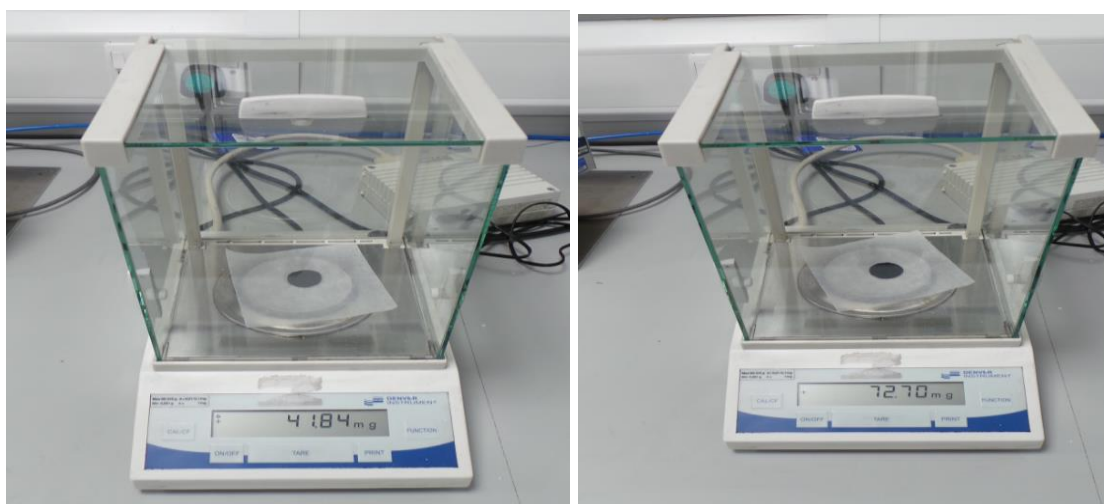
In this section, the amount of the MPL applied to the surfaces of the carbon substrate, and the coating application technique employed are discussed. For the purpose of

experimental reproducibility, in each set, there were 6 carbon substrates from the same batch of carbon paper (i.e. SGL 10BA).

The following procedures were employed to determine the amount of the MPL coated on the surface of the carbon substrate. The GDL samples were weighed before and after coating, see Figure 3.8. In Figure 3.8(a), the initial weight of the carbon substrate sample was measured (41.84 mg). The expected loading by weight for the GDL sample was determined by adding the estimated value of carbon-PTFE loadings per sample as shown in Table 3.4, to the initial weighed value of the carbon substrate, and obtaining the expected weight value for the amount of carbon-PTFE loading on the surface of the GDL sample. The actual weighed value of the GDL sample after coating was measured, as shown in Figure 3.8(b). Further, the initial weighed value of the GDL sample before coating was subtracted from the actual weighed value of GDL sample after coating and the difference in the weighed value was obtained. The difference in the weighed value for the amount of carbon-PTFE loading was divided by the surface area of the sample (5.069 cm^2) and the actual amount of carbon-PTFE loading on the sample surface was obtained, see Table 3.6. This mainly determines the amounts of the MPL ink that have been coated on the surface of the tested GDL sample. Table 3.6 summarises a list of the procedural steps for the estimation of the amount of Carbon-PTFE coated on one-side of the GDL sample surface by weight. However, these estimation methods and procedures have been used to determine (i) the actual amount of carbon-PTFE loading, (ii) the amounts of the MPL composition required, (iii) the thickness of the GDL after coating, and (iv) the MPL thickness. Table 3.6 lists the estimated values for 2.5 mg/cm^2 of 40 wt.% PTFE loadings, for a set of prepared samples. Clearly, the estimated values are relatively close to the magnitude value (4.17 mg/cm^2) presented in Table 3.5. It should be noted that the variations in the values compared with the pre-estimated value (i.e. 4.17 mg/cm^2) are due

to the slight variation in the coating. However, this has been taken into account in Section 3.4. Also, all the other estimated values for the prepared samples are summarised in Appendix C.

For coating the GDL samples, the samples were stuck to a heated plate, as shown in Figure 3.9, and the formed slurry was manually sprayed onto them using a gun (Badger 100™ LG, USA). Nitrogen gas was used for applying the slurry on the surfaces of the GDL samples. The temperature of the plate was set to about 80 °C in order to evaporate the volatile components as the slurry was applied to the substrate. The MPL-coated GDL samples were heat-treated and the processing is discussed in the next section.



(a)

(b)

Figure 3.8. Photographs of the measured GDL sample by mass weight (a) before coating, and (b) after coating.

Table 3.6. The estimation of the amount of Carbon-PTFE coated on one-side of the GDL sample surface by weight.

Sample	Initial weight, wt1(mg)	Expected weight, wt2(mg) + 21.15	Actual weight, wt*(mg)	Difference, Δwt^* [wt*-wt(1)]	$\frac{\Delta wt}{5.069}$ (mg/cm²)
1	49.01	70.16	71.16	22.15	4.37
2	43.95	65.10	66.57	22.62	4.46
3	48.13	69.28	72.40	24.27	4.79
4	46.75	67.90	69.97	23.22	4.58
5	41.10	62.25	62.51	21.41	4.22
6	42.97	64.12	67.76	24.79	4.89

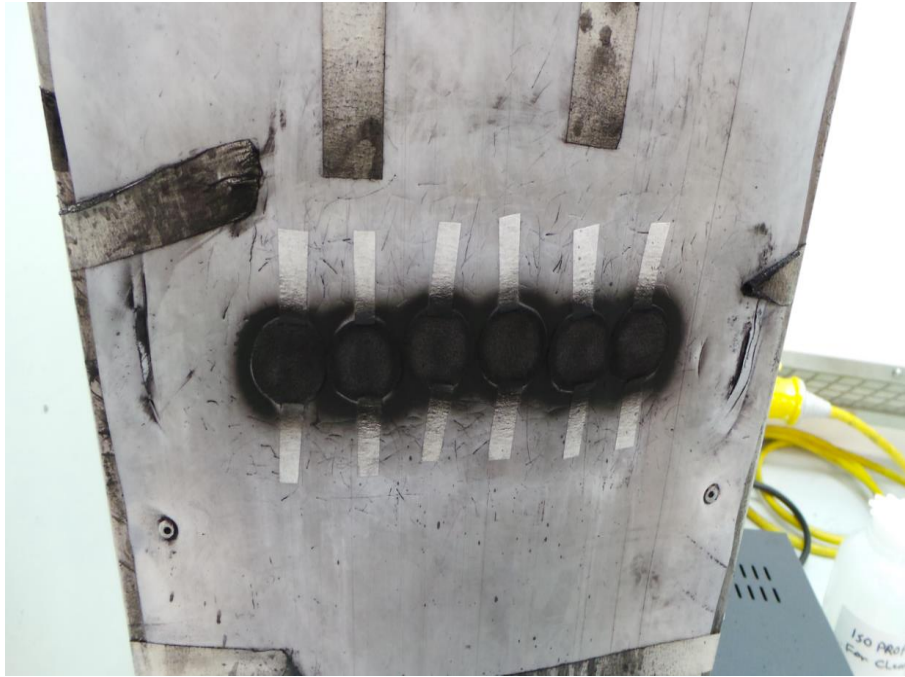


Figure 3.0.9. Photograph of a set of samples after coating and heat treated at temperature 80 °C of the heated plate.

3.2.4 Sintering setup

Figure 3.10 shows the sintering setup furnace for the heat-treatment. The furnace was set for three stages of the temperature, namely 120, 280 and 350 °C for 1 hour, 30 minutes and 30 minutes, respectively. For, each set of 6 samples prepared, 3 samples were used for sintering and other 3 samples were non-sintered. Nitrogen gas was flowing into the furnace for about 20 minutes to heat treated the tested samples.

Further, the gas permeability of the coated samples were experimentally measured before and after heat-treatment and sintering in order to evaluate the effects of the latter process.

The morphology of the MPLs before and after heat-treatment was examined through the SEM images of the surfaces of the coated samples. In addition, the gas permeability of the MPL-coated GDL samples were measured before and after sintering.



Figure 3.0.10. Photograph of the furnace used for the heat-treatment of the GDL samples.

3.2.5 Calibration of the flow meter

The flow controller was calibrated by setting a given flow on the controller, and measuring the time taken for a soap film in a small glass tube connected to the flow controller outlet to move a given distance corresponding to a known volume. Thus the volumetric flow rate is determined for the given flow controller setting, and this is repeated for a number of flow controller settings in the working range of the flow controller. The experimental setup includes: a mass flow meter EK model 202 blue Hasting with its associated controller, ranging from 0 to 10 litre per minute, a small marked glass tube, and a squeeze bulb to create the bubbles, see Figure 3.11, which depicts the calibration setup.

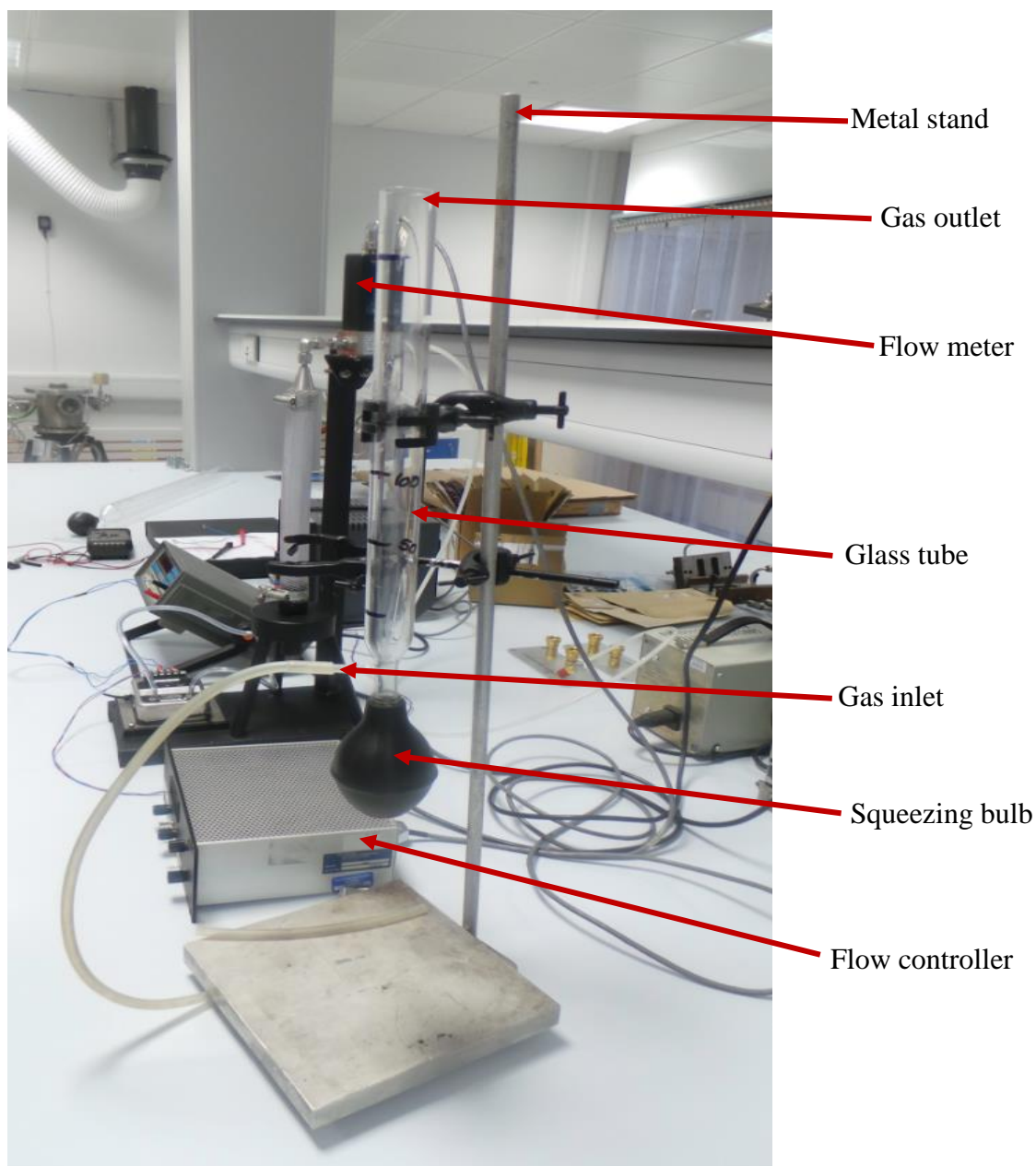


Figure 3.11. Photograph of the calibration setup for the flow meter.

The gas flow was compressed air. The rubber bulb on the glass tube was squeezed and bubbles were formed. A stopwatch was used to measure the time taken for a bubble to move between two fixed points on the tube. For the best results to be obtained, several bubbles were formed, five to six seconds apart, and a well-formed bubble was considered time (t) in second (s). However, caution must be taken not to continuously squeeze the

bulb because this causes a froth to form on the walls and of this makes the timing difficult. Further, the measurement values were recorded, then the volumetric flow rate was calculated by employing the following equation:

$$Q = \frac{\text{Volume of cylinder}}{\text{Time in second (s)}} \quad (3.1)$$

$$Q = \frac{\pi r^2 h (m^3)}{t(s)} \quad (3.2)$$

where Q is the volumetric flow rate of air, r is the radius of the tube, h is the height of the tube which is the distance between the two marked points on the cylinder and t is time, s. The flow rate of the calibrated flow meter was corrected for variation of temperature and pressure as follows, Nield and Bejan (2013):

$$\text{Flow rate} = Q (m^3s^{-1}) \times \frac{T(K)}{T_{rm}(K)} \times \frac{P_r(m)}{P(m)} \quad (3.3)$$

where T is the standard temperature of 273.15 K, P is the standard pressure of 1013.25 mb, T_{rm} and P_r are the room temperature of 295.65 K measured using a thermometer and the pressure of 1015 mb was taken from the BBC (British Broadcasting Corporation) weather. However, the variations in the measured temperature and recorded pressure was found to be negligible. Finally, the flow rate in cubic metre per second is multiplied by 6×10^4 to be converted to litres per minute.

Tables 3.8, shows the calibration experimental data for the calibration. The calibration curve is constructed based on the measurement data summarised in Table 3.7. The values obtained for the volumetric average flow rate was plotted against the setting points of the mass flow meter EK2. Figure 3.12 shows the calibration of the flow meter for flow rate as a function of voltage signal (i.e. X = set point from EK2).

Table 3.7. The experimental data for voltage signal used for the calibration curve flow rate.

X = Set Point From EK2	Y = Average Flow Rate (l /min)
1.5	1.703
2.5	2.724
3.5	3.766
4.5	4.827
5.5	5.837
6.5	6.887
7.5	7.971
8.5	9.220

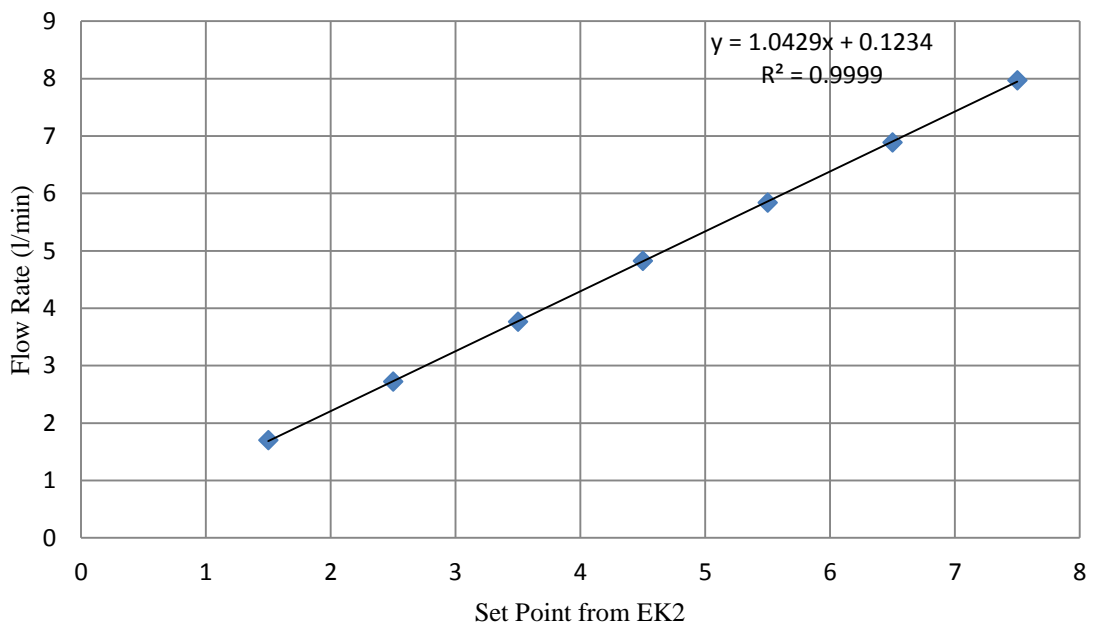


Figure 3.12. The calibration curve for a 10 litre per minute mass flow meter for the calculation of pressure drop for the flow across the samples.

Table 3.8. Experimental data for the flow meter calibration of a litre/minute flow meter.

Set point from flow controller	Time (s)	Average time (s)	Volume of Cylinder = $\pi r^3 h$ (m ³)	Volumetric flow rate: Q (m ³ /s)	Flow rate (m ³ /s)	Flow rate (lit/min)
1.5	39.73	39.42	1.21x10 ⁻⁰³	3.07 x 10 ⁻⁰⁵	2.84x10 ⁻⁰⁵	1.70
	39.57					
	39.40					
	39.06					
	39.36					
2.5	24.19	24.64		4.91x10 ⁻⁰⁵	4.54x10 ⁻⁰⁵	2.72
	24.63					
	24.87					
	24.81					
	24.71					
3.5	17.81	17.83		6.78x10 ⁻⁰⁵	6.28x10 ⁻⁰⁵	3.766
	17.79					
	17.86					
	17.83					
	17.84					
4.5	13.94	13.91		8.69x10 ⁻⁰⁵	8.05x10 ⁻⁰⁵	4.83
	13.73					
	13.90					
	13.99					
	13.98					
5.5	11.43	11.50		1.05x10 ⁻⁰⁴	9.73x10 ⁻⁰⁵	5.84
	11.52					
	11.43					
	11.52					
	11.61					
6.5	9.59	9.75		1.24x10 ⁻⁰⁴	1.15x10 ⁻⁰⁴	6.89
	9.70					
	9.88					

	9.65					
	9.92					
7.5	8.46	8.422		1.44×10^{-04}	1.33×10^{-04}	7.97
	8.50					
	8.32					
	8.48					
	8.35					
8.5	7.41	7.28		1.66×10^{-04}	1.54×10^{-04}	9.22
	7.43					
	7.45					
	7.59					
	7.59					

3.2.6 Gas permeability setup

The measurement and estimation of the gas permeability of the porous media are primary factors which could influence characterisation of porous gas diffusion media. Gurau et al. (2006) described an estimation method, applied to GDM with different components of the carbon substrates (GDLs) and MPLs. Also, Ismail et al. (2011) estimated the gas permeability of the microporous layers by employing similar estimation method in Gurau et al. (2006). Clearly, the basic approach that is require to determine the influencing parameters is discussed by Blanco and Wilkinson (2010).

The experimental setup and procedures for the measurements of the through-plane gas permeability is described in this section. Figure 3.13 shows the in-house experimental setup for the measurement of the through-plane gas permeability of the tested GDL samples. This typical setup has been previously employed in Ismail et al. (2011) and this setup and procedures have been adopted to measure the through-plane gas permeability of the GDL.

The setup consists of upstream and downstream fixtures and the GDL sample is positioned between the upper and lower fixtures (Figure 3.14). It should be noted that the diameter of the GDL sample is 2.5×10^{-2} m, and after the fixing of the sample between the two fixtures of the setup, the diameter reduces to 2.0×10^{-2} m. The gas flows across the sample at a fixed rate (set from flow control) and the resulting pressure drop was measured by pressure sensors and taking the voltage signal readings through the Multimeter.

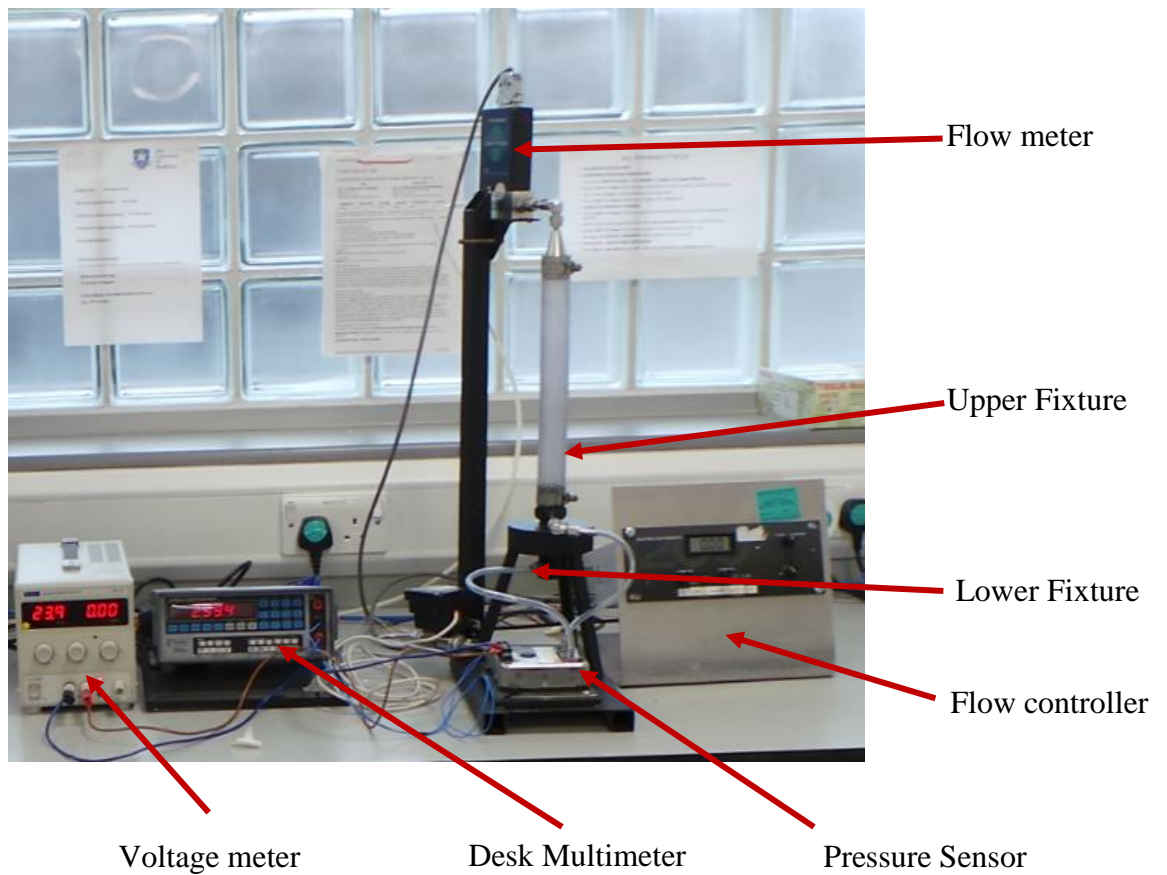


Figure 3.13. The experimental setup of the through-plane gas permeability of the tested GDL samples.

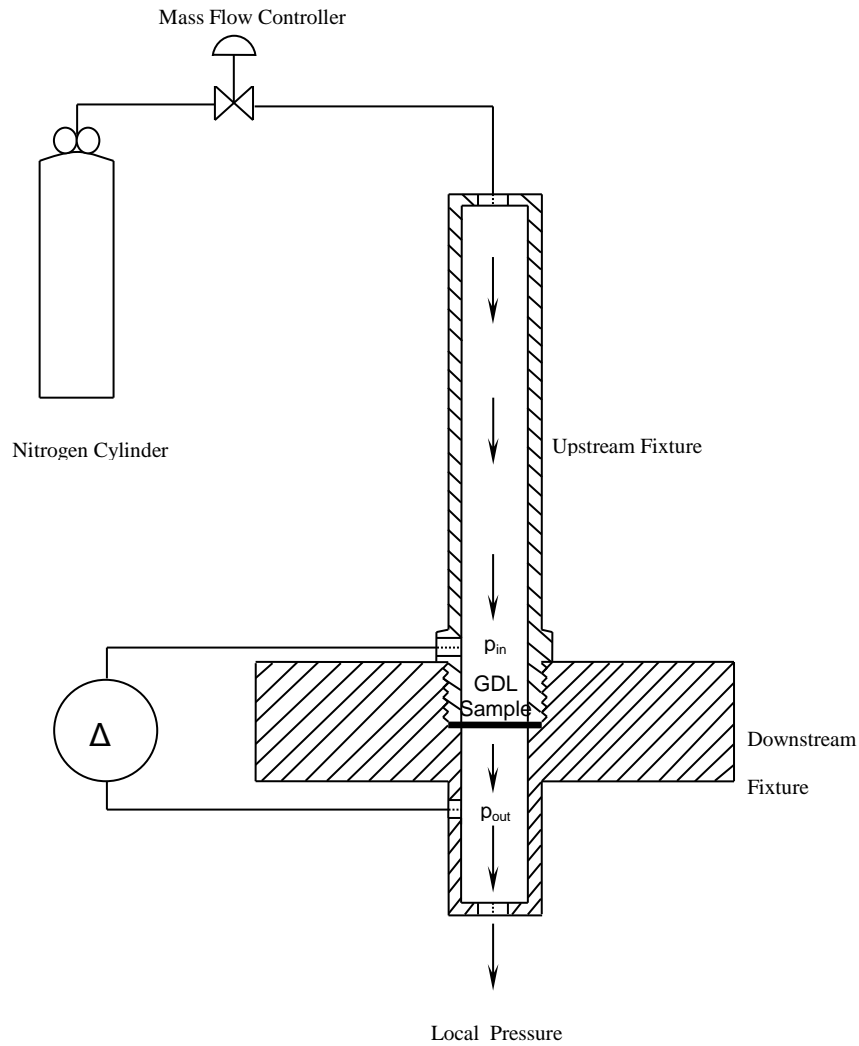


Figure 3.14. Schematic diagram of the experimental setup.

The pressure drop across the sample was measured at 8 equal-interval values of the flow rate, namely 0.00, 0.48, 0.97, 1.47, 1.96, 2.46, 2.95 and 3.45 Pa. The flow controller used was an HFC-202 (Teledyne Hastings, UK) with a range of 0.0-0.5 SLPM and the differential pressure sensor used was a PX653 (Omega, UK) with a range of ± 12.5 Pa.

The experimental methods employed have been focused on the measurement, characterisation and determination of the through-plane gas permeability of the GDL

samples before and after coating, particularly the effects of microporous layers (MPLs) when it is adding to the porous carbon substrates (GDLs).

The pressure drop for the six samples prepared from a SGL 10BA sheet was measured before and after coating. The experimental data obtained from the voltage signals values at different flow rates were used to calculate the pressure drops for each GDL sample. The data analysis of the calculations process is discussed in more detail in the next section.

3.3. Data analysis

Darcy's law is a generalised relationship on the state for the flow in porous media which is shown to be a proportionality constant between the flow rate and the applied pressure difference (Nield and Bejan, 2013; Wang, 2004). Darcy's law includes the volumetric flow rate which is a function of the flow area, thickness of the porous layer, fluid pressure and a proportionality constant of the porous media (Shou et al., 2013). In addition, the pressure drop across the porous diffusion layer is as a function of the friction between the reactant gas and the flow field across the porous media, namely the gas diffusion layers (GDLs), microporous layers (MPLs) and catalyst layers (CLs), Barbir (2013).

Darcy's law is employed in this thesis since (i) the viscous resistance is one of the major causes for the pressure drop across the porous media, especially if the gas velocity is sufficiently small, Ismail et al. (2011), (ii) sufficiently low flow rates, the maximum Reynolds number was 3, and then the inertial losses are negligible, and (iii) used to characterised the laminar flow across porous layers, and linearly relates the volume-average velocity with the pressure gradient, particularly through-plane gas permeability, Shou et al. (2013).

However, the gas flow rate used was sufficiently small for Darcy's law to be used to calculate the through-plane gas permeability of the porous layers with the following associated parameters before and after MPL coating, after MPL sintering and the MPL penetration into the substrate.

3.3.1 Darcy's law

Consequently Darcy's law is employed, which is given as follows:

$$\frac{\Delta P}{L} = \frac{\mu}{k} v \quad (3.4)$$

$$v = \frac{Q}{\pi \frac{D^2}{4}} \quad (3.5)$$

where ΔP is the pressure drop across the sample, L is the thickness of the sample, μ is the dynamic fluid viscosity of the nitrogen gas at the test temperature (20 °C), k is the gas permeability of the porous GDL sample, and v is the velocity of the flowing gas, Q is the volumetric flow rate and D is the diameter of the sample exposed to the flow. However, the inertial resistance is important to be considered if relatively high flow rates are used, a modified version of Darcy's law, namely the Forchheimer equation, is normally used to account for the inertial pressure losses.

3.3.2 MPL thickness and gas permeability

The carbon substrate and MPL are typically layered in the coated GDL, the pressure drop across the coated sample is expressed as follows, Wang et al. (2006):

$$\Delta P_{\text{GDL}} = \Delta P_{\text{MPL}} + \Delta P_{\text{sub}} \quad (3.6)$$

where ΔP_{GDL} , ΔP_{MPL} , and ΔP_{sub} are the pressure drops through the coated GDL, MPL and the carbon substrate, respectively. From Equation (3.4), Equation (3.6) can be written as follows:

$$\frac{\mu L_{GDL} v}{k_{GDL}} = \frac{\mu L_{MPL} v}{k_{MPL}} + \frac{\mu L_{sub} v}{k_{sub}} \quad (3.7)$$

where L_{GDL} , L_{MPL} , and L_{sub} are the thicknesses of the coated GDL, the MPL and carbon substrate respectively, and the k_{GDL} , k_{MPL} , and k_{sub} are gas permeability values for the coated GDL, the MPL and the carbon substrate, respectively. Clearly, equation (3.7) was used to solve for the gas permeability of the MPL:

$$k_{MPL} = \frac{L_{MPL}}{\frac{L_{GDL}}{k_{GDL}} - \frac{L_{sub}}{k_{sub}}} \quad (3.8)$$

As mentioned in Section 3.2.2, the thickness of the MPL was estimated locally using cross-sectional SEM images at as many points as possible in order to have a well-representative value of the thickness of the MPL in Section 4.4. However, the gas permeability of the carbon substrate used was estimated by fitting the experimental data of the pressure gradients as a function of the velocity to equation (3.4).

3.3.3 MPL penetration and gas permeability

In this section, a method to estimate the penetration of the MPL into the carbon substrate on the GDL gas permeability is analysed.

Figure 3.14 shows schematic representation of a method for estimating the MPL penetration into a porous carbon substrate. The resistance of a porous material that is permeable with very small pores, but does not permit penetration of the MPL into it, and the permeability of material after coating can be ascribed to the resistance of the gas flow distance through its flow pathways, Blanco and Wilkinson (2010).

The MPL thickness penetration was calculated by employing the total resistance expression as follows:

$$R_{\text{tot}} = R_{\text{mpl}} + R_{\text{sub}} \quad (3.9)$$

where, R_{mpl} and R_{sub} are the resistance values for the MPL and the material sample, respectively, and R_{tot} is the total resistance of the material. Equation (3.9) can also be expressed as follows:

$$\frac{L_{\text{tot}}}{k_{\text{tot}}} = \frac{L_{\text{mpl}}}{k_{\text{mpl}}} + \frac{L_{\text{sub}}}{k_{\text{sub}}} \quad (3.10)$$

where L_{tot} is the total thicknesses of the material, L_{mpl} is the thickness of the MPL coated on the material and L_{sub} is the thickness of the material before coating, k_{tot} is the gas permeability of the coated material, k_{mpl} is the gas permeability of the MPL and k_{sub} is the gas permeability of the material before coating. In this case, a material, namely the membrane filter was used, as described in Section 3.1. The gas permeability of the MPL with no penetration was calculated using Equation (3.8) in Section 3.3.2. Further, the gas permeability of the MPL with penetration was determined. From Equation (3.10), the total thickness of the MPL is estimated as follows:

$$L_{\text{mpl}} = L_{\text{vis-mpl}} + L_{\text{pen}} \quad (3.11)$$

where $L_{\text{vis-mpl}}$ is the visible MPL thickness and L_{pen} is the MPL penetration into porous carbon substrate, see Figure 6.2. If Equation (3.11) is substituted into Equation (3.10), then the following expression provides a relationship between the visible MPL thickness and the penetration:

$$\frac{L_{\text{tot}}}{k_{\text{tot}}} = \frac{L_{\text{vis}} + L_{\text{ptn}}}{k_{\text{mpl}}} + \frac{L_{\text{sub}}}{k_{\text{sub}}} \quad (3.12)$$

$$L_{\text{pen}} = k_{\text{mpl}} \left[\frac{L_{\text{tot}}}{k_{\text{tot}}} - \frac{L_{\text{sub}}}{k_{\text{sub}}} \right] - L_{\text{vis}} \quad (3.13)$$

As the gas permeability value of the MPL with no penetration has been estimated, and the other parameters are known, namely the gas permeability of the coated GDL (k_{tot}), the total thickness of the coated GDL (L_{tot}), gas permeability and thickness of the carbon substrate. Then, the amount of MPL penetration material into the porous carbon substrate can be calculated by using Equation (3.13), which presents the method employed to determine the penetration of the MPL into porous carbon substrate using a permeable and non-penetrable material as described in Section 3.1.

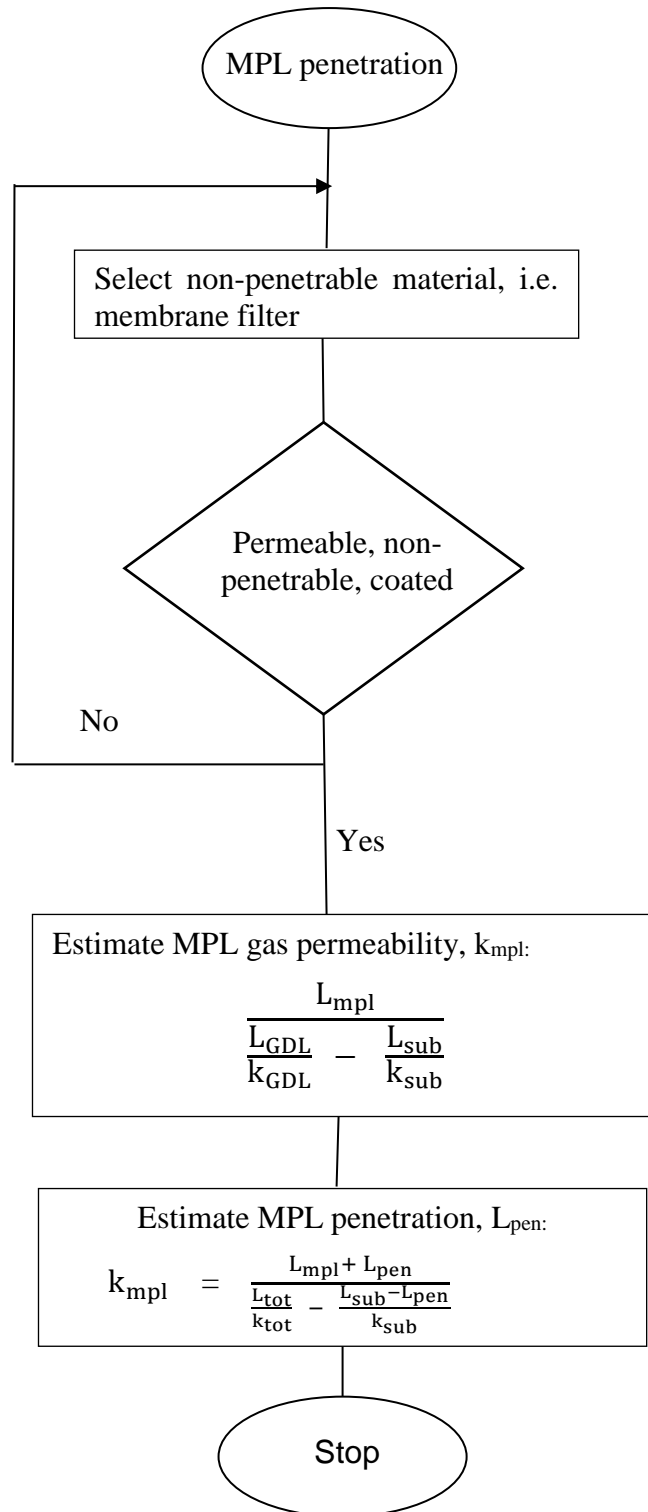


Figure 3.15. Schematic representation of a method for estimating the MPL penetration into a porous carbon substrate.

3.4. Uncertainty and error analysis

In this thesis, the experimental measurements were performed on the following equipment, materials and parameters: calibration of the flow meter, thickness of the carbon substrate before and after coating, carbon black particles loading, PTFE loading, carbon-PTFE loading by weight. In order to reduce measurement errors, the measurements are repeated several times and the mean and standard deviation methods were utilised for estimating the measurement errors within the 95 % confidence interval (Figures 3.15 – 3.19). Figure 3.15 shows the experimental data for amount of carbon-PTFE loading in the MPL as a function of PTFE loading in the MPL. The carbon black loading in the MPL is kept constant at 0.5, 1.0, 1.5, 2.0 and 2.5 mg/cm² while, the PTFE loading varies over the range 0, 10, 20, 30, 40 and 50 wt.%, respectively. For deducing the measurement error of uncertainty for the carbon-PTFE loading in the MPL, the error bars estimate the 95 % confidence interval calculated for the MPL slurry coated on the surfaces of the six samples as mentioned in Section 3.2.3 (see Figure 3.16). Figure 3.16 presents the amount of the MPL ink coated on a set of six GDLs samples taken from the same sheet, the carbon-PTFE loading in the MPL increases as the PTFE loading for the two carbon blacks used as a material for the MPL, namely Ketjenblack and Vulcan carbon black. However, the measurement error bar has been estimated for coating one-side of the surface of the tested samples, see Figure 3.16.

Experimental measurements

The following steps have been taken to calculate the measurement errors of the investigation:

1. Estimated gas permeability of each 6 samples for a set of group.
2. Calculate the mean of the samples, that is, average the 6 samples permeability.

- Calculate the standard deviation for the 95 % confidence interval by employing, Moffat (1988);

$$\frac{(n - 1) * \text{STDV}(x)}{\text{SQRT}(n)}$$

where n-1 is the degrees of freedom (df) for the number of tested samples, n, x is the standard deviation of tested samples. Additionally,

$$\text{Mean}(x) = \frac{\sum(x_i)}{n}$$

where n is the total number of tested samples.

- Calculate the maximum and minimum values as follows:

$$\text{Mean}(x) \pm \text{Standard Deviation}$$

- Finally, the degrees of freedom is simply the number of measurements (n) – the number of calculated quantities (1), hence $df = n-1$.

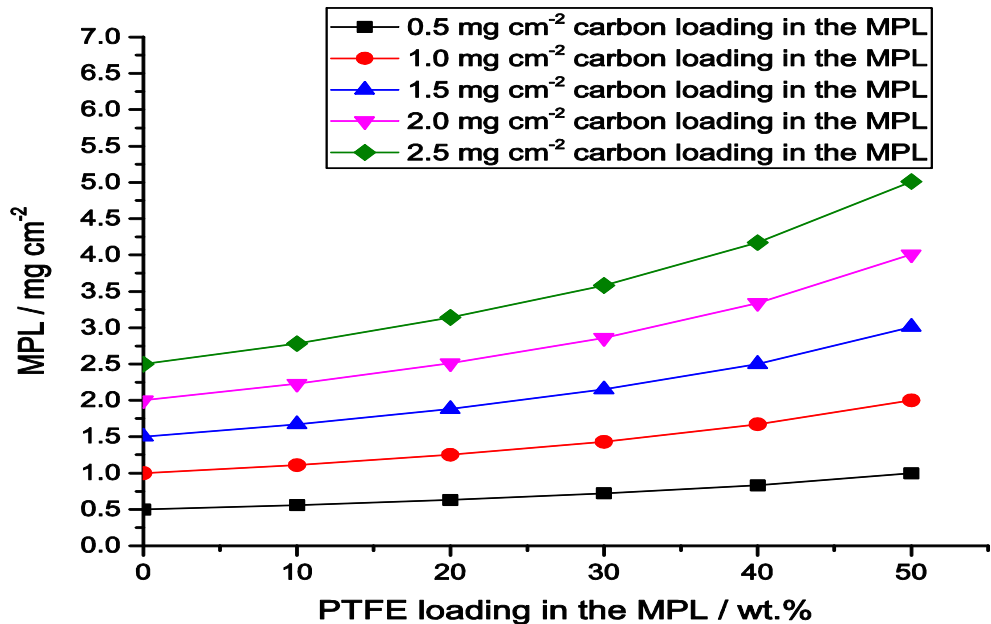
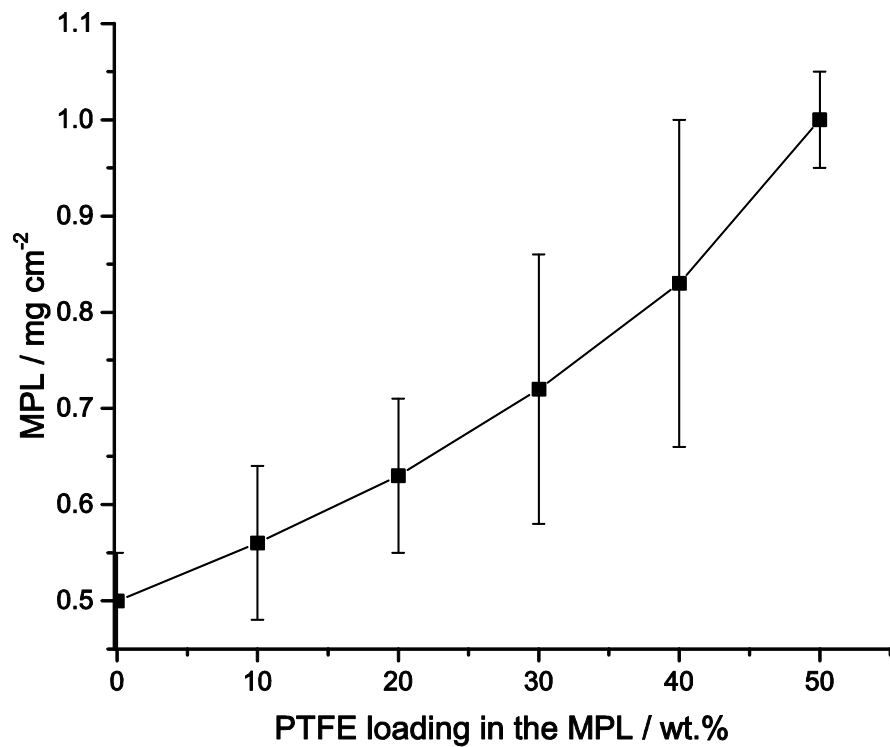
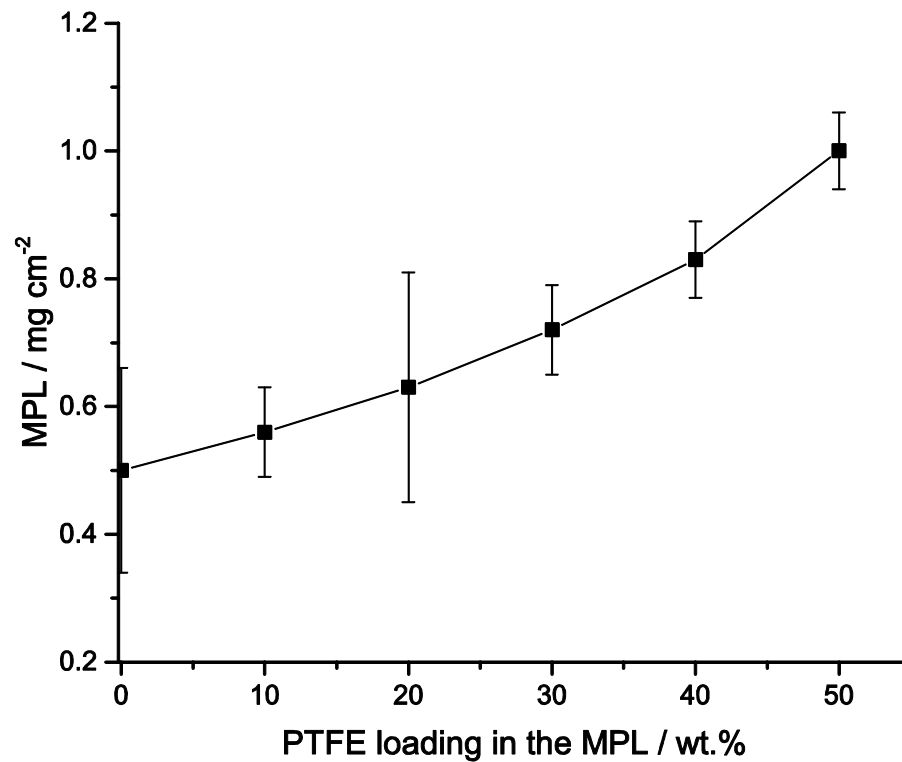


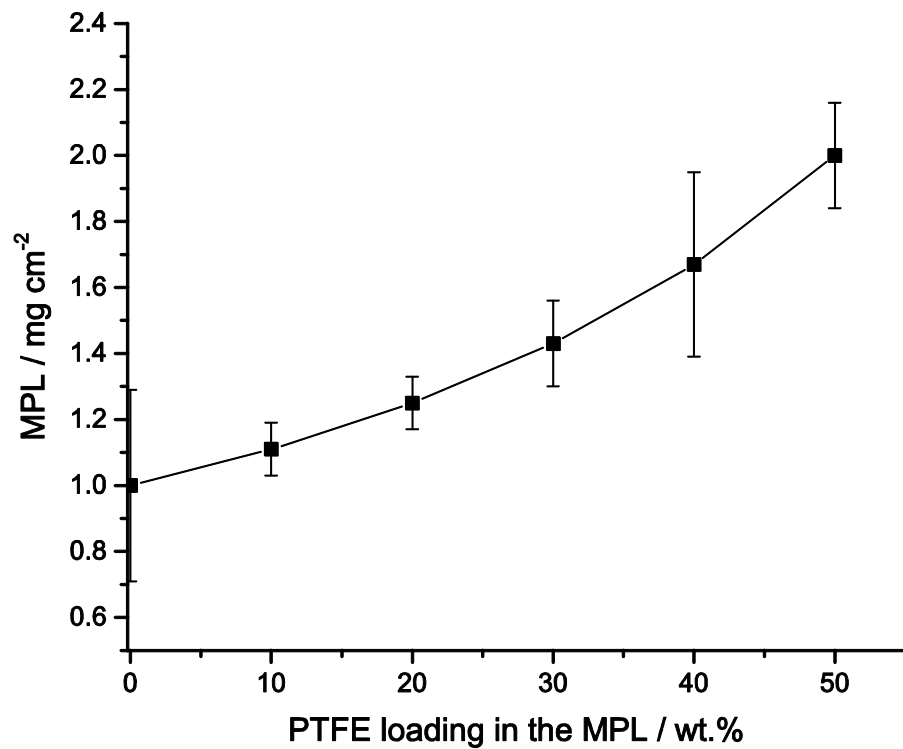
Figure 3.16. Amount MPL slurry coating on the top of one-side of the carbon substrate sample surfaces.



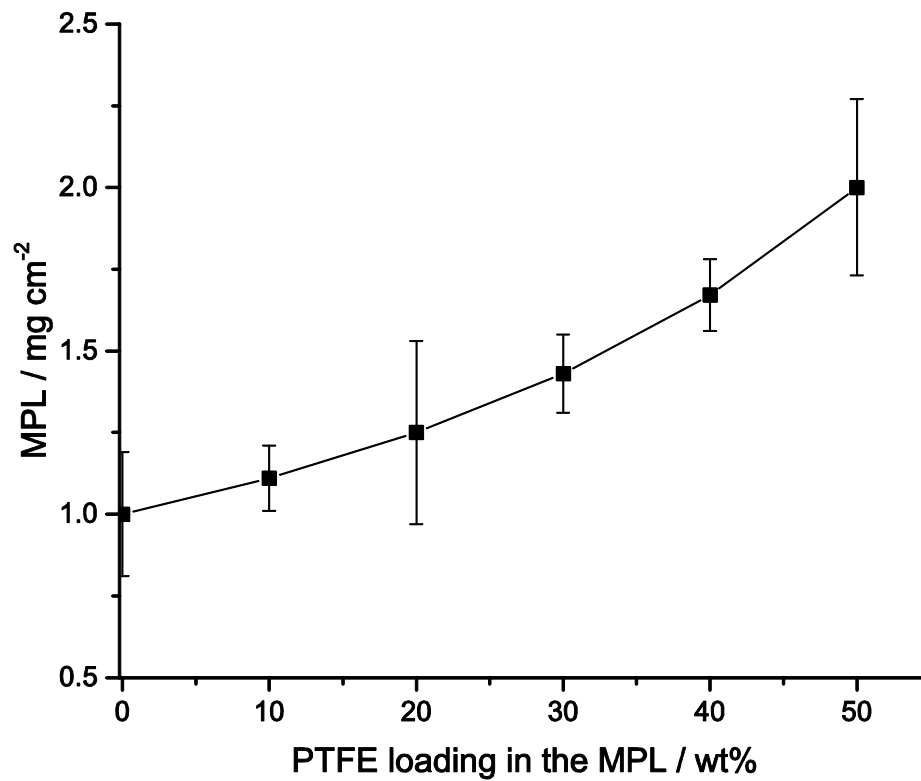
(a) 0.5 mg/cm² Ketjenblack carbon black loading in the MPL.



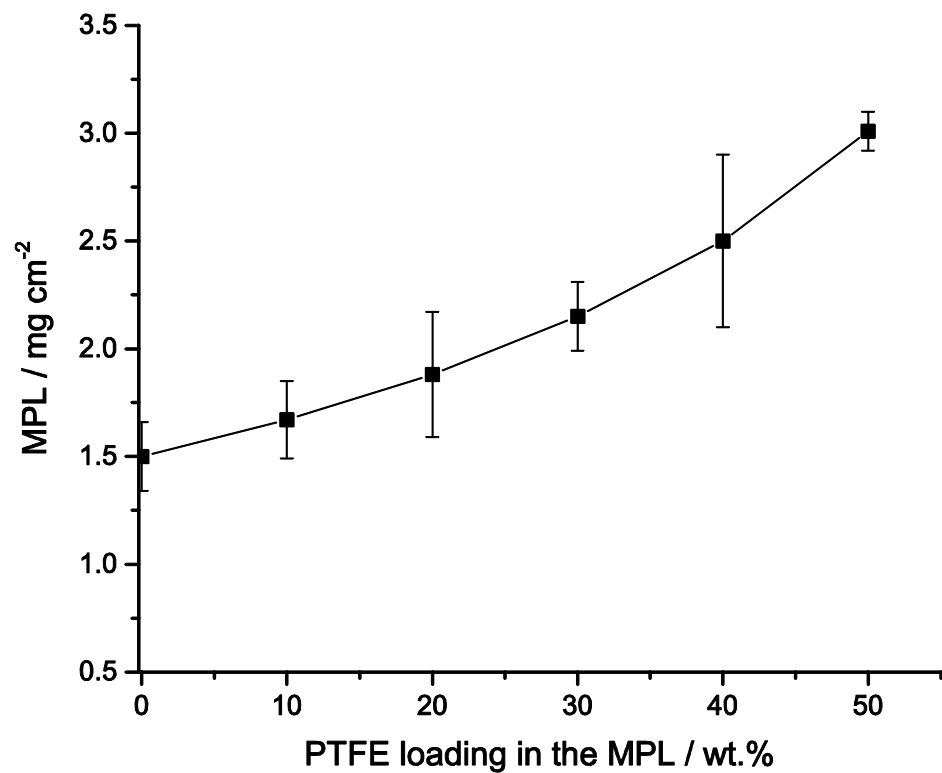
(b) 0.5 mg/cm² Vulcan carbon black loading in the MPL.



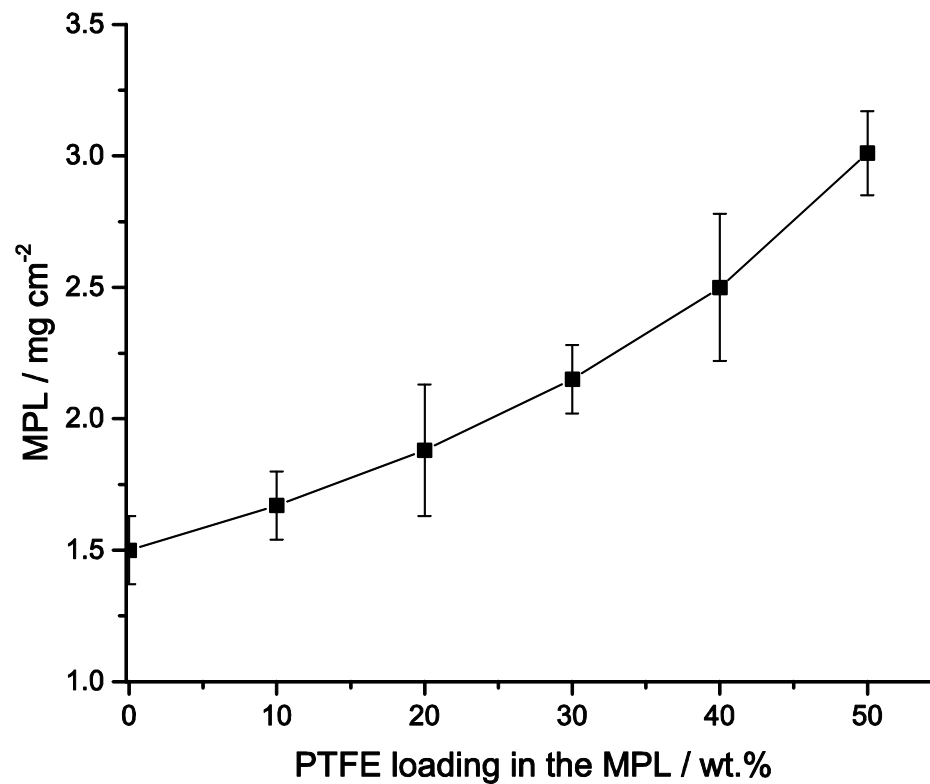
(c) 1.0 mgcm² Ketjenblack carbon black loading in the MPL.



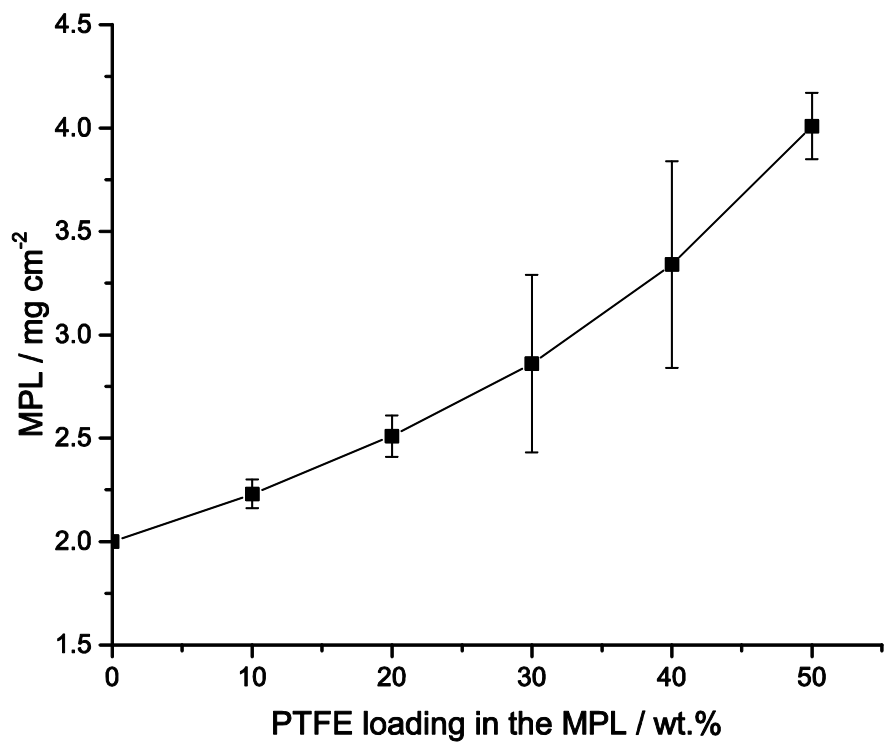
(d) 1.0 mg/cm² Vulcan carbon black loading in the MPL.



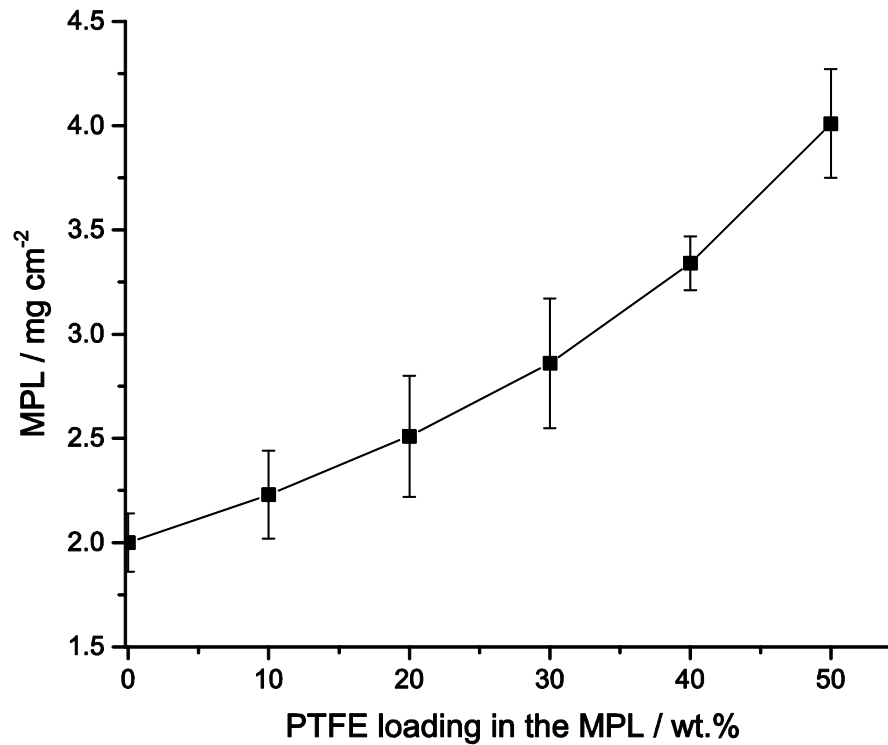
(e) 1.5 mg/cm^2 Ketjenblack carbon black loading in the MPL.



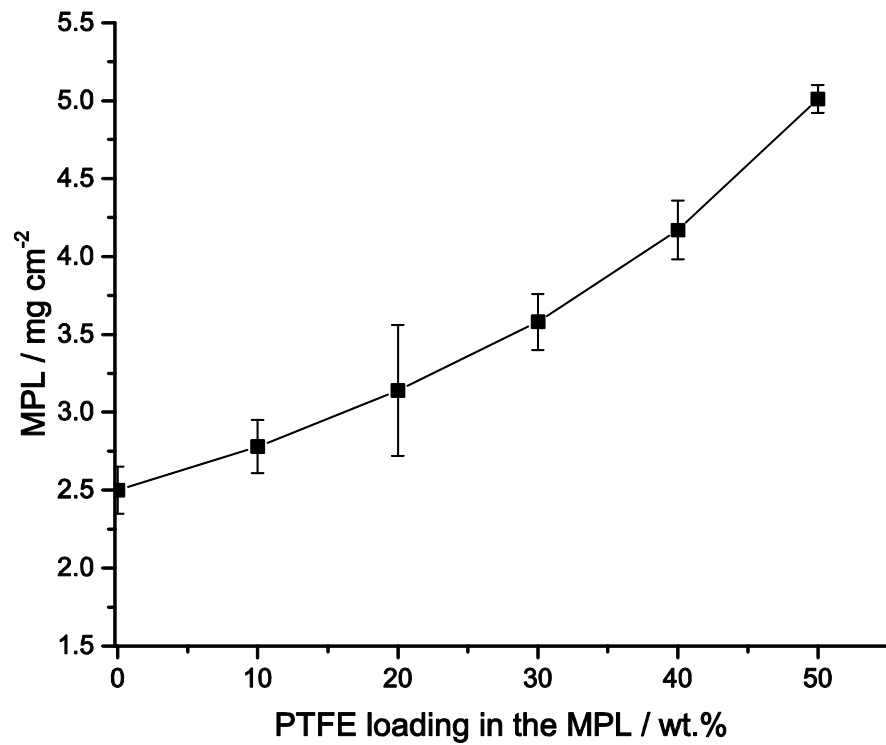
(f) 1.5 mg/cm^2 Vulcan carbon black loading in the MPL.



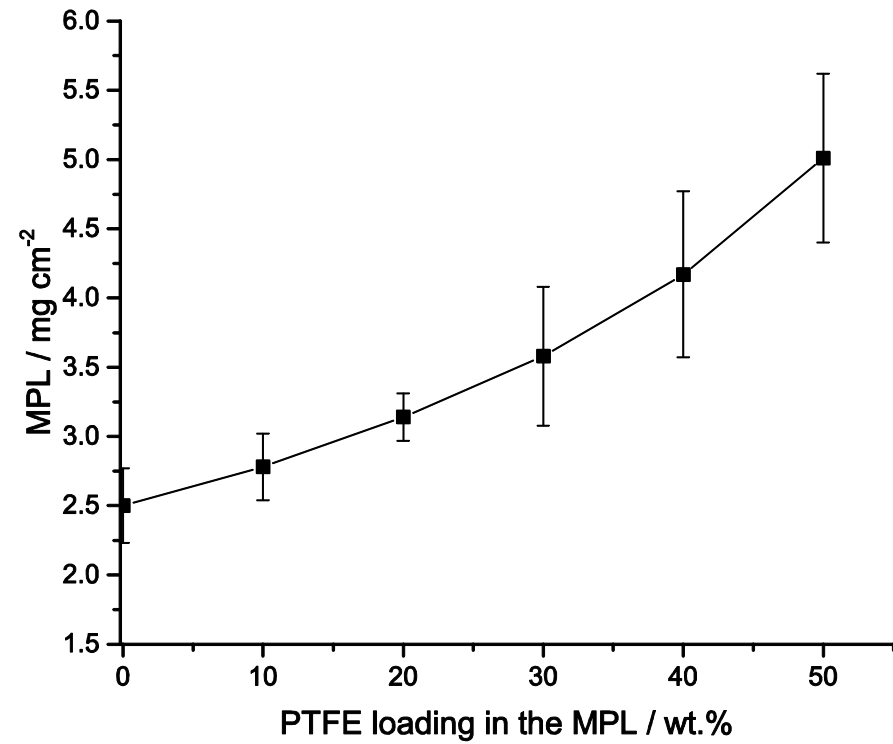
(g) 2.0 mg/cm² Ketjenblack carbon black loading in the MPL.



(h) 2.0 mg/cm² Vulcan carbon black loading in the MPL.

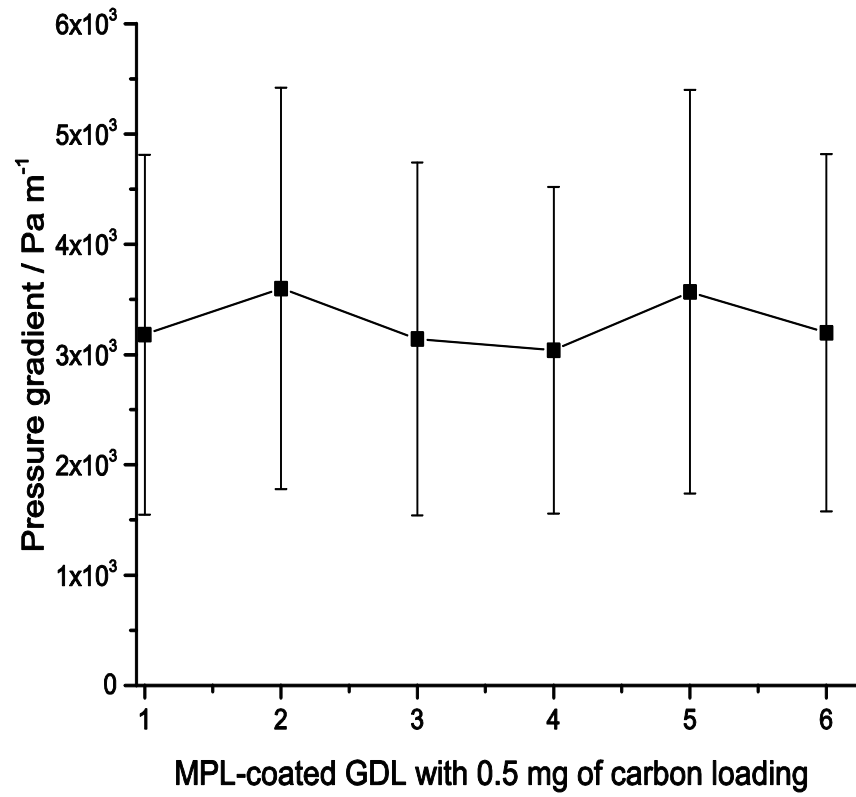


(i) 2.5 mgcm² Ketjenblack carbon black loading in the MPL.

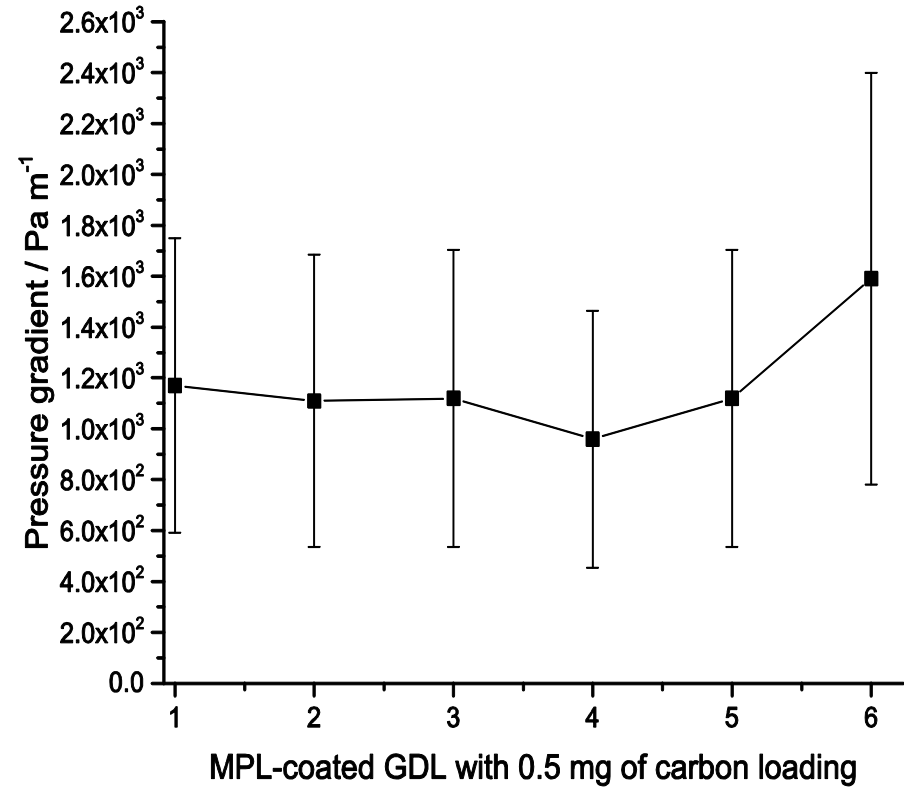


(j) 2.5 mg/cm² Vulcan carbon black loading in the MPL.

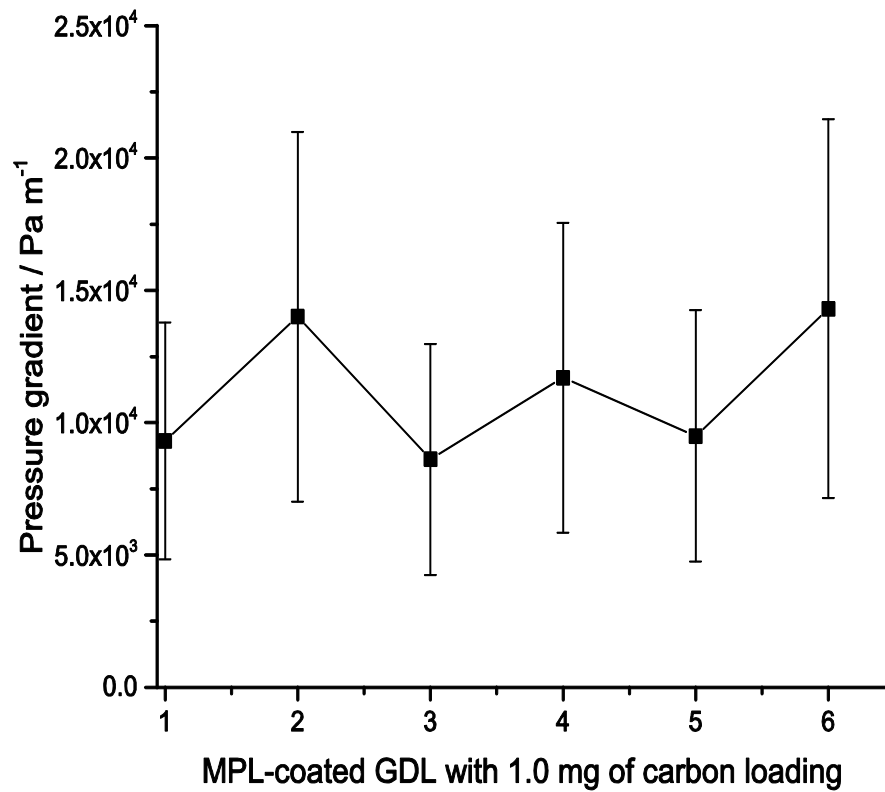
Figure 3.17. The estimation of the amount of Carbon black type-PTFE loading in the MPL coated on one-side of the GDL sample surface by weight and measurement error bars of 95 % conf. int.



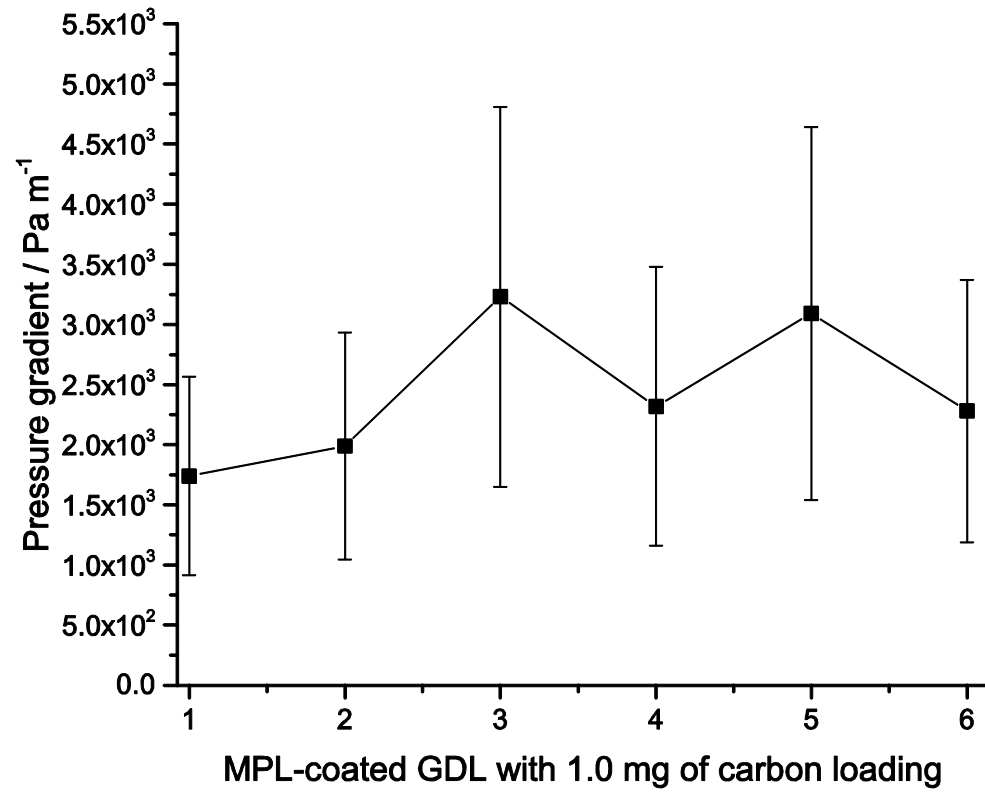
(a)



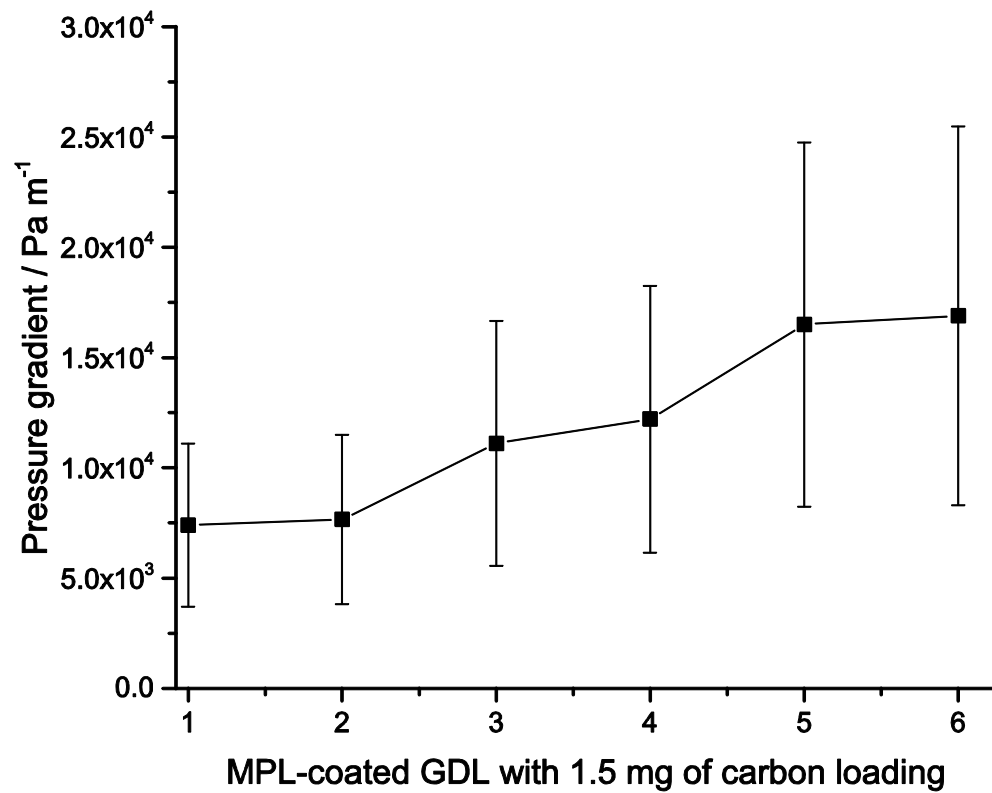
(b)



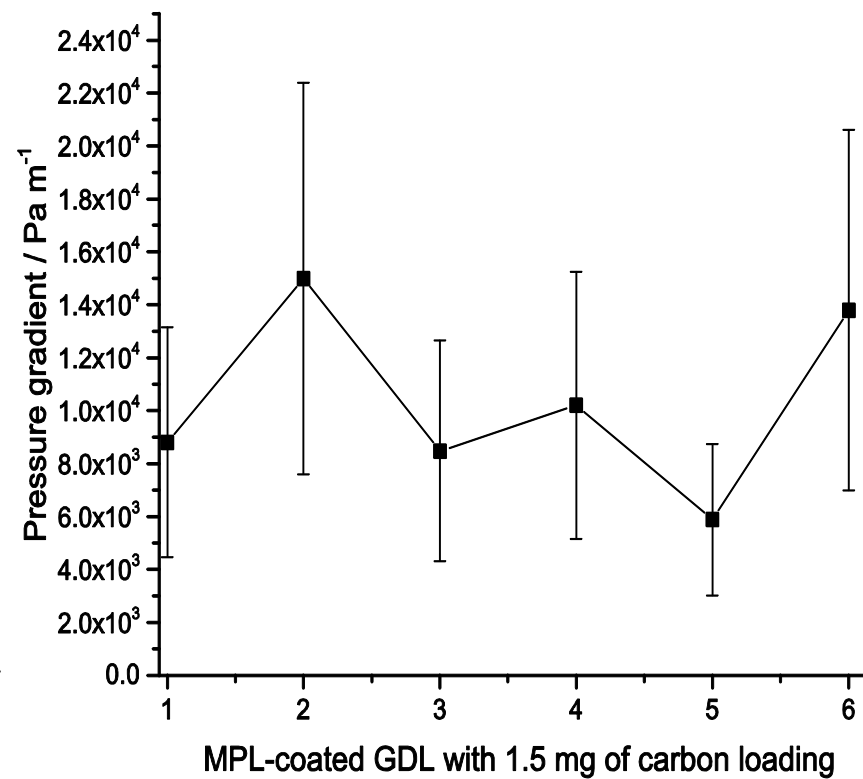
(c)



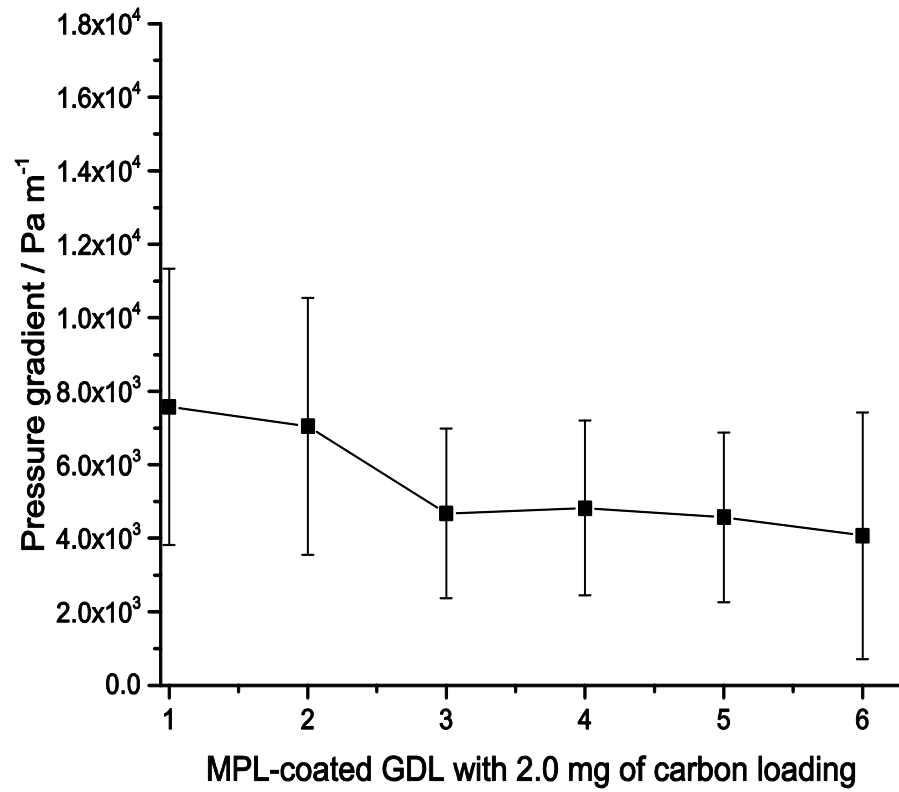
(d)



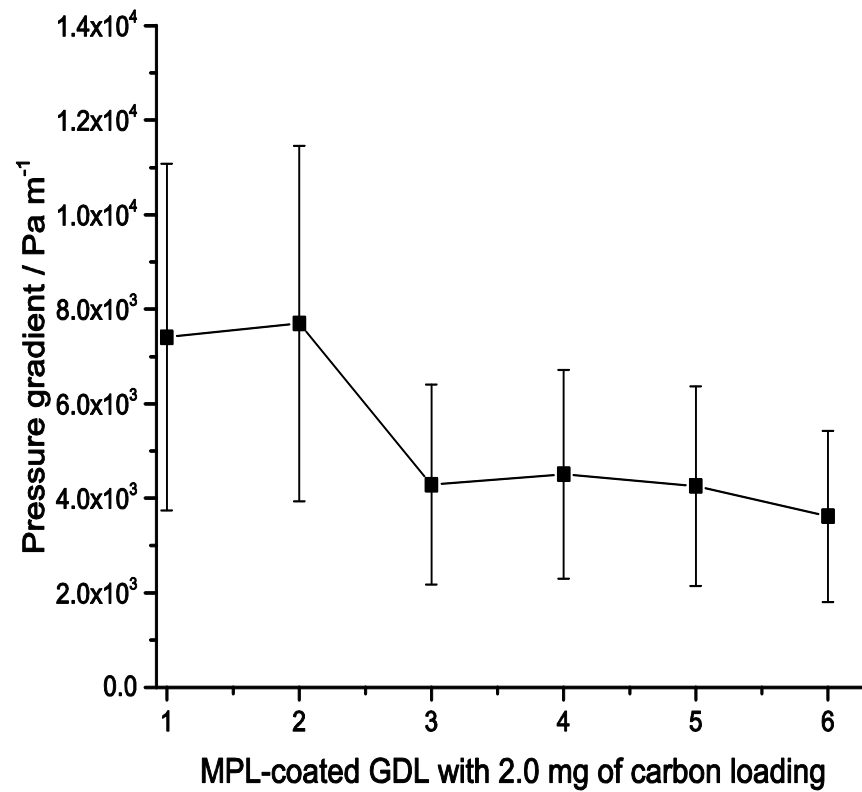
(e)



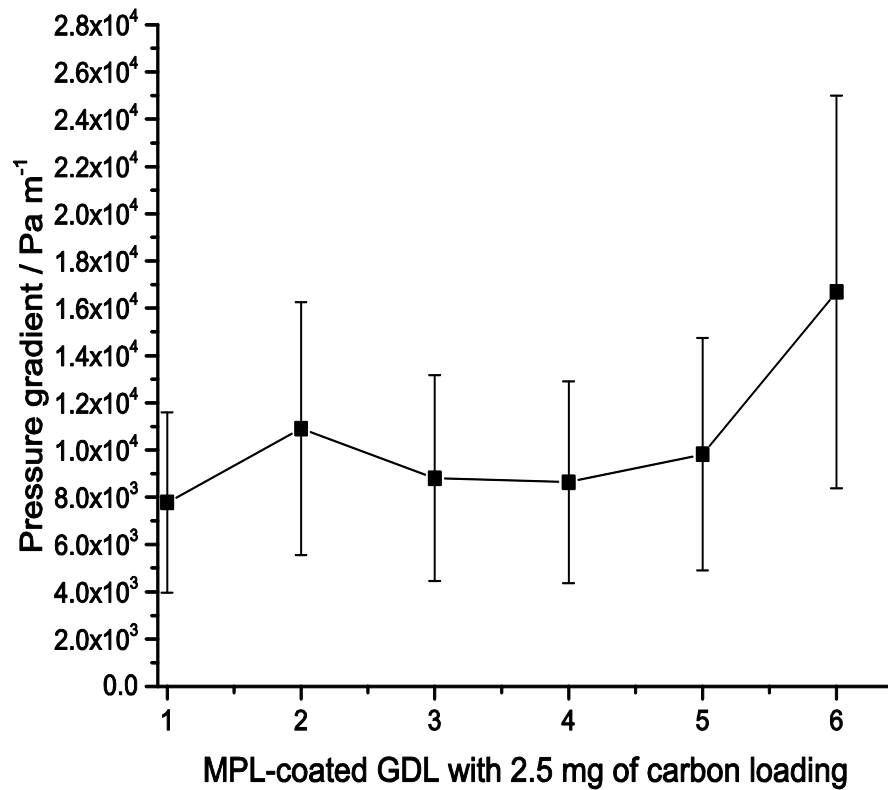
(f)



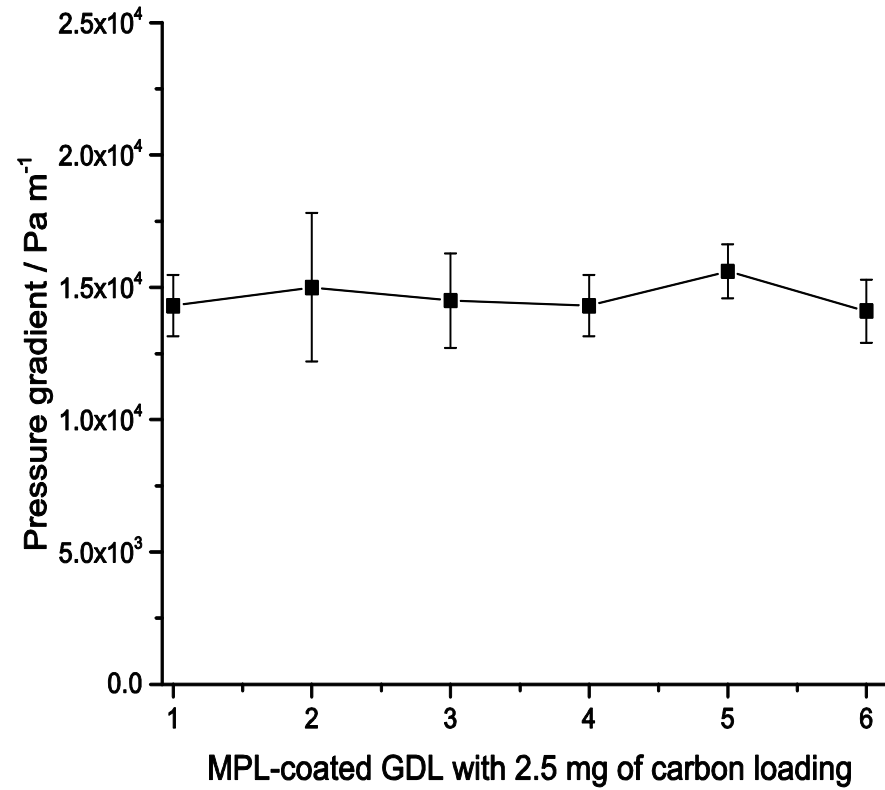
(g)



(h)

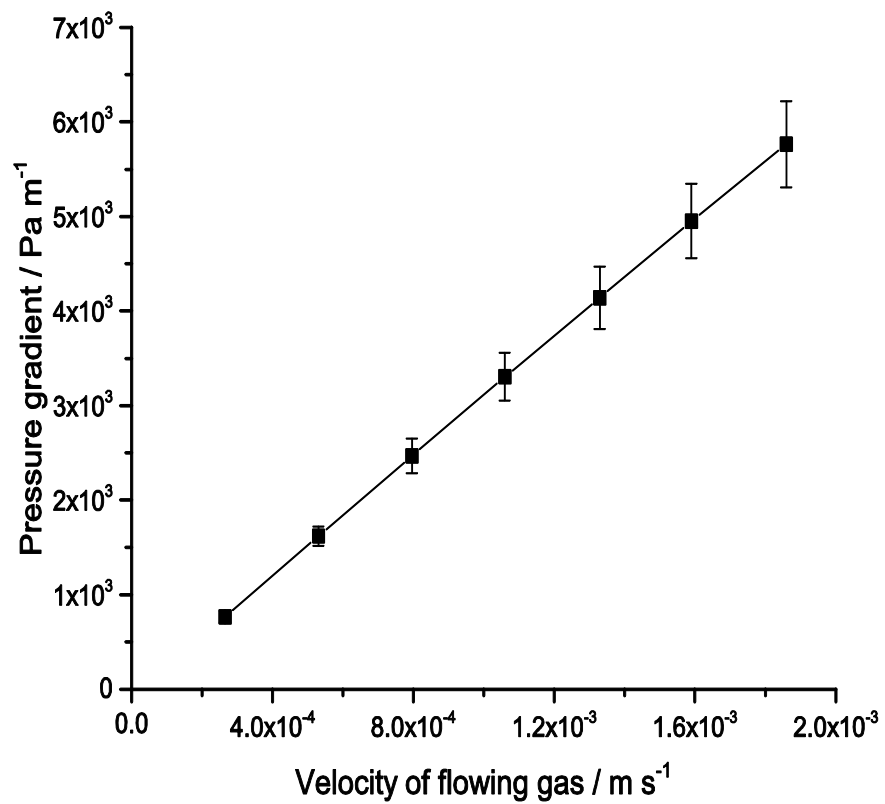


(i)

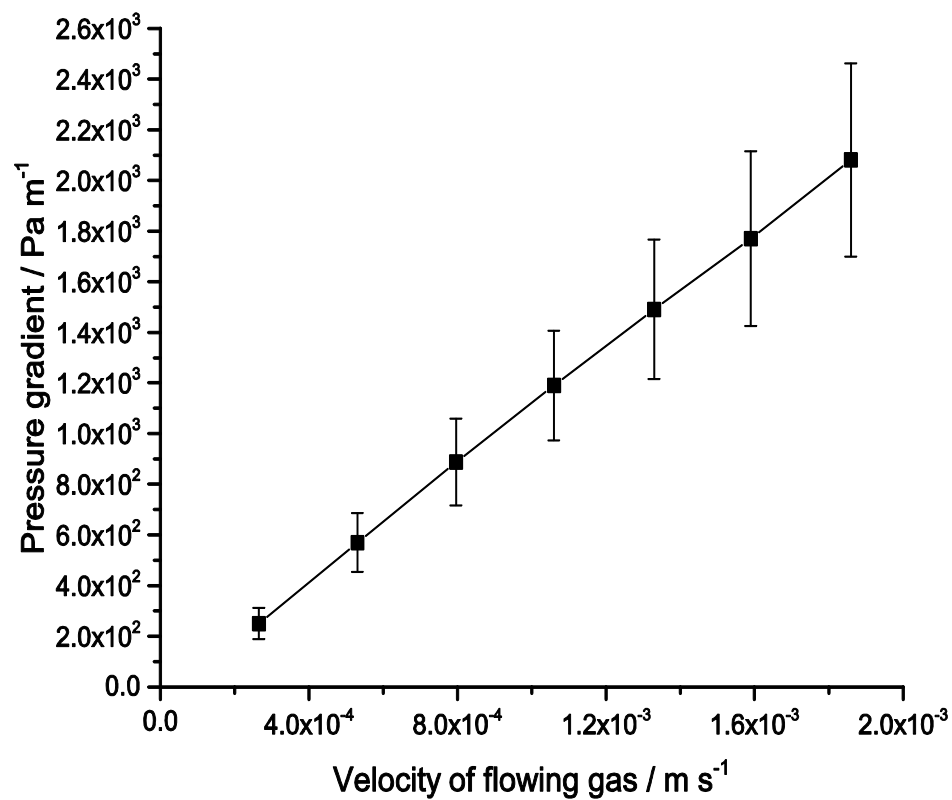


(j)

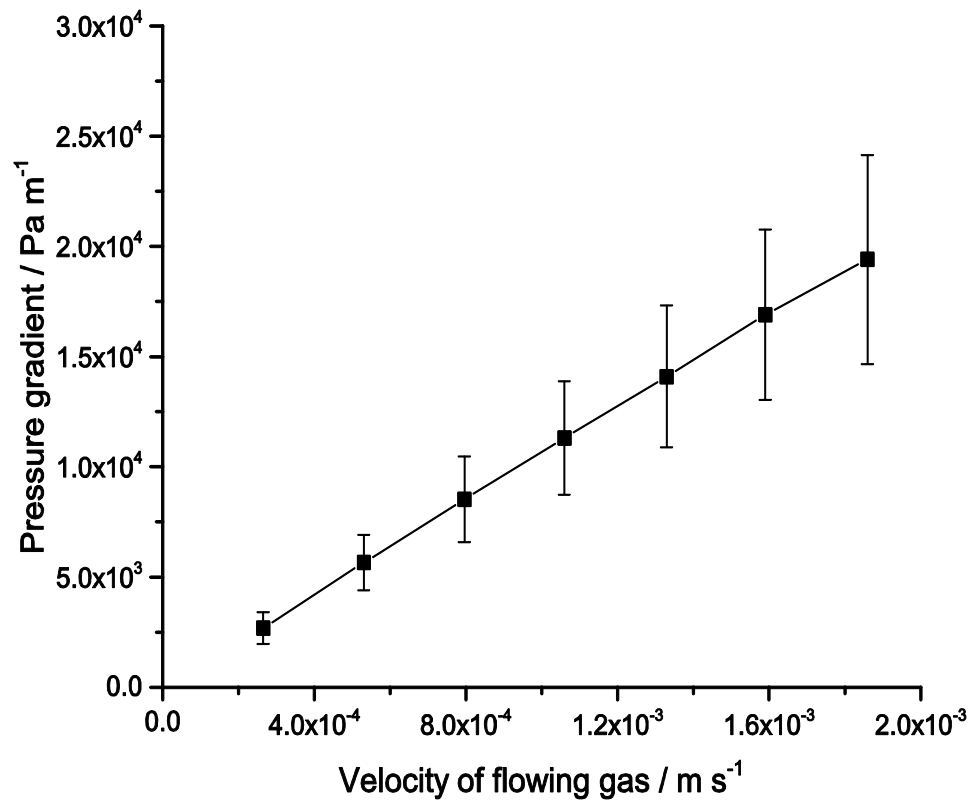
Figure 3.18. The measurement error bars of 95% confidence interval for pressure gradient of MPL-coated GDLs with Vulcan for each of 6 tested samples of 20 wt.% PTFE.



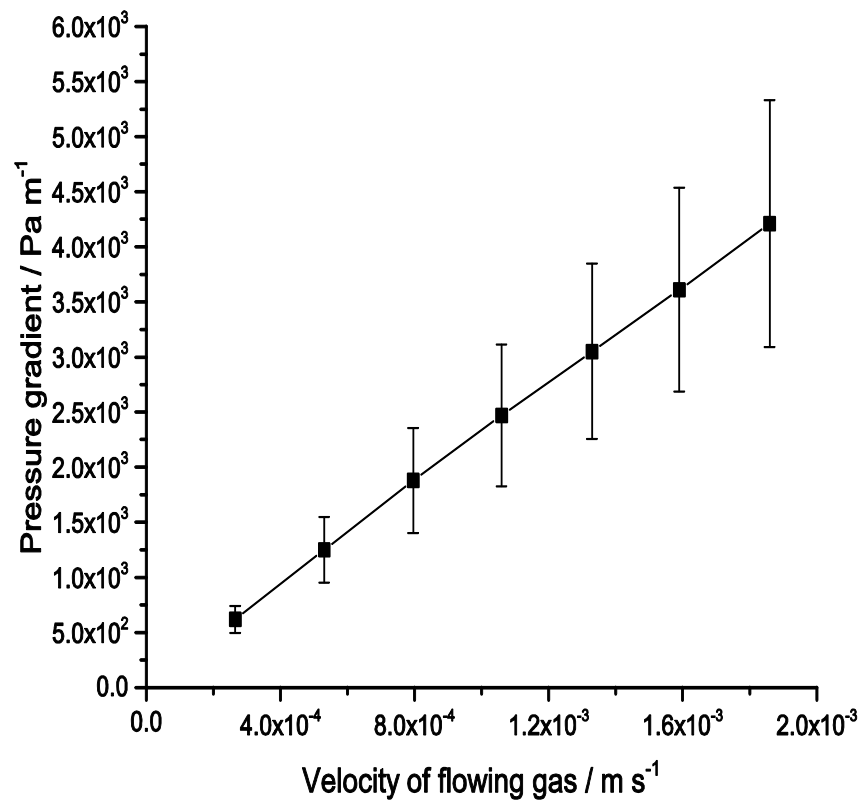
(a) 0.5 mg/cm² Ketjenblack loading



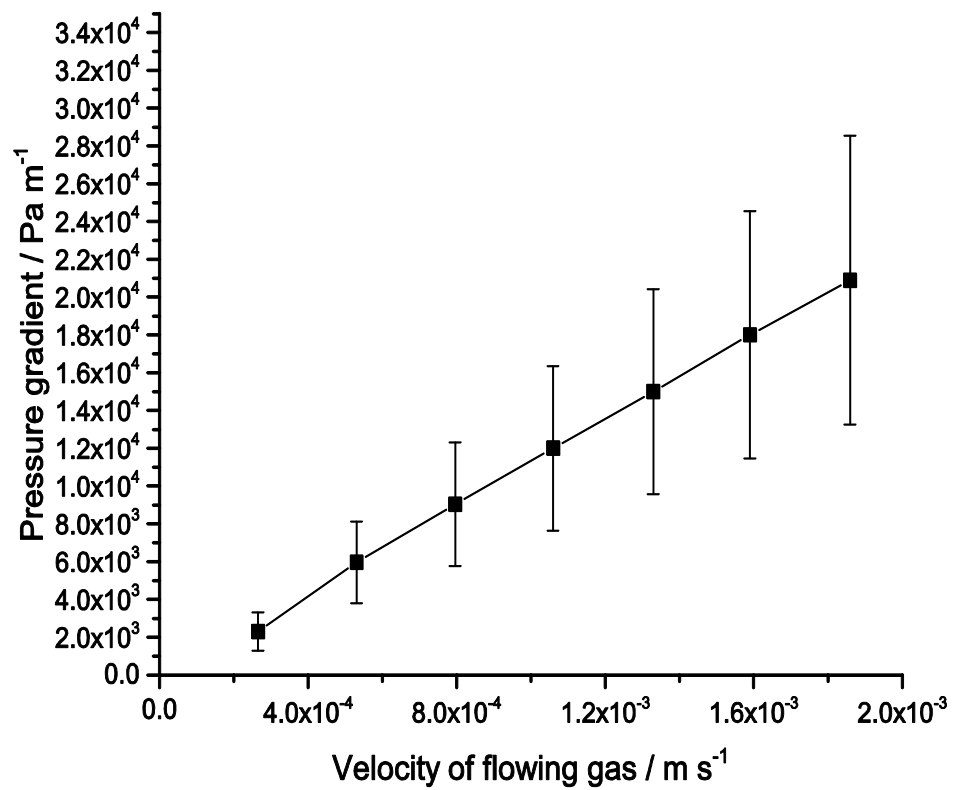
(b) 0.5 mg/cm² Vulcan loading



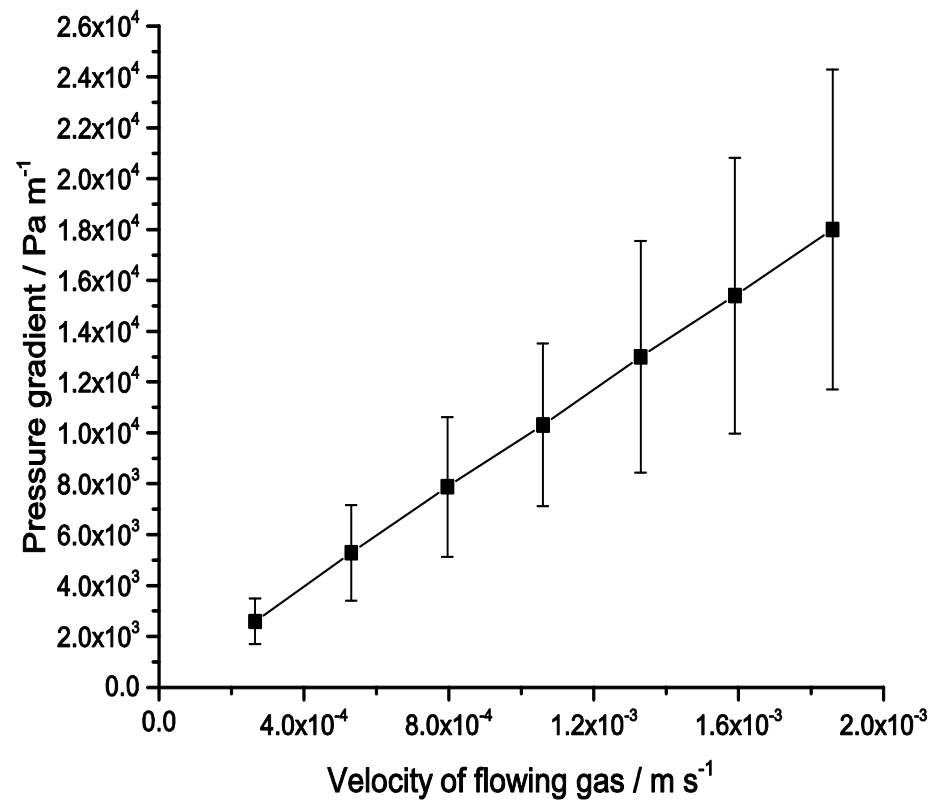
(c) 1.0 mg/cm² Ketjenblack loading



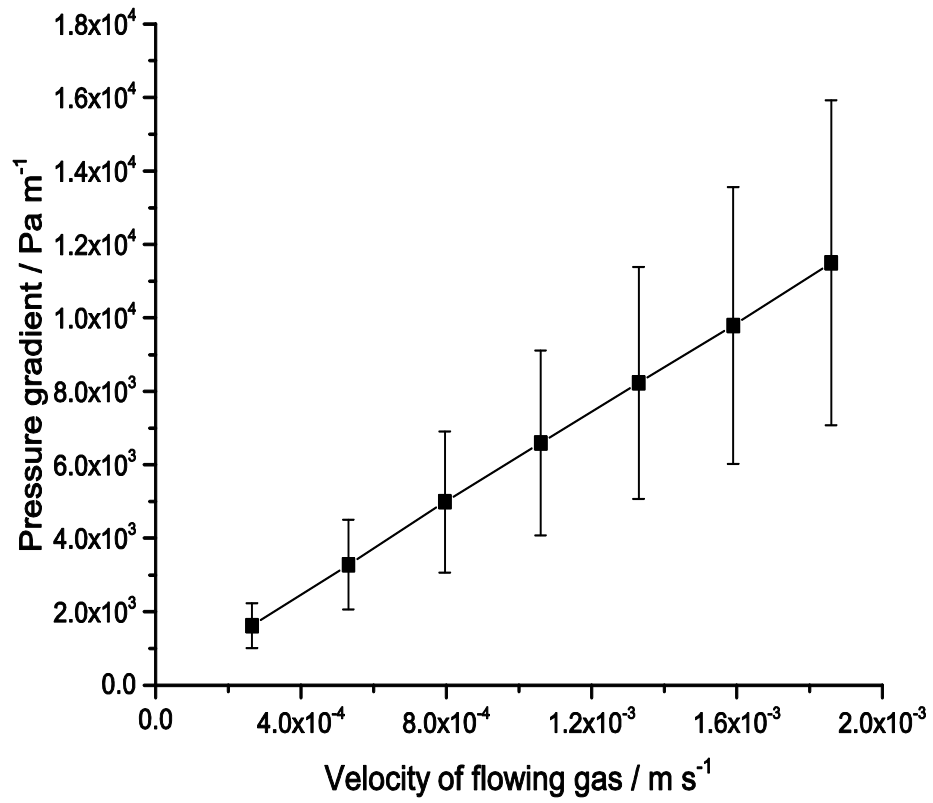
(d) 1.0 mg/cm² Vulcan loading



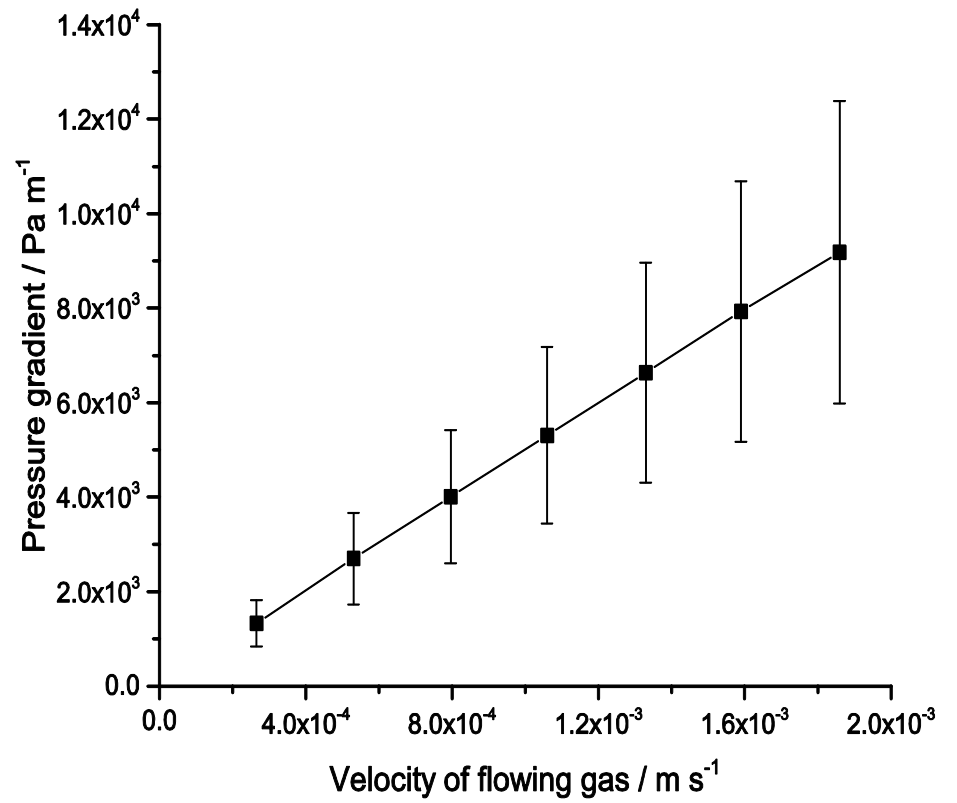
(e) 1.5 mg/cm² Ketjenblack loading



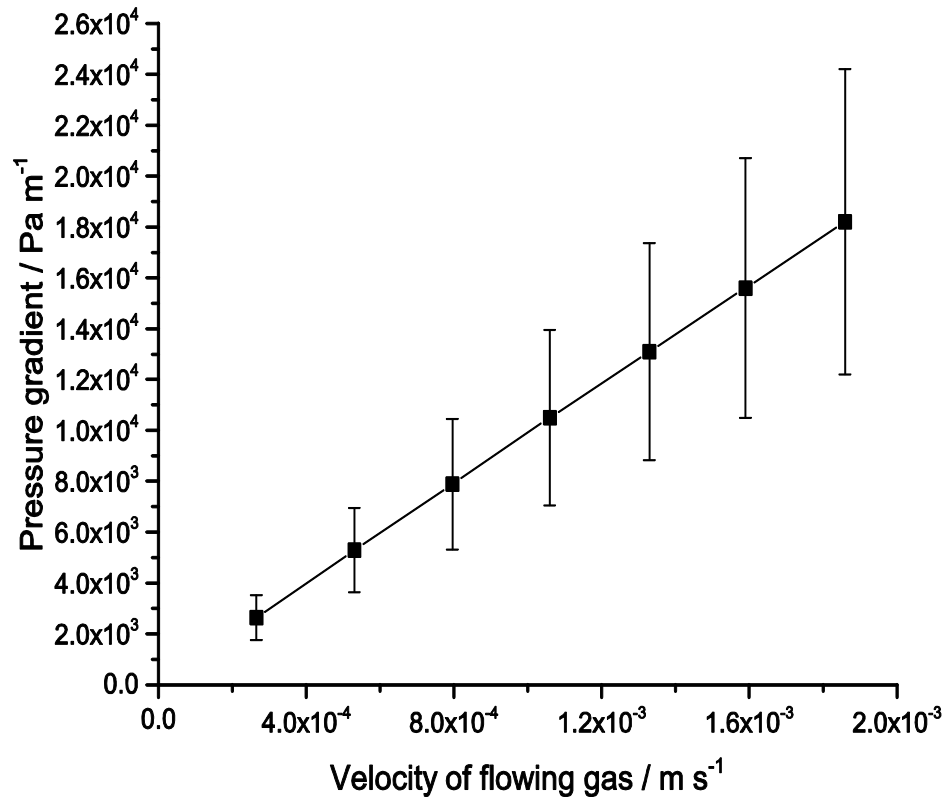
(f) 1.5 mg/cm² Vulcan loading



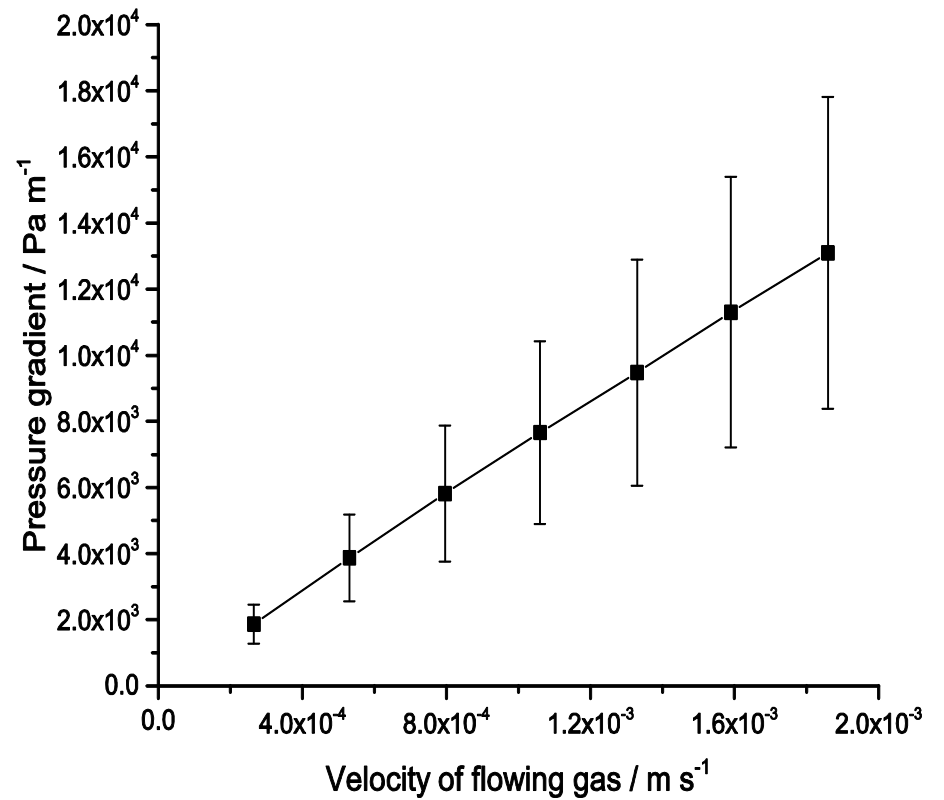
(g) 2.0 mg/cm² Ketjenblack loading



(h) 2.0 mg/cm² Vulcan loading

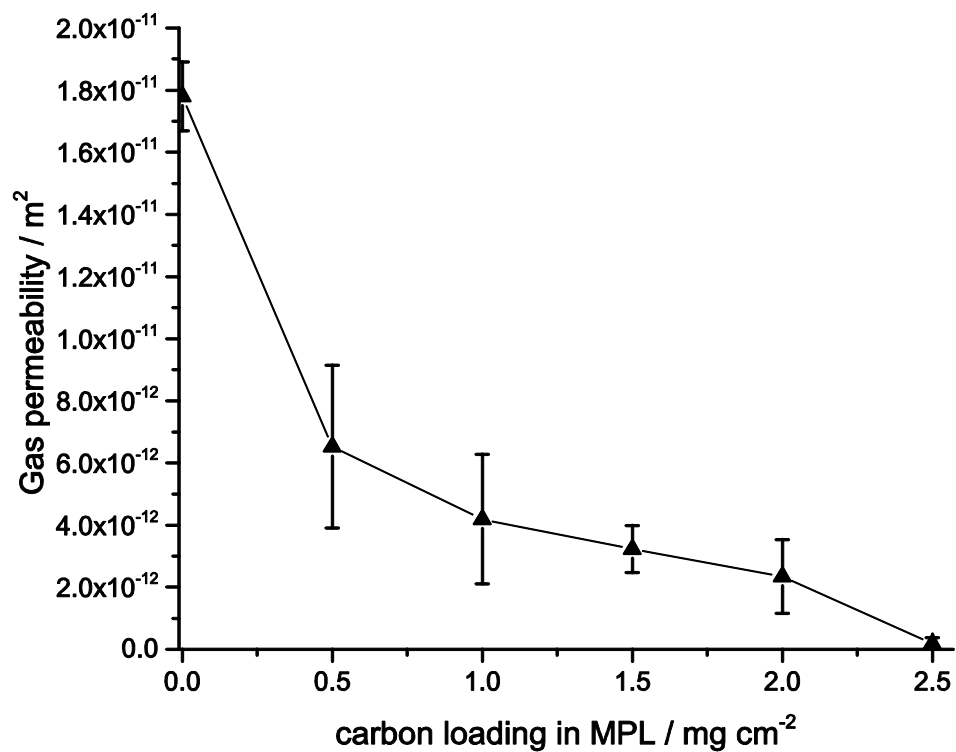


(i) 2.5 mg/cm² Ketjenblack loading

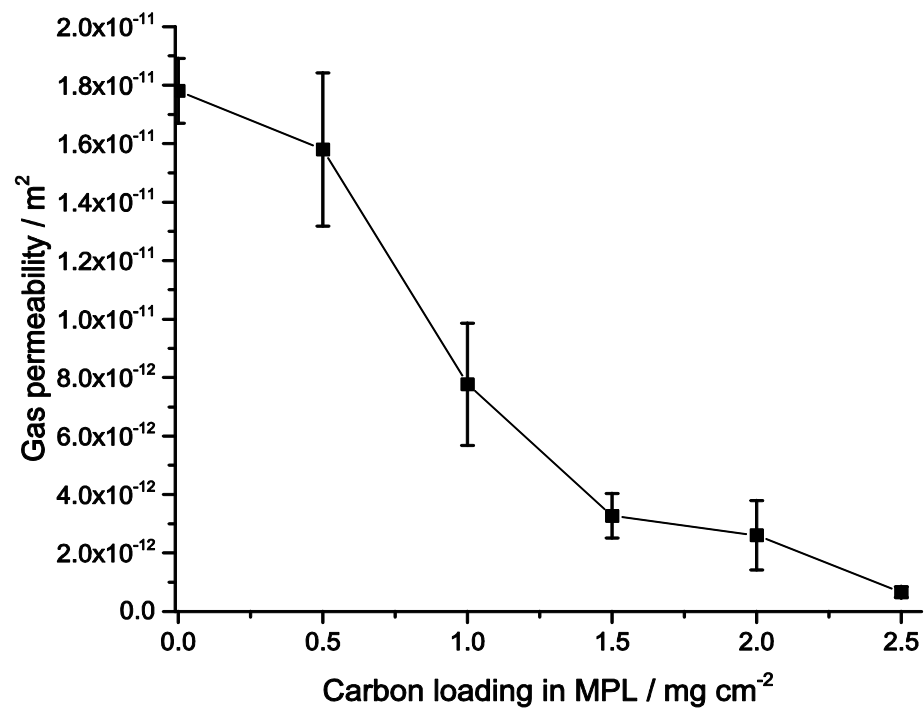


(j) 2.5 mg/cm² Vulcan loading

Figure 3.19. The measurement error bars of 95% confidence interval for pressure gradient as a function of velocity of flowing gas across MPL-coated GDLs with Ketjenblack and Vulcan carbon blacks of 20 wt.% PTFE.

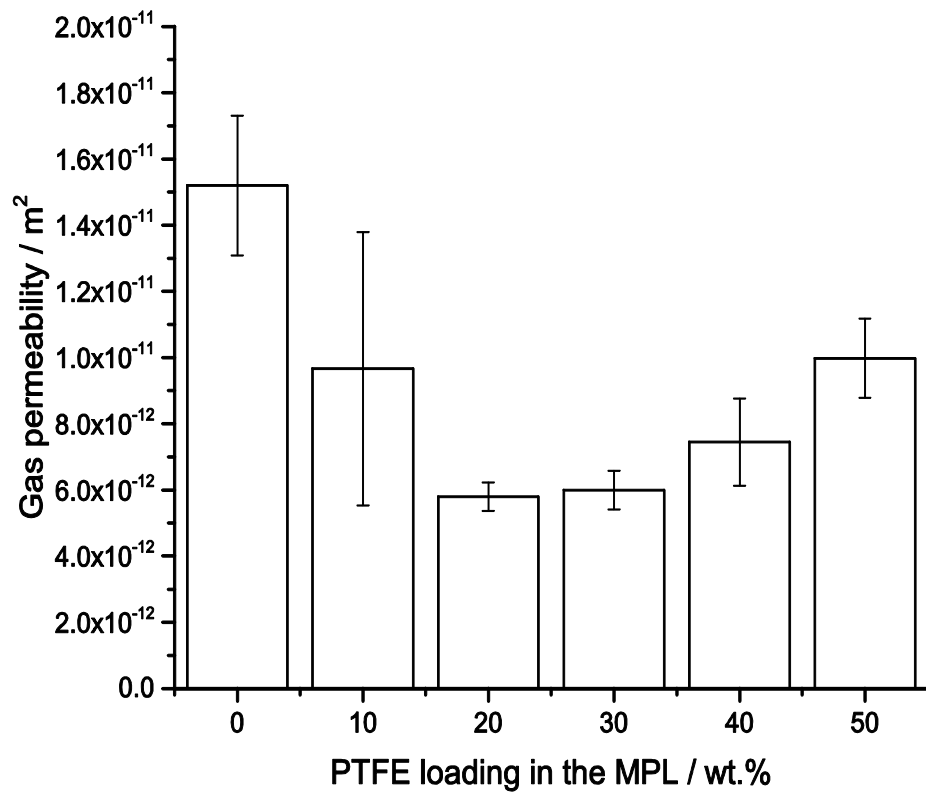


(a)

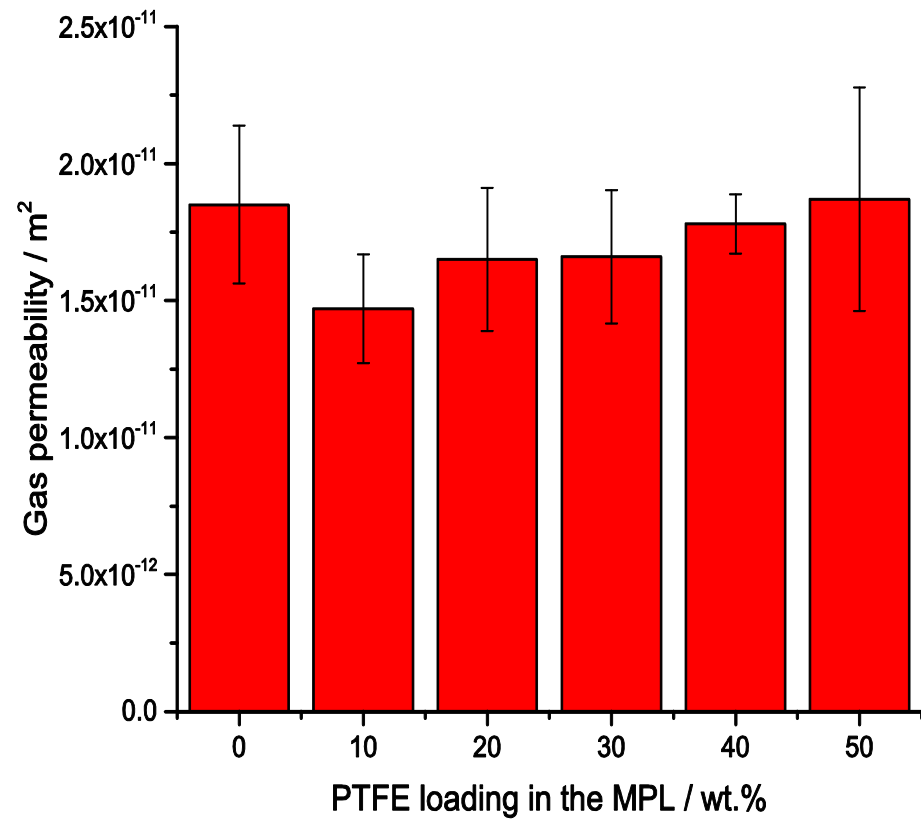


(b)

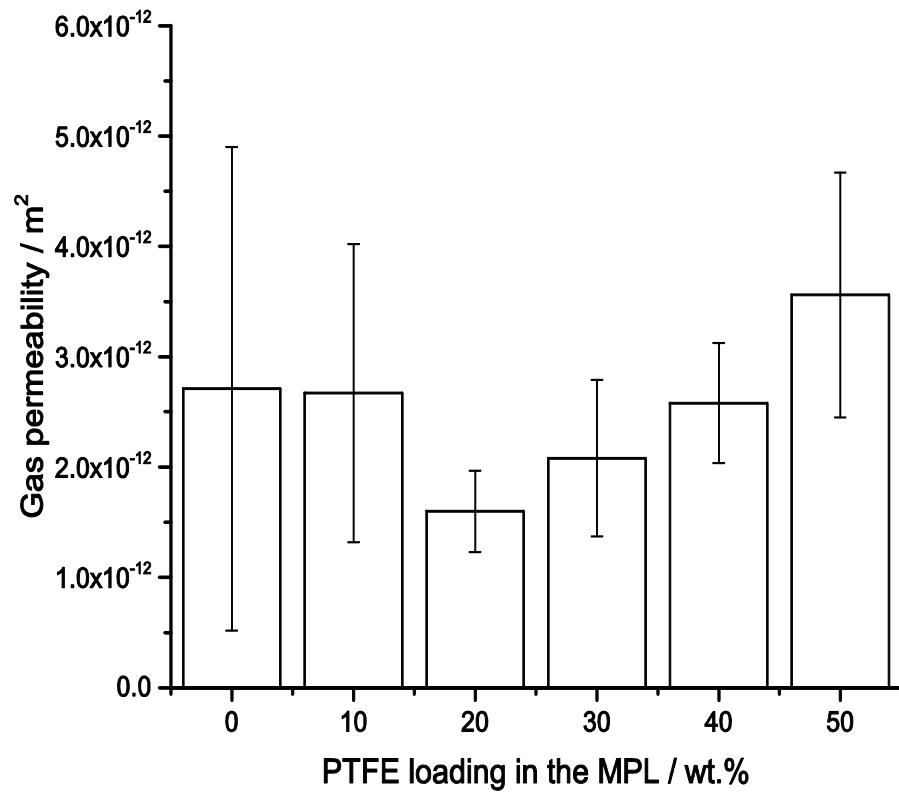
Figure 3.20. The measurement error bars of 95% confidence interval for gas permeability of MPL-coated GDLs as a function of carbon loading in the MPL with (a) Ketjenblack and (b) Vulcan carbon blacks with 20 wt.% PTFE.



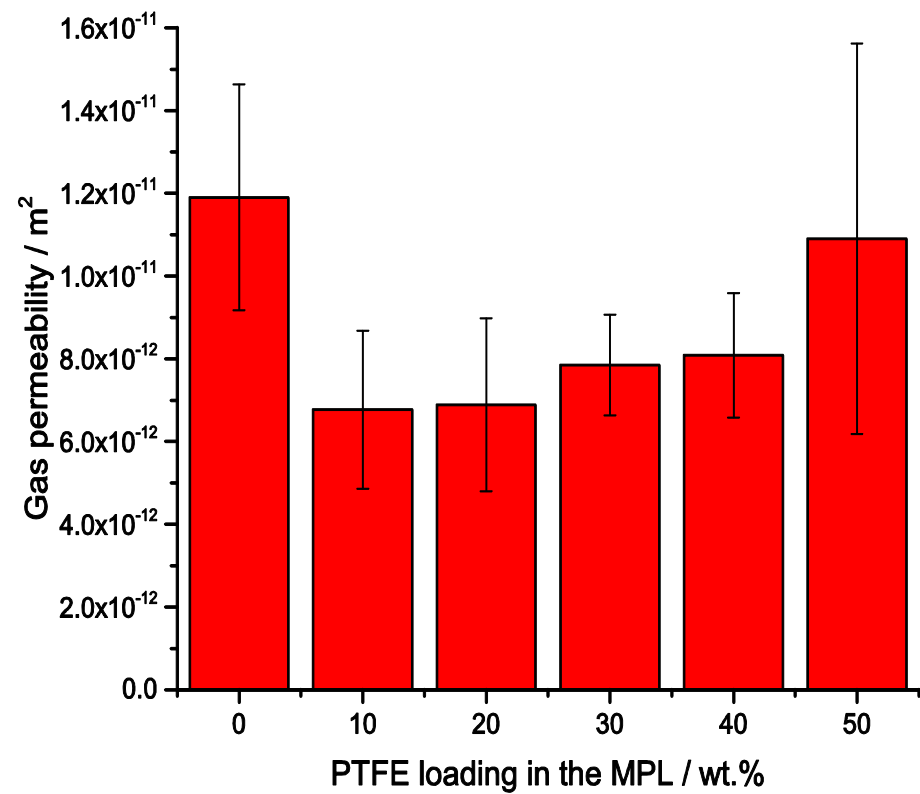
0.5 mg/cm² Ketjenblack loading



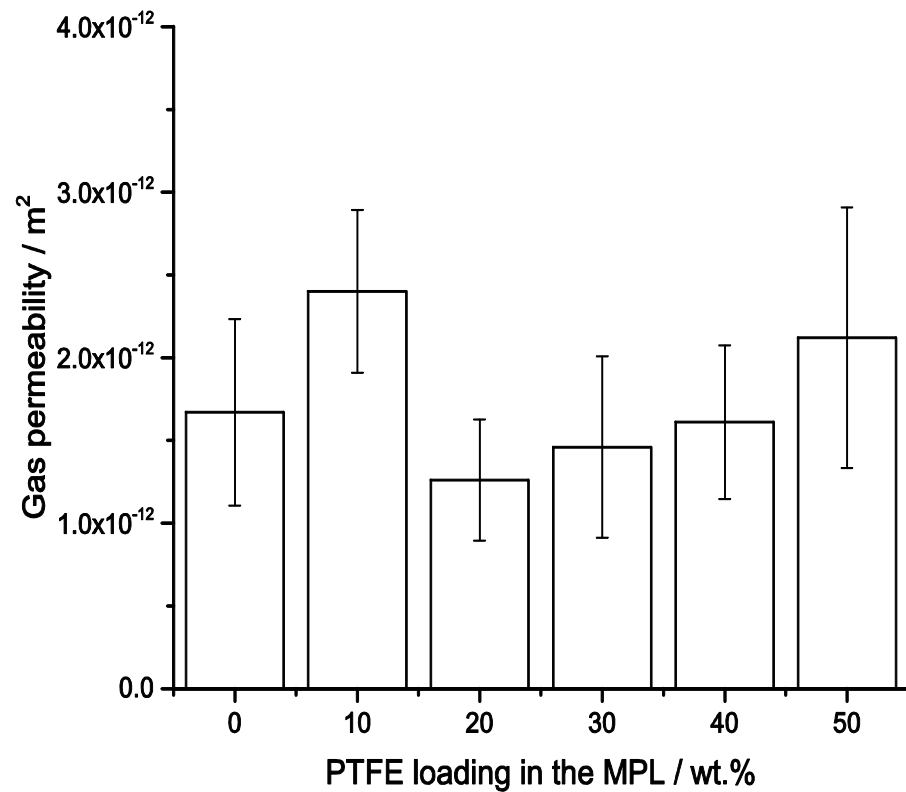
0.5 mg/cm² Vulcan loading



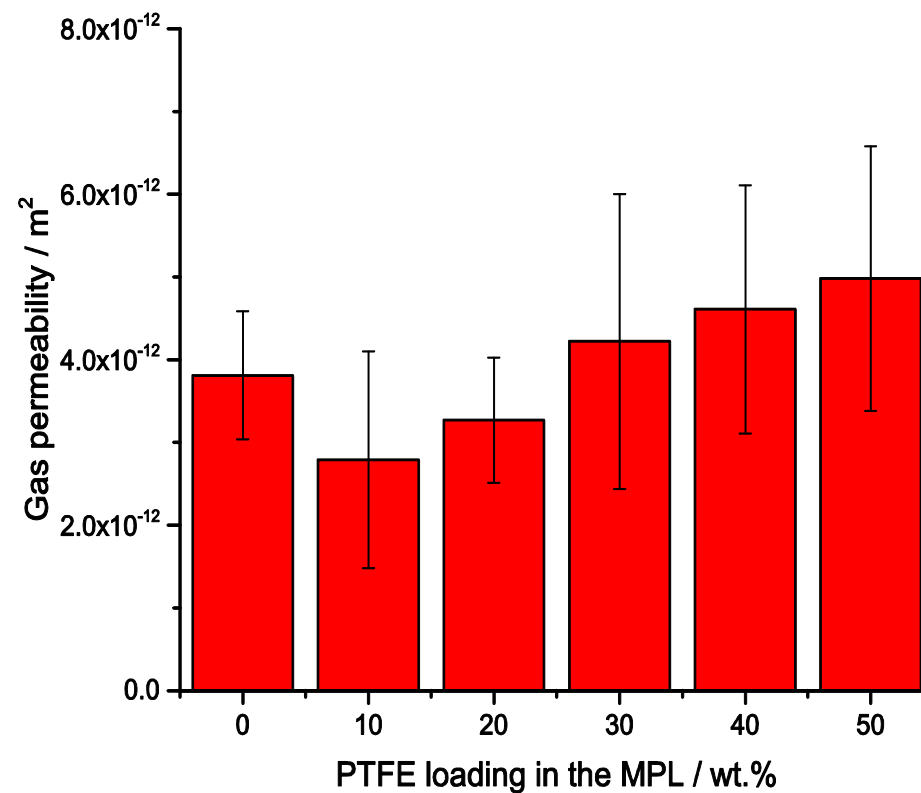
1.0 mg/cm² Ketjenblack loading



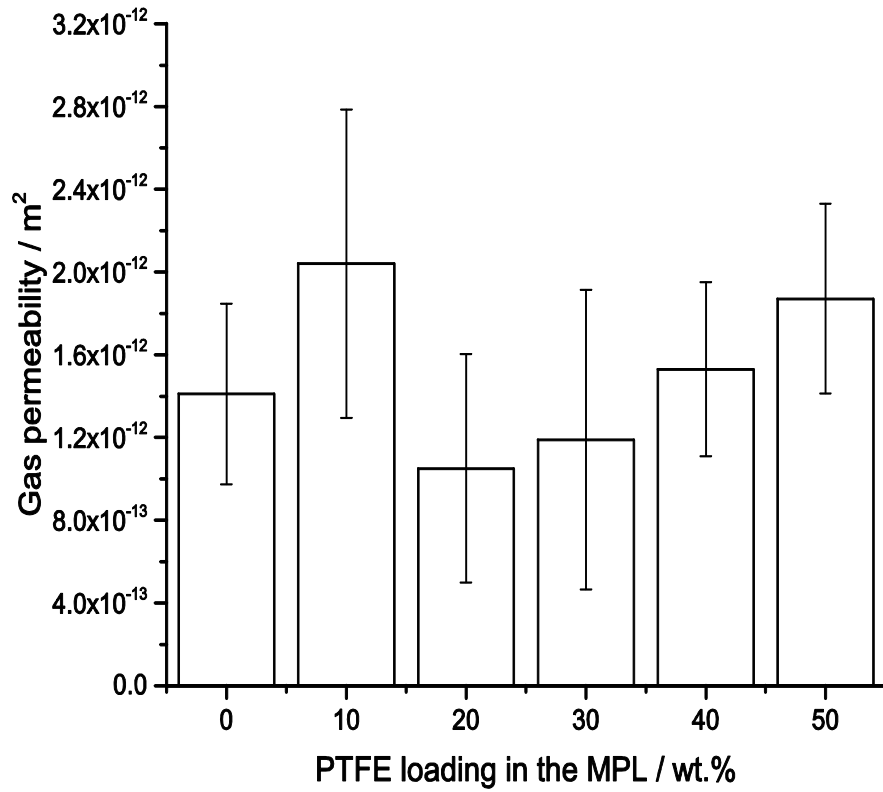
1.0 mg/cm² Vulcan loading



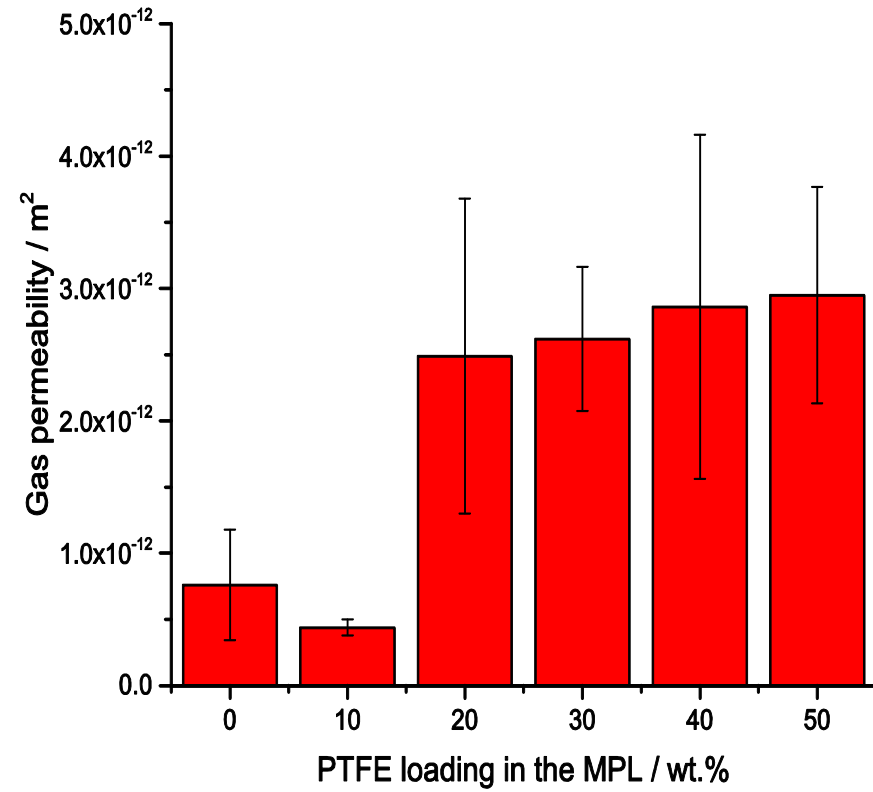
1.5 mg/cm² Ketjenblack loading



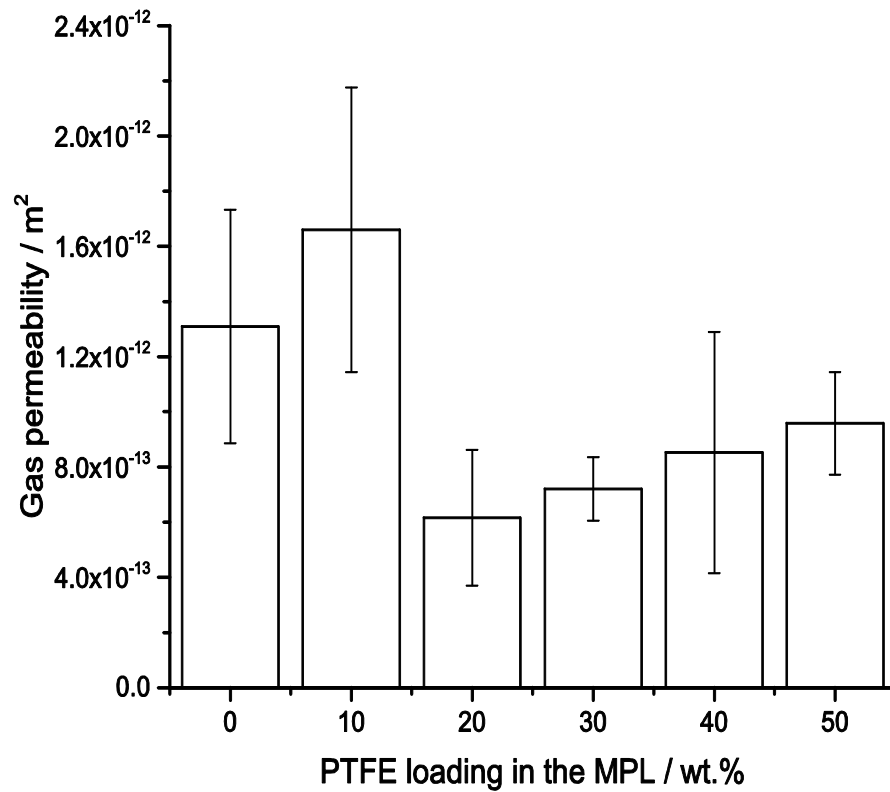
1.5 mg/cm² Vulcan loading



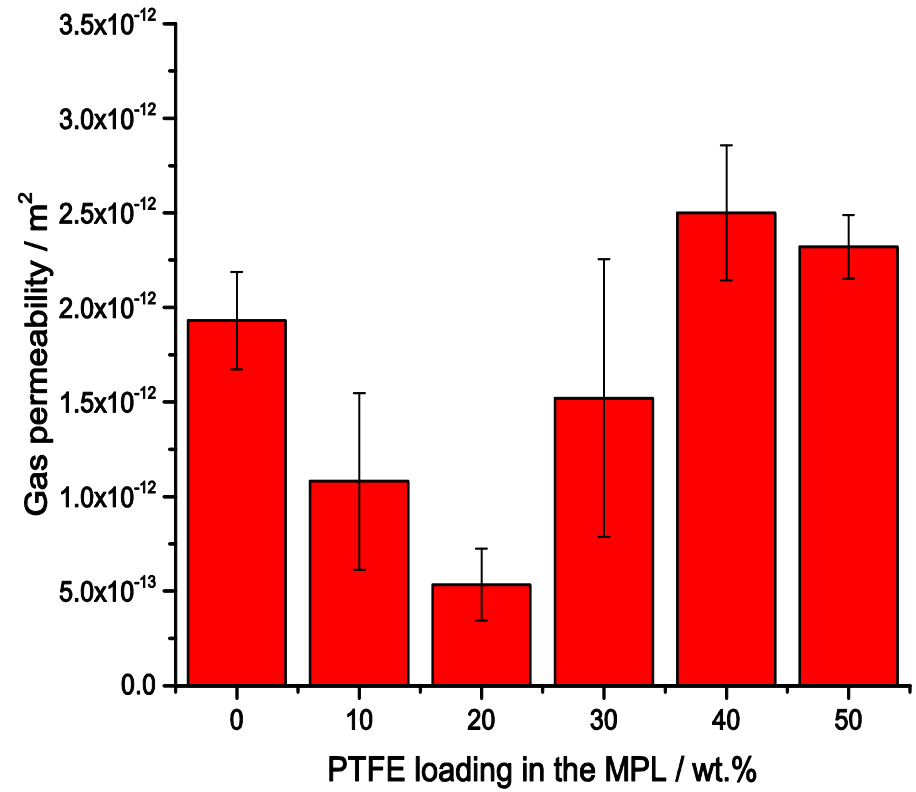
2.0 mg/cm² Ketjenblack loading



2.0 mg/cm² Vulcan loading

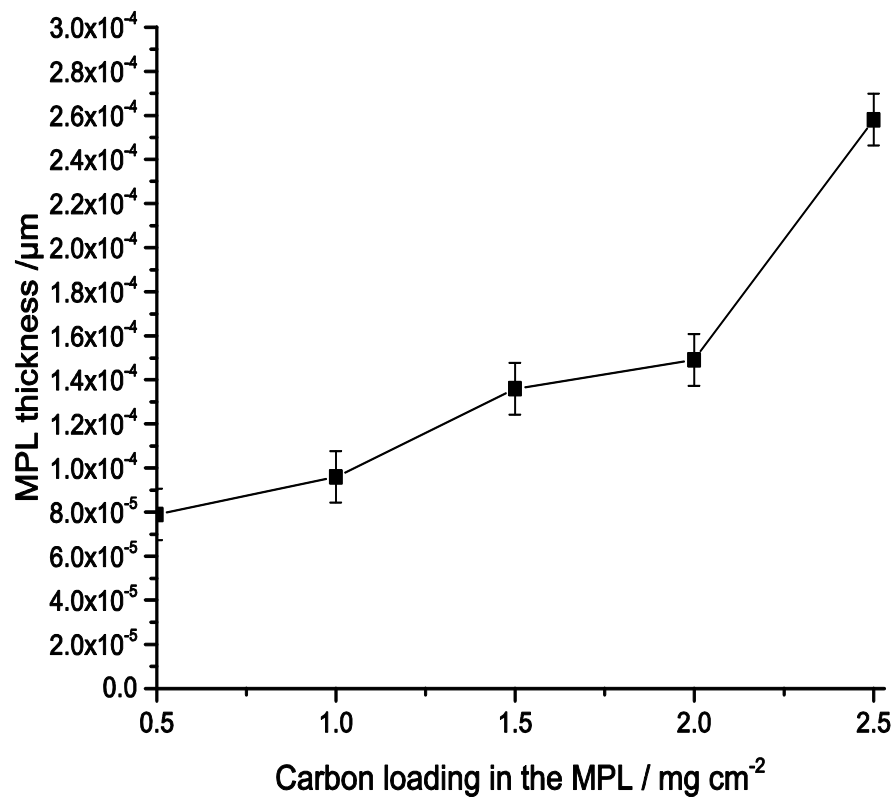


2.5 mg/cm² Ketjenblack loading.

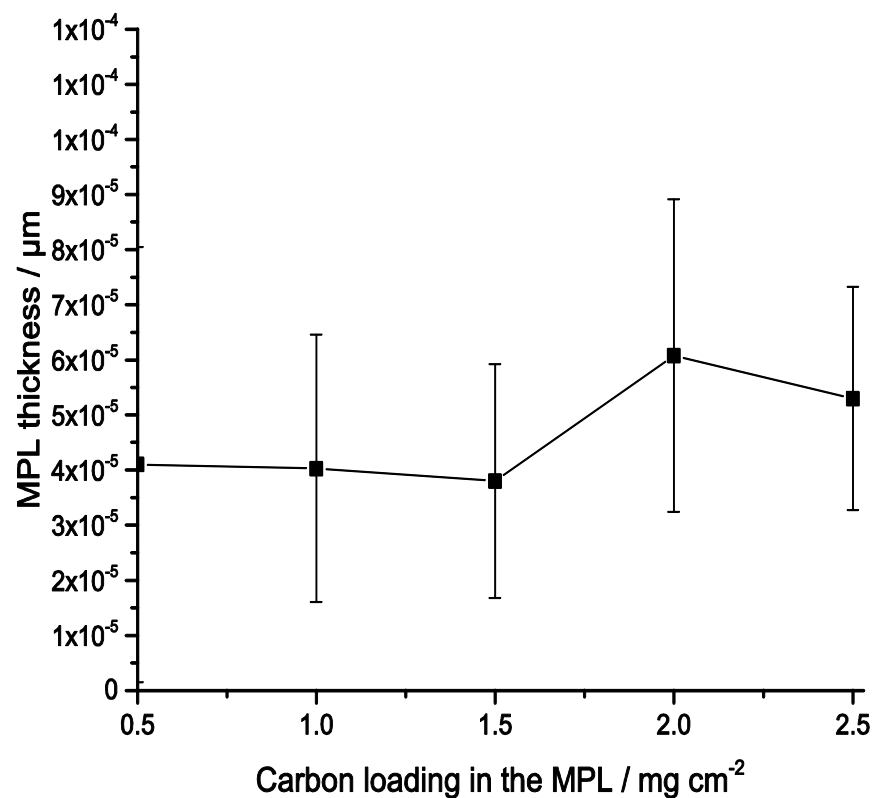


2.5 mg/cm² Vulcan loading.

Figure 3.21. The measurement error bars of 95% confidence interval for gas permeability of MPL-coated GDLs as a function of PTFE loading in the MPL with Ketjenblack and Vulcan carbon blacks.

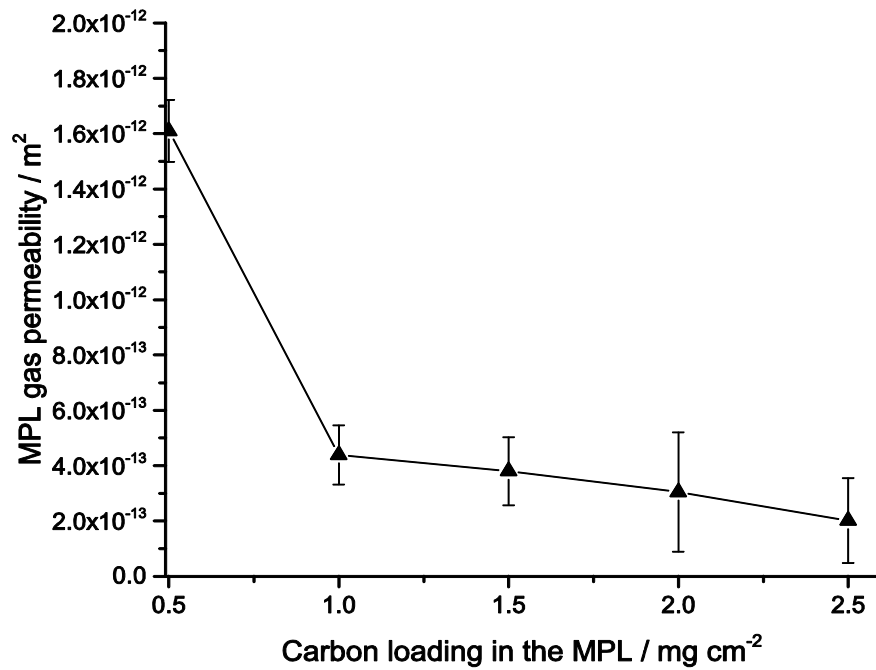


(a) MPL-Ketjenblack.

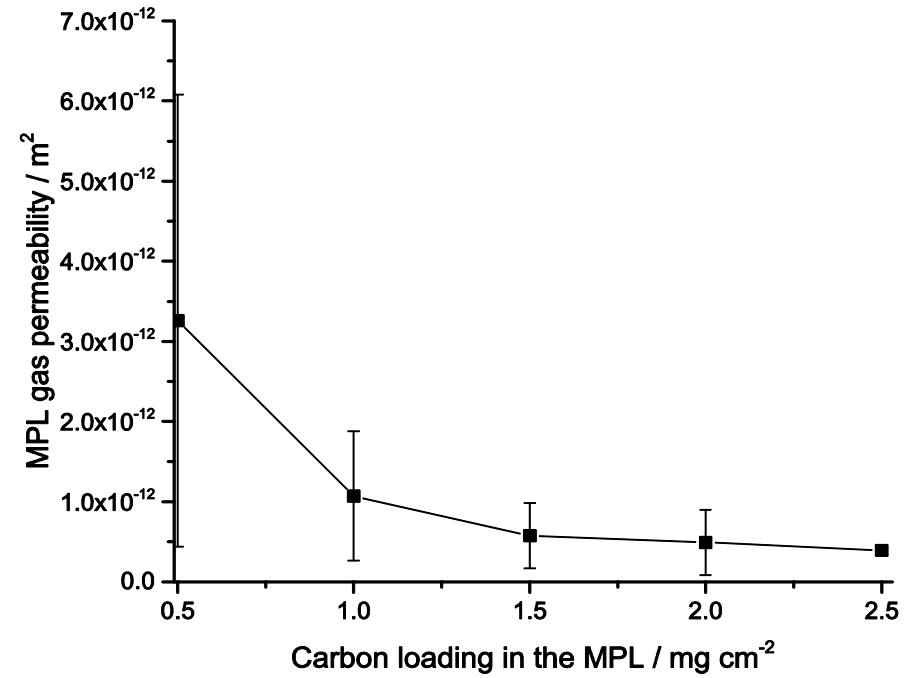


(b) MPL-Vulcan.

Figure 3.22. The measurement error bars of 95% confidence interval for MPL thickness as a function of carbon loading in the MPL with (a) Ketjenblack and (b) Vulcan carbon blacks.



MPL-Ketjenblack



MPL-Vulcan

Figure 3.23. The measurement error bars of 95% confidence interval for gas permeability of MPL as a function of carbon loading in the MPL with Ketjenblack and Vulcan carbon blacks.

3.5. Summary

This chapter has presented the techniques and methodology adopted to experimentally estimate the through-plane gas permeability of the porous gas diffusion media in PEFCs. The experimental techniques explored the materials and methods used for preparing the gas diffusion media, namely MPLs and MPL-coated GDLs. In addition, a new method for preparing the MPL materials and the coating on the porous material (i.e. membrane filter) which is permeable, but does not allow MPL penetration into its pores.

Chapter 4

The effects of Carbon black as the material used for the Microporous Layer of Gas Diffusion Media

A detailed knowledge of the reacting gas transport from the porous gas diffusion media (GDM), namely the gas diffusion layer (GDL) and microporous layer (MPL) to the active site of the catalyst layers is crucial in the performance of polymer electrolyte fuel cells (PEFCs). The performance of the GDM is varied by changing the physical characteristics of the porous media used in PEFCs (Amirinejad et al., 2006). In order to ensure the presence of a sufficient amount of the reactant gases for the reaction in the catalyst layers, the GDM must be able to demonstrate high transport properties (Tamayol et al., 2012, Wu et al., 2012).

Gas permeability is one of transport properties that signals how effective the convective transport is within the porous media used in the membrane electrolyte assembly (MEA) components of the PEFCs (Tadbir et al., 2015 and Lindermeir et al., 2004). However, the comprehensive gas permeability values of the GDL before and after adding MPL, have not been reported in the literature by taking into account the effects of the carbon black loadings and carbon black types. Also, the effects of sintering the MPL on the gas permeability of the coated GDL has not previously been evaluated.

Several studies have been reported on the gas permeability coefficients of the GDLs and MPLs. Wang et al. (2010) reported the correlation between the gas and liquid permeability of some GDLs, and experimentally determined the liquid water saturation level. The gas permeability was measured through the pre-saturated sample, and it increases as the pressure drop displaced by the liquid phase. In addition, the gas

permeability of the GDLs have been measured before and after the wet sample. Also, the saturation level was estimated based on the difference between before and after the wet samples; however, they have not been taken into account the presence of the MPL.

El-kharouf et al. (2012) reported the through-plane gas permeability of the GDL after adding MPL. The results show that adding MPL to the GDL, the thickness, the fibre density and PTFE loading significantly have effects on the gas permeability of the GDL after coating. Also, they have not considered the possible effects of carbon loadings and carbon types, respectively, on the overall thickness of the GDL after coating that affect the gas permeability of the GDLs.

Park et al. (2006) have experimentally investigated the carbon loadings in the MPL coated to the GDL and found that there is a significant influence on the pore diameter and the total pore volume in the GDLs. The results show that by increasing the carbon loading in the MPL, the average pore diameter and total volume of the GDL reduces and the total volume decreases. Clearly, the results indicate the significant effects of the MPL coated to the GDL, but how these affect the gas permeability of the GDL after coating was not reported.

Further, the influence of the uniform distribution of the PTFE loading in the MPL by sintering has on the gas permeability of the MPL-coated GDL was not considered. Jordan et al. (2000) studied the effect of altering the PTFE distribution loading in the MPL. Also, they considered two carbon types, namely Acetylene and Vulcan carbon blacks. They reported that the maximum power density is obtained with a sintered MPL with an Acetylene carbon black of loading 1.9 mg cm^{-2} . The maximum power density of the cells performance was operated with oxygen, while the air operation maximum power density is attained with a loading 1.25 mg cm^{-2} , a sintered MPL with same Acetylene black.

However, there have been no thorough investigations on the effects of carbon types and loadings in the MPL of the coated GDLs gas permeability of GDL before and after coating. Also, taking into account the effects of sintering, the MPL added to the GDL sintering effect has not been considered on the gas permeability of the coated GDL.

In this chapter, the gas permeability of the GDM, i.e. the GDL and MPL used in the PEM fuel cells has been experimentally investigated. In addition, the effects of sintering the MPL with different carbon types of loading on the gas permeability of the coated GDL has been evaluated. In the first stage, the through-plane gas permeability of the carbon substrate both before and after coating, were measured, and in the second stage, the through-plane gas permeability of the coated GDL after sintering was investigated by considering the effects of different carbon types. Finally, the through-plane gas permeability of the MPL has been estimated.

4.1 Through-plane gas permeability of the carbon substrate

In order to investigate the gas permeability of the gas diffusion layers when MPL is present, the through-plane gas permeability of the porous carbon substrate has been measured. Figure 4.1 shows typical scanning electron microscope (SEM) micrographs for the surface of the SGL 10BA carbon substrate before coating. The gas permeability of the GDL before coating was calculated by fitting the experimental data of the pressure gradients as a function of the gas velocity to Equation (3.4). Figure 4.2 shows a typical pressure gradient as a function of the gas velocity used to estimate the gas permeability.

The average thickness of 30 carbon paper samples was estimated to be about 370 ± 40 μm . The averaged through-plane gas permeability for the carbon substrate tested samples was found to give a gas permeability value of the GDL before coating to be 2.08 ± 0.33

$\times 10^{-11} \text{ m}^2$. This value is in good agreement with those reported in the literature for the same substrate, namely $1.80 \times 10^{-11} \text{ m}^2$ Ithonen et al. (2004). On the other hand, the value is lower than $2.72 \times 10^{-11} \text{ m}^2$ as reported by Ismail et al. (2011), and $3.74 \times 10^{-11} \text{ m}^2$ Gostick et al. (2006).

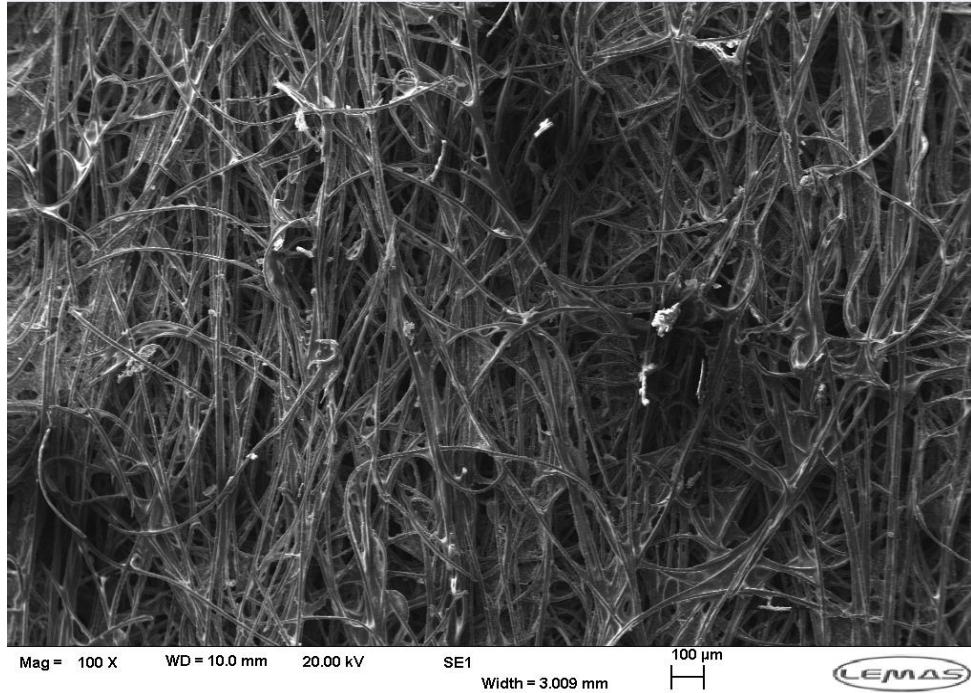


Figure 4.1. A typical SEM image for the surface area of a SGL 10BA carbon substrate.

4.2 Through-plane gas permeability of MPL-coated GDLs

The through-plane gas permeability values of the coated GDLs with MPL for two types of carbon black loadings have been determined. The effects of the carbon loading and carbon type in the MPL on the gas permeability of the MPL-coated GDLs have been investigated. Figure 4.3 shows a typical SEM image for the surface of a GDL after coating with MPL. It is worth noting that the PTFE loading in the MPL is kept constant

at 20 wt.%, as this is a value frequently used in the literature, Kitahra et al. (2010), Park et al. (2006) and Uchida et al. (1995).

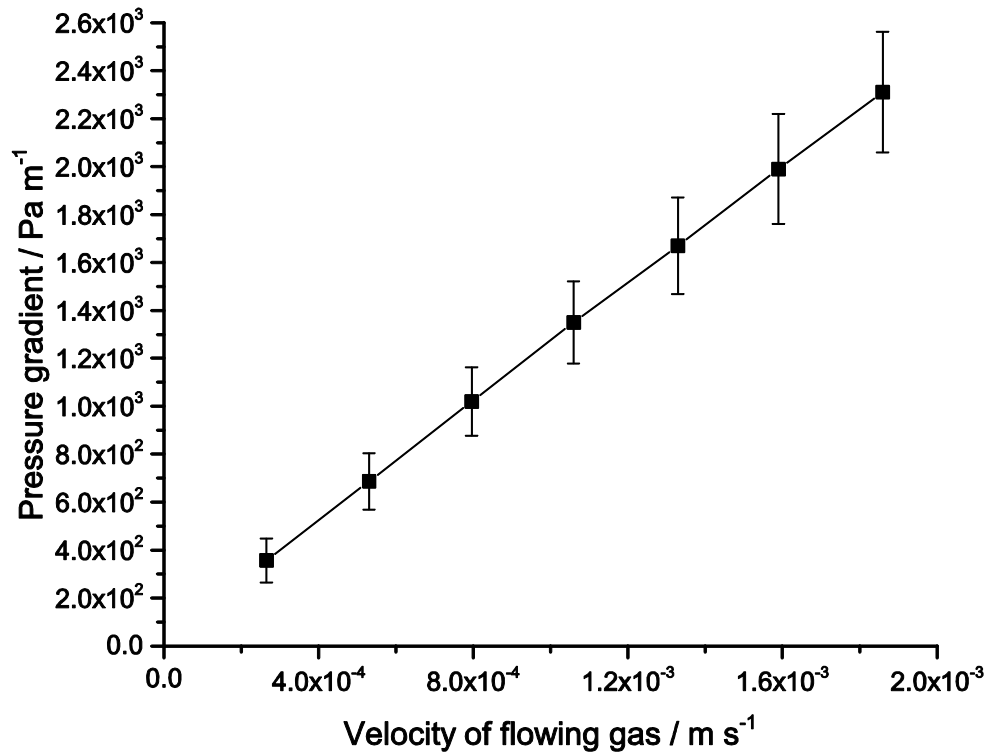


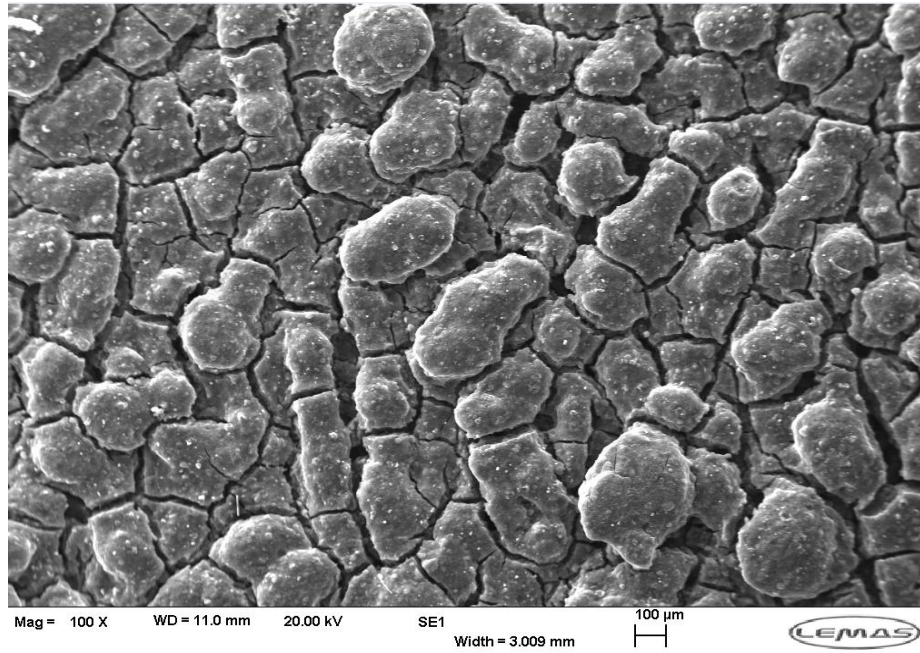
Figure 4.2. Measured pressure gradient as a function of the gas velocity for a SGL 10BA sample. The solid line represents the linear pressure gradient-velocity curve.

Figure 4.4 presents the experimental data of the pressure gradient-velocity curve for the GDLs after coating with various carbon loadings for Ketjenblack carbon black. Also, Figure 4.5 shows experimental data of the pressure gradient as a function of the gas velocity for the MPL-coated GDLs with various carbon loading of Vulcan carbon black. However, the pressure gradients of each set of set tested samples are linear and increases as the carbon loadings in the MPLs increases, and the distributions are shown in the form of 95 % confidence intervals, see Figure 3.19 (Chapter 3).

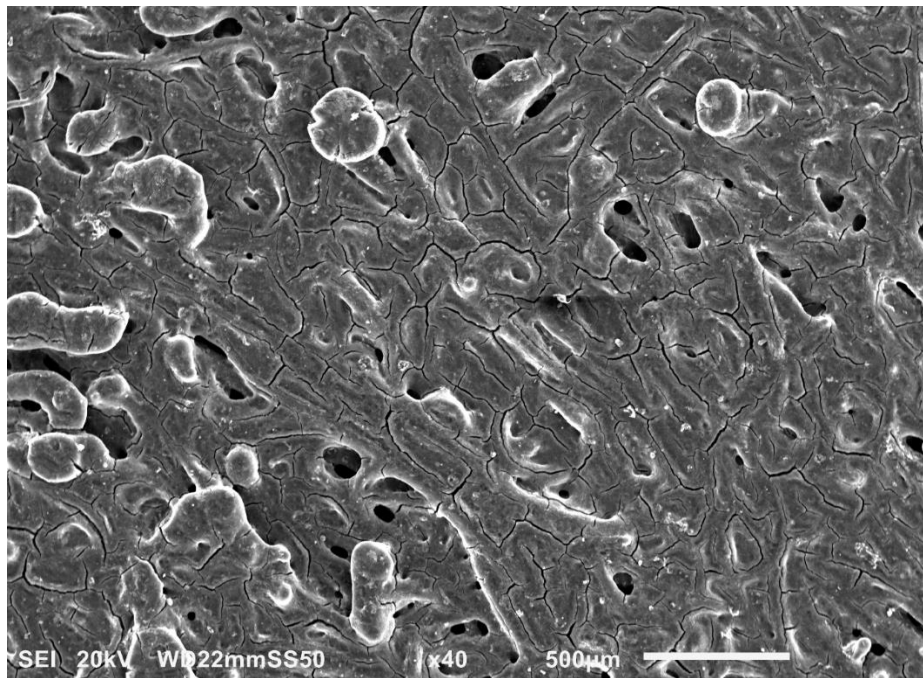
The gas permeability values for the MPL-coated GDL samples were calculated using Equation (3.4). From the curves, the experimental data shows a linear trend of the gas pressure gradients as the velocity of the gas flow increases, see Figures 4.4 and 4.5. These figures indicate that, for the given velocity, the pressure gradient increases as the carbon loading increases in the MPL. This is as a result of the increases in the thickness as the carbon loading increases in the MPL. The gas permeability value is the average gas permeability for six samples of the same carbon loading in the MPL. Further, a comparison is made for various carbon loadings in the MPL with two different carbon types that are discussed in Sub-section 3.2.1, which is based on the carbon types utilised in this thesis.

4.2.1 Effects of carbon loading

The significant effects of the carbon loading in the MPL on the gas permeability of MPL-coated GDLs is the increase in the total thickness of the coated GDL. The value of the thickness was obtained by using Equation (3.8). As the carbon loading in the MPL gradually increases from 0.5 to 2.5 mg/cm² of carbon black, the corresponding thickness of the coated GDL increases. Figure 4.6 indicates the total thickness of the coated GDLs as a function of carbon loading in the MPL. Given that the averaged thicknesses of the coated GDLs attained are 414 ±11, 435 ±18, 488 ±17, 497 ±20, 519 ±34 μm with MPL carbon loadings of 0.5, 1.0, 1.5, 2.0 and 2.5 mg/cm², respectively. This shows that the gas travel paths across the porous layers of the coated GDLs increases as the carbon loading increases and the corresponding thickness of the coated GDL. The indicated trend of the increase in the amount of carbon loading in the MPL increasing the thickness of the MPL-coated GDL is in agreement as reported by Liu and Chang (2013) and Ko et al. (2010).



(a)



(b)

Figure 4.3. Typical SEM image for the surface area of the MPL-coated GDL sample, (a) MPL-coated GDL with Ketjenblack carbon black, and (b) MPL-coated GDL with Vulcan carbon black.

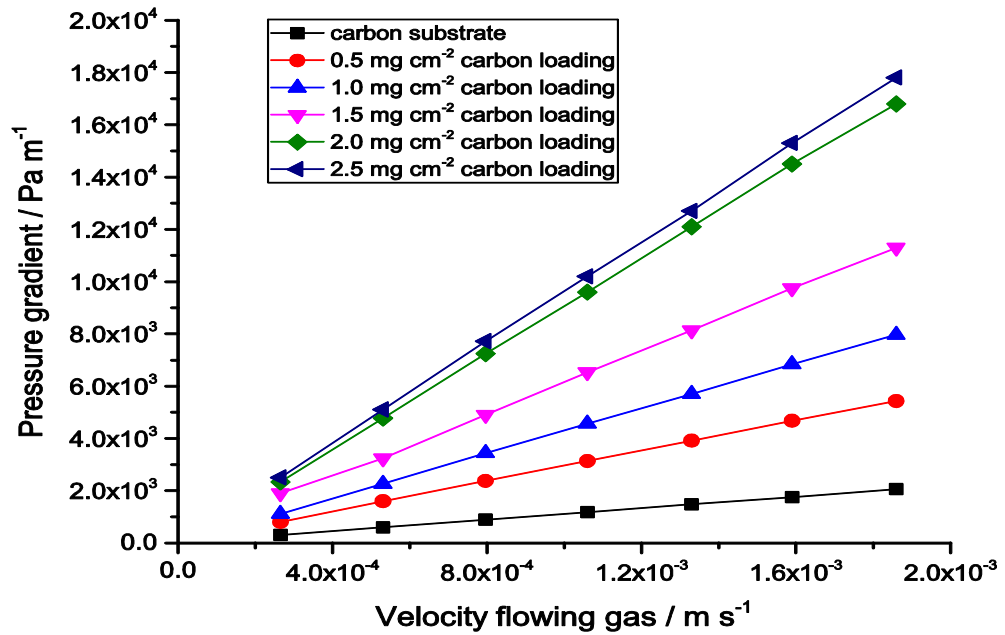


Figure 4.4. Measured pressure gradient as a function of the nitrogen gas velocity for the MPL-coated carbon substrates with various carbon loadings in the MPL for 20 wt.% PTFE, and before and after, coating the GDL with MPL using Ketjenblack carbon black.

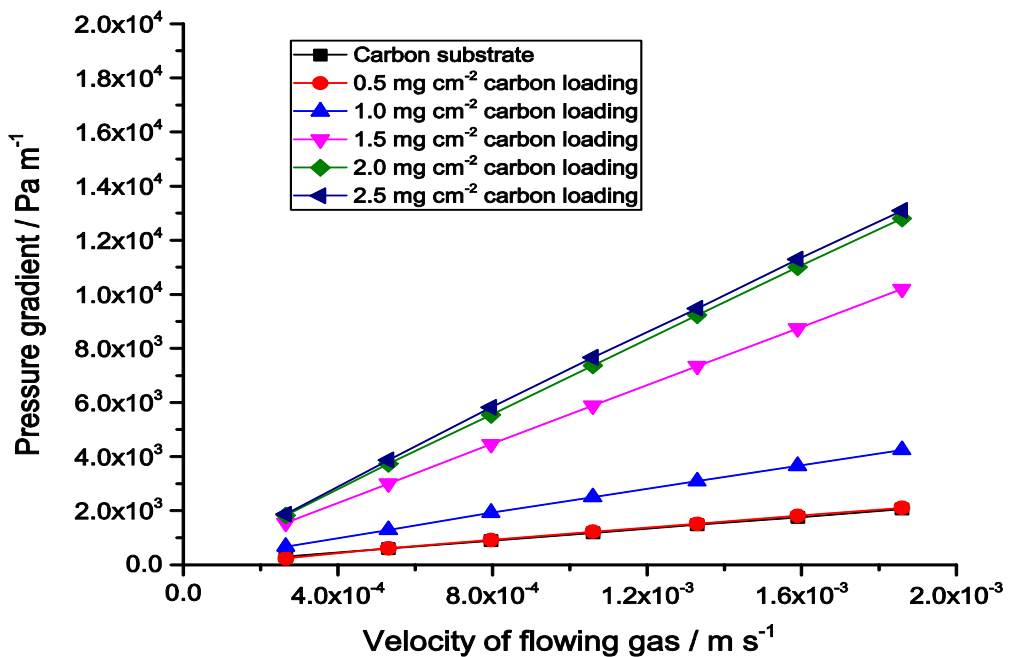


Figure 4.5. Measured pressure gradient as a function of the nitrogen gas velocity for the MPL-coated carbon substrates with various carbon loadings in the MPL of 20 wt.% PTFE, and before and after, coating the GDL with MPL using Vulcan XC-72R carbon black.

The gas permeability values of the MPL-coated GDLs are displayed with a progressive and rapid decrease in the averaged gas permeability of the GDLs after coating. Figure 4.7 shows the through-plane gas permeability as a function of the carbon loading in the MPL for the coated-GDLs after coating. This indicates that, as the MPL carbon loading increases, the total GDL thickness increases after coating and clearly, the gas permeability of the coated GDL decreases.

Furthermore, the gas permeability reduces as the carbon loading in the MPL increases as a result of an increase in the pressure drop of the MPL-coated GDL. The resistance of the flowing gas across the MPL-coated GDL increases as the carbon loading increases, Figures 4.4 and 4.5. This clearly indicates that changing in the properties of the GDL before and after coating, namely the porosity and pore size distribution have been attributed to the changes in the MPL properties, such as the micro-pores, meso-pores and macro-pores by the carbon black loading in the MPL (Park et al., 2006, Chen and Chang, 2013). However, the gas permeability of the GDL after adding the MPL decreases as the capillary pressure of the coated GDL decreases based as the carbon loading increases in the MPL (Pharoah, 2005, Tamyol et al., 2012, Kim et al., 2013). The gas permeability values of the MPL-coated GDLs are lower than those of the base carbon substrate by an order of magnitude at the 95 % confidence intervals (Figure 3.20) .

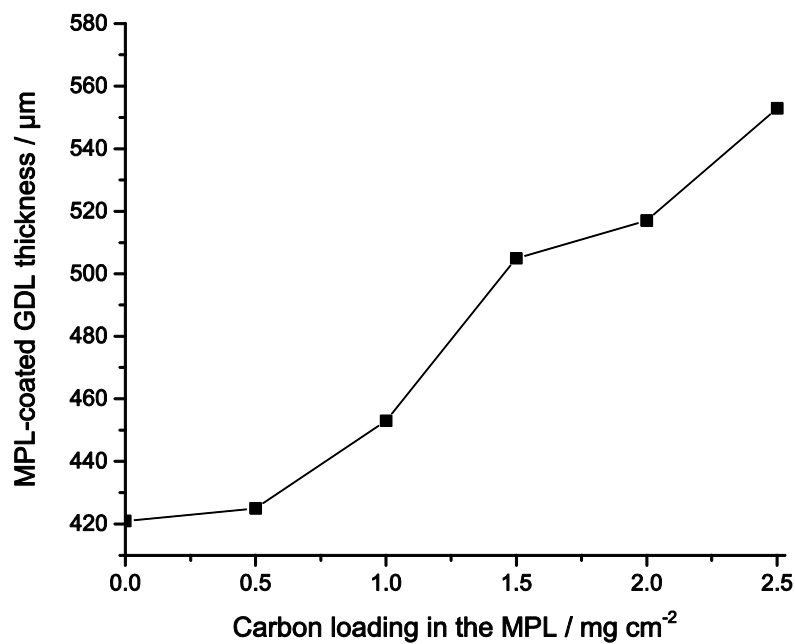


Figure 4.6. Thickness of the carbon substrate before and after coating.

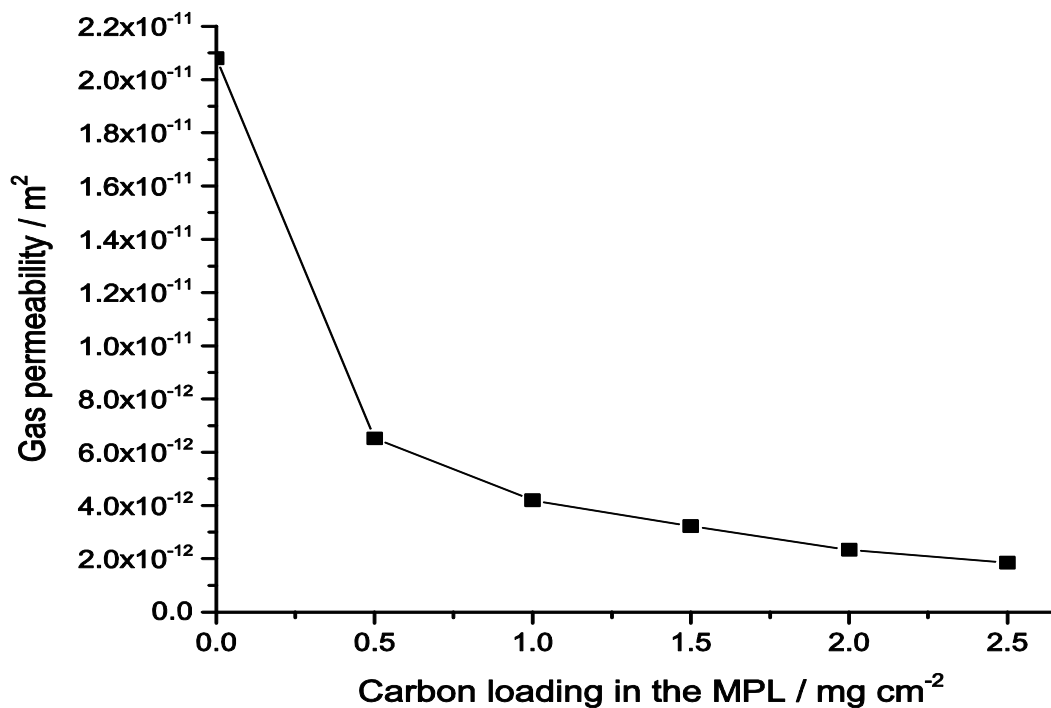


Figure 4.7. Through-plane gas permeability of the MPL-coated GDLs with various amounts of carbon loading in the MPL with 20 wt.% PTFE.

4.2.2 Effects of carbon black type

Figure 4.8 illustrates the thicknesses of the MPL-coated GDLs investigated measured using the MPLs loaded with various amounts of the two carbon blacks, namely Ketjenblack and Vulcan carbon blacks. It shows that the use of the MPLs with Vulcan carbon black coated GDL thickness is less compared to the MPLs with Ketjenblack carbon black coated GDL. This is as a result of the MPL dispersion and the penetration into the carbon substrate (Jordan et al., 2000 and Kitahara et al., 2010), and the characteristic properties of the MPL structure based on the carbon black structure, such as the breadth of the pore size distribution that is loading in the MPL (Prasanna et al., 2004 and El-kharouf et al., 2013). Clearly, the thickness of the MPL increases as the loading of the carbon powder increases in the MPL that is adding to the surface of the carbon substrate.

The through-plane gas permeability values of the GDL after coating with the different MPLs of different carbon types have been determined. Figure 4.9, presents the through-plane gas permeability as a function of the carbon type that is the loading in the MPL. The distributions of raw data for all carbon loadings in the MPL on the results are shown in the form of 95 % confidence intervals, see Figures 3.18 and 3.20. Also, the standard deviations for each data points in the figures and the results are tabulated in Appendices C and D. The gas permeability of the coated GDLs with MPLs made of Vulcan carbon black have higher values compared to the MPL-coated GDLs with Ketjenblack carbon black. Clearly, the results indicate that the properties of the carbon blacks utilised affect the properties of the MPLs, such as the micropores, mesopores and macropores (Park et al., 2006, El-kharouf et al., 2012).

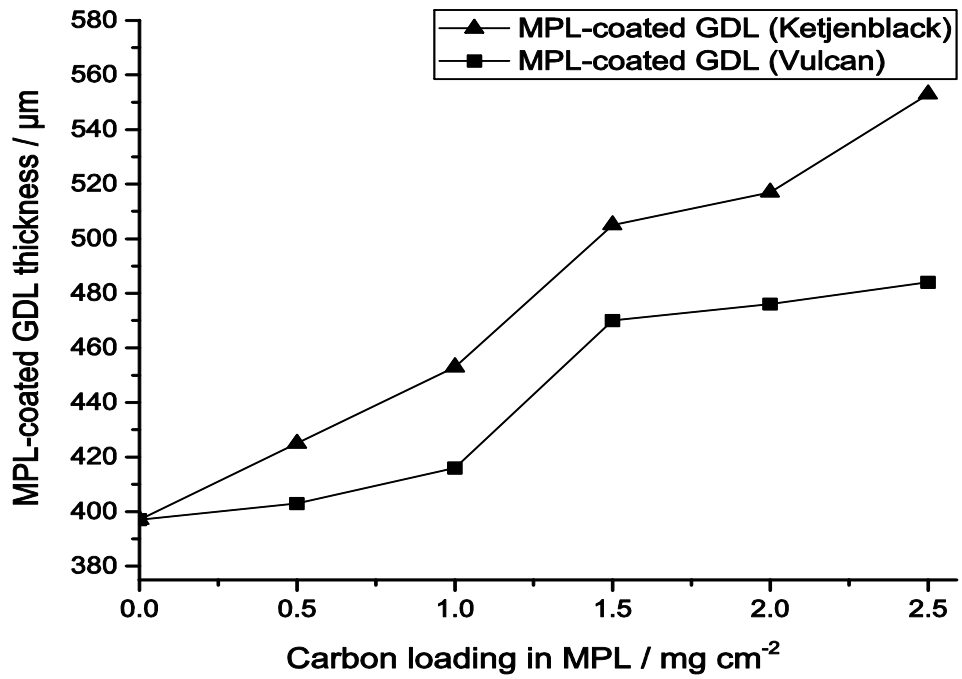
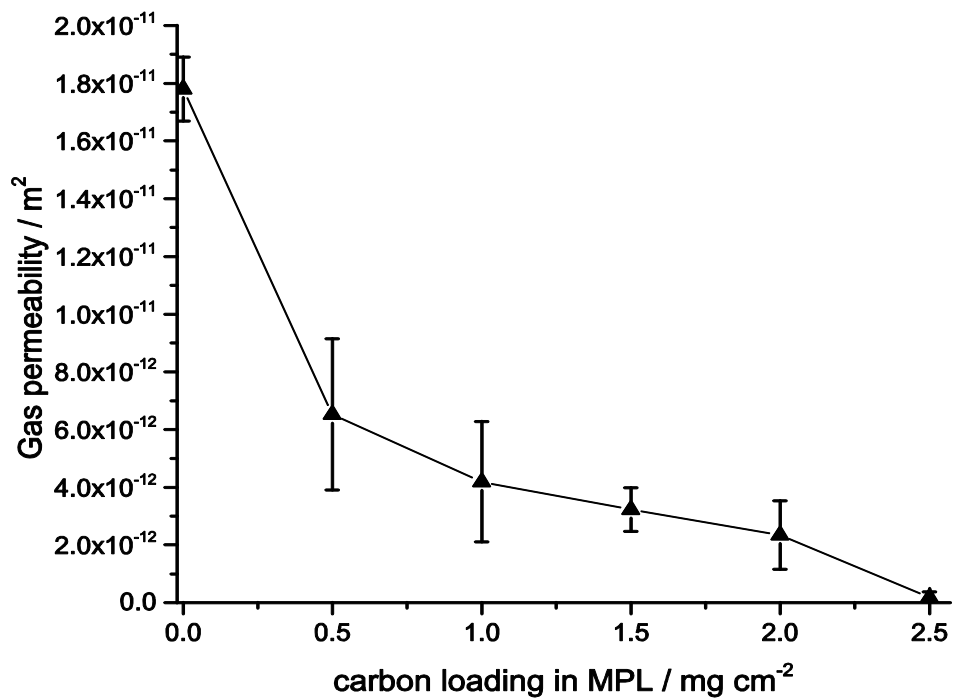
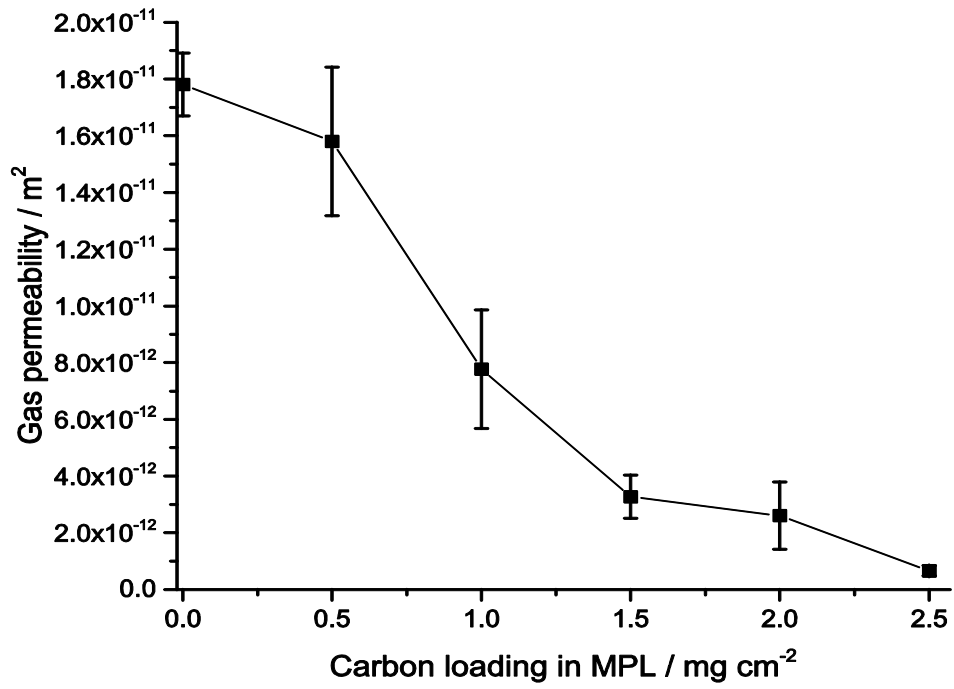


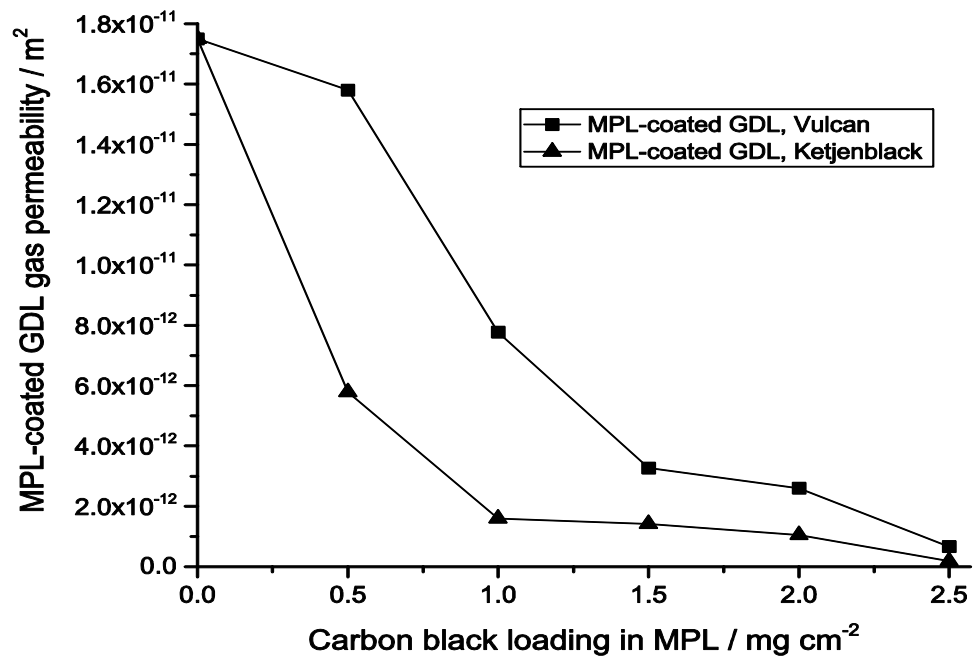
Figure 4.8. MPL-coated GDL thickness as a function carbon loading in the MPLs. Two different carbon types, ▲ Kejenblack carbon black and ■ Vulcan XC 72R carbon black.



(a)



(b)



(c)

Figure 4.9. Through-plane gas permeability as a function of carbon loading of coated GDLs for different carbon black type loadings in the MPL, (a) ▲ Kejenblack carbon black and (b) ■ Vulcan XC 72R carbon black.

4.3 Effects of sintering

Figure 4.10 shows the gas permeability of the MPL-coated GDL before and after sintering. The results show that, regardless of the carbon loading and carbon black used in the MPL, the through-plane gas permeability of the coated GDLs decreases after sintering. This is as a result of the uniform distribution of the PTFE loading in the MPL. The gas permeability of the coated GDLs for the loading 0.5 mg/cm^2 of Ketjenblack carbon black slightly decreases after sintering but significantly reduces for the loading Vulcan carbon black. For a carbon loading 2.5 mg/cm^2 in the MPL of both types of carbon blacks, the gas permeability slightly decreases after sintering.

Further, these results indicate that when the carbon loading is varied and the PTFE loading is kept constant, sintering the MPL with higher carbon loading from 2.5 mg/cm^2 has a negligible influence on the gas permeability of the coated GDL. However, the most likely spreading effect that sintering has on the MPL material is clear in loadings from 0.5 mg/cm^2 (Vulcan) to 1.5 mg/cm^2 for both type of carbon black, respectively. This is most likely due to the physical properties and uniform distribution of the PTFE within the MPL, see Figure 4.11. Additionally, sintering narrows down the cracks that exist in the MPL (due to the above mentioned spreading effect) and which eventually increases the gas (mass) resistance.

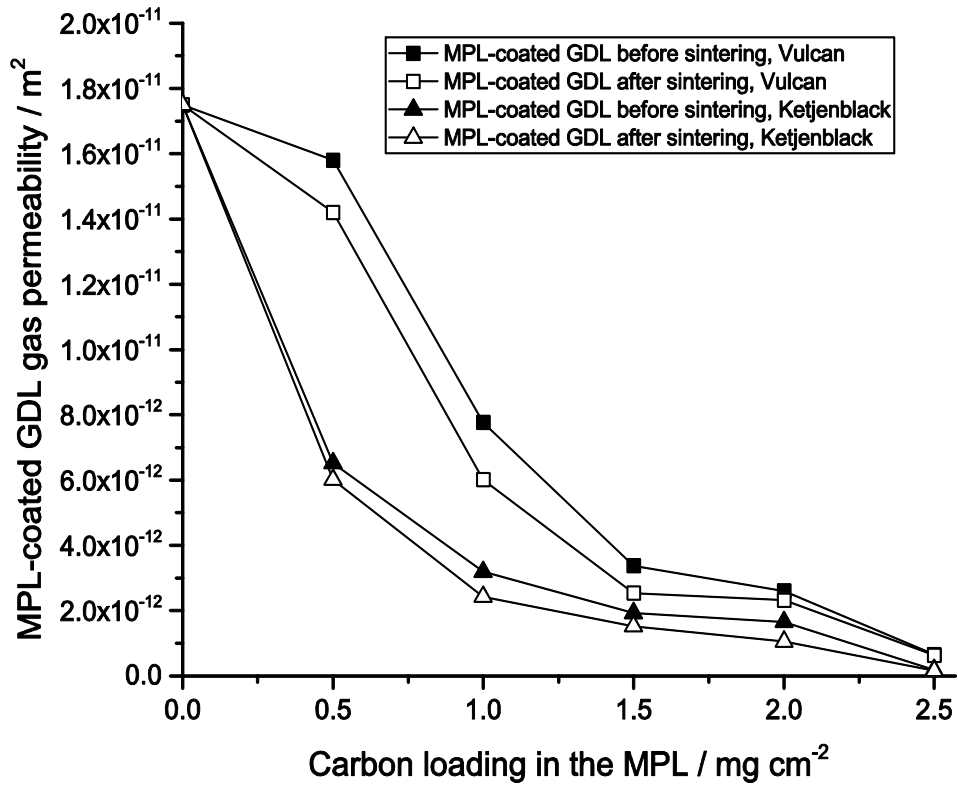
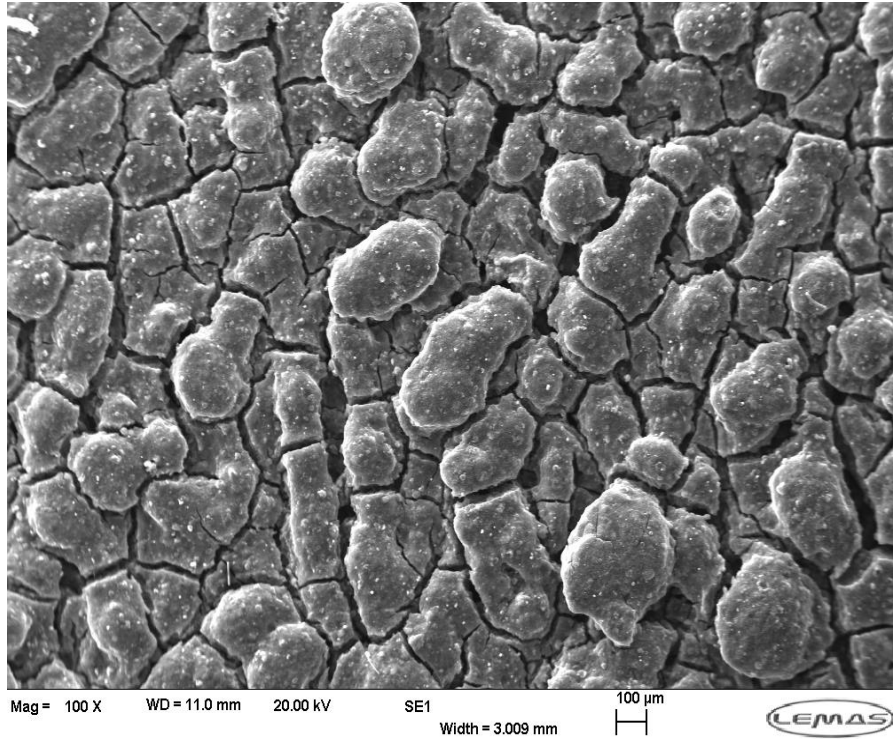
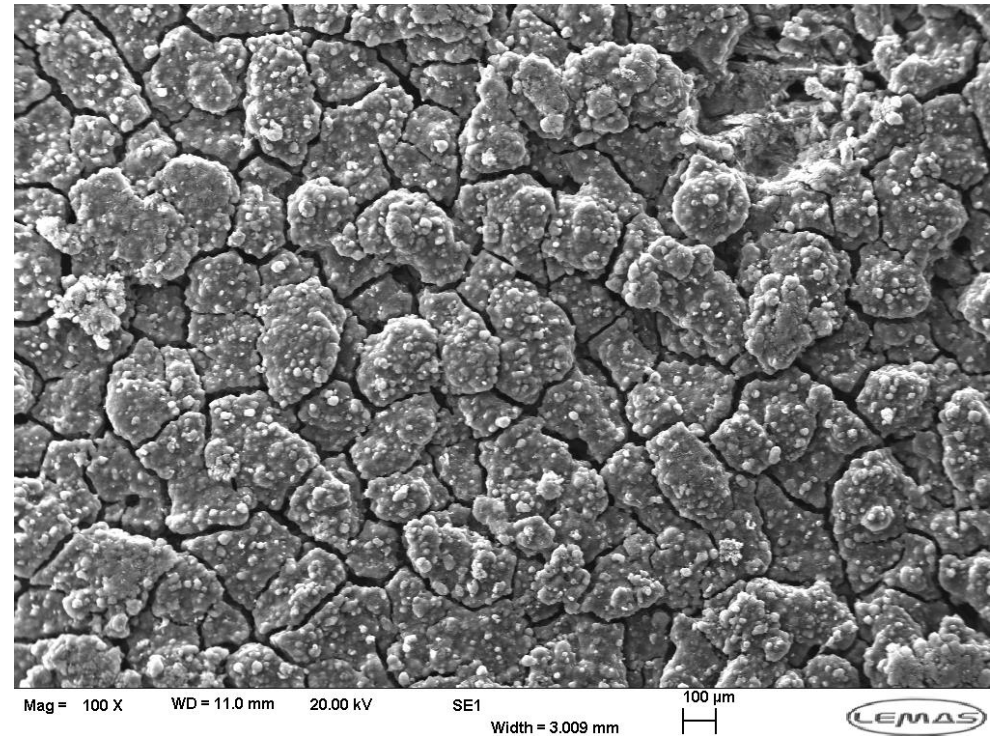


Figure 4.10. Through-plane gas permeability of MPL-coated GDLs before and after sintering as a function of carbon loading in the MPL, for comparison of the effects of sintering on the MPLs coated on GDLs with 20 wt.% PTFE.

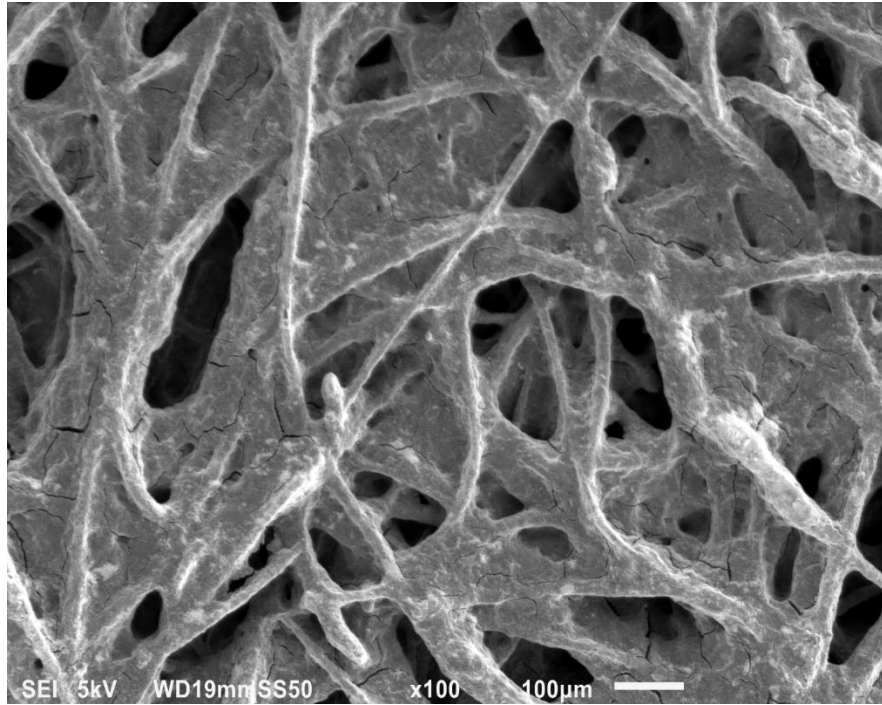


(a)

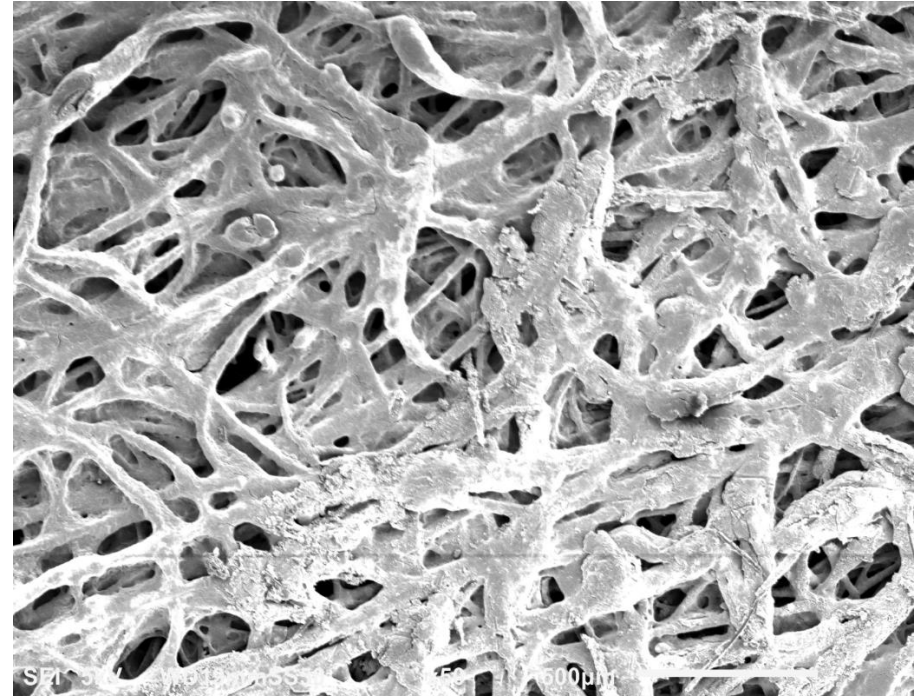


(b)

Figure 4.11. SEM images for the MPL with 1.5 mg/cm² Ketjenblack of 20 wt.% PTFE carbon loading (a) before sintering, and (b) after sintering.



(a)



(b)

Figure 4.12. SEMs images for the MPL with 1.5 mg/cm² Vulcan of 20 wt.% PTFE carbon loadings (a) before sintering, and (b) after sintering.

4.4 Through-plane gas permeability of MPLs

The gas permeability values of the MPLs (microporous layers) that are coated onto the surface of the carbon substrates have been estimated and compared when using both Ketjenblack carbon black and Vulcan carbon blacks as materials for the MPLs. Equation (3.8) was used to estimate the through-plane gas permeability of the MPLs of coated SGL 10BA samples. The thickness of the MPL, and all the other parameters required to estimate the gas permeability of the MPL, were determined as explained in Chapter 3 (Sections 3.1 and 3.2).

Figure 4.13 shows the MPL thickness values as a function of the carbon loading in the MPL. In Yu et al. (2005), the procedures adopted for the MPL thickness have been estimated in this study through the use of cross-sectional SEM images of the coated GDLs, see Figure 4.13. It clearly indicates that the thickness of the MPL increases as non-independent carbon type but as carbon loading in the MPL. However, there is a significant difference in the MPL with Ketjenblack carbon black material and MPL with Vulcan carbon black thicknesses, which are based on the carbon types that have been used as materials for the MPL, i.e. the MPL with Vulcan black thickness is less than that of the Ketjenblack carbon black (MPL). These results indicate that the properties of the carbon type used affects the MPL coated onto the substrate, namely the thickness, dispersion and density, pore size, pore volume and distribution, see Table 3.3 (Prasanna et al., 2004, El-kharouf et al., 2012). Further, it is clear from the Figure 4.13 that the thickness of the coated MPL is varies widely for the different carbon black types.

The effects of the MPLs with the different carbon blacks used in PEFCs (polymer electrolyte fuel cells) on the gas permeability of the porous layers, by considering the thickness, have been investigated, see Figure 4.15. Clearly, from this figure the gas

permeability of the MPL with Ketjenblack is higher compared with that of the Vulcan MPL (Figure 4.15), and this may be due to the effects of the thickness and the carbon blacks that significantly affect the through-plane permeability of both the MPLs.

Furthermore, the gas permeability of the MPL decreases with increasing the carbon loading, but, this should not be the case due to uncertainty estimation of the MPL thickness. Regardless, of the carbon loading, the gas permeability values should ideally have been the same values for all the coated samples. Since the composition of the MPLs is the same for all the MPLs: 80 wt.% carbon loading and 20 wt. % PTFE content. In other words, the MPL material does not change as the carbon loading changes. Therefore, its gas permeability value should be ideally the same as the latter is an intrinsic property of the material, Ismail et al. (2010). This signifies that the current approach of estimating the MPL gas permeability, by either using a micrometre or cross-sectional images of the MPL-coated GDLs, it appears to lead to rather inaccurate results. This is most likely due to the significant penetration of the MPL materials into the body of the carbon substrates which leads to an uncertainty in the estimation of the MPL thickness.

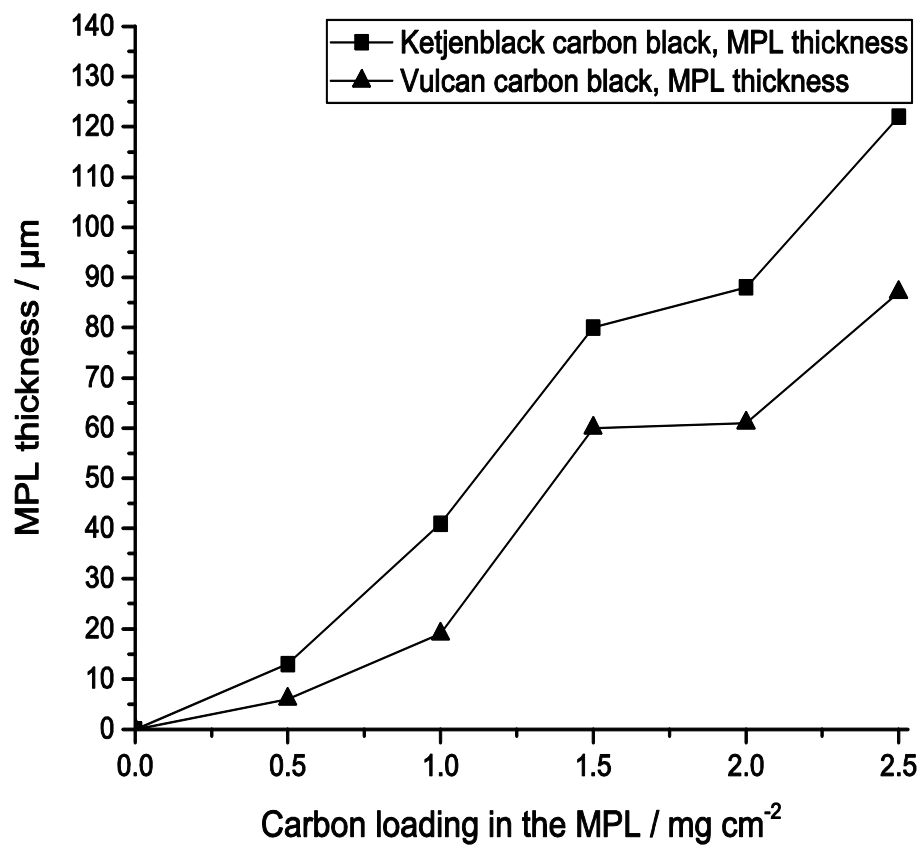


Figure 4.13. MPL thickness as a function of carbon loading in the MPL for (a)▲ Ketjenblack carbon black and (b)■ Vulcan carbon black as materials for the MPLs.

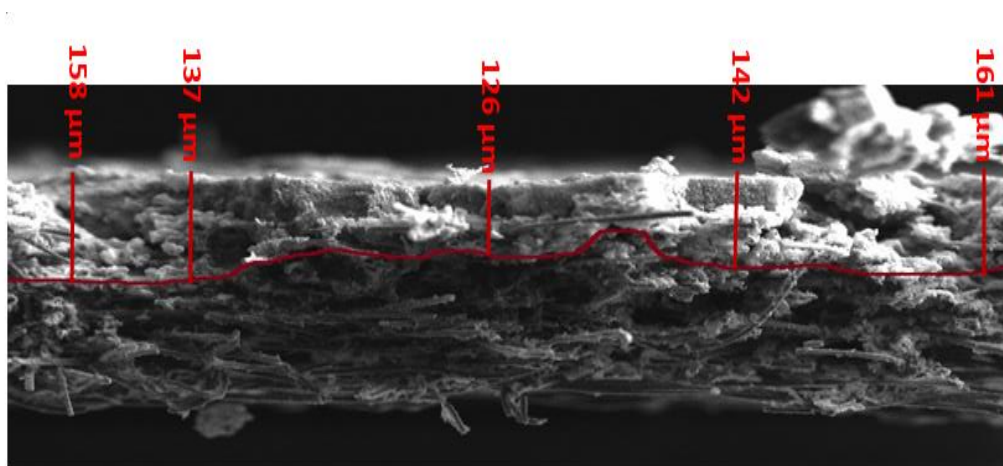


Figure 4.14. A typical SEM cross-sectional micrograph of an MPL-coated GDL for MPL with Ketjenblack carbon black.

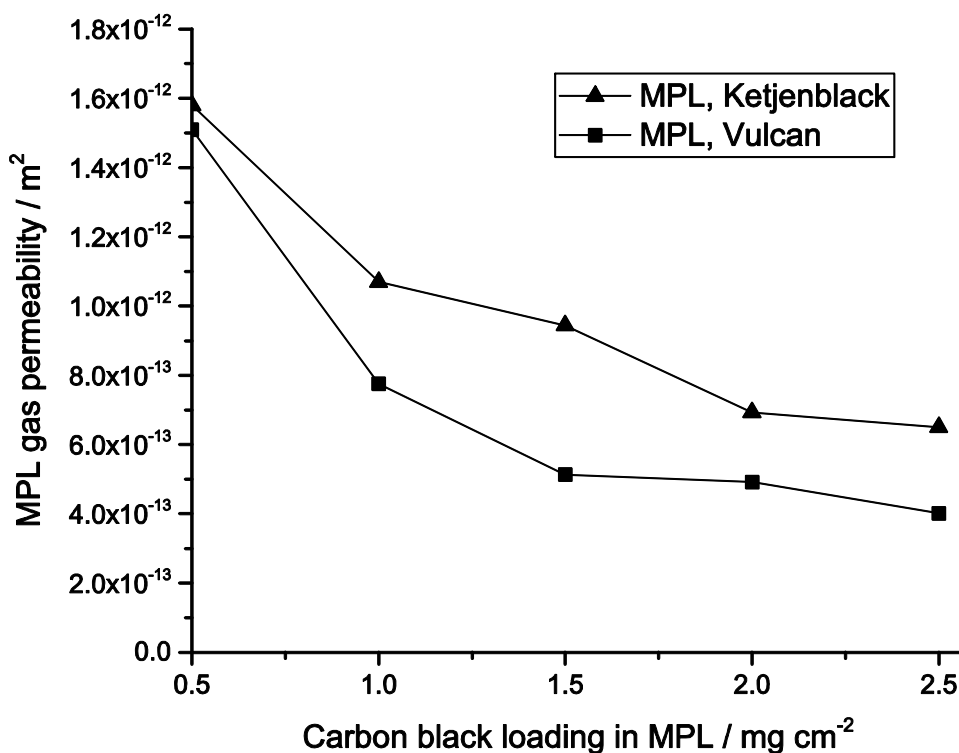


Figure 4.15. Through-plane gas permeability of the MPL as a function of carbon black loading in the MPL with two different carbon blacks (a) Ketjenblack carbon black and (b) Vulcan carbon black.

4.5 Conclusions

The through-plane gas permeability of the gas diffusion media and sintering have been experimentally investigated. The gas permeability of the GDLs coated with MPLs having various carbon loadings have been estimated using two types of commonly-used carbon blacks, namely Ketjenblack and Vulcan carbon black.

The gas permeability of the MPL was estimated through employment of (i) the measured permeability and thickness of the GDL before and after the MPL-coating, and (ii) the cross-section SEM images of the coated GDLs to estimate the thickness of the MPLs.

The main conclusions from this study are as follows:

- The MPL-coating reduces the gas permeability of the GDL by at least one order of magnitude and this is clearly due to the significantly lower gas permeability of the MPLs.
- The gas permeability of the MPL was found to change significantly with the carbon loading, despite the use of the invariable weight composition for all the MPLs coated, namely 20 wt.% PTFE and 80 wt.% carbon black. This is mainly due to the inaccurate estimation of the MPL thickness using either the micrometre or the cross-sectional images SEM of the coated GDL which do not account for the penetration part of the MPL.
- The MPL sintering was found to slightly decrease the gas permeability of the GDL as it appears to narrow the gaps between the cracks in the MPL.
- Finally, it should be noted that all of the findings in this study are applicable to both the carbon blacks investigated. Also, the gas permeability of the MPL-coated GDLs with Ketjenblack carbon black is less than that of the MPL-coated GDLs with Vulcan carbon black. While, in order of the MPLs, the gas permeability of the MPL with Vulcan carbon black is higher compared with that of the Ketjenblack carbon black, see Figures 4.9 and 4.14.

This study has highlighted the need to accurately determine the effects of the MPL thickness and the penetration into substrate, despite the fact that the carbon black type is non-independent of the carbon loading in the MPL. In addition, the composition of the MPL effects on the through-plane gas permeability of the porous gas diffusion media used in the PEFCs and requires further investigation.

Chapter 5

The Effects of the Composition of the Microporous Layer on the Through-plane Gas Permeability of the Gas Diffusion Media

As a result of the experimental studies which were performed on the effect of carbon black loading in the microporous layer (MPL) on the through-plane gas permeability of the coated gas diffusion layer (GDL) in Chapter 4, and in order to understand the effects of the composition of the MPL coated GDL, the effects of the polytetrafluoroethylene (PTFE) loading in the MPL with various carbon loadings have been investigated in this thesis.

It is common practice to treat GDLs with MPL coating for better transport phenomena within the GDLs used in polymer electrolyte fuel cells (PEFCs). The composition of the porous gas diffusion media (carbon substrates and microporous layers) plays an important role on the performance of the cells, Ramasamy et al. (2008) and Kim et al. (2013).

Velayutham et al. (2007) investigated the effect of the PTFE loadings in the porous gas diffusion layers (carbon substrate and microporous layer) of the MEAs on the performance of the PEMFC (polymer electrolyte membrane fuel cell) tested under ambient pressure. They reported that the MEAs with microporous layer of 20 wt.% of PTFE performed better compared with those loadings of 10 and 32 wt.% PTFE, respectively. The carbon loading in the MPL has been kept constant, and the comparative loadings of both the PTFE and carbon in the MPL by considering different amounts of carbon loadings have not been taken into account in this case.

Park et al. (2008) studied the effects of the PTFE loading in the MPL on the proton exchange membrane (PEM) fuel cell water management. They measured the cumulative

pore volumes in the GDLs after coating for different PTFE loadings in the MPLs. The amount of PTFE content in the MPL was varied from 10, 20, 30 and 40 wt.%, and the carbon loading was kept constant at 2.0 mg/cm². They reported that the cumulative pore volume in the pore size of the MPL reduces from 30 to 0.01 μm with increases in the PTFE loading in the MPL as a result of decreases in the porosity of the MPL. In addition, as the PTFE loading in the MPL varies, that is, increases from 10 to 40 wt.%, the threshold pressure value for the liquid water flow increases from 1.8 to 3.5 kPa. However, they did not determine the effect of different PTFE contents and carbon loadings in the MPL on the gas permeability of the GDLs after coating.

Further, Kim et al. (2013) studied the effects of the microstructure and carbon black compositions of the MPL in a direct methanol fuel cell. Their investigations focused on the important roles that the MPL plays in the anode side of the cell and considered the control of the water transport and the gas (methanol) on the performance of the MEA under the operation of highly concentrated methanol. They reported that the gas permeability of the gas diffusion layers (GDLs) after coatings was significantly dependent on the cracks in the MPLs compared with the thickness of the MPLs which is based on the effects of the different carbon black types of compositions in the MPLs. In their report, the PTFE loadings was kept constant at 25 wt.%, however, the effect of the amount of Vulcan XC 72R carbon black used has not been taken into account.

Chen and Chang (2013) experimentally investigated the effects of the composition of MPL at the cathode side and considered the PTFE and carbon black loadings on the performance of the PEMFC. The performance of the PEMFC was evaluated under different relative humidity at the air inlet. They reported that the optimal performance of the cell depends on the MPL composition with 1.5 mg/cm² carbon black and 20 wt.%

PTFE loadings at different air relative humidity. Also, they noted that increasing the PTFE loading in the MPL improves the performance of the cell at a lower relative humidity state. However, the effect of the relative amount of carbon black types and PTFE loading in the MPLs on gas permeability of the gas diffusion media in their experiments is unclear.

Mangal et al. (2015) experimentally studied the mass transport in a PEMFC by investigating the through-plane permeability and molecular diffusivity in the GDLs. They found that an increase in the PTFE loadings in the GDLs have a significant effect, either “positive” or “negative”, on the permeability and diffusivity. However, they did not consider the relatively matching PTFE – carbon loadings in the MPL, and the effect of the carbon black types have not been taken into account.

In general, it is clear that the illustrated literature review highlights the lack of in-depth experimental investigations of the effects of the composition of the microporous layer (MPL) on the through-plane gas permeability of MPL-coated GDLs of the PEMFCs. In the present study, the through-plane gas permeability of the GDLs after coating with the MPL has been investigated, considering the effects of the composition of the MPL added to the GDLs. In addition, the effects of the PTFE loadings in the MPL with two different carbon types, namely Ketjenblack EC-300JD and Vulcan XC-72R have been presented and discussed in detail in this chapter.

5.1 PTFE loading in the MPL

Figures 5.1 and 5.2 show the experimental data for the pressure gradient as a function of velocity of flowing gas (nitrogen) across the MPL-coated GDLs with different compositions of the MPLs. The carbon loadings in the MPL varied from 0.5, 1.0, 1.5, 2.0

and 2.5 mg/cm^2 , and also the PTFE loadings varied between 0 and 50 wt.%. Two different carbon blacks have been used in this study, namely Ketjenblack EC-300JD and Vulcan XC-72R. It is observed that at a given velocity, the pressure gradient curve is linear. The pressure gradient curves for the MPL-coated GDLs with 0.5 mg/cm^2 carbon black with various PTFE loadings of the two carbon black types have been considered.

In Figure 5.1, the MPL-coated GDLs have a minimum pressure gradient at 20 wt.% PTFE loading and maximum pressure gradient observed at 30 wt.% PTFE loading in the MPL. Also, it is shown that the MPL-coated GDLs with 0 wt.% PTFE and the substrate have mostly the same values for the pressure gradient and they are between 20 and 50 wt.% PTFE of the MPL-coated GDLs. Whilst the pressure gradient values of 10 and 40 wt.% PTFE loading in the MPL-coated GDLs are slightly closer in magnitude and both the coated GDLs are below the MPL-coated GDLs of 30 wt.% PTFE and above the MPL-coated GDL of 50 wt.% PTFE, respectively. However, the pressure gradient values of the MPL-coated GDLs indicate the significant loading of the PTFE when the carbon loading is kept at a constant value in the MPLs.

Figure 5.2 shows that the minimum pressure gradient is observed in the substrate, and a maximum pressure gradient is exhibited in the MPL-coated GDLs with 40 wt.% PTFE loading in the MPLs, respectively. The significant variations in the pressure gradient values shown in both figures is as a result of the carbon black characteristic property that affects the porosity of the treated gas diffusion layers used in the polymer electrolyte fuel cells (Ramasamy et al., 2008). Similar results are also obtained at the other compositions with higher carbon loadings, see Table 5.1.

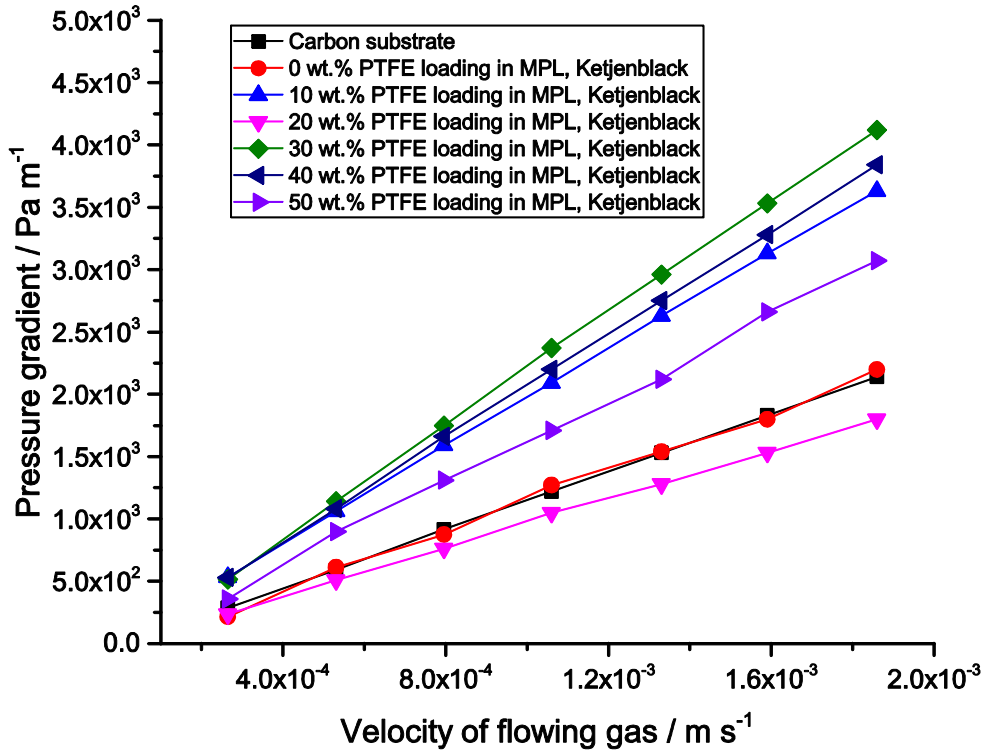


Figure 5.1. Measured pressure gradient as a function of the nitrogen gas velocity for the MPL-coated carbon substrates with different PTFE loadings in the MPL for 0.5 mg/cm² Ketjenblack carbon black.

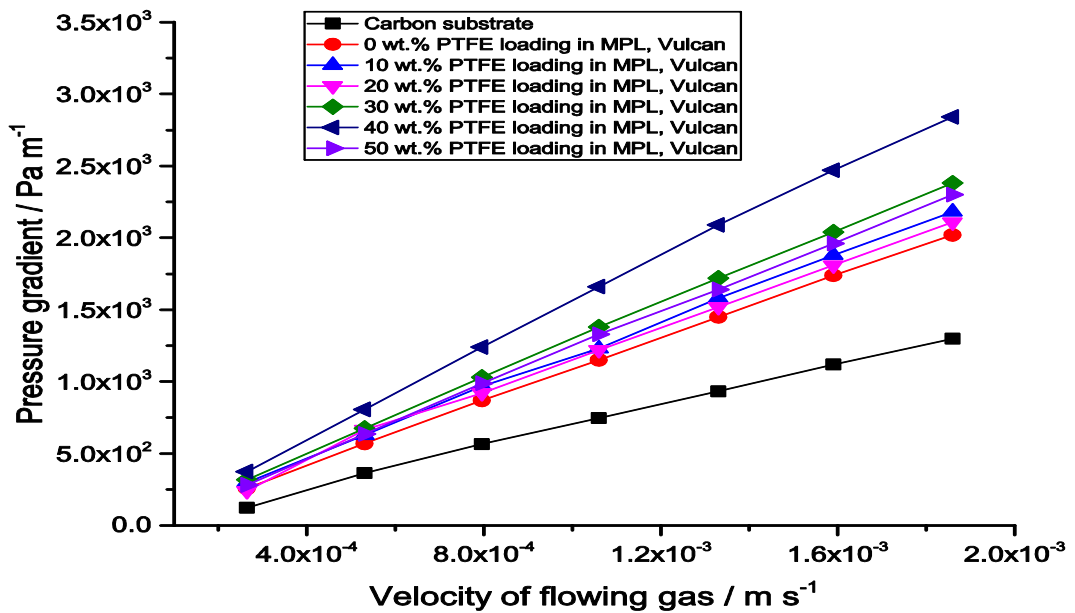


Figure 5.2. Measured pressure gradient as a function of the nitrogen gas velocity for the MPL-coated carbon substrates with different PTFE loadings in the MPL of 0.5 mg/cm² Vulcan carbon black.

Table 5.1. The through-plane gas permeability of the MPL with Ketjenblack and Vulcan carbon blacks.

Carbon loading, mg/cm ²	PTFE loading, wt.% and gas permeability, m ²											
	0		10		20		30		40		50	
	Ketjenblack	Vulcan	Ketjenblack	Vulcan	Ketjenblack	Vulcan	Ketjenblack	Vulcan	Ketjenblack	Vulcan	Ketjenblack	Vulcan
0.5	1.36×10 ⁻¹¹	3.95×10 ⁻¹¹	2.41×10 ⁻¹²	4.92×10 ⁻¹²	8.22×10 ⁻¹³	2.29×10 ⁻¹²	1.10×10 ⁻¹²	9.65×10 ⁻¹²	1.66×10 ⁻¹²	1.78×10 ⁻¹¹	4.01×10 ⁻¹²	4.95×10 ⁻¹¹
1.0	6.91×10 ⁻¹³	1.06×10 ⁻¹²	4.67×10 ⁻¹³	6.89×10 ⁻¹³	2.59×10 ⁻¹³	4.15×10 ⁻¹³	2.89×10 ⁻¹³	8.55×10 ⁻¹³	4.31×10 ⁻¹³	1.09×10 ⁻¹²	5.56×10 ⁻¹³	2.13×10 ⁻¹²
1.5	5.19×10 ⁻¹³	8.19×10 ⁻¹³	5.79×10 ⁻¹³	1.86×10 ⁻¹³	3.27×10 ⁻¹³	1.56×10 ⁻¹³	3.24×10 ⁻¹³	3.24×10 ⁻¹³	3.83×10 ⁻¹³	4.29×10 ⁻¹³	6.68×10 ⁻¹³	4.56×10 ⁻¹³
2.0	4.51×10 ⁻¹³	3.43×10 ⁻¹³	5.43×10 ⁻¹³	3.06×10 ⁻¹³	1.66×10 ⁻¹³	3.00×10 ⁻¹³	3.99×10 ⁻¹³	3.77×10 ⁻¹³	5.22×10 ⁻¹³	5.07×10 ⁻¹³	7.18×10 ⁻¹³	6.16×10 ⁻¹³
2.5	4.83×10 ⁻¹³	1.93×10 ⁻¹²	5.61×10 ⁻¹³	1.08×10 ⁻¹²	1.40×10 ⁻¹³	4.75×10 ⁻¹³	1.61×10 ⁻¹³	1.52×10 ⁻¹²	3.13×10 ⁻¹³	2.50×10 ⁻¹²	4.15×10 ⁻¹³	2.32×10 ⁻¹²

5.1.1 Effects of the carbon black loading

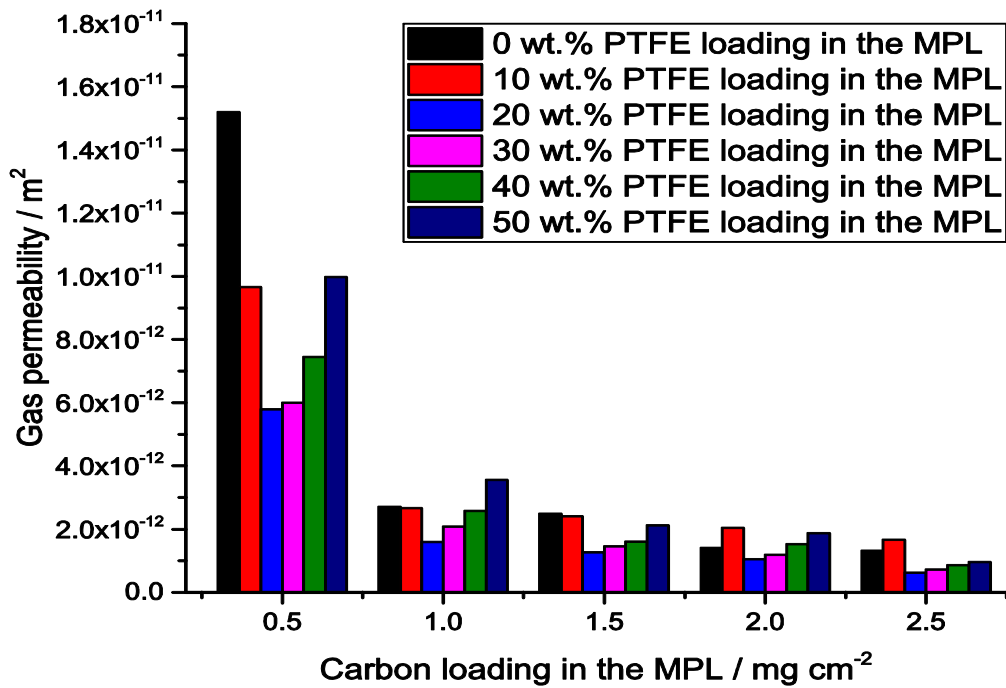
Figures 5.3 (a) and (b) present the through-plane gas permeability of the MPL-coated GDLs as a function of the carbon loading in the MPL for the Ketjenblack EC-300JD and Vulcan XC-72R carbon black. A set of MPL composition is a combination of the carbon loadings, namely 0.5, 1.0, 1.5 and 2.5 mg/cm² with different PTFE loading varying in the range 0, 10, 20, 30, 40 and 50 wt.%. The figures show that the gas permeability values of the composition of the GDLs after coating with a composition of the MPL reduces by an order of magnitude as the carbon loading increases from 0.5 to 2.5 mg/cm² and as well as the PTFE contents in the MPL.

In Figure 5.3(a), the coated GDLs with MPLs of Ketjenblack EC-300JD carbon loading from 0.5, 1.0, 1.5 to 2.5 mg cm⁻², the gas permeability reduces at PTFE loadings of (i) 0 wt.% (85.39, 15.23, 9.38 7.92 and 7.35) %, (ii) 10 wt.% (54.27, 15, 13.48, 11.46 and 9.32) %, (iii) 20 wt.% (33.71, 11.69, 8.20, 6.69 and 4.05) %, (iv) 30 wt.% (33.71, 11.66, 8.20, 6.69 and 4.05) %, (v) 40 wt.% (4.85, 14.49, 9.05, 8.60 and 4.79) %, and (vi) 50 wt.% (56.07, 20, 11.91 and 10.51) %, respectively. Compared with Figure 5.3 (b), similar results are obtained as the magnitude of the gas permeability values of the MPL-coated GDLs composition decreases with Vulcan XC-72R carbon black loadings in the MPL. The gas permeability value magnitude of the compositions 0.5, 1.0, 1.5 and 2.5 mg/cm² Vulcan XC-72R carbon black and PTFE loadings at (i) 0 wt.% (88.94, 57.21, 18.32, 3.65 and 9.78) %, (ii) 10 wt.% (70.67, 32.55, 13.41, 2.11 and 5.19) %, (iii) 20 wt.% (79.33, 33.13, 15.72, 11.97 and 11.97)%, (iv) 30 wt.% (79.81, 37.74, 20.29, 12.60 and 7.31) %, (v) 40 wt.% (85.58, 38.85, 22.16, 13.75 and 12.02) %, (vi) 50 wt.% (89.90, 52.40, 23.94, 14.18, and 11.15) %, respectively. However, the gas permeability of the coated GDLs with Ketjenblack EC-300JD and Vulcan XC-72R loadings as the material of the MPLs

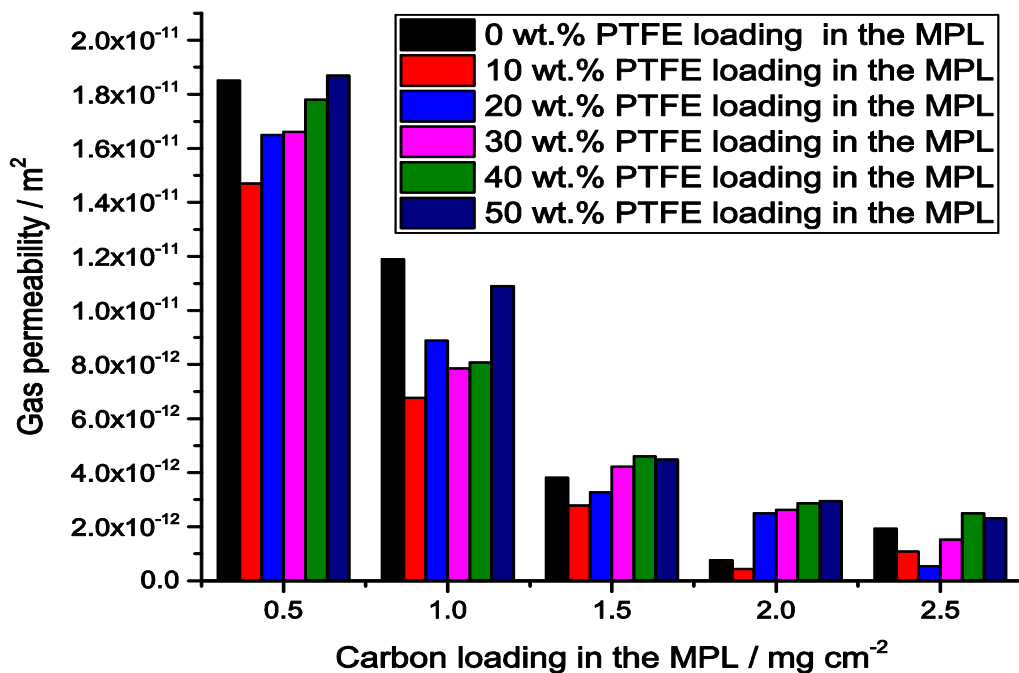
show common trends with a decrease as the carbon loading increases in the composition of the MPL coated to the porous GDLs. The decrease in the gas permeability value is mainly attributed to the decrease in the pore size and pore volume of the GDL when the MPL is coated on the carbon substrate (Park et al., 2006). Also, the decrease in the gas permeability by increasing the carbon loading in the MPL is as a result of an increase in the thickness of the MPL coated onto the GDL samples as illustrated in Figure 5.4, Orogbemi et al. (2016). In Section 3.4, 95 % confidence range of these gas permeability values are presented, see Figure 3.20.

In Figure 5.4, it was found that there is an increase in the thickness of the scanning electron micrographs (SEMs) of the typical cross-section images of the MPL-coated GDLs as the amount of carbon particle loadings in the MPL increases from 0.5 to 2.0 mg cm⁻², respectively. For Figure 5.4, 20 wt.% PTFE loading in the MPLs for coated GDLs is considered. From this figure, it is observed that the SEM images show that the averaged thickness of the MPL is about at 86, 100, 143 and 145 μm for 0.5, 1.0, 1.5 and 2.0 mg/cm² Ketjenblack EC-300JD carbon black loading, respectively.

Further, the PTFE loading is sensitive to the carbon loading in the MPL-coated GDL. Figure 5.3(a), shows that the gas permeability of the coated GDL with PTFE loading of 0 to 10wt.%, decreases for the 0.5 mg/cm² carbon loading, remains almost the same for 1.0 mg/cm² carbon loading and increases for the 1.5 and 2.5 mg/cm² carbon loadings. However, the MPL-coated GDLs with 0.5 mg/cm² carbon loading of PTFE ranges from 0 to 50 wt.% compositions of both MPLs have the highest gas permeability values in both Figures 5.3(a) and (b), respectively. This is mainly due to the insufficiency of the 0.5 mg/cm² carbon black to completely cover the large pores on the surface of the carbon substrate, see Figure 5.5.



(a)



(b)

Figure 5.3. Through-plane gas permeability as a function of carbon loading in the MPL (a) Ketjenblack and (b) Vulcan.

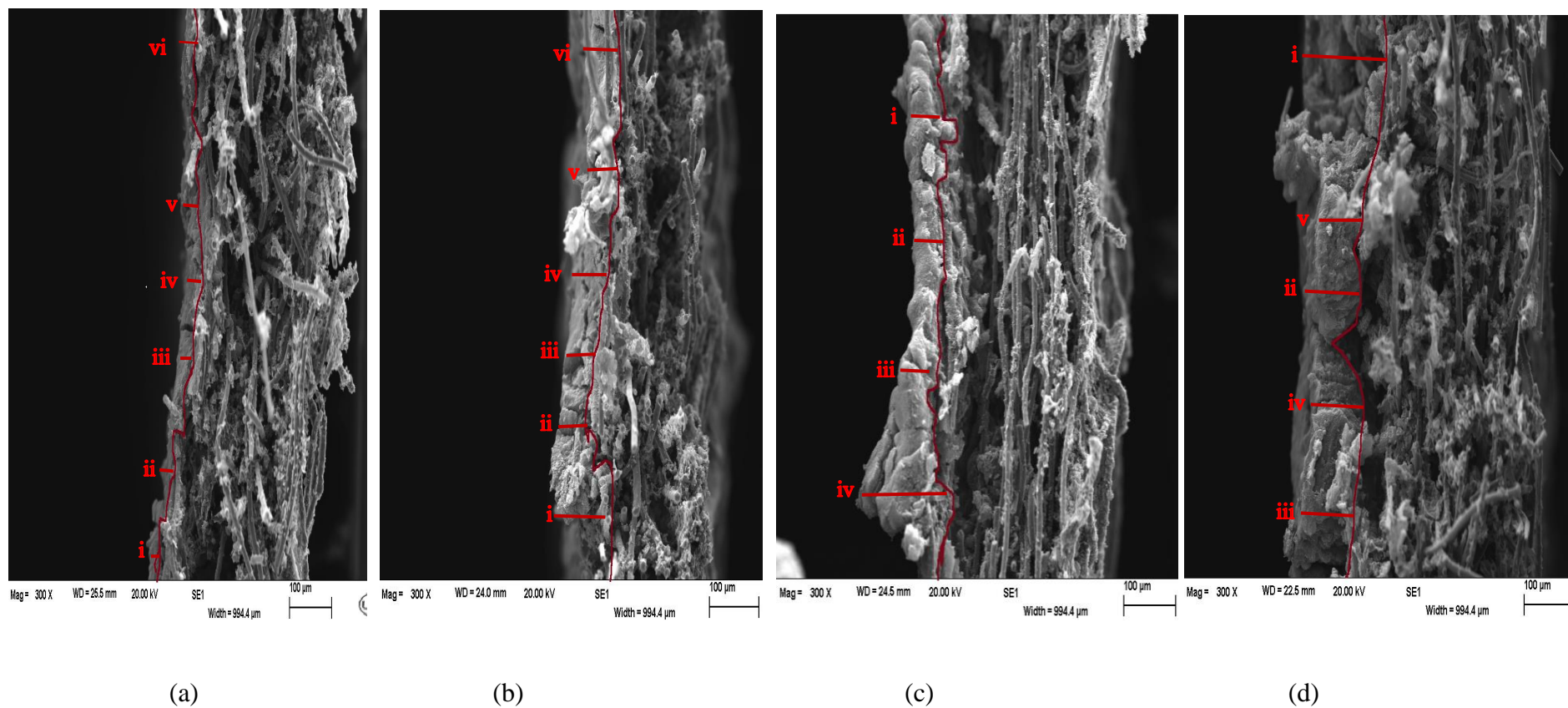


Figure 5.4. SEMs of cross-sectional images of the coated GDLs with Ketjenblack carbon black loadings of (a) 0.5 mg/cm², the MPL thickness (i = 121, ii = 79, iii = 99, iv = 79, v = 64, and vi = 74) μm. (b) 1.0 mg/cm², the MPL thickness (i = 116, ii = 106, iii = 96, iv = 100 and v = 84) μm. (c) 1.5 mg/cm², the MPL thickness (i = 138, ii = 117, iii = 152, iv = 166, v = 145) μm. (d) 2.0 mg/cm², the MPL thickness (i = 168, ii = 142, iii = 126, iv = 137, v = 158) μm.

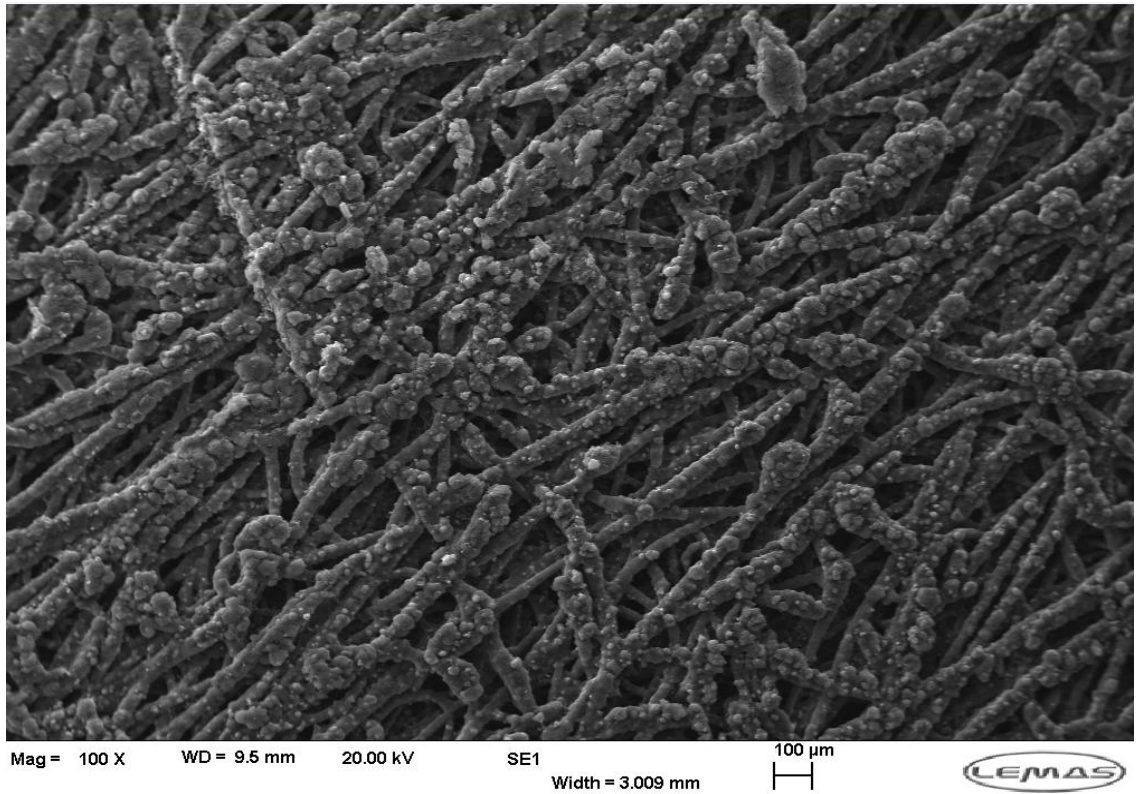


Figure 5.5. SEM image for the surface of the MPL with Ketjenblack of 0.5 mg/cm² and 20 wt.% PTFE.

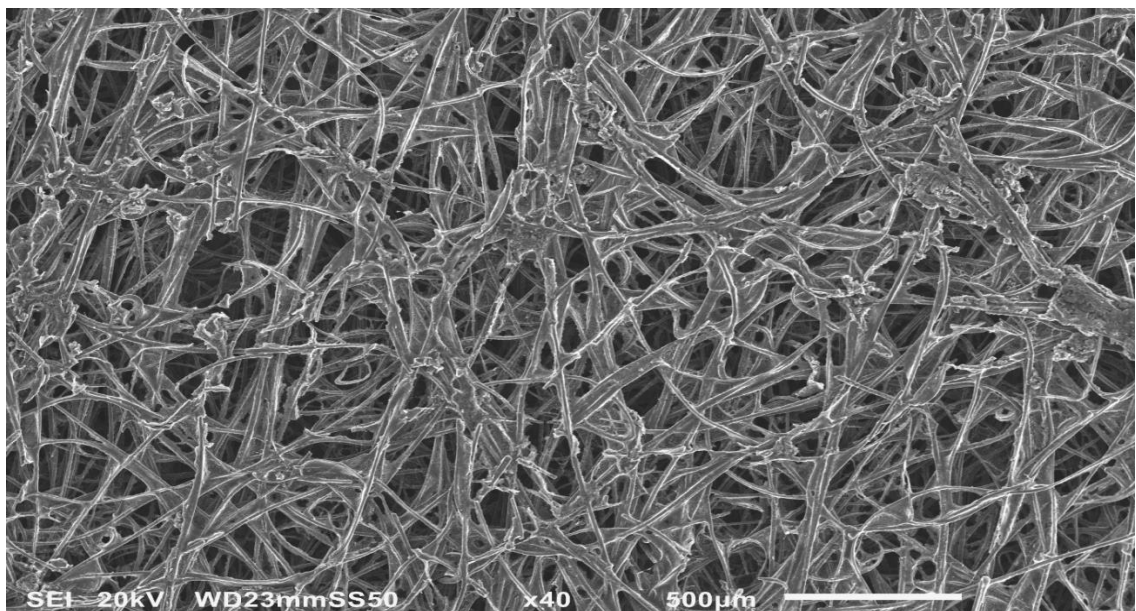


Figure 5.6. SEM for the surface of the MPL with Vulcan XC-72R of 0.5 mg/cm² and 20 wt.% PTFE.

In Figure 5.5, the skeleton of the carbon substrate clearly shows after coating with 0.5 mg/cm² carbon black at 20 wt.% PTFE loading. This indicates the large gaps that exist between the gas permeability values of the coated GDL with 0.5 mg/cm² and all other coated GDLs with higher carbon loadings. Additionally, this significantly shows that when increasing the carbon loading and adding some high content of the PTFE as material to the carbon black reduces the size of the large pores and consequently decreases the gas permeability, Mangal et al. (2015). However, for relative high carbon loadings, namely 1.0, 1.5 and 2.5 mg/cm² carbon black, the high carbon loading is apparently sufficient to completely cover the large pores on the surface of the substrate.

5.1.2 Effects of the carbon black types

Figures 5.7 (a) and (b) show the estimated through-plane gas permeability of the MPL-coated GDLs as a function of the PTFE loading in the MPL for various considered carbon loadings, namely 0.5, 1.0, 1.5 and 2.5 mg/cm². The two figures present the gas permeability of the MPL-coated GDLs with Ketjenblack EC-300JD, Figure 5.7 (a) and Vulcan XC-72, Figure 5.7(b) carbon blacks, respectively. The same kind of PTFE loading in the MPL, and identical preparation methods were applied to prepare the two sets MPLs slurry for both Ketjenblack and Vulcan carbon of the MPL-coated GDLs. The distributions are shown in the form of 95 % confidence interval in Figure 3.21.

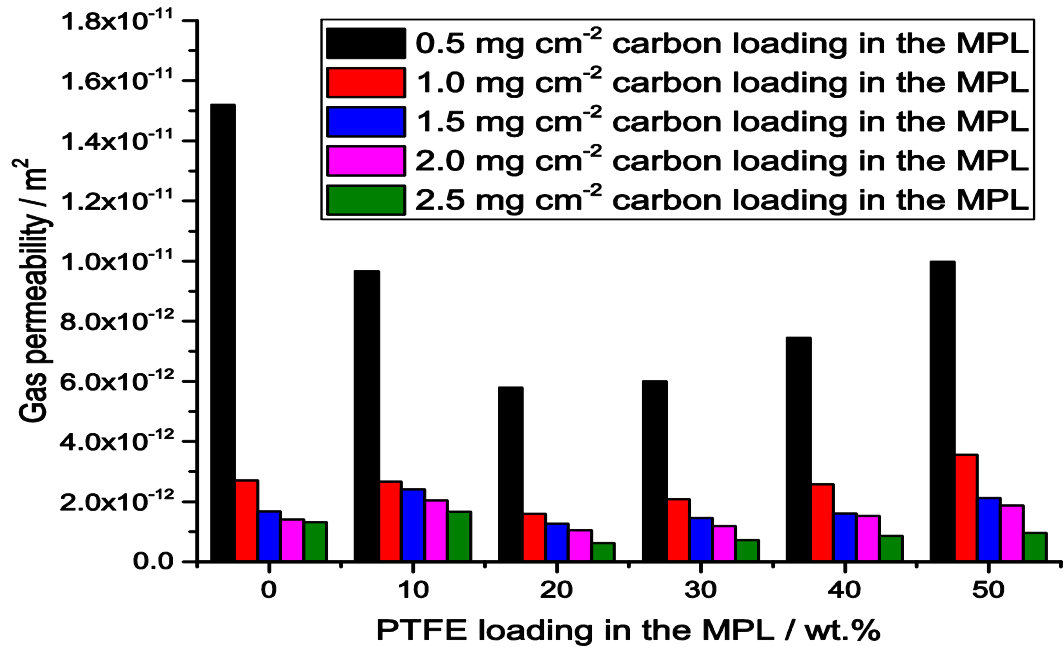
There is a significant difference in the gas permeability of the coated GDLs for the two cases. In Figure 5.7 (a), with 20 wt.% PTFE loading, the gas permeability of the coated GDLs increases with increasing PTFE loading in the MPL compared to the gas permeability obtained in Figure 5.7 (b), the gas permeability increases after 10 wt.% PTFE loading in the MPL. For Figure 5.7 (a), the results obtained are in good agreement with the literature, this justifying that the relatively large PTFE particles could not

penetrate the relatively small pores within the carbon agglomerate but the larger pores between these agglomerates, Su et al. (2016). The sizes of the agglomerate increases and there is an increase in the porosity of the MPL, Orogbemi et al. (2016). Also, the pore sizes of the MPL decreases with increasing the PTFE loading in the MPL, and this shows that the PTFE reduces the porosity of the MPL, Park et al. (2008) and Uchida et al. (1995).

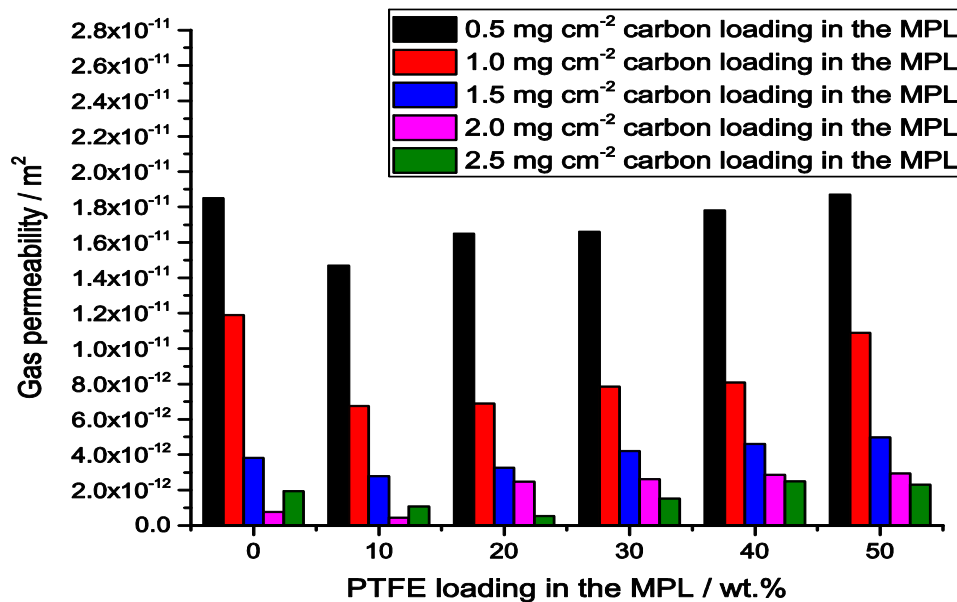
The gas permeability of the GDL decreases when the PTFE content is increased in the MPL from 10 to 20 wt.% PTFE in Figure 5.7 (a). Compared with Figure 5.7 (b), this significant difference is not obtained when Vulcan XC-72R carbon black is considered as the material in an MPLs with different PTFE loadings. Clearly, in Figure 5.7 (a) the results obtained indicate that the increase in the content of the PTFE loading increases the thickness of the MPL. In addition, the PTFE loading is not sufficiently adequate to make a positive-increasing influence compared with its negative-increasing thickness effect. This means that in this case the gas permeability increase by the positive effect is more than offset by the negative effect, Park et al. (2004).

Figure 5.7 (b) shows that all the samples have a decrease in the gas permeability with the PTFE compositions increasing from 0 to 10 wt.%. This is because the coated GDL with Vulcan XC-72R carbon black (MPL) apparently fills the pores without increasing the MPL thickness coated onto the GDLs (Park et al., 2004). Despite their similar trends of an increase of gas permeability attained at the higher PTFE loading in the MPL. The various PTFE loadings with Vulcan XC-7R carbon black loadings in the MPL-coated GDLs reveals much less gas permeability variation as compared with the same PTFE compositions and the Ketjenblack EC-300JD carbon black loading in the MPLs. It should be noted that the gas permeabilities are higher in the Figure 5.7(b), although they do not

have the same sensitivity to PTFE loading. However, the 1.0 mg/cm² carbon loading is where the increase in the thickness and decrease in the gas permeability are the competing effects for the 10 wt.% PTFE loadings are counterbalanced as shown in Figure 5.7 (a).



(a)



(b)

Figure 5.7. The through-plane gas permeability of the MPL-coated GDLs as a function of the PTFE loading for various carbon loadings, (a) gas permeability of MPL-coated GDLs with Ketjenblack carbon black, and (b) gas permeability of MPL-coated GDLs with Vulcan carbon black.

5.2 Effect of sintering

The gas transport and liquid water flow within the porous media are linked with the hydrophobicity characteristics property of the gas diffusion media in general. The ability of the gas transport property of the porous media can be illustrated by the gas permeability the porous carbon substrates, and PTFE contents in the GDLs together with the MPL coated which can be used to characterise the hydrophobicity property exhibited by the porous media, Ismail et al. (2010). Meanwhile, the hydrophobicity is the ability of managing of liquid water and its flooding in the MEA porous media components, Gurau et al. (2006).

However, the PTFE loading in the MPL can either cause a decrease or increase in the gas transport and water flow in the fuel cell. For a uniform distribution of the PTFE in the applied MPLs to the GDLs, sintering of the MPL-coated GDLs is an influencing factor that improves the performance of the porous gas diffusion media used in the fuel cell, see Bevers et al. (1996), Jordan et al. (2000) and Rohendi et al. (2014).

For the effect of sintering on the gas permeability of the MPLs with different PTFE loadings, Figure 5.8 shows the through-plane gas permeability of MPL coated GDL as a function of PTFE loading in the MPL before and after sintering. The MPLs are sintered at a temperature of 350 °C for 30 minutes. In this case, the effect of sintering on MPLs made of Ketjenblack and Vulcan carbon blacks with different PTFE loading has been considered. The carbon loading is kept constant at 1.5 mg/cm² and the PTFE content in the MPLs varies in the range from 0 to 50 wt.%. The gas permeability values for the MPL-coated GDLs are evaluated before and after sintering for the MPLs with different PTFE contents. Generally, the gas permeability of the coated GDL is reduced after sintering as discussed in Section 4.3.

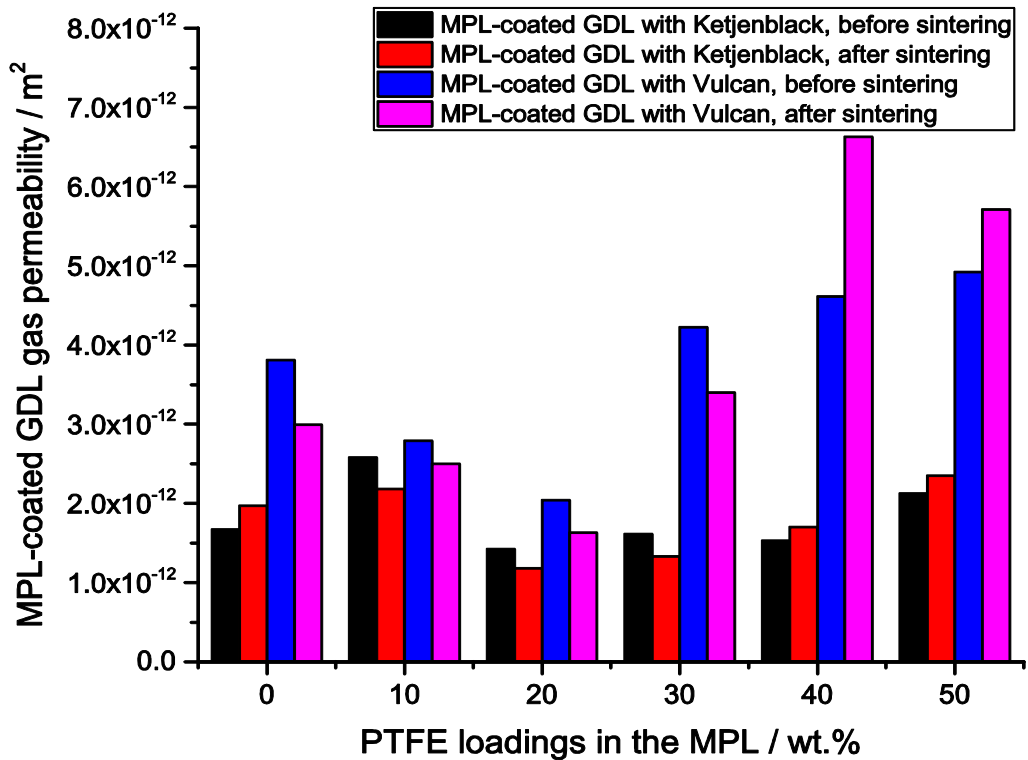


Figure 5.8. Through-plane gas permeability of MPL-coated GDLs before and after sintering as a function of PTFE loading in the MPL, for comparison of the effects of sintering on the MPLs coated on the GDLs with different PTFE (wt.%) consist of 1.5 mg/cm².

In the case of the MPL-coated GDLs for the loadings of 0, 40 and 50 wt.% PTFE in Figure 5.8, the gas permeability of the coated GDLs increases after sintering. For MPLs with 0 wt.% PTFE of Ketjenblack carbon black, this increase is as a result of physical properties of the Ketjenblack carbon black, such as pore volume, see Table 3.2. For the MPLs with 40 and 50 wt.% PTFE loading, the gas permeability increases after sintering in the MPLs with both Ketjenblack and Vulcan carbon blacks. On other hand, the gas permeability of the MPL-coated GDLs reduces for the MPLs loading of 10, 20 and 30 wt.% PTFE after sintering.

The results show that, regardless of carbon type loading, when the amount of the PTFE loading is higher than 30 wt.% in the MPLs after sintering the gas permeability increases

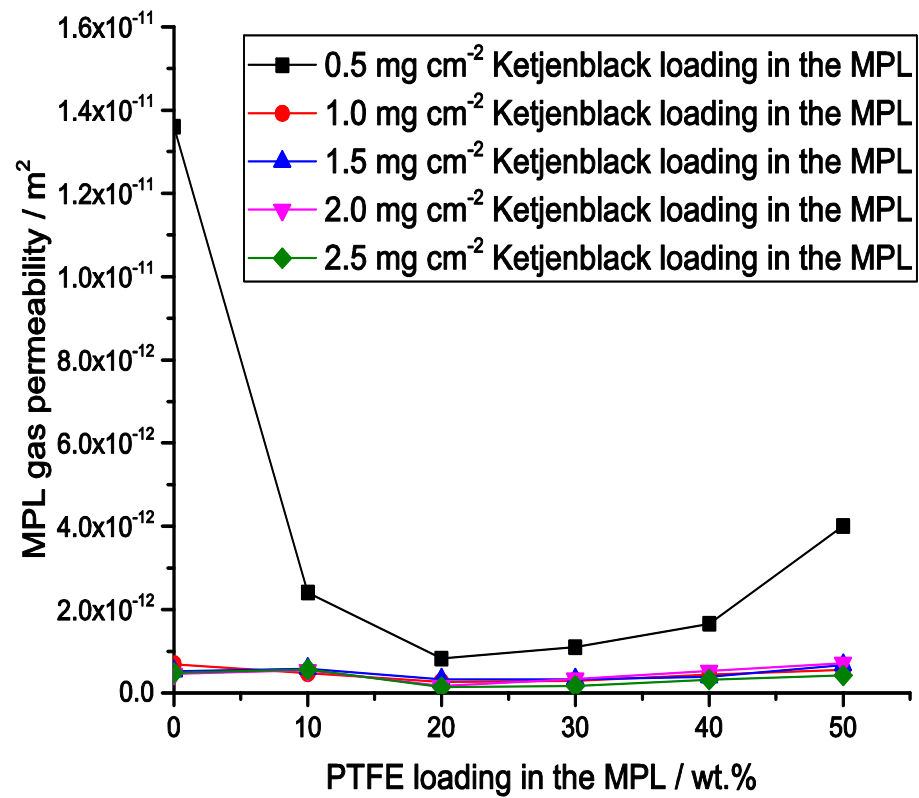
rather than decreases as observed in Section 4.3. Clearly, the results indicate the complex relationship between the PTFE and carbon loading in the MPL, uniform distribution of the PTFE in the MPL, and PTFE influence on the gas transport properties of the coated GDL. In addition, the agglomeration of the carbon-PTFE particles in the MPL structure is affected with respect to the sintering and the amounts of the PTFE contents in the MPL. Also, the sintering of different PTFE loading regardless of the carbon type and loading in the MPL has characterised the gas transport property (gas permeability) and hydrophobicity for water-repellent substances in the PEM fuel cells, Rohendi et al. (2014).

5.3 Through-plane gas permeability of MPLs

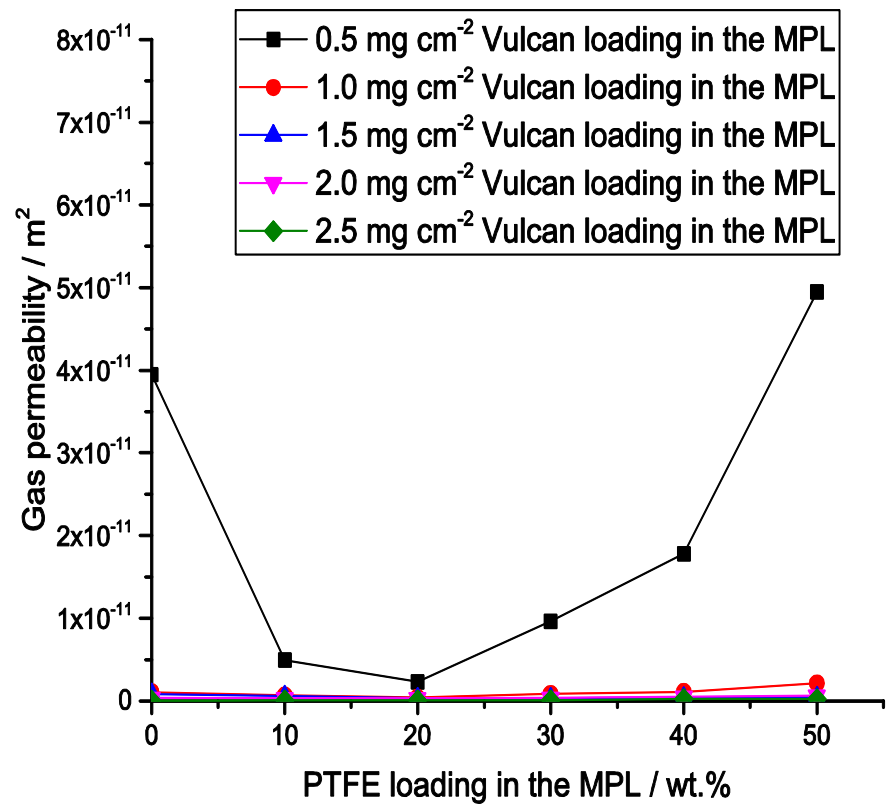
In Section 3.3, Equation (3.8) was used to estimate the through-plane gas permeability of the microporous layers of the coated gas diffusion layers. Figure 5.9 shows the calculated MPL gas permeability values as a function of the PTFE loading for all the Ketjenblack and Vulcan carbon loadings investigated. As anticipated, the trends of the gas permeability of the MPLs are generally in good agreement with those of the MPL-coated GDLs. The gas permeability values of the MPLs have the same PTFE loading, and the MPLs of the carbon types considered have the same composition for all the above MPLs. Figure 5.9(a), shows that the MPLs with 10 wt.% PTFE loading must ideally all have the same gas permeability value as the weight compositions of those MPLs, i.e. 10 % PTFE and 90 % Ketjenblack carbon loading. Similarly, the same results are obtained in most of all the other MPLs compositions, namely 10, 20, 30, 40 and 50 wt.% PTFE loadings, see Figure 5.9(b). However, this is not the case for the MPL gas permeability values in Figure 5.9(c) – (d) where there is a significant variation in the gas permeability values for the

MPLs of the same composition. The variation in the gas permeability is as a result of the significant penetration of the MPL and the carbon black type used as the material of the MPL in the porous carbon substrates. In conclusion, an accurate estimation of the MPL thickness and the penetration and subsequently the gas permeability of the MPL are required as discussed in Chapter 6.

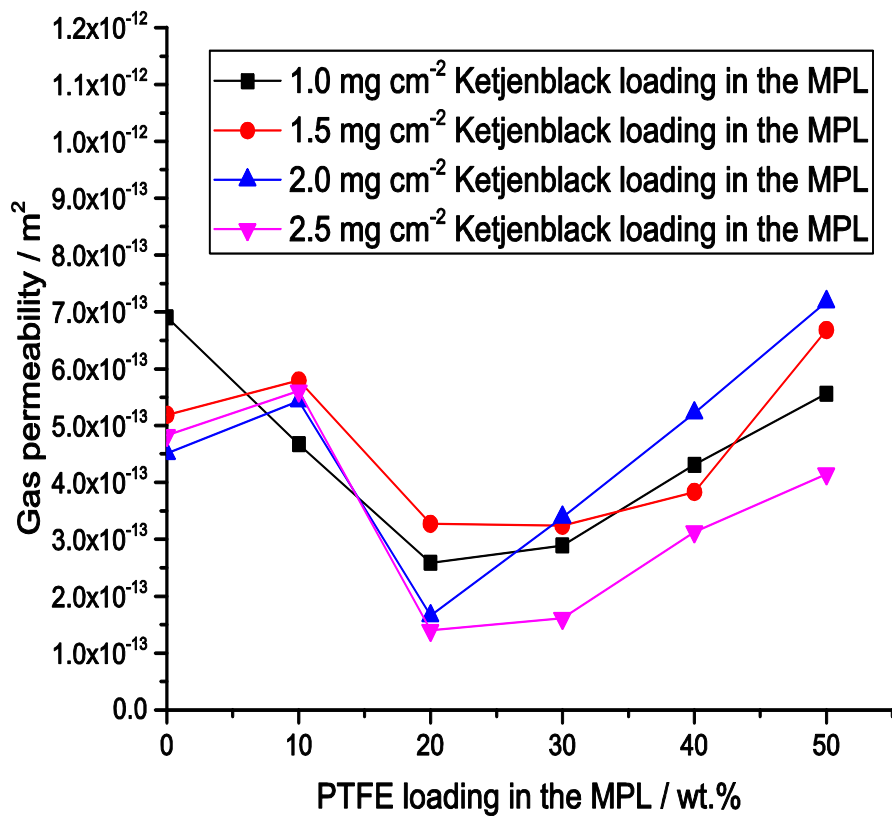
Figure 5.10 shows the SEMs micrographs of the surfaces of the MPLs with Ketjenblack and Vulcan carbon black, respectively. A comparison of the surfaces of the MPLs with Ketjenblack and Vulcan carbon black as material is considered relatively to the PTFE loading in the MPLs. The SEM images of the surfaces demonstrate the pore structure of the coated GDLs. It is visible in the surfaces of the MPL-Vulcan images that only some range of pores compare to MPL-Ketjenblack surfaces, which indicate that the surface structure of the MPLs with the two carbon black types is clearly different and in agreement with the SEMs surfaces images measured and analysed by Yu et al. (2005). However, the importance of this result can help in the process of electrode design for low-cost and maximising the efficiency of porous electrode materials used in the PEM fuel cell.



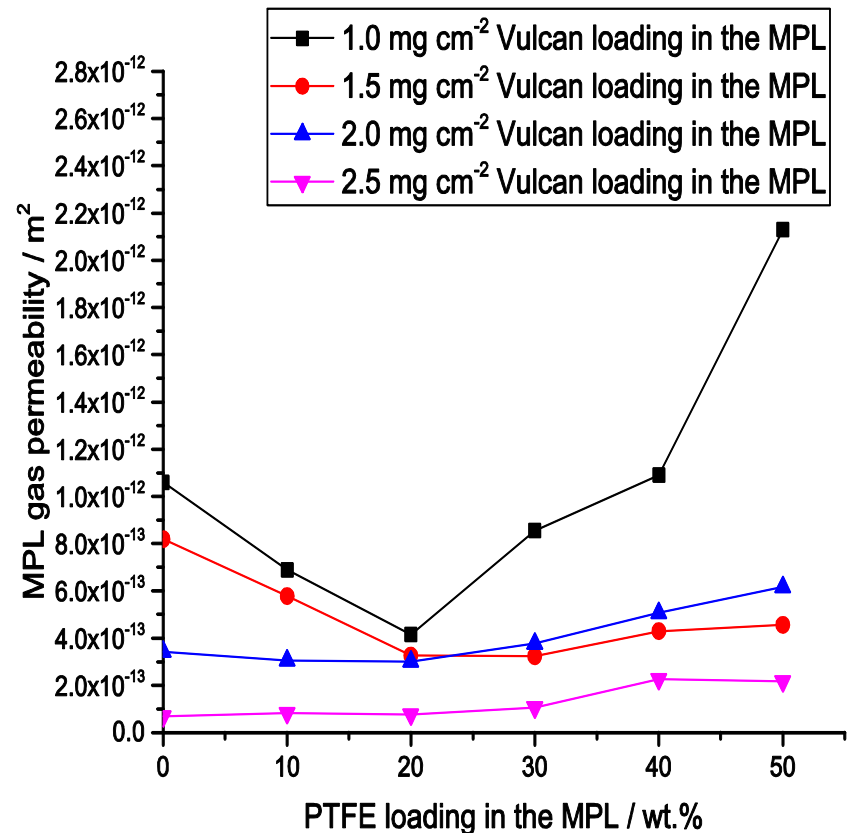
(a)



(b)

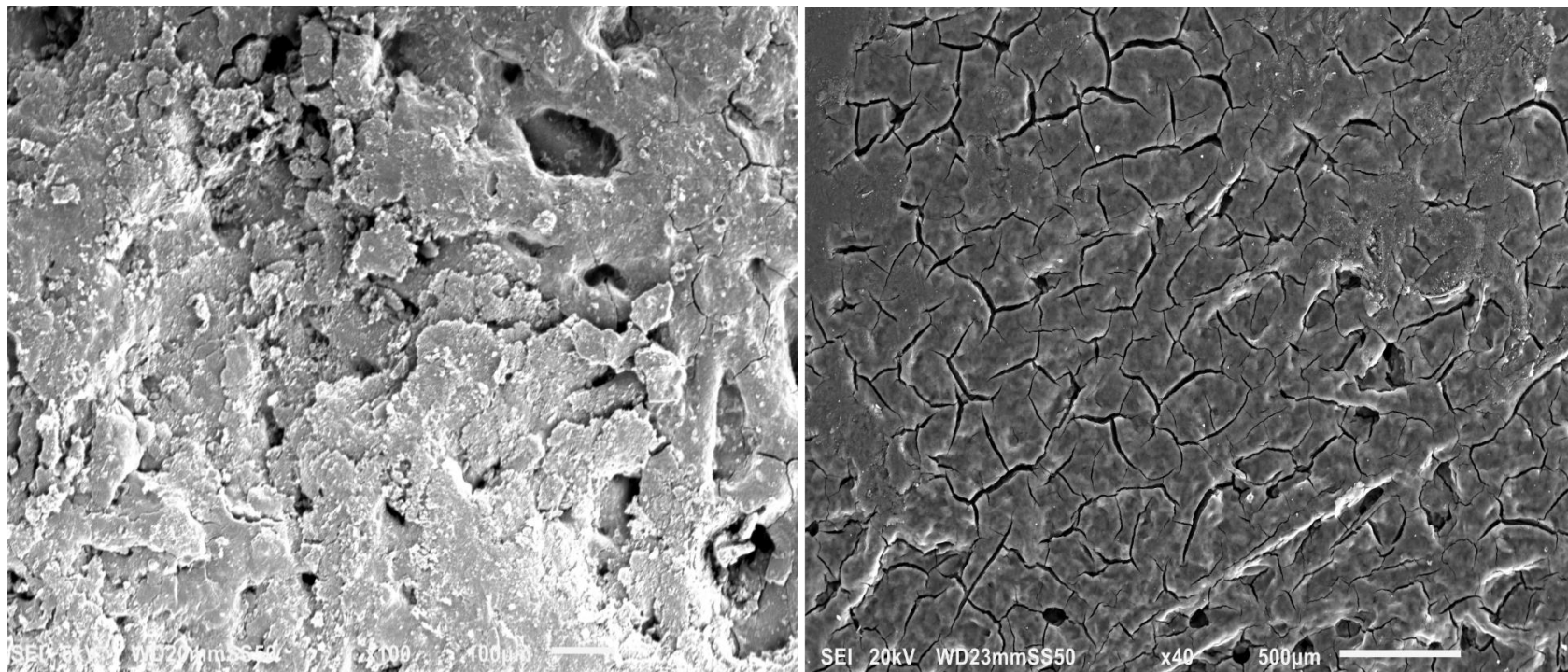


(c)



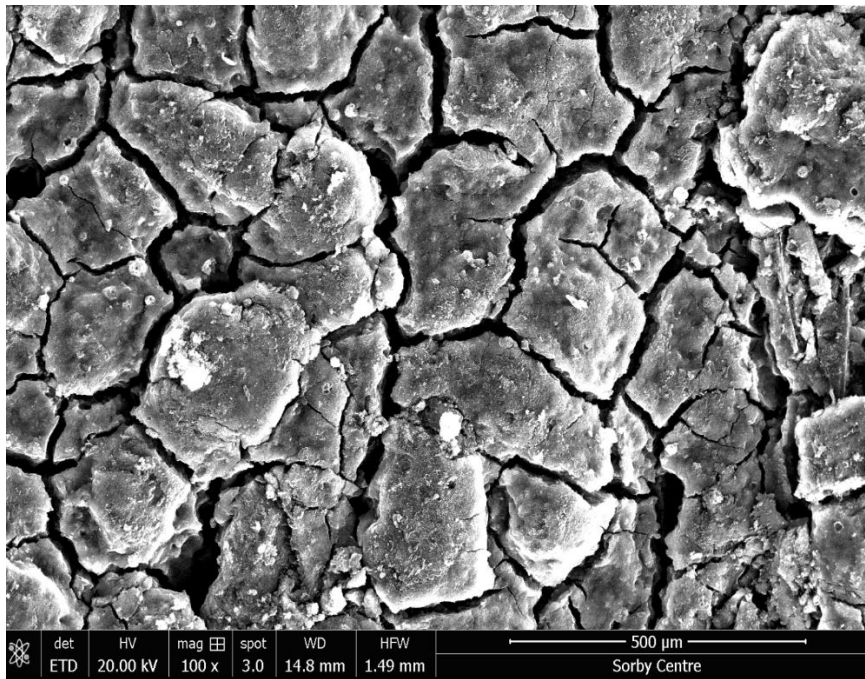
(d)

Figure 5.9. (a)-(b) The curves representing the gas permeability of the MPL as a function of PTFE loading for various Ketjenblack EC-300JD and Vulcan XC-72R carbon black, and (c) - (d) the curves after excluding the 0.5 mg/cm² carbon loading curve from (a)-(b).

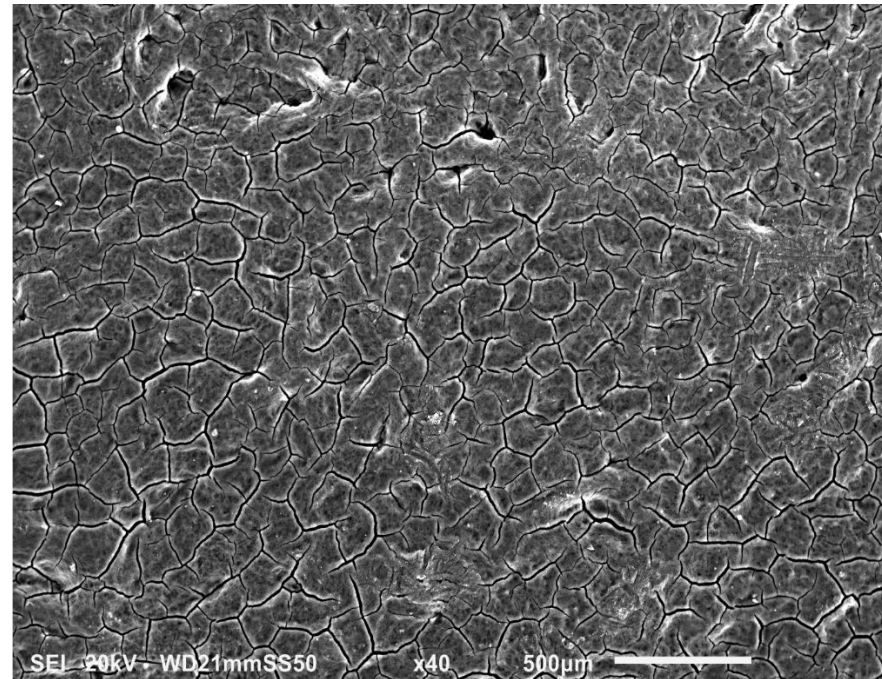


(a) 2.0 mg/cm² Ketjenblack with 0 wt.% PTFE.

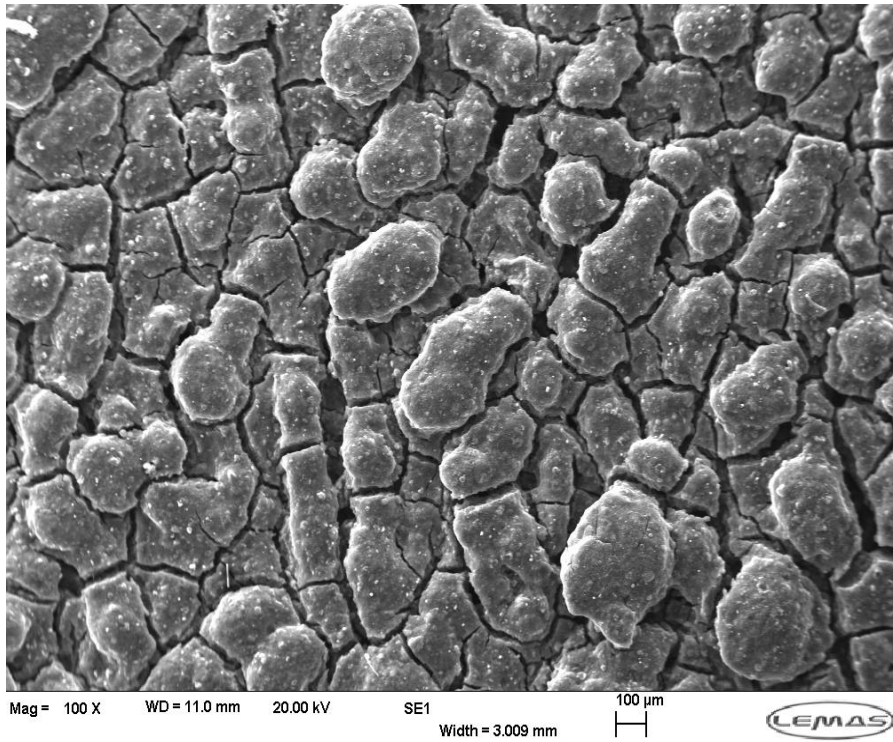
(b) 2.0 mg/cm² Vulcan with 0 wt.% PTFE.



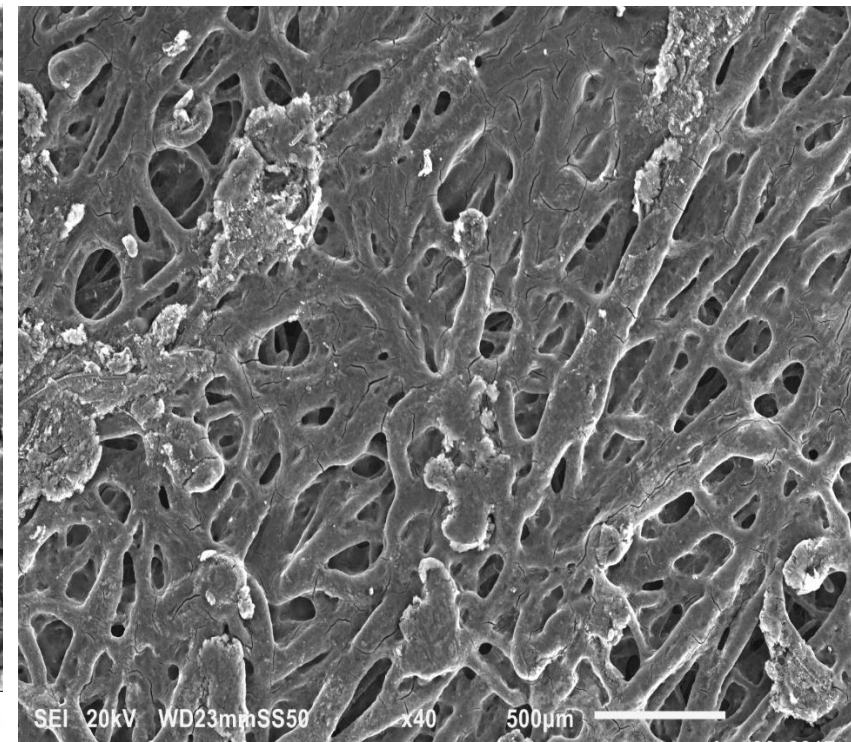
(c) 2.0 mg/cm² Ketjenblack with 10 wt.% PTFE.



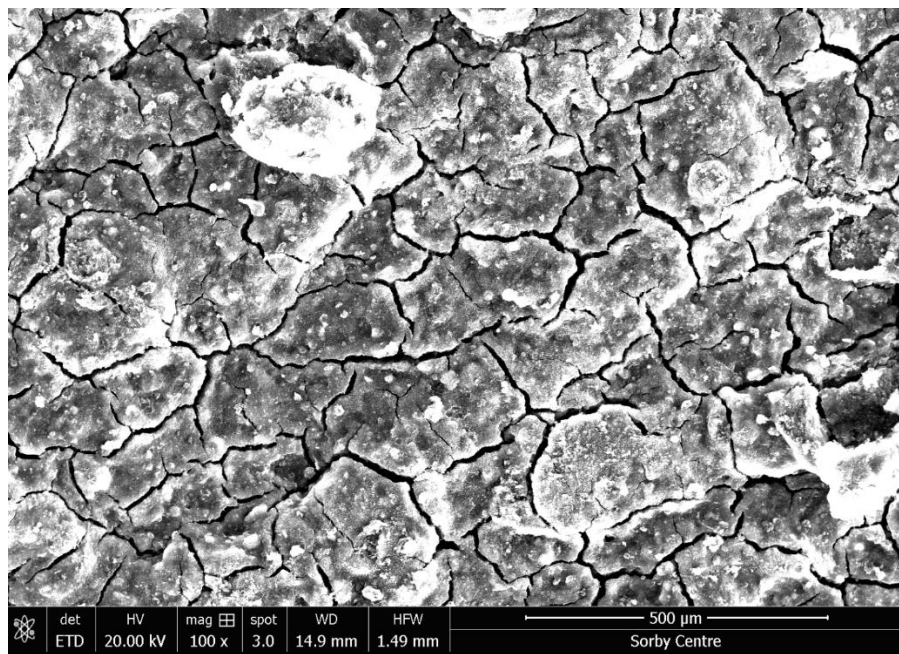
(d) 2.0 mg/cm² Vulcan with 10 wt.% PTFE.



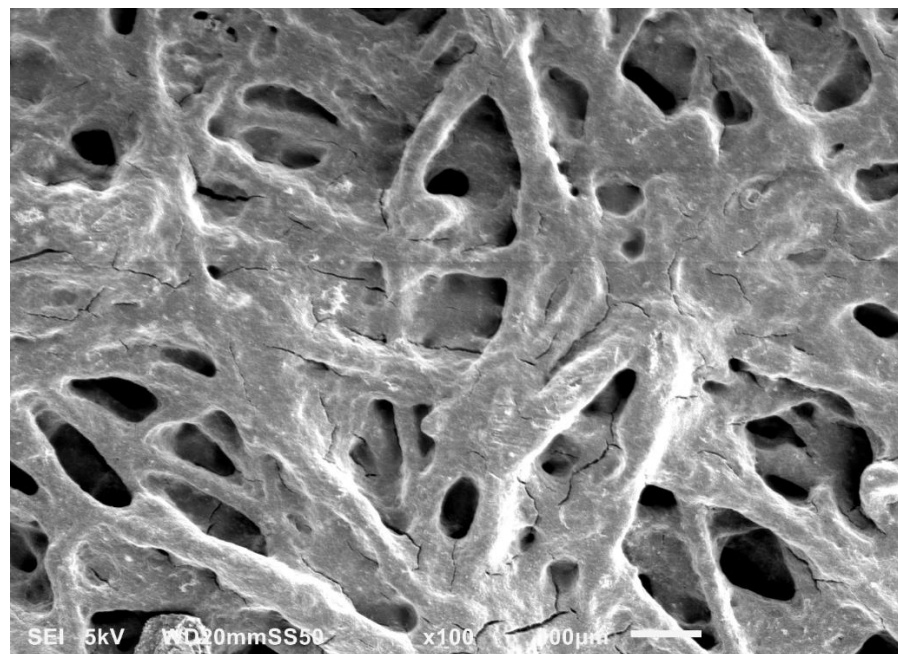
(e) 2.0 mg/cm^2 Ketjenblack with 20 wt. % PTFE.



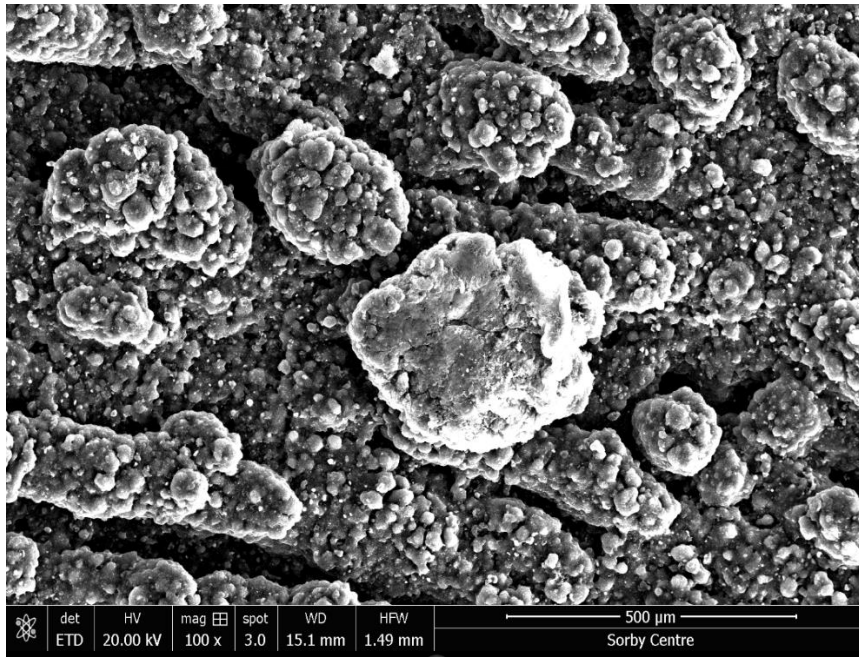
(f) 2.0 mg/cm^2 Vulcan with 20 wt.% PTFE.



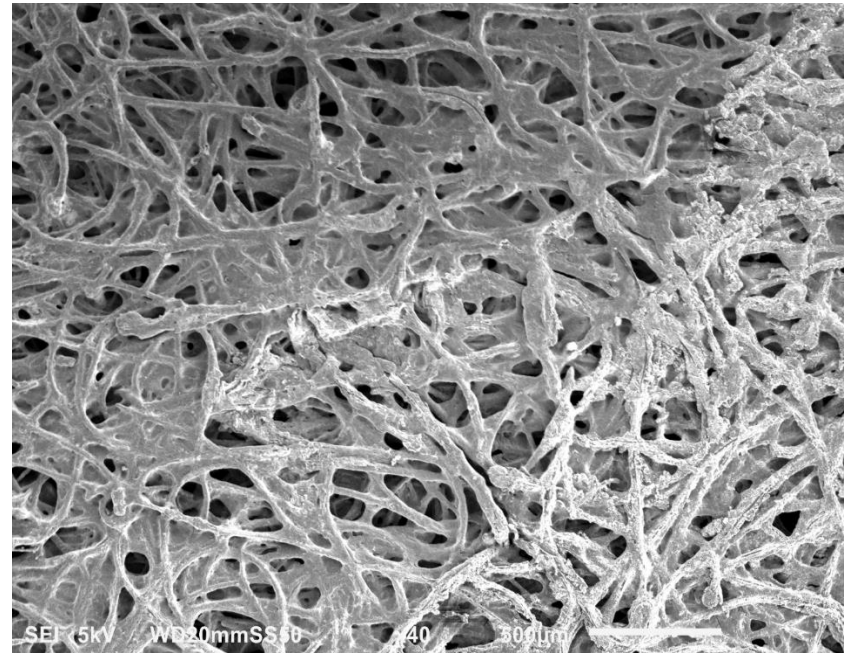
(g) 2.0 mg/cm² Ketjenblack with 30 wt.% PTFE.



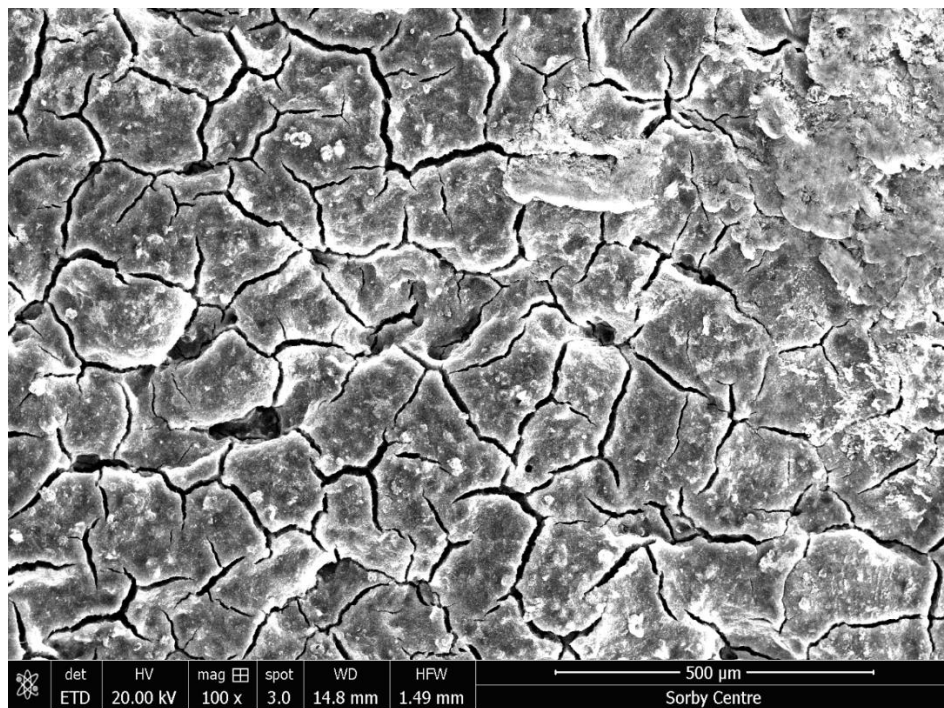
(h) 2.0 mg/cm² Vulcan with 30 wt.% PTFE.



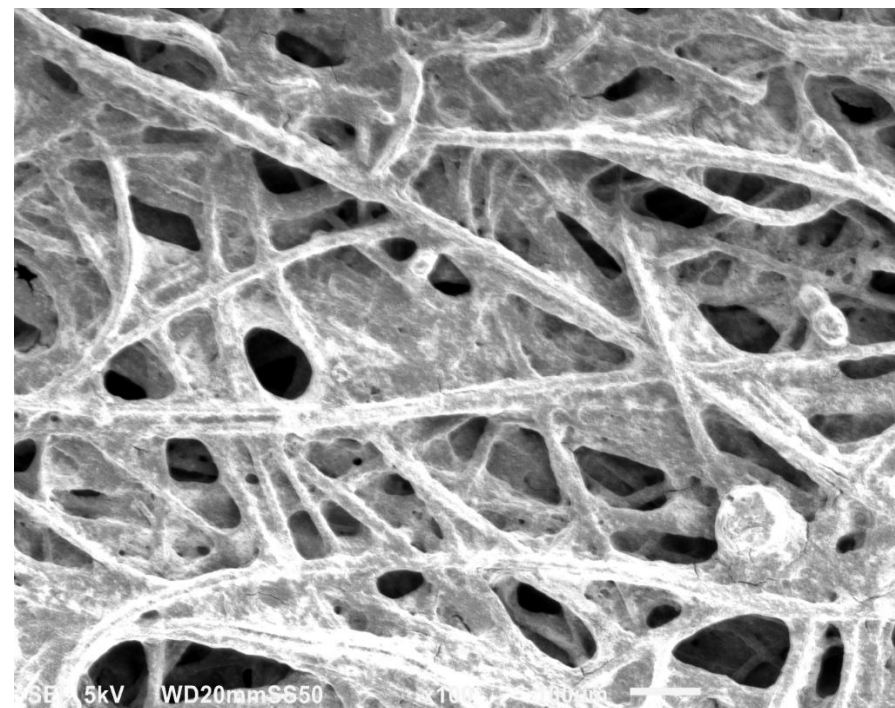
(i) 2.0 mg/cm² Ketjenblack with 40 wt. % PTFE.



(j) 2.0 mg/cm² Vulcan with 40 wt. % PTFE.



(k) 2.0 mg/cm² Ketjenblack with 50 wt. % PTFE.



(l) 2.0 mg/cm² Vulcan with 50 wt.% PTFE.

Figure 5.10. SEMs images for the surfaces of the MPL with PTFE loadings ranging from 0 to 50 wt. % PTFE, and 2.0 mg/cm² of Ketjenblack and Vulcan carbon black.

5.4 Conclusions

The effects of the composition of the microporous layers on the through-plane gas permeability of the gas diffusion layers has been investigated. The gas permeability is found to decrease as the carbon loading increases at a given PTFE loading. This is as a result of the increase in the thickness of the MPL and property of the carbon black.

The main conclusions from this study are as follows:

- For all the investigated carbon loadings of the carbon blacks, the gas permeability of the GDL was found to be a minimum at 20 wt.% PTFE loading for the Ketjenblack EC-72R and 10 wt.% PTFE loading for all the Vulcan XC-72R, apart from 2.5 mg/cm² in Figure 5.3(b).
- For all the investigated carbon loadings of the carbon blacks, the GDL gas permeability was found to increase when the PTFE loading of the MPL increases from 10 to 50 wt.% PTFE loading in the MPL for Vulcan XC-72R and 20 wt.% PTFE loading in the MPL for the Ketjenblack EC-300JD. This is due to the increase in the porosity of the MPL induced by the large PTFE particles and the characteristic properties of the carbon blacks used as the material in the MPL.
- The GDL gas permeability was found to decrease when the PTFE loading of the MPL is increases from 10 to 20 wt.% PTFE for all the investigated Ketjenblack EC-300JD carbon loadings. This is most likely to be as a result of the increase in the MPL thickness and the pore size of the Ketjenblack carbon black that results in higher mass transport resistance.

- For Ketjenblack EC-300JD, the effects of the PTFE loading in the MPL on the GDL gas permeability significantly depends on the carbon loading of the PTFE in the range 0 to 10 wt.%. (i) for a carbon loading of 0.5 mg/cm^2 , the coated GDL gas permeability decreases with increasing the MPL-PTFE loading, (ii) for a carbon loading of 1.0 mg/cm^2 , the coated GDL gas permeability remains almost the same, and (iii) for a carbon loading of 1.5 to 2.0 mg/cm^2 , the GDLs gas permeability increases with increasing PTFE loading. These results are explained in Chapter 6 considering the competing effects of (a) the MPL coverage of the surface of the carbon substrate, (b) the increase in the MPL porosity due to the addition of the PTFE particles, and (c) the carbon blacks properties.
- The influence of the compositions of the MPLs and the following sintering on through-plane gas permeability is measured and discussed, in addition to sintering effect of different PTFE loadings. The results show that the MPL surface structure depends on the carbon black used as material for the MPL and it is found that the MPLs surfaces and structure of the two carbon blacks are significantly different.

In this study, the through-plane gas permeability of the MPLs of all the cases investigated were determined. The results were found to follow the same general trends as those of the MPL-coated GDLs. This study has highlighted the need to accurately determine the MPL thickness and the penetration of the MPL thickness, since the gas permeability values of the MPLs with the same composition were found to significantly vary due to the MPL penetration into the porous carbon substrate.

Chapter 6

An Estimation of the Microporous Layer Thickness

In this chapter, the effect of microporous layer penetration into polymer electrolyte fuel cells carbon substrates has been investigated. The significant penetration of the MPL material into the body of the carbon substrates has shed information on the uncertainty in the estimation of the MPL thickness in Kitahara et al. (2010). A method has been described to accurately estimate the thickness of MPL and also accurately calculate the gas permeability of the MPL by determining the MPL penetration into the carbon substrates.

As a result of the gas diffusion layers (GDL) structure, design and performance, the GDL must have its central nature of the effective interface with other thin layers, namely microporous layers (MPLs) and catalyst layers (CLs). The characterisation of the GDL is based on its central nature by adding MPLs to the surfaces for tailoring the structure and the composition of the GDL. Also, the properties of the MPL by adding to the surface of the GDL have to be better understood. The transport properties of the GDL depend on its structure before and after adding the MPLs onto the surface, Zamel and Li (2013). To have a comprehensive understanding of the GDL after coating with an MPL, the characteristic properties of the MPL, namely the carbon loading, carbon type, thickness, etc. have to be determined. These properties of the MPL have to be experimentally investigated and numerically validated.

The transport properties of the GDL before and after coating with an MPL have been experimentally and numerically studied and reported in the literature. Lin and Nguyen (2005) tested two types of carbon substrates, namely SGL SIGRACET carbon paper and Toray TGPH carbon paper, and MPLs coated to the surfaces of the carbon papers. The

effect of the thickness of the carbon papers before and after coating were investigated on the electrode flooding and performance of a cell in a PEM fuel cell. They reported that the two factors that mainly affected the pressure drop are, the thickness of the gas diffusion media and the liquid water saturation level. The effect of the MPL visible thickness has been investigated, however, the effect of the penetration of the MPL into the carbon substrates of the GDLs after coating has not been previously investigated.

Gurau et al. (2007) characterised the transport properties, namely the absolute permeability, in GDLs for PEMFCs (proton exchange membrane fuel cells). They described a method for the estimation of the absolute gas permeability in the in-plane and through-plane directions in order to determine the viscous and inertial permeability values of the GDL and MPL, respectively. The method was used to estimate the permeability values of (i) the porous GDL before coating, and (ii) the GDL after coating with various thickness layers of the MPLs. Also, the method was employed to determine the permeability values of the coated GDLs with MPLs of different carbon types and PTFE (polytetrafluoroethylene). However, the method has been applied to calculate the thickness of the MPL, but they have not considered the penetration of the MPL effect on the permeability values of the GDLs used in the PEMFCs.

Kitahara et al. (2010) clarified the effect of the MPL thickness and the penetration into the substrate on the in-plane and through-plane air permeability. The authors reported that the MPL penetration into the substrate influences the through-plane and in-plane gas permeability of the GDL after coating. The penetration thickness enhances the in-plane permeability of the coated GDLs, while the MPL penetration thickness decreases the cross-sectional area of the coated GDLs. The penetration thickness was estimated by comparing the in-plane permeability values of the GDLs before and after coating. They

reported that the thickness of penetration was unable to be obtained directly by employing the in-plane permeability value ratio. Also, the boundary between the MPL and the substrate was unclear when using SEM micrographs to observe the MPL penetration. However, the use of a permeable and non-penetrable material has not been used and taken into account the effect of the carbon types.

Furthermore, Kim et al. (2013) investigated the effects of different carbon powders used as materials for MPLs have on the performance of high concentration methanol fuel cell. They considered the parameters that influence the properties of the MPLs porous materials in the components of MEAs of a cell, namely thickness and gas permeability. Kim et al. found that the thicknesses of the prepared MPLs with 5 different types of the carbon powders are about 30 μm , while their gas permeability coefficients are different, which can be attributed to the physical characteristics of the carbon type. However, they did not account for the penetration of the MPL material into the porous carbon substrate for the five carbon powder types. Though, it is agreed that the gas permeability of the coated GDLs with these different MPLs materials are depending on cracks in the MPLs than the thickness of the MPLs. Moreover, for the MPLs having the same characteristic physical properties, such as densities, should have shown close gas permeability coefficients, which has not been investigated nor mentioned in this case.

In the present study, a method to estimate the MPL penetration into the substrate has been developed. The method is applied initially to a permeable and non-penetrable membrane filter material after coating and subsequently to the MPL-coated GDL with different carbon loadings of two different carbon types. The method is used to determine (i) the gas permeability of the MPL with no penetration of different carbon loadings and carbon black types, (ii) the MPL penetration thickness of different carbon loadings with the same

composition, (iii) the actual MPL thickness of the carbon loadings and gas permeability, and (iv) the overall effect of the MPL penetration on the through-plane gas permeability of porous gas diffusion media.

6.1. MPL with penetration

The gas permeability values of microporous layers (MPLs) greatly vary, particularly in the modelling investigations. Figure 6.1 shows that the experimental determination of the through-plane gas permeability values of MPLs are in the order of 4.29 to $6.42 \times 10^{-13} \text{ m}^2$ and 5.59 to $7.79 \times 10^{-13} \text{ m}^2$ for Ketjenblack and Vulcan carbon blacks, respectively.

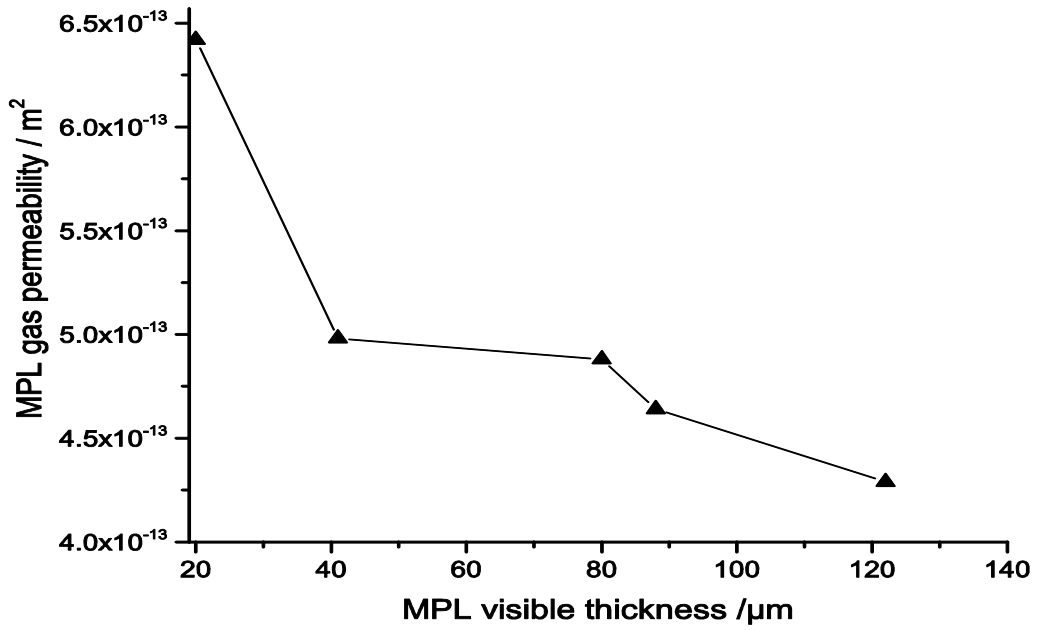
Values of the MPL gas permeability are determined as a function of thickness of the MPL, where the thickness of the MPL is obtained as the amount of carbon loading in the MPL, range 0.5 and 2.5 mg/cm^2 . Figure 6.1(a) shows that the gas permeability values of the MPLs with Ketjenblack carbon black change as a function of MPL visible thickness. The thickness value of the MPL increases as the carbon loading in the MPL increases, and also, similar results are obtained in Figure 6.1 (b), for the MPLs made of Vulcan carbon black. A comparison of the measured thickness values for the two figures clearly show that the thickness values of the Vulcan carbon black (MPLs) are less in magnitude than that of the Ketjenblack carbon black (MPL), as shown in Table 6.1.

Similarly, the gas permeability values vary as a result of the visual thickness measurements of the MPL without considering the influence of the penetration of the MPL material into the porous carbon substrates. The values of the gas permeability of the MPLs for Ketjenblack carbon black and Vulcan carbon black are different in magnitude values, i.e. the MPL gas permeability values of the Ketjenblack carbon black is high in values than that of Vulcan carbon black, see Figure 6.2. This indicate that the carbon

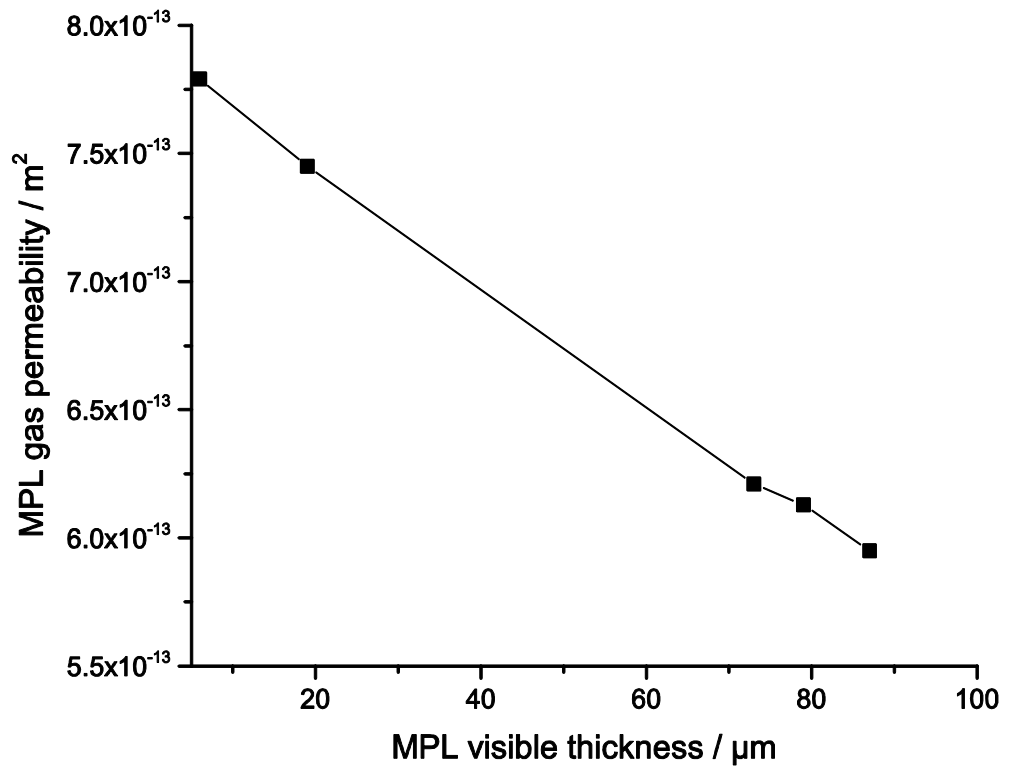
black type used as a material for the microporous layer has a significant effect on the gas permeability of the MPL. It has to be noted that the composition of the MPLs is fixed, such as 20 % of PTFE and 80 % of the carbon loading, and the effects of carbon black types are significant on the values of the gas permeability, the thickness, and the penetration of the MPL.

However, the difference in the thickness values and gas permeability values of the Ketjenblack and Vulcan MPLs are mainly due to the characteristic properties of the carbon blacks and which are in good agreement with Yu et al. (2005).

Further, the effect of the MPL visible thickness as a function of carbon loading for two different carbon black types on factors that influence the MPL physical properties has been reported in the literature, for example see Park et al. (2006), Ismail et al. (2011) and Kim et al. (2013). Also, it has been reported in the literature that the gas permeability values of the MPL of the same composition adding to the porous carbon substrate has not been close in order of magnitude values (Kim et al., 2013), this is as a result of the penetration of the MPL material into the porous carbon substrate, Kim et al. (2013) and Kitahara et al. (2010). Clearly, the values of the gas permeability of both the Ketjenblack carbon black and Vulcan carbon black as materials for the MPLs are significantly decreased as the MPLs thicknesses increase, which can be ascribed to the increase in the carbon black powder loading in the MPL, as shown in Figures 6.1 and 6.2. The 95 % confidence interval of the distribution of carbon loading on thicknesses and gas permeability of the MPL are shown in Figures 3.22 and 3.23.



(a)



(b)

Figure 6.1. Through-plane gas permeability of the MPL as a function of the MPL visible thickness of (a) Ketjenblack carbon black, and (b) Vulcan carbon black, as the materials of the MPLs.

Table 6.1. Measured thickness values for the microporous layers of Ketjenblack and Vulcan carbon blacks using SEM.

Carbon black type	0.5 mg/cm ² carbon loading	1.0 mg/cm ² carbon loading	1.5 mg/cm ² carbon loading	2.0 mg/cm ² carbon loading	2.5 mg/cm ² carbon loading
Ketjenblack (MPL / μm)	18±3.3	41±2.5	80±1.10	88±2.3	122±3.10
Vulcan (MPL / μm)	6±4.0	19±1.0	73±5.3	79±2.2	87±5.1

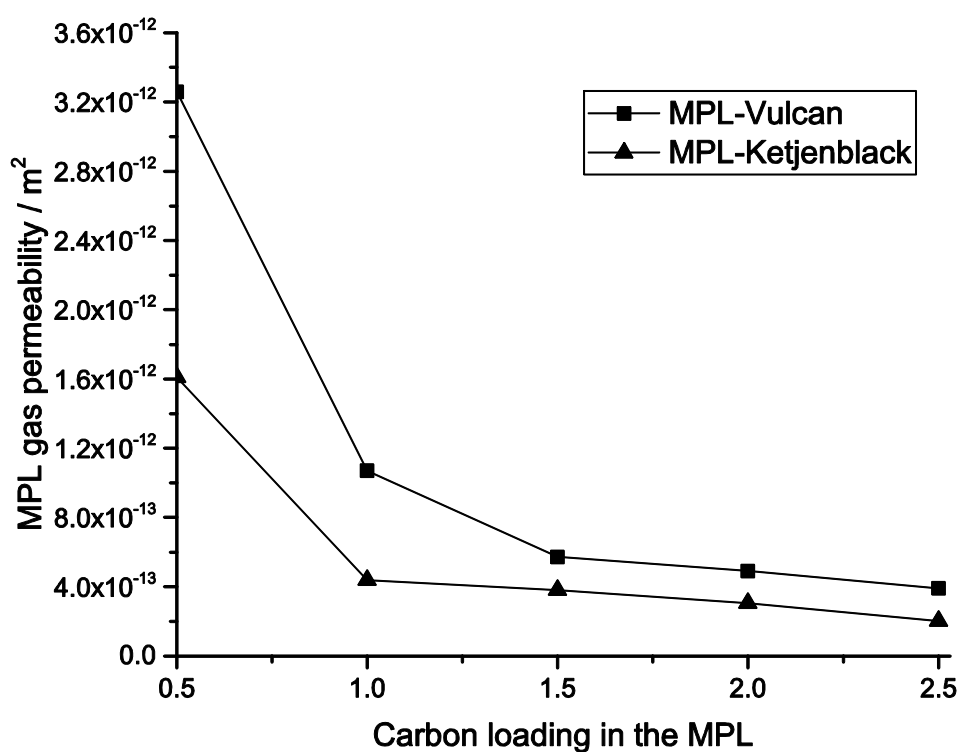


Figure 6.2. Gas permeability of the MPL as a function of the carbon black loading in the MPL, for a comparison of the (a) Ketjenblack carbon black, and (b) Vulcan carbon black, as the materials of the MPLs.

Figure 6.3 depicts a schematic diagram for the cross-sectional view through the MPL-coated GDLs and makes a distinction between the visible thickness of the MPL (L_{mpl}) and the MPL penetration (L_{pen}). Assumptions are made towards the calculation of the MPL thickness that (i) the penetrating part has the same properties as the visible part of the MPL, and (ii) the porosity and pore size of the porous carbon substrate visible part is not significantly affected due to the flow of the gas. This figure is used to describe the parameters required for determining the penetrating values for the MPLs after adding the MPL to one side surface of the carbon substrate.

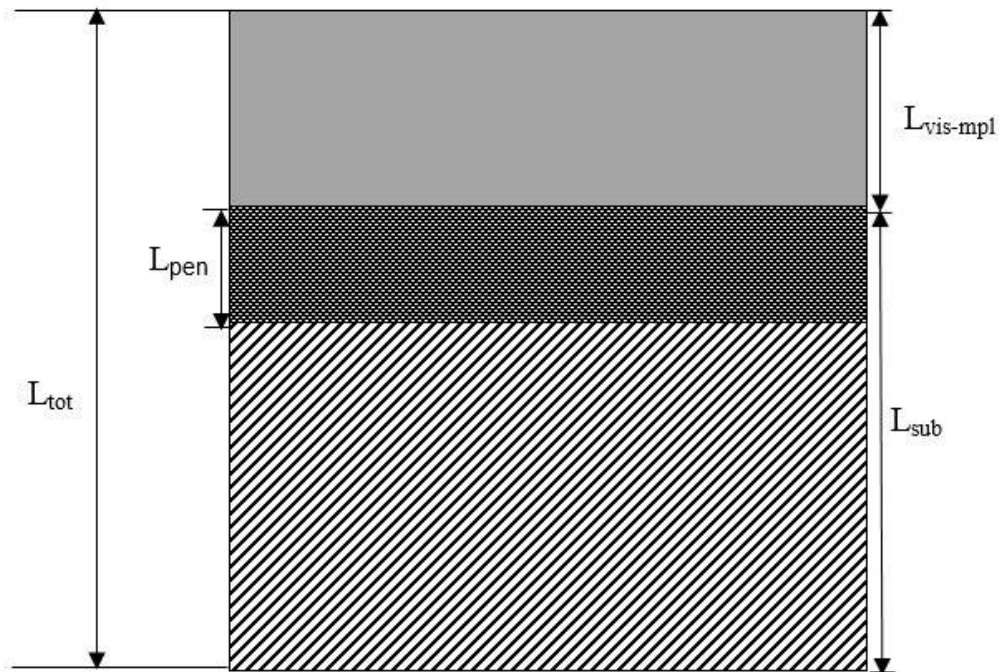


Figure 6.3. A schematic diagram for the cross-section of the MPL-coated GDL and the penetration of the MPL into the carbon substrate.

The effect of the visible MPL thickness as a function of carbon loading for two different carbon black types, namely Ketjenblack and Vulcan, on the estimation of the through-plane gas permeability values of the MPL is discussed in the next section.

6.1.1 MPL thickness with penetration

When an MPL is coated to the surface of the carbon substrate with carbon loadings 0.5, 1.0, 1.5, 2.0 and 2.5 mg/cm², the visible MPL thicknesses varied from 20 to 122 μm (Ketjenblack carbon back), and 6 to 87 μm (Vulcan carbon black) as shown in Figure 6.4 and summarised in Table 6.1.

The average gas permeability of the GDL before coating (k_{sub}) and the thickness (L_{sub}) are estimated to be $1.78 \times 10^{-11} \text{ m}^2$ and $397 \pm 60 \text{ μm}$ in Section 4.1. On the addition of MPL to one side of the GDL, it is observed that there is a significant increase in the thickness of the GDLs in relatively the same amount of the carbon loading in the MPL, as shown in Figure 6.4.

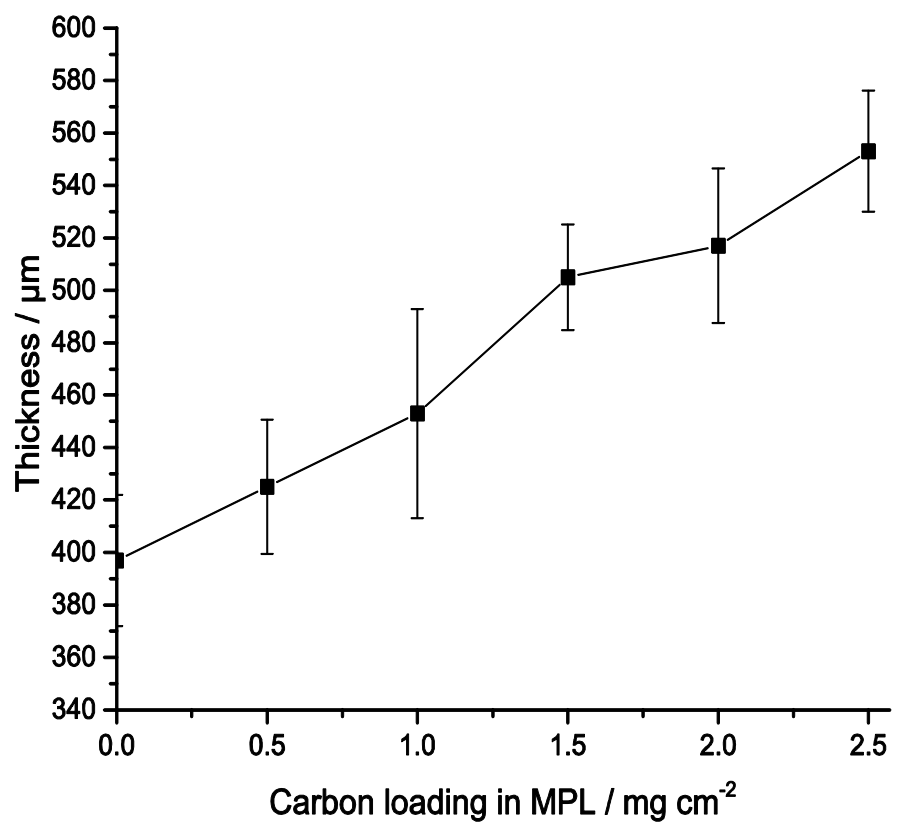
Figure 6.4 shows the thickness of the MPL-coated GDL as a function of the carbon loading in MPL. The estimation of the visible MPL thickness is determined by employing the following expression, Ismail et al. (2011):

$$L_{\text{mpl}} = L_{\text{tot}} - L_{\text{sub}} \quad (6.1)$$

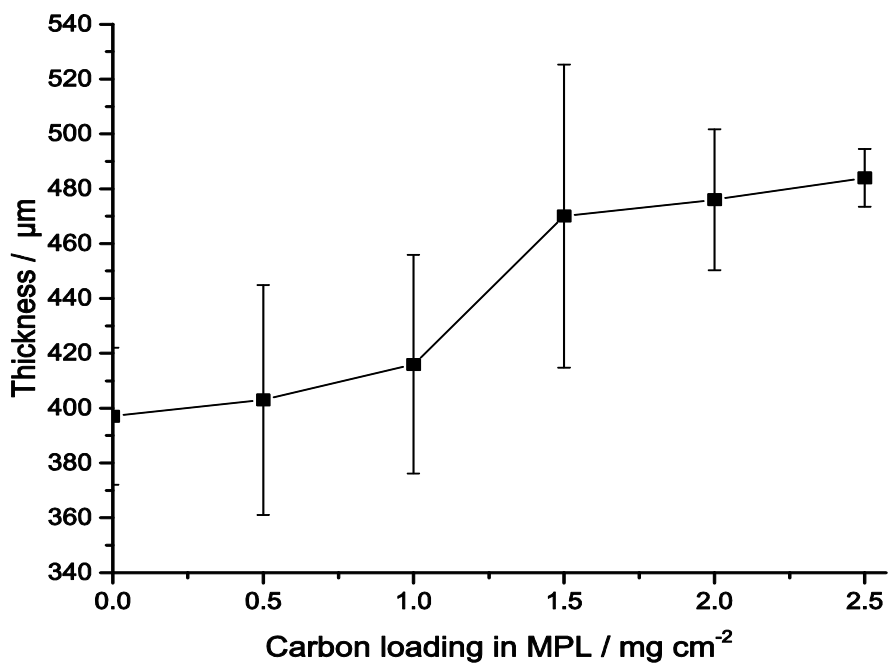
where L_{sub} , L_{tot} and L_{mpl} are the thickness of the carbon substrate, MPL-coated GDL and MPL. The values of the visible MPL thickness significantly depends on the amount of (i) carbon loading, and (ii) carbon black type, as shown in Figure 6.4.

In Figure 6.4, similar common trends are observed towards the orders of magnitude of the values of the MPL-coated GDLs thickness and the carbon black types, and the thickness value of the carbon substrate from the same batch of carbon paper sheet is $397 \pm 25 \text{ μm}$. Figure 4 (a-b) shows the 95 % confidence interval for variation in thicknesses of MPL-coated GDLs due to application of MPL to the surface of carbon substrate. Clearly, the magnitude of the MPL-coated GDLs thickness with Vulcan carbon black is

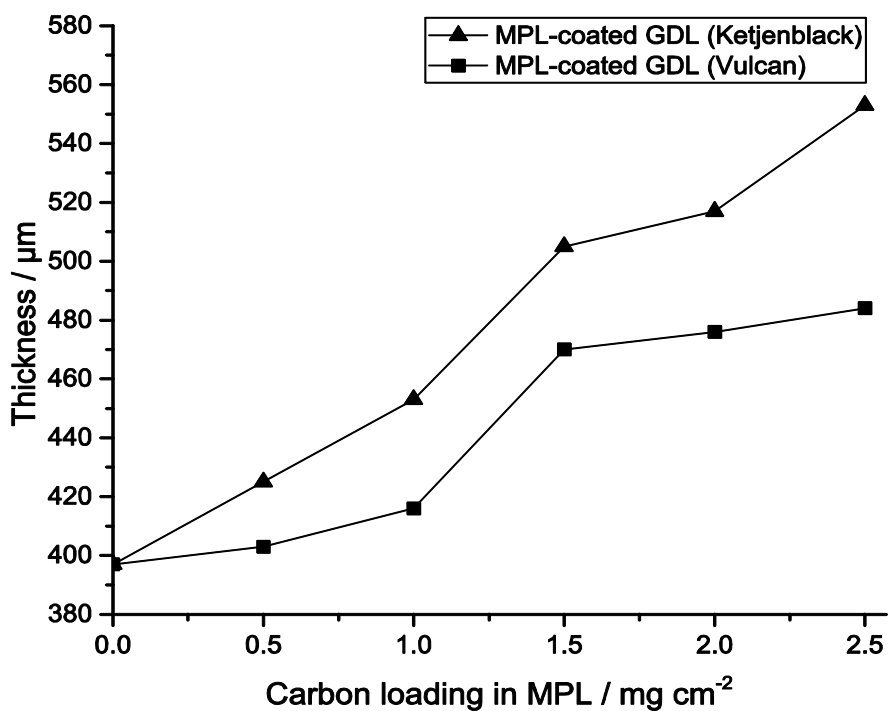
less compared with the thickness magnitude of the coated GDL with MPL of Ketjenblack (Figure 4c). However, the two different carbon blacks exhibit similar trends of increasing as the amount of carbon loading in the MPL increases. This simply indicates that the thickness of the GDLs after coating significantly depends on (i) the amount of carbon loading, and (ii) carbon black type.



(a)



(b)



(c)

Figure 6.4. The MPL-coated GDL thickness as a function of carbon loading and carbon type utilised as materials in the MPL (a) Ketjenblack, (b) Vulcan and (c) comparison of MPLs thicknesses.

In Figure 6.5, the visible thickness of the MPLs with Ketjenblack carbon black is higher compared with Vulcan carbon black. Also, the visible MPL thickness of the MPLs increases as the carbon loading increases in the MPL. This means that the properties of the carbon particles type use as material for the MPL have a significant influence on the thickness of the MPL that is added to the GDL. For the Ketjenblack carbon black, it has a surface area of $950 \text{ m}^2/\text{g}$ and this is higher than that of Vulcan which is about $254 \text{ m}^2/\text{g}$, see Table 3.2. Further, the MPL gas permeability can also be determined, and this is discussed in the next section.

6.1.2 MPL gas permeability with penetration

Equation (3.8) is used to estimate the gas permeability of the MPLs for each set of carbon loading, as shown in Figure 6.2. Through-plane gas permeability of the MPL decreases as the carbon loading in the composition of the MPL increases, which relate to the measured visible thickness of the MPL increases, see Figure 6.2.

In Figure 6.2, the through-plane gas permeability of the MPLs have been estimated with uncertainties of constant values of the measured thicknesses of the MPLs, and this is due to the effect of the MPL penetration to the porous substrate. However, Figure 6.5 shows the effect of the visible MPL thickness on the through-plane gas permeability of the MPL.

The thickness layer of the visible MPL of $122 \text{ }\mu\text{m}$ ($2.5 \text{ mg}/\text{cm}^2$ carbon loading) has the lowest gas permeability compared with all other less thicknesses (thin layers), namely $20, 41, 80$ and $88 \text{ }\mu\text{m}$ in Figure 6.1 (a). Also, a decrease in the MPL visible thickness from $87 \text{ }\mu\text{m}$ of $2.5 \text{ mg}/\text{cm}^2$ to $6, 19, 73$ and $79 \text{ }\mu\text{m}$ of $0.5, 1.0, 1.5, 2.0 \text{ mg}/\text{cm}^2$, the gas permeability values of the MPLs increase in Figure 6.1(b).

The amount of the carbon loading in the MPL apparently determines the thickness of the MPL. Clearly, the results show that the thickness of the MPL has a significantly effect on the gas permeability of the MPL.

In addition, the effect of the carbon black utilised as the material in the MPL on the through-plane gas permeability is significant. The results show that the through-plane gas permeability of the MPL with Ketjenblack are less compared with the through-plane gas permeability values for Vulcan as shown in Figure 6.2. This is due to the significant influence of the penetration of the MPL material into the body of the carbon substrates, more information on the reason for the uncertainty in the estimation of the MPL thickness has been given by Kitahara et al. (2010).

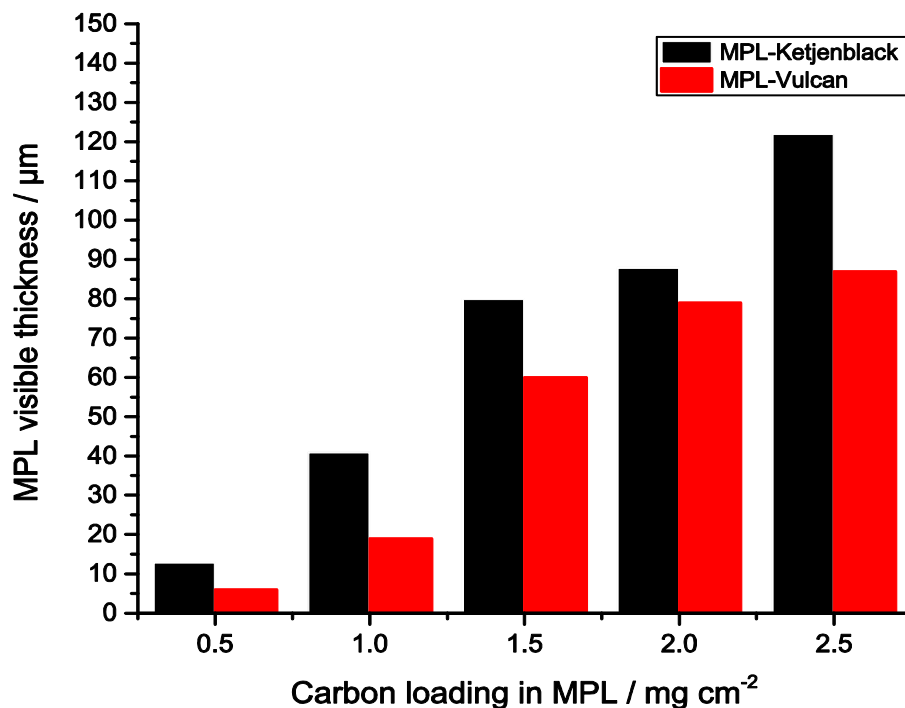


Figure 6.5. Comparison of the MPL visible thickness as a function of the carbon loading and carbon type utilised as materials in the MPL.

The accurate estimation of the gas permeability of the MPL requires that the actual estimation of the thickness of the MPL considering the penetration, and this is discussed in the next section.

6.2 MPL without penetration

As mentioned in Section 3.3.3, knowing the gas permeability value (k_{tot}) and the thickness (L_{tot}) of the porous material, namely the membrane filter after coating, then, the thickness (L_{mpl}) of the MPL may be determined from Equation (6.1), and which the actual permeability value (k_{mpl}) of the MPL is determined, from the following equation Ismail et al. (2011):

$$k_{mpl} = \frac{L_{mpl}}{\frac{L_{tot}}{k_{tot}} - \frac{L_{sub}}{k_{sub}}} \quad (6.2)$$

where L_{sub} is the thickness of the membrane filter substrate and k_{sub} is the gas permeability of the membrane filter substrate before coating. The L_{mpl} represents the MPL visible thickness, as described in Figure 6.3.

Figure 6.6. shows a SEM cross-sectional image view for the membrane filter after coating with MPL, and clearly the membrane filter does not permit the penetration of the MPL.

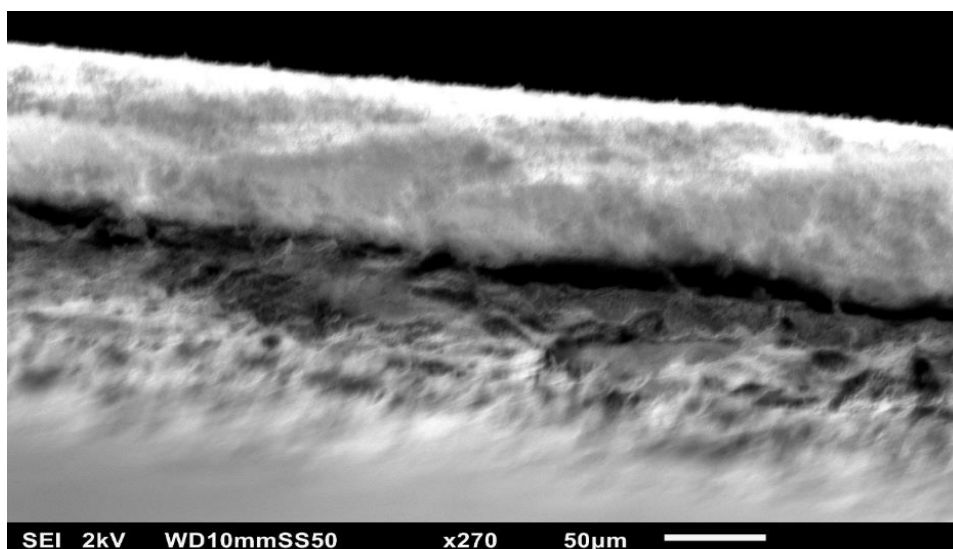


Figure 6.6. SEM cross-sectional image view for the membrane filter after coating with MPL.

6.2.1 MPL gas permeability

The gas permeability and the thickness of the membrane filter substrate before coating is estimated to be $4.25 \times 10^{-13} \text{ m}^2$ and $160 \text{ }\mu\text{m}$. For all other parameter values estimated for determining the (i) gas permeability of the membrane filter after coating, and (ii) the MPL-coated membrane filter thickness. Table 6.2 lists the parameter values of the two carbon loadings (0.5 and 1.0 mg/cm^2) for the two carbon blacks utilised as materials in the MPLs coated on one side of the surface of the membrane filter substrates. Figure 6.7 shows some the SEMs cross-sectional images of membrane filter after coating with 0.5 mg/cm^2 of Ketjenblack carbon black, and coated Vulcan XC-72R carbon black.

Equation (6.2) is used to calculate the through-plane gas permeability of the MPL, average gas permeability of the MPL with Ketjenblack carbon black $2.89 \pm 0.02 \times 10^{-13} \text{ m}^2$ for 0.5 mg/cm^2 and for Vulcan carbon black it gives a value of $5.31 \pm 0.03 \times 10^{-14} \text{ m}^2$. The actual estimated thickness of the MPL with the same composition depends on the amount of the carbon loading. Figure 6.8 shows the MPL thickness of the non-penetrable

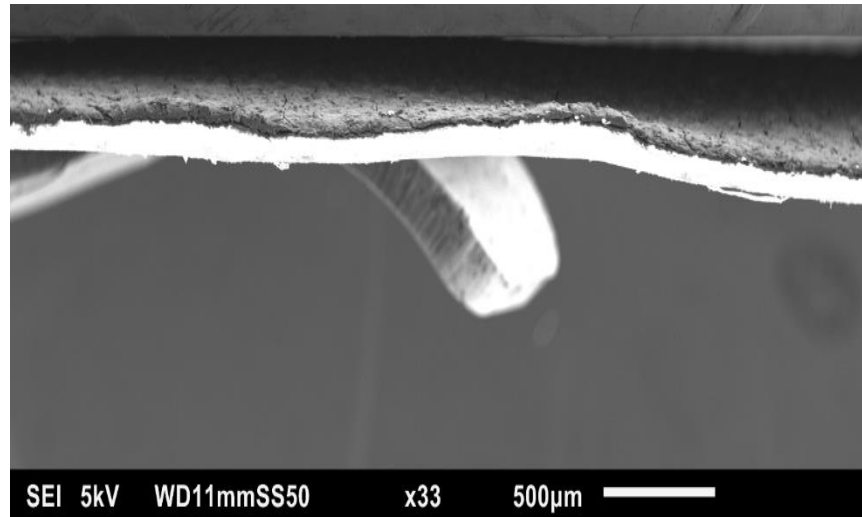
material as a function of the carbon loading. Clearly, the effect of sensitivity of carbon blacks on the thickness of the MPL is observed.

Also, the type of the carbon black used as the material in the MPLs have a significant effect on the thickness and the gas permeability of the MPLs. Figure 6.9 shows the gas permeability values of the MPLs for the Ketjenblack and Vulcan carbon black as a function of the carbon loadings in the MPLs. It is found that the thicknesses of the MPLs with Ketjenblack carbon black have higher magnitude values than the thicknesses of the MPLs with Vulcan carbon black for the two carbon loadings, as shown in Figures 6.8.

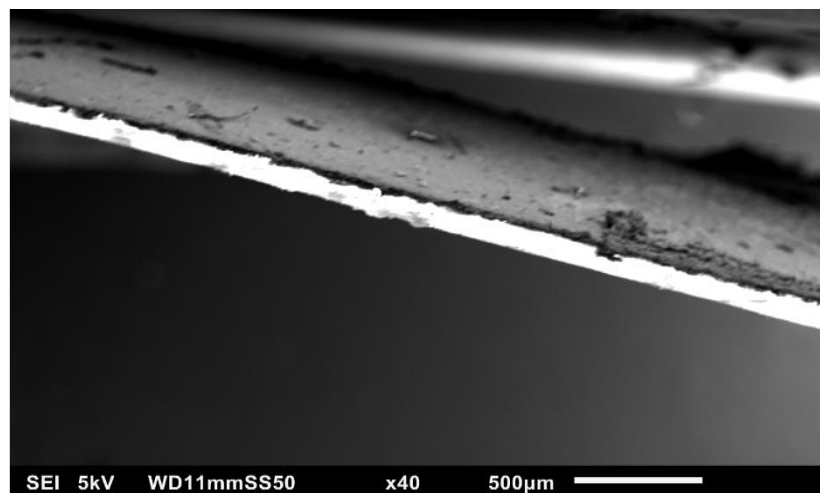
The values of the through-plane gas permeability of the MPLs with no penetration are estimated and used to estimate the penetration of the MPL into the porous carbon substrates. However, the values of the MPL gas permeability have been confidently calculated to estimate the amount of the MPL penetration into the carbon substrates.

Table 6.2. List of the parameters values estimated for the two types of MPLs with no penetration.

Parameters description	0.5 mg/cm² carbon blacks		1.0 mg/cm² carbon blacks	
	Ketjenblack	Vulcan	Ketjenblack	Vulcan
gas permeability / m²	4.04×10^{-13}	3.39×10^{-13}	3.90×10^{-13}	2.66×10^{-13}
L_{coated} / μm	180	166	198	175



(a)



(b)

Figure 6.7. SEMs of (a) a coated membrane filter with 0.5 mg/cm^2 cross-sectional image of Ketjenblack EC-300JD carbon black, and (b) a coated membrane with 0.5 mg/cm^2 cross-sectional image of Vulcan XC-72R carbon black.

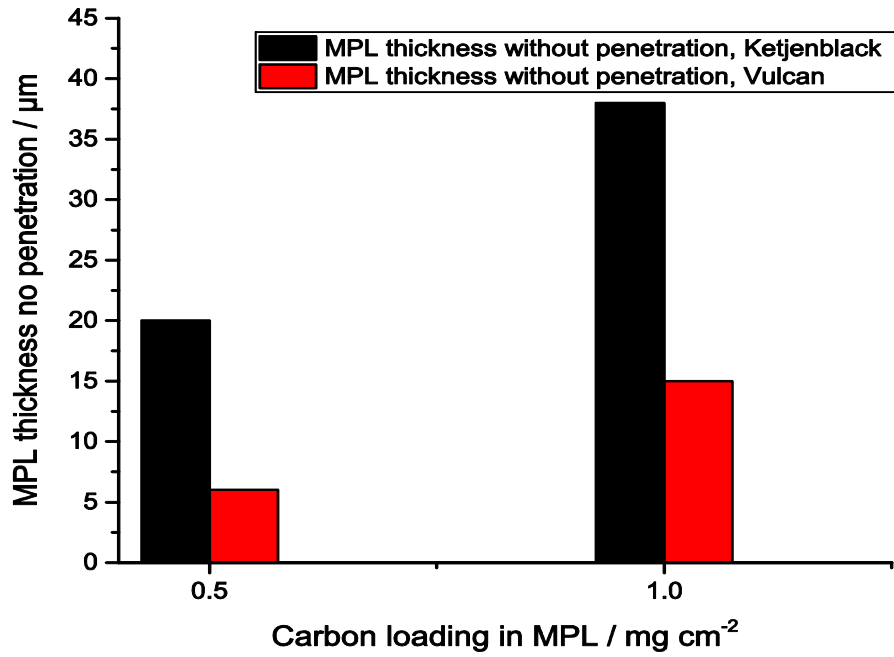


Figure 6.8. The MPL visible thickness without penetration as a function of the carbon loading in the MPL.

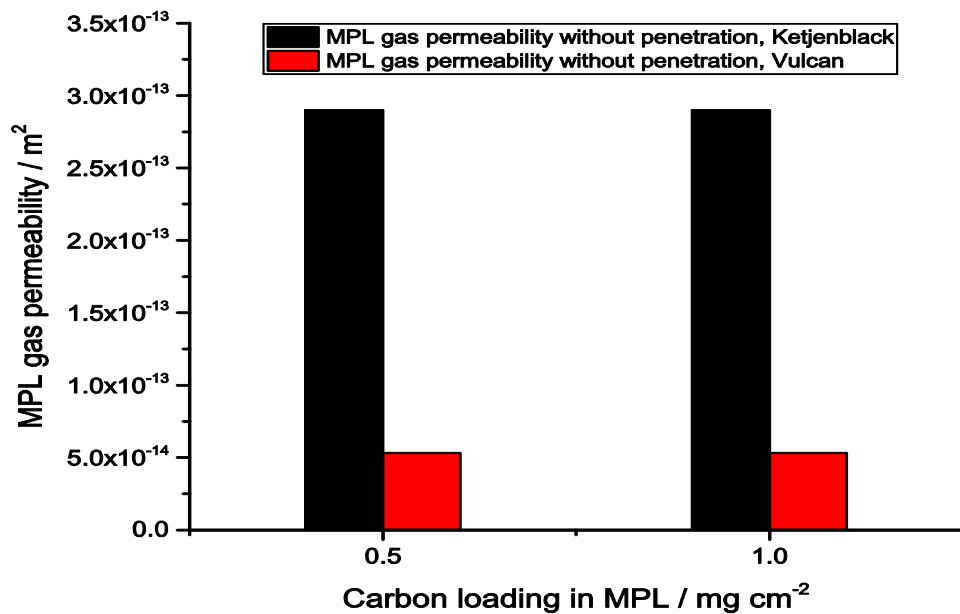
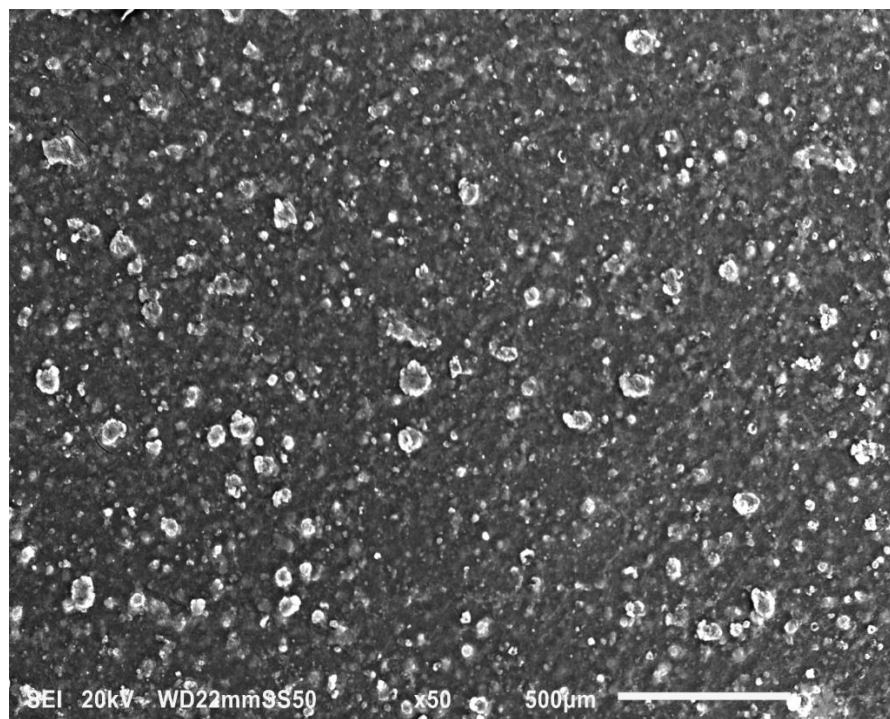


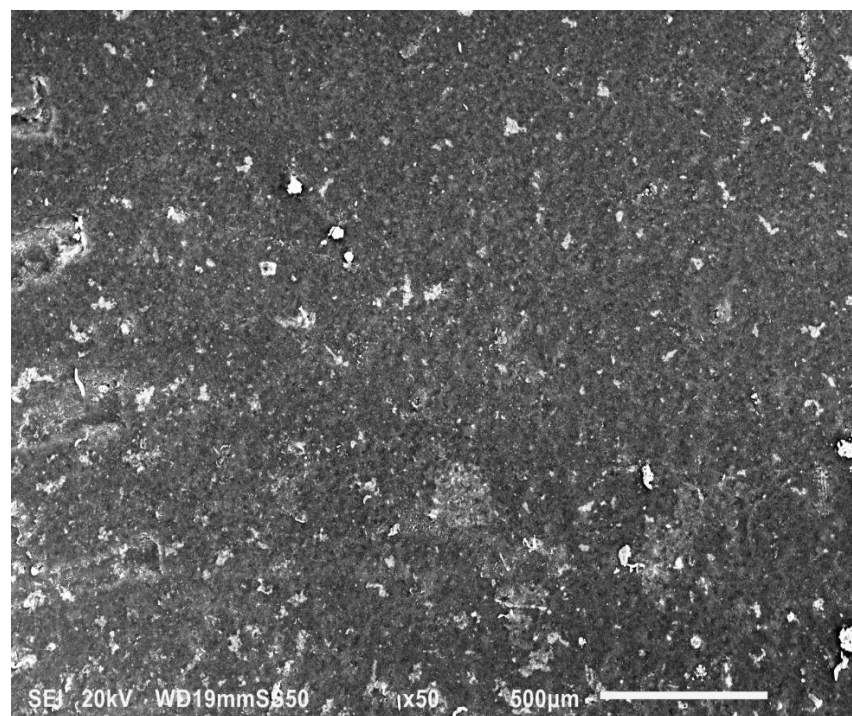
Figure 6.9. Through-plane gas permeability of MPL without penetration as a function of the carbon loading for the Ketjenblack and Vulcan carbon blacks.

Figure 6.10 (a)-(j) present the scanning electron micrographs (SEMs) of the surfaces of the MPLs with Ketjenblack and Vulcan carbon black for the filter membrane with no penetration, respectively. The SEMs of the surface of the MPL were taken with the JEOL JSM-6010LA SEM under an accelerating voltage of 20 kV.

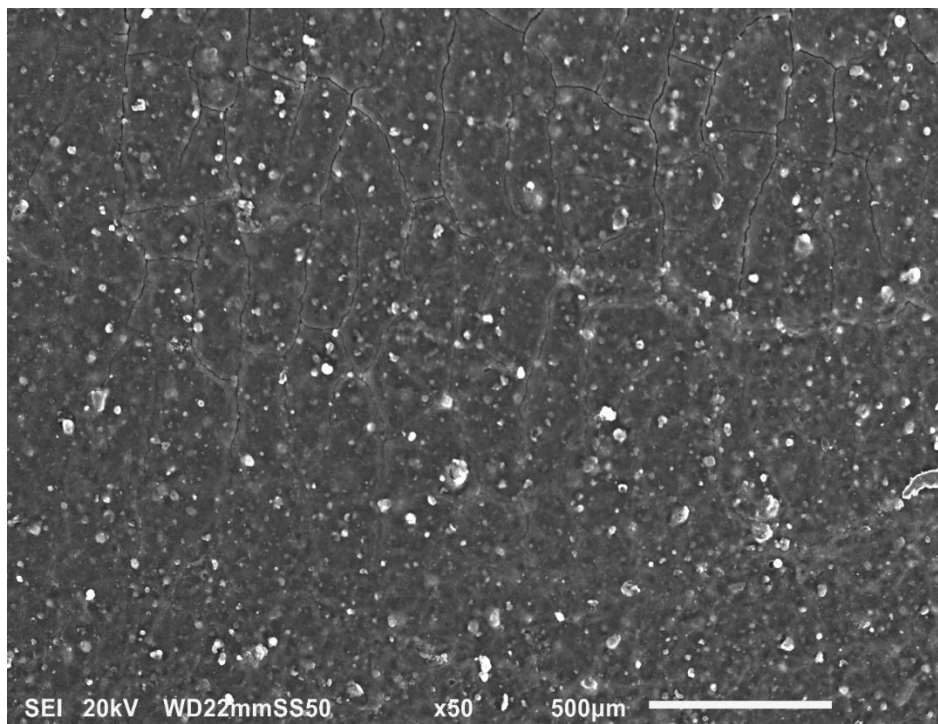
It should be noted that the same amount of carbon black and PTFE loadings in the MPL, i.e. 2.0 mg/cm² of carbon black and 20 wt.% PTFE, and identical preparation technique were applied to prepare the surfaces of the two layers. A comparison of the surfaces of the MPLs, showed no significant difference of the micromorphology of the surfaces of the two MPL layers in Figure 6.10 (a) and (b), the cracks on the surface insignificant, due to the dominant effect of the amount of PTFE content (i.e. 20 wt.%) over the carbon loading (0.5 mg/cm²). Further, it is clearly observed the cracks of the surfaces as the carbon loading in the MPLs increases from 1.0 mg/cm² to 2.5 mg/cm² while, the PTFE loading remained constant at 20 wt.%, see Figures 6.10 (c)–(j). it should be noted that, there is significant difference of cracks on the surfaces of the MPLs and clear indication of the surface morphology structure of the MPLs, which is an evidence that the MPLs made from the two carbon blacks are different.



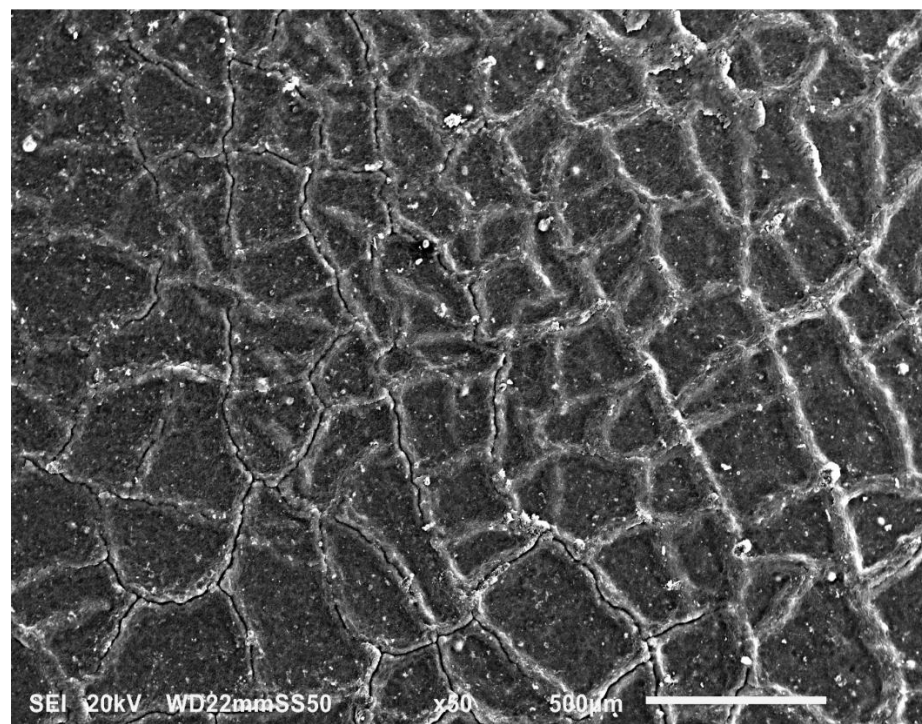
(a) 0.5 mg/cm^2 Ketjenblack and 20 wt.% PTFE loadings.



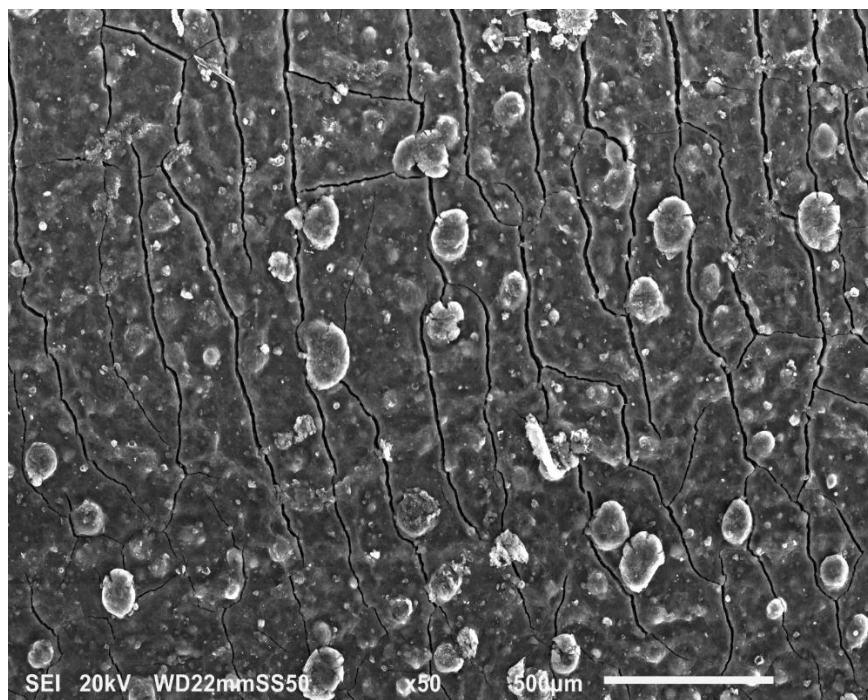
(b) 0.5 mg/cm^2 Vulcan and 20 wt. %PTFE loading.



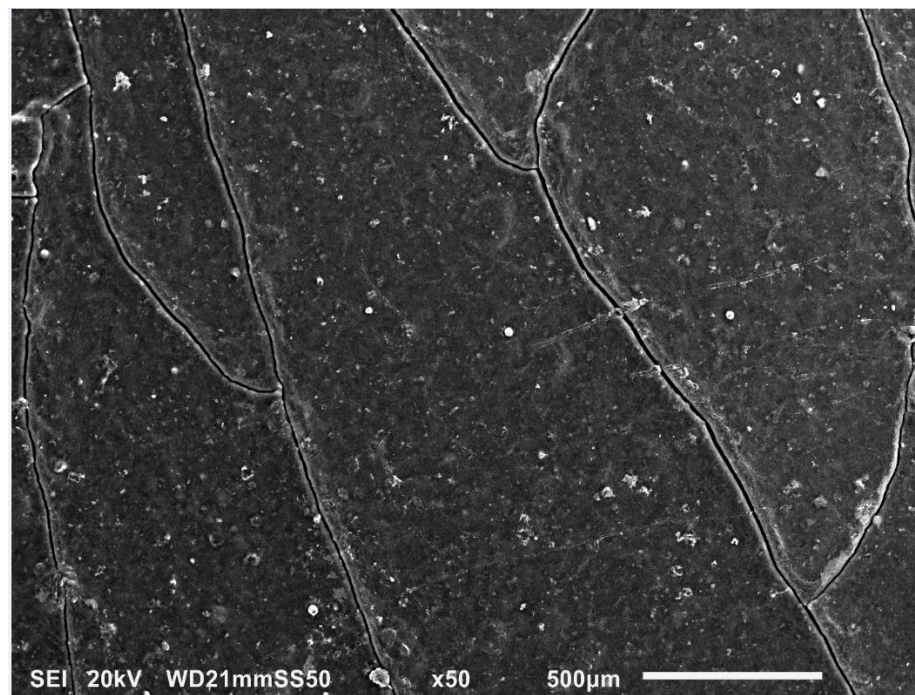
(c) 1.0 mg/cm² Ketjenblack and 20wt. % PTFE loadings.



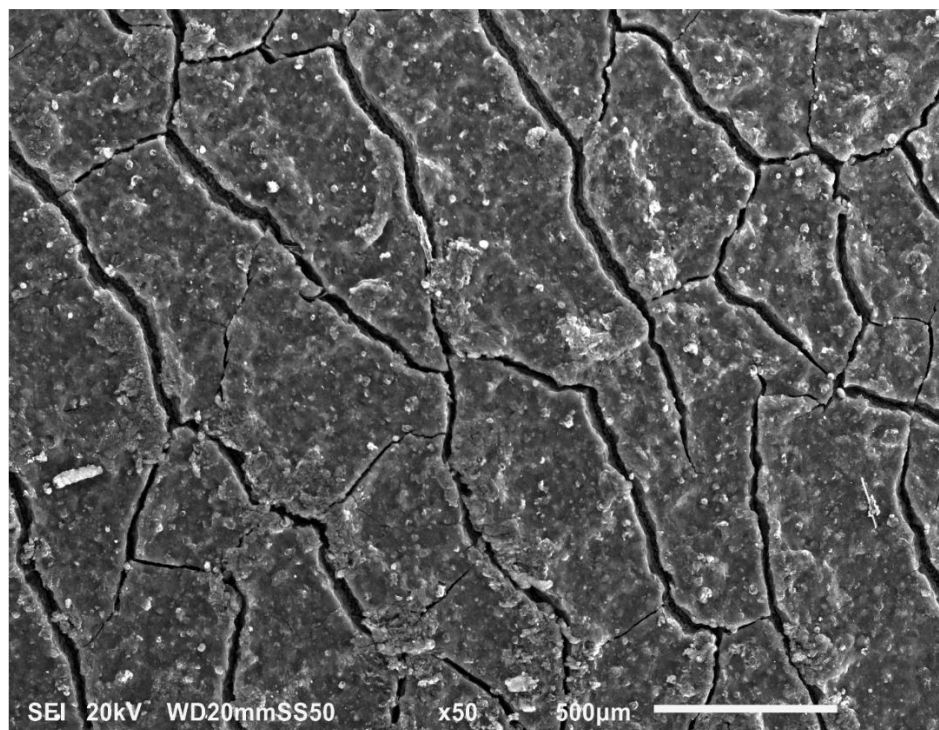
(d) 1.0 mg/cm² Vulcan and 20wt.% PTFE loadings.



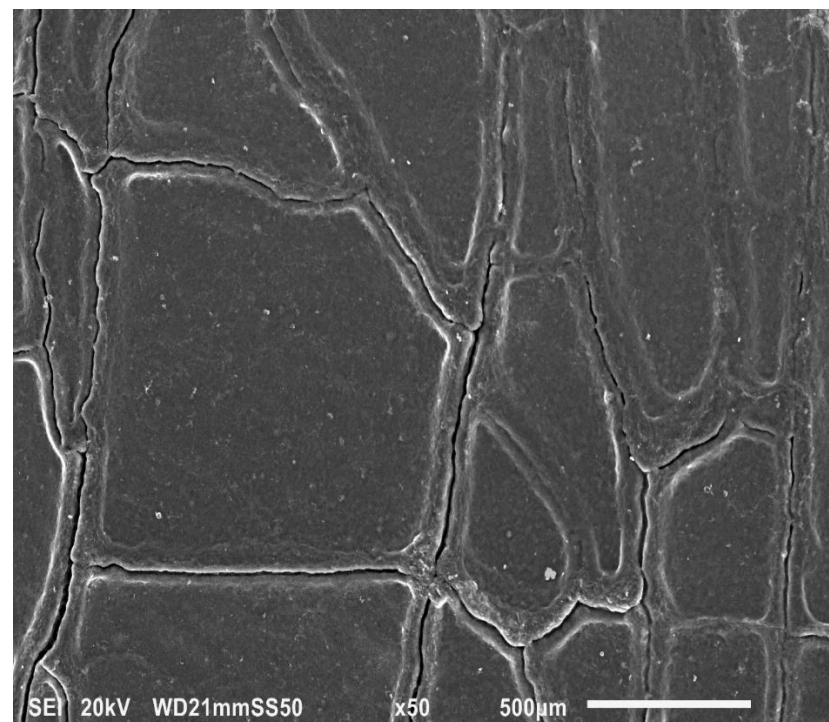
(e) 1.5 mg/cm² Ketjenblack and 20 wt.% PTFE loadings.



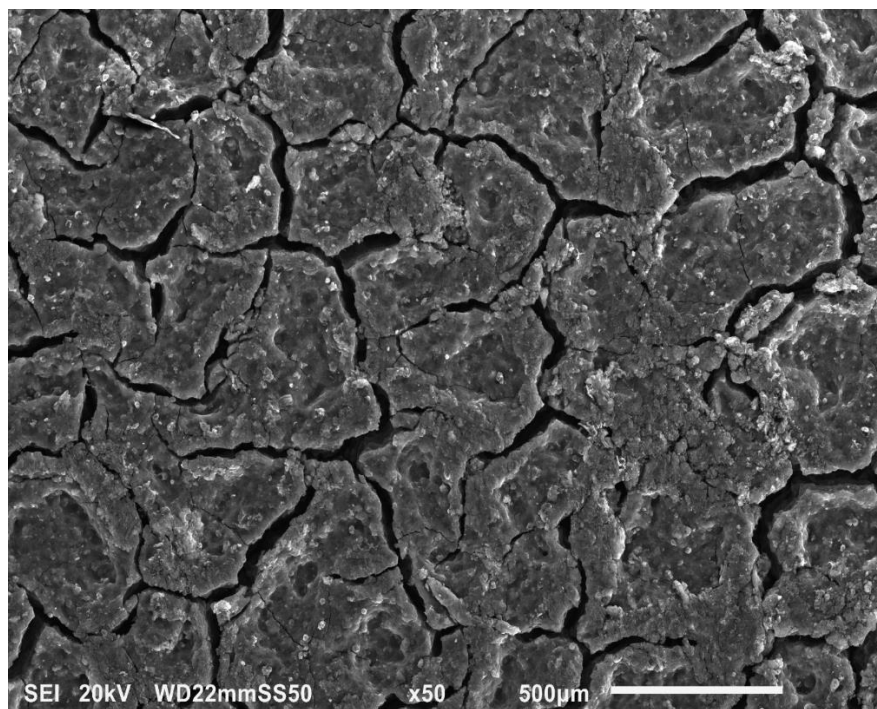
(f) 1.5 mg/cm² Vulcan and 20 wt.% PTFE loading.



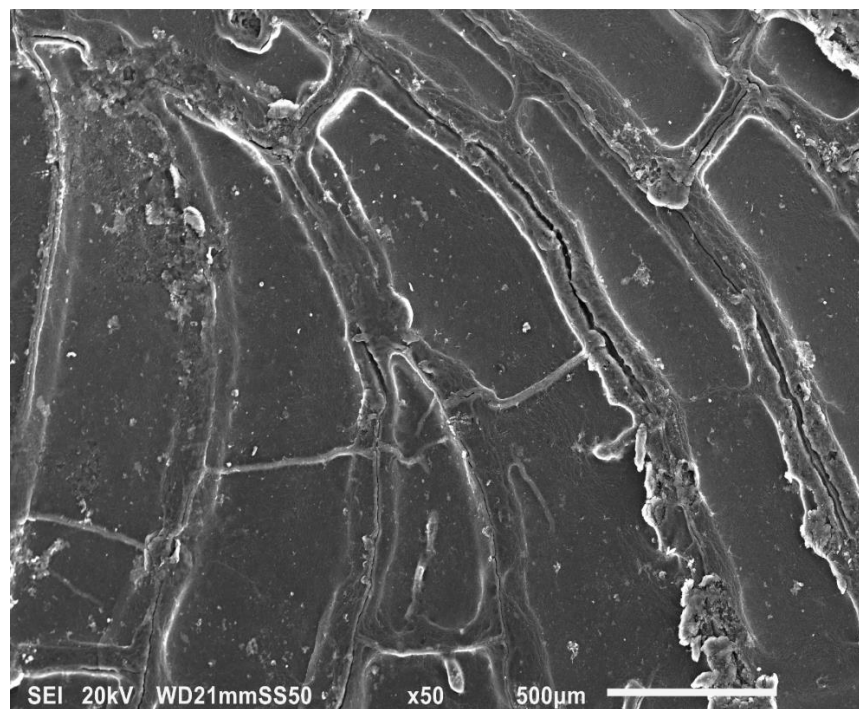
(g) 2.0 mg/cm² Ketjenblack and 20 wt.% PTFE loadings.



(h) 2.0 mg/cm² Vulcan and 20 wt. % PTFE loadings.



(i) 2.5 mg/cm² Ketjenblack and 20 wt.% PTFE loadings.



(j) 2.5 mg/cm² Vulcan and 20 wt.% PTFE loadings.

Figure 6.10. SEMs images for the surfaces of the MPL with various Ketjenblack and Vulcan carbon black loadings of 20 wt.% PTFE.

6.2.2 MPL penetration into the carbon substrate

The effect of the MPL penetration into the carbon substrates is significant. Therefore, Equation (6.2) is slightly modified to account for the penetration of the MPL material to the porous carbon substrate:

$$k_{\text{mpl}} = \frac{L_{\text{mpl_vis}} + L_{\text{pen}}}{\frac{L_{\text{tot}}}{k_{\text{tot}}} - \frac{L_{\text{sub}} - L_{\text{pen}}}{k_{\text{sub}}}} \quad (6.2)$$

where $L_{\text{mpl_vis}}$ is the visible MPL thickness of the carbon substrate and k_{mpl} is permeability of the MPL without penetration, L_{sub} is the visible thickness of the carbon substrate, and L_{pen} is the penetration thickness into the porous carbon substrate. It should be noted that the penetration part of the MPL includes carbon fibres from the carbon substrate, see Figure 6.3.

For simplification, it is assumed in equation (6.2) that the presence of the carbon fibres in the penetration part of the MPL has no effect on its characteristics, such as porosity and pore size Kitahara et al. (2010) and Kim et al. (2013). Therefore, having estimated the MPL gas permeability with no penetration, Equation (6.2) can now be used to estimate the amount of the MPL penetration into the porous carbon substrate as follows:

$$\frac{L_{\text{mpl_vis}} + L_{\text{pen}}}{K_{\text{mpl}}} = \frac{L_{\text{tot}}}{K_{\text{tot}}} - \frac{L_{\text{sub_vis}} - L_{\text{pen}}}{K_{\text{sub}}} \quad (6.3)$$

Therefore, knowing the following values: $L_{\text{mpl_vis}}$, k_{mpl} , L_{tot} , k_{tot} , $L_{\text{sub_vis}}$, and k_{sub} experimentally, then the MPL penetration (L_{pen}) into the porous carbon substrate can be determined. Figure 6.11 shows the penetration of the MPL coating into the porous carbon substrate as a function of the carbon loading in the MPL. This figure presents a

comparison of the penetration of the MPL materials of the two different carbon black types (i.e. Ketjenblack and Vulcan) and the amount of their penetration into the substrate.

From Figure 6.11 it can be seen that the penetration thickness of the MPL relative to the amount of carbon loading is significant, and as the amount of carbon loading increases, then penetration increases. This means that a decrease in the penetration of the MPL thickness into the carbon substrate increases the cross-sectional area of the porous substrate Kitahara et al. (2010), see Figure 6.12.

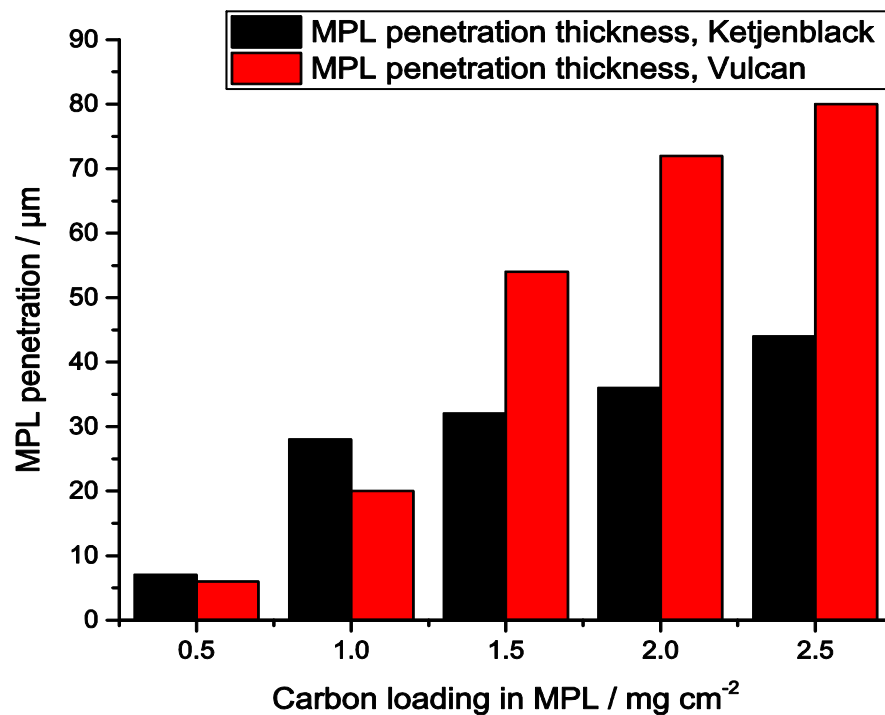


Figure 6.11. Comparison of the MPL penetration thickness of the carbon loading and carbon type.

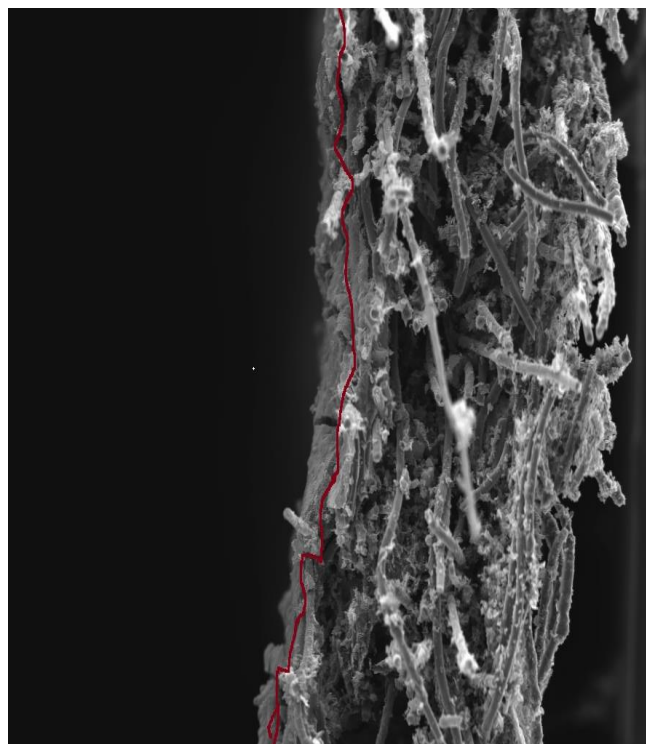
Figure 6.12 shows that the boundary between the visible MPL and the substrate is not clear in order to observe the penetration of the MPL material, and the calculations of the thicknesses of the MPLs have been discussed in Section 5.1, see Figure 5.4. Further, the penetration of the MPL thickness of the Ketjenblack carbon black is of a higher

magnitude at 0.5 and 1.0 mg/cm² carbon loading compared to that of the Vulcan carbon black. With the Vulcan carbon black, the MPL penetration thickness is of a higher magnitude compared with that if the Ketjenblack carbon black as the loading of the related carbon black increases from 1.5 to 2.5 mg/cm² in Figure 6.11. This could be attributed to that when preparing the MPL ink then the size of the Vulcan carbon black agglomerates are smaller than that of the Ketjenblack agglomerates. This indicates that the Vulcan agglomerates have less difficulty in penetrating the porous carbon substrate.

Table 6.3 presents a comparison of the visible and penetration of the MPL thickness of Ketjenblack and Vulcan carbon blacks relative to the amount of carbon loading in the MPL. Clearly, the significant influence of the MPL penetration on the estimation of the total MPL thickness significantly depends on (i) the amount of carbon loading in the MPL, and (ii) the typical carbon black used as the material for the MPL.

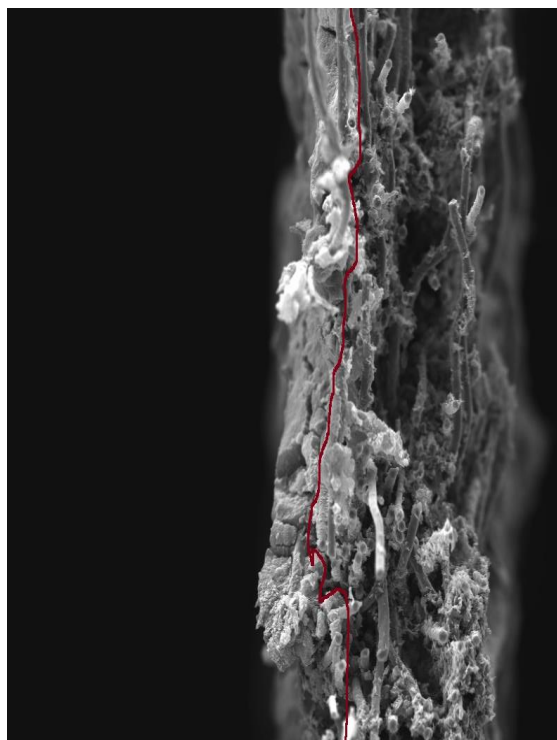
Table 6.3. A comparison of the MPL visible thickness and penetration of the two carbon types for the different carbon loadings in the MPL.

Carbon loading /mg cm ⁻²	MPL with Ketjenblack EC-300JD		MPL with Vulcan XC-72R	
	Visible thickness / μm	Penetration thickness / μm	Visible thickness / μm	Penetration thickness / μm
0.5	20	7	6	6
1.0	41	28	19	20
1.5	80	32	73	54
2.0	88	36	79	72
2.5	122	44	87	80



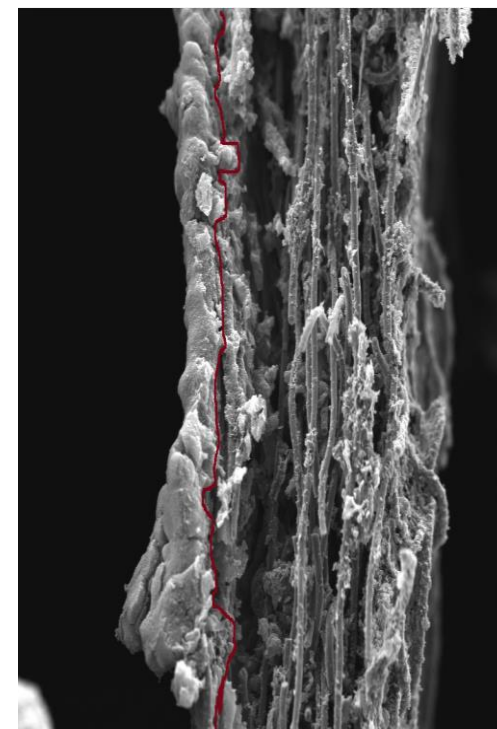
Mag = 300 X WD = 25.5 mm 20.00 kV SE1
Width = 994.4 μ m 100 μ m

0.5 mg/cm² carbon loading.



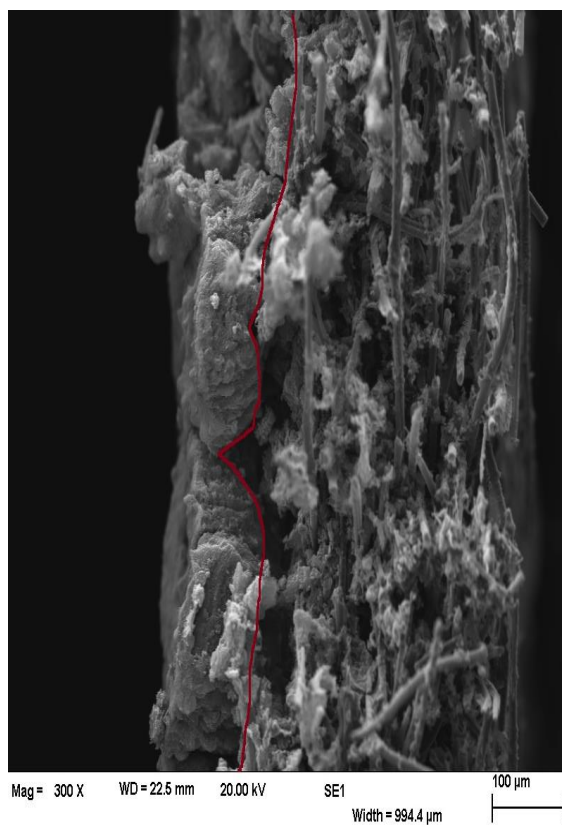
Mag = 300 X WD = 24.0 mm 20.00 kV SE1
Width = 994.4 μ m 100 μ m

1.0 mg/cm² carbon loading.

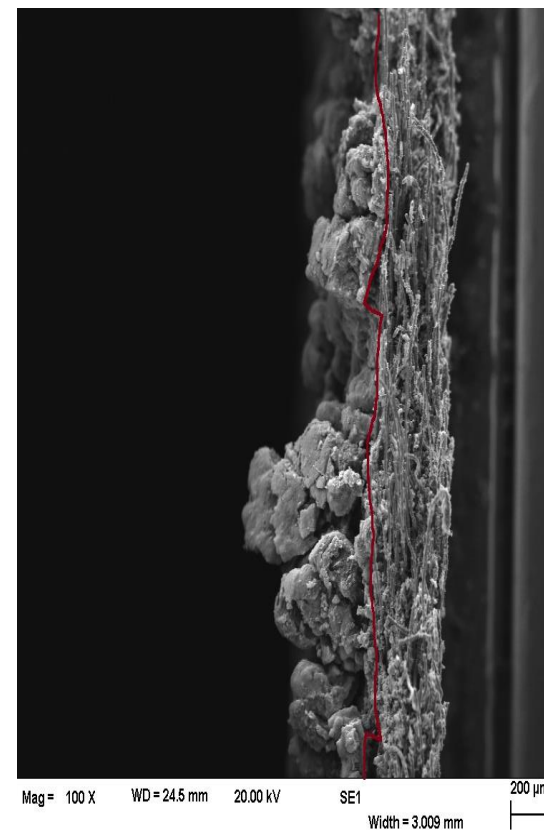


Mag = 300 X WD = 24.5 mm 20.00 kV SE1
Width = 994.4 μ m 100 μ m

1.5 mg/cm² carbon loading.



2.0 mg/cm² carbon loading.



2.5 mg/cm² carbon loading.

Figure 6.12. The SEMs cross-sectional images for the visible MPL thickness and the penetration of the coated GDLs with carbon black.

Furthermore, the overall effect of the MPL penetration thickness on the estimation of the MPL thickness is that the values of the total MPL thickness added to the porous carbon substrate surfaces (GDLs) have been under-estimated, in particular those reported in the modelling literature by Inamuddin et al. (2011) and Yuan et al. (2010). Table 6.4 presents a comparison of the total MPL thickness of the two different carbon black types used as the materials in the MPLs in this study. The table provides an estimate of the total thickness of the MPL and gives estimation of the total thickness of the MPL-coated GDL. This gives a more comprehensive set of information than most of the assumptions that are made in the literature.

Table 6.4. A comparison of the MPL total thickness and the GDL total thickness after the coating of two different carbon types for various carbon loadings in the MPL.

Carbon loading /mg/cm ²	MPL with Ketjenblack EC-300JD		MPL with Vulcan XC-72R	
	MPL total thickness / μm	MPL-coated GDL thickness / μm	MPL total thickness / μm	MPL-coated GDL thickness / μm
0.5	27 \pm 11	439 \pm 5	12 \pm 8	409 \pm 4
1.0	69 \pm 11	481 \pm 9	39 \pm 6	480 \pm 4
1.5	112 \pm 12	524 \pm 12	127 \pm 11	497 \pm 6
2.0	124 \pm 11	536 \pm 9	203 \pm 74	504 \pm 9
2.5	166 \pm 12	578 \pm 5	253 \pm 31	507 \pm 3

In addition, experimental determination of through-plane gas permeability values have been significantly overdetermined due to the visible MPL thickness used as the total estimate of the MPL thickness. The effect of the MPL penetration has been always assumed in modelling the MEA components of PEM fuel cell, by excluding the

penetration thickness of the MPL material into the porous substrate. Apparently, the composition of the MPLs added to the GDL is almost the same.

6.3 Conclusions

In this chapter, the estimation of the MPL penetration thickness for two different carbon black types with various amounts of carbon loading have been determined. A novel method has been used to estimate the amount of the penetration of the MPL material into the porous carbon substrate (GDL). Based on the results obtained, the following conclusions are obtained:

- The penetration thickness of the MPL into the porous carbon substrate is significantly sensitive to the carbon loading in the MPL. This implies that the amount of the carbon loading in the MPL corresponds to the thickness and the penetration of the MPL added to the total thickness of the GDL after coating, and the MPL thickness and the penetration increase as the carbon loading in the MPL increases.
- The carbon black used as the material for the MPL has a significant effect on the MPL thickness and the penetration. This is because the carbon black particle characteristic properties are sensitive to the dispersion of the MPL coated onto the surface of the porous substrate.
- Gas permeability value of the MPL obtained is close in value for the thickness of the MPL with no penetration, and for the different loadings of the same carbon black in the MPLs.

- The MPL thickness is underestimated in the literature as the MPL penetration has not been accounted for, and the results obtained give comprehensive information on the computational modelling of porous media used in polymer electrolyte membrane (PEM) fuel cells.

Having concluded the above, it must be stressed that the gas permeability of the microporous layer that is added to the porous gas diffusion layer in the fuel cell is overestimated.

Further, a decrease in the MPL thickness significantly determines the penetration of MPL material into the carbon substrate, and the across the sectional area of the MPL-coated GDLs used in the PEFCs, however, it enhances the in-plane flow. Therefore, it is of importance to always consider the penetration thickness of the MPL as it significantly affects both the experimental and numerical modelling of the gas diffusion media used in PEM fuel cells.

Chapter 7

Conclusions and Possible Future Work

In this thesis, the primary parameters that affect the performance of the porous materials used in the construction and the design of the gas diffusion media of membrane electrode assemblies (MEAs) have been studied. The gas permeability of the porous gas diffusion materials, namely the gas diffusion layers (GDLs) and microporous layers (MPLs) is experimentally investigated. For this to be achieved, an in-house experimental approach has been employed in order to investigate the effects of (i) carbon black as the material used for the microporous layers, and the sintering of the microporous layers, (ii) compositions of the microporous layer, and (iii) the microporous layer penetration on the gas permeability of the gas diffusion media.

The knowledge contributions (novelty) of this thesis are summarised in the next section of this chapter, which is followed by all the main conclusions from the experimental work performed, and the suggestions on possible future work are also highlighted in this chapter.

7.1 Contribution to Knowledge

The research which has been conducted in this thesis has contributed to knowledge in the following fields:

- Through-plane gas permeability of the coated GDLs decrease after coating with the MPL, slightly reduces after sintering the MPL-coated GDL, and the gas permeability of the MPL-coated GDL made of Ketjenblack carbon black is less than that of the MPL-coated GDLs with MPL of Vulcan carbon black before and

after sintering. The experimental estimations of the gas permeability value are of important in the case of the MPL, in particular after sintering since much information on the reactant gases transport of the MPL itself is required to understand the material interactions in the design and modelling of the fuel cells.

- Further, the novel aspects of this thesis have been highlighted as follows: the gas permeability decreases as the carbon loading increases at a given PTFE loading, the gas permeability of the coated GDL is a minimum at 20 wt.% PTFE loading in the MPL-Ketjenblack carbon black coated GDL and 10 wt.% PTFE loading for the MPL-Vulcan carbon black coated GDL.

The gas permeability increases when the PTFE loading of the MPL increases from 10 to 50 wt.% PTFE loading in the MPL-Vulcan carbon black coated GDLs and 20 wt.% PTFE loading for the MPL-Ketjenblack carbon black coated GDLs. In addition, the gas permeability of the coated GDL with MPL-Ketjenblack carbon black decreases when the PTFE loading of the MPL increases from 10 to 20 wt.%. The gas permeability of 0.5 mg cm⁻² carbon loading decreases with increasing the PTFE in the range 0 to 10 wt.%, for 1.0 mg/cm² carbon loading, the gas permeability remains almost the same and the gas permeability increases between 1.5 and 2.0 mg/cm² carbon loading as the PTFE loading in the MPL increases. The minimum gas permeability was found at 20 wt.% PTFE loading for both the MPLs of the Ketjenblack carbon black and Vulcan carbon black.

The estimation of the MPL penetration thickness for the Ketjenblack carbon black and Vulcan carbon black with various amounts of their loadings in the MPLs have been provided through this study. In addition to that, a novel method has been described and used to estimate the amount of the penetration of the MPL material into the porous carbon substrate (GDL).

- Furthermore, the sensitivity of the penetration of the MPL material into the substrate, determined by the amounts of the carbon loadings and carbon types used, have been evaluated in this thesis. In addition to that, as the PTFE loadings increase in the compositions of the MPLs, the thickness of the MPL relatively increase. The significant effect on the MPL thickness and the penetration has also been evaluated for the modelling of the PEM fuel cells. However, a microscopic change in the composition of the MPL dramatically has an effect on the characteristic properties of the porous media, which can result in a significant change in both the porous media and the PEM fuel cell performance.
- Finally, the actual estimated gas permeability values for different loadings of the carbon black in the MPLs of 0.5 and 1.0 mg/cm² have been obtained, and it has been shown that the gas permeability of the microporous layer that is added to the porous diffusion layer in the fuel cell is underestimated by the literature.

7.2 Conclusions

In order to have a comprehensive information on the gas permeability of the gas diffusion media, i.e. MPL and GDL used in the PEM fuel cells, this work provides an experimental study of the investigated effects on the gas permeability of the MPLs.

- In Chapter 4, the gas permeability of the gas diffusion layers before and after coating have been experimentally investigated. Also, the effects of sintering the

MPLs on the gas permeability of the coated gas diffusion layers (GDLs) have been determined.

The gas permeability of the GDLs coated with MPLs, which have different amounts of carbon loadings have been estimated using two different types of commonly used commercial carbon powders, namely Ketjenblack and Vulcan carbon black. The MPL-added reduces the gas permeability of the GDL, the MPL sintering was found to slightly decrease the gas permeability of the GDL, and the gas permeability of the MPL made of Ketjenblack carbon black is less than that of the MPL-coated GDLs with MPL of Vulcan carbon black. In the order of MPLs, the gas permeability values of the MPL-Vulcan carbon black is higher compared with that of the MPL-Ketjenblack carbon black.

- In Chapter 5, the effects of the compositions of the MPLs on the through-plane gas permeability of the gas diffusion layers was investigated. The gas permeability is found to decrease as the carbon loading increases at a given PTFE loading.

The gas permeability of the GDL is found to be a minimum at 20 wt.% PTFE loading for the MPL-Ketjenblack carbon black and 10 wt.% PTFE loading for the MPL-Vulcan carbon black. The gas permeability is found to increase when the PTFE loading of the MPL increases from 10 to 50 wt.% PTFE loading in the MPL-Vulcan carbon black and 20 wt.% PTFE loading for the MPL-Ketjenblack carbon black. In addition, the coated GDL with MPL-Ketjenblack carbon black was found to decrease when the PTFE loading of the MPL increases from 10 to 20 wt.% PTFE, for all the Ketjenblack carbon loadings investigated.

The gas permeability of 0.5 mg/cm² carbon loading decreases with increasing the PTFE in the range 0 to 10 wt.%, for 1.0 mg/cm² carbon loading, the gas

permeability remains almost the same and the gas permeability increases between 1.5 and 2.0 mg/cm² carbon loading as the PTFE loading in the MPL increases. The minimum gas permeability was found at 20 wt.% PTFE loading for both the MPLs of the Ketjenblack carbon black and Vulcan carbon black.

- Finally, in Chapter 6 an estimation of the MPL penetration thickness for the Ketjenblack carbon black and Vulcan carbon black with various amounts of loadings in the MPLs have been determined. In addition, a novel method has been used to estimate the amount of the penetration of the MPL material into the porous carbon substrate (GDL).

The sensitivity of the penetration of the MPL material into the substrate is determined by the amounts of the carbon loadings and carbon types used. The amount of the carbon loading in the MPL corresponding to the thickness and the penetration of the MPL added to the total thickness of the GDL after coating. The MPL thickness and the penetration increases as the carbon loading in the MPL increases.

It was found that the carbon black used as the material for the MPL has a significant effect on the MPL thickness and the penetration. The estimations of the MPL penetration depth, and the thickness of the layer will enhance the accuracy of the predictions of the gas transport and water flooding in the modelling of the multi-phase flow under operational conditions of high-efficiency in the PEM fuel cell.

It has been shown through the novel method used the value of the MPL gas permeability that is close in value for the different loadings of the carbon black in the MPLs, and which has been proved that the gas permeability of the microporous

layer that is added to the porous diffusion layer in the fuel cell is underestimated by the literature.

Therefore, this study can aid in enabling the realistic and accurate simulation of multi-phase flows, namely the gas transport and liquid water through the porous media with highly non-uniform pore sizes, and complete understanding of how MPL properties affect the efficiency of the PEM fuel cell performance.

7.3 Possible future work

The gas transport inside the porous media is closely related to the MPL-coated GDLs structural characteristics, which plays an important role on the conversion of energy in the PEM fuel cell. In this thesis, the bare GDLs are usually 320-440 μm thick, a common commercial GDL material, namely SGL 10BA is a porous carbon substrate based for the porous media. The GDL properties and parameters, such as thickness and gas permeability have been utilised to characterise the features of the microporous layer, and this has provided possible solutions (results) and explanation for the reconstructing of the porous gas diffusion media micro-layer that have been developed for several stochastic models in the literature. However, MPLs applied to the GDLs exhibit different effects on the gas transport characteristics of the porous gas diffusion media. It should be pointed out that the investigations effects and results discussed in this study are valid only when the properties of the MPL, i. e. thickness and gas permeability, are considered and it may need a further study on the influence of other possible affecting factors.

This study highlights the factors that affect the gas transport properties, namely the gas permeability of the porous materials used in the construction and design of the MPL components of PEM fuel cells. However, more research is required in order to investigate

many parameters that do affect the tailoring of the gas diffusion media effective and efficiency performance of the porous gas diffusion materials in PEM fuel cells, in particular the MPLs that are added to the carbon substrates, and there is a need for further investigations, for example,

- the effect of different carbon substrates (i.e. GDLs) on the investigation of the different sintering time at different sintering temperatures of the MPLs on the gas permeability of the microporous layers coated to the porous materials. In this study, the sintering temperature is at 350 °C for 30 minutes and this is in good agreement with what has been reported in much of the literature, see Chen and Chang (2013), Ko et al. (2010), Kim et al. (2013), Kannan et al. (2006), Han et al. (2006) and Hwang et al. (2011). However, many authors have reported different sintering temperatures and time which can affect the heat treatment of the MPLs coating. For the purpose of porous material requirements and how well the materials satisfy the efficiency of the fuel cell in the modelling of the components, further investigations are required in order to have a better understanding of the sintering different compositions of the MPLs at different sintering temperatures for varying sintering times on the gas transport properties of the porous material used.
- not only should the effect of the compositions of the MPLs on the permeability of the porous media and the MPLs be considered since the effects of the composite of the carbon blacks in the composition of the MPL itself are unknown for the gas permeability of the porous media. Therefore, the development of a numerical simulation that takes into account the gas permeability in the small pores of the MPL with composite carbon black materials has to be investigated. However, this

is another aspect of the cost of the porous materials used in PEM fuel cell for the effective performance of the porous media within the MEA components.

- the effects of the reactant gas flow rates on the gas permeability of the microporous layers compositions and composites carbon materials, and the gas diffusion media are also still under active research. Thus, the small velocity of gas flow has been considered, since the viscous resistance to the gas flow is a major cause of the pressure drop, which in turn is related to the rate of the chemical reactions that take place at the catalyst layer interface. This effect can be studied from the perspective of utilising higher gas velocities that take into account the inertial resistance, when considering the compositions of the microporous layers along with the porous carbon substrates.

Bibliography

- Appleby, A. J. (1992). Fuel cell technology and innovation. *Journal of Power Sources*, 37, pp. 223 – 239.
- Afshari, E, Ziaei-Rad, M., Dehkordi, M. M. (2016) Numerical investigation on a novel zigzag-shaped flow channel design for cooling plates of PEM fuel cells. *Journal of the Energy Institute*, pp. 1-12.
- Antolini, E., Passos, R. R., Ticianeli, E. A. (2002) Effect of the carbon powder characteristics in the cathode gas diffusion layer on the performance of polymer electrolyte fuel cells. *Journal of Power Sources*, 109, pp. 477-82.
- Amirinejad, M., Rowshanzamir, S., Eikani, M. H. (2006) Effects of operating parameters on performance of a proton exchange membrane fuel cell. *Journal of Power Sources*, 161. pp. 872-875.
- Barbir, F. (2013) *PEM fuel cells: Theory and practice*. Elsevier. 2nd edition. Chapter 4: pp. 73 – 117.
- Belkhir, Z., Zeroual, M., Saidani, N. (2011.) A two-dimensional analysis of mass transport in proton exchange membrane fuel cells: influence of porosity and permeability. *International Journal of Chemical and Environmental Engineering*, 2, pp. 390 -394.
- Barbir, F. PEM (2013) *Fuel Cells: Theory and Practice*, 2nd Edition. Elsevier Academic Press. Chapter 1. pp. 8-13.
- Blanco, M. and Wilkinson, D. P. (2010) Diffusion layer. In: D. P. Wilkinson, J. Zhang, R. Hui, J. Fergus and X. Li. *Proton exchange membrane fuel cells: materials properties and performance*. USA, CRC Press. Chapter 4. pp. 196-197.

Boyle, G., Everret, B. and Alexander, G. (2012) Introducing renewable energy. In: G. Boyle. *Renewable Energy: Power for a sustainable future*, 3rd edition. UK, Oxford University Press. Chapter 1: pp. 7-17.

Barbir, F. (2013) *PEM Fuel Cells: Theory and Practice*, 2nd Edition. Elsevier Academic Press. Chapter 2. pp. 17-26.

Bevers, D. Rogers, R. Bradke, M. V.(1996) Examination of the influence of PTFE coating on the properties of carbon paper in polymer electrolyte fuel cells. *Journal of Power Sources*, 63. pp. 193-201.

Barbir, F. (2013) *PEM Fuel Cells: Theory and Practice*, 2nd Edition. Elsevier Academic Press. Chapter 7. pp. 217-218.

Barge, L. M., Kee, T. P., Doloboff, I. J., Hampton, J. M. P., Ismail, M., Pourkashainian, M. Zeytounian, J., Baum, M. M., Moss, J. A., Lin, C. K., Kidd, R. D., Kanik, I. (2014) The fuel cell model of abiogenesis: A new approach to origin-of-life simulations. *Astrobiology*, 14. pp. 254-270.

Barbir, F. (2013) *PEM Fuel Cells: Theory and Practice*, 2nd Edition. Elsevier Academic Press. Chapter 12. pp. 469.

British Broadcasting Corporation (BBC) Weather. www.bbc.co.uk/weather/

Clean Fuel Cell Energy for Today (1999). Developments in proton exchange membrane fuel cells. *Platinum Metals Rev.*, 43, pp. 14 – 17.

Çengel, Y. A. and Cimbala, J. M. (2006) *Fluid Mechanics: Fundamentals and Applications*. McGraw-Hill Companies, New York. Chapter 15: p. 818.

- Choi, B. W., Chung, S. J., and Shin, D. R. (1996) Microstructure of PTFE and acid absorption behaviour in PTFE-bonded carbon electrodes. *International Journal of Hydrogen Energy*, 27, pp. 541-46.
- Chen, H. H., Chang, M. H. (2013) Effect of cathode microporous layer composition on proton exchange membrane fuel cell performance under different air inlet relative humidity. *Journal of Power Sources*, 232, pp. 306-9.
- Chang, H. M., Chang, M. H. (2013) Effect of gas diffusion layer with double-side microporous layer coating on polymer electrolyte membrane fuel cell performance. *Journal of Fuel Cell Science and Technology*, 10, pp. 021005-10.
- Carrigy, N. B., Pant, L. M., Mitra, S., Secanell, M. (2012) Knudsen diffusivity and permeability of PEMFC microporous coated and gas diffusion layers for different polytetrafluoroethylene loadings. *Journal of The Electrochemical Society*, 160 (2), pp. F81-F89.
- Carrette, L., Friedrich, K. A., Stimming, U. (2001) Fuel cells – fundamentals and applications. *Fuel cells*, 1, pp. 5-39.
- Edmund, G., Brown J.R. (2012) California energy commission: Integrated energy policy report update. pp. 1-108.
- El-kharouf, A., Mason, T. J., Brett, D. J. L., Pollet, B. G. (2012) Ex-situ characterisation of gas diffusion layers for proton exchange membrane fuel cells. *Journal of Power Sources*, 218. pp. 393-404.
- Feroldi, D., Basualdo, M. (2012) PEM fuel cells with bio-ethanol processor systems. *Green Energy and Technology*, 87, pp. 49-72.

Gostick, J. T., Fowler, M. W., Pritzker, M. D., Ioannidis, M. A., Behra, L. M. (2006) In-plane and through-plane gas permeability of carbon fibre electrode backing layers. *Journal of Power Sources*, 162 (1), pp. 228-238.

Gurau, V., Bluemle, M. J., De Castro, E. S., Tsou, Y. M., Zawodzinski Jr., T. A., Mann Jr., J. A. (2006) Characterization of transport properties in gas diffusion layers for proton exchange membrane fuel cells 1: Wettability (internal contact angle to water and surface energy of GDL fibers). *Journal of Power of Sources*, 160, pp. 1156-1162.

Giorgi, L., Antolini. E., Pozio, A., Passalacqua, E. (1998) Influence of the PTFE content in the diffusion layer of low-Pt loading electrodes for polymer electrolyte fuel cells. *Electrochimica Acta*, 43, pp. 3675 – 80.

Gibson, P., Gibson, H. S., Rivin, D. (2001) Electrode permeability and flow-field configuration: influence on the performance of a PEMFC. *Colloids and Surfaces A: Physicochemical and Engineering Aspect*, 187-188, pp.469-481.

Gurau, V., Bluemle, M. J., De Castro, E. S., Tsou, Y. M., Zawodzinski, T. A. Jr., Mann, J. A. Jr. (2007) Characterization of transport properties in gas diffusion layers for proton exchange membrane fuel cells 2. Absolute permeability. *Journal of Power Sources*, 165 (2), pp. 793-802.

Hoffmann, P. (2012) Tomorrow's Energy: hydrogen, fuel cells, and the prospects for a cleaner planet. London, The MIT Press, 2012. Chapter 5: pp. 89 – 91.

Hu, G., Li, G., Zheng, Y., Zhang, Z., Xu, Y. (2014) Optimization and parametric analysis of PEMFC based on an agglomerate model for catalyst layer. *Journal of the Energy Institute*, 87, pp. 163 – 174.

Haile, S. M. (2003) Fuel cell materials and components. *Acta Materialia*, 51, pp. 5981 – 6000.

Hossain, M., Islam, S. Z., Pollard, P. (2013) Investigation of species transport in a gas diffusion layer of a polymer electrolyte membrane fuel cell through two-phase modelling. *Renewable Energy*, 51, pp. 404-418.

Hoogers, G., 2003 (ed.). Fuel cell technology handbook. Florida: CRC Press LLC.

Ismail, M. S., Damjanovic, T. Hughes, K., Ingham, D. B., Ma, L., Pourkashanian, M., Rosli, M. (2010) Through-plane permeability for untreated and PTFE-treated gas diffusion layers in proton exchange membrane fuel cells. *Journal of Fuel Cell Science and Technology*, 7, pp.1-7.

Ihonen, J. Mikkola, M., Lindbergh, G. (2004) Flooding of gas diffusion backing in PEFCs physical and electrochemical characterization. *Journal of the Electrochemical Society*, 151 (8), pp. A1152-A1161.

Ismail, M. S., Hassanpour, A., Ingham, D. B., Ma, L., Pourkashanian, M. (2012) On the compressibility of gas diffusion layers in proton exchange membrane fuel cells. *Fuel Cells*, 3, pp. 375-383.

Ismail, M. S., Borman, D., Damjanovic, T., Ingham, D. B., Pourkashanian, M. (2011) On the through-plane permeability of microporous layer-coated gas diffusion layers used in proton exchange membrane fuel cells. *International Journal of Hydrogen Energy*, 36, pp. 10392-10402.

Ismail, M. S., Damjanovic, T., Ingham, D. B., Pourkashanian, M. Westwood, A. (2010) Effect of polytetrafluoroethylene-treatment and microporous layer-coating on the

electrical conductivity of gas diffusion layers used in proton exchange membrane fuel cells. *Journal of Power Sources*, 195, pp. 2700-2708.

Ismail, M. S., Hughes, K. J., Ingham, D. B., Ma, L., Pourkashanian, M. (2012) Effects of anisotropic permeability and electrical conductivity of gas diffusion layers on the performance of proton exchange membrane fuel cells. *Applied Energy*, 95, pp. 50-63.

Ismail, M. S., Damjanovic, T., Ingham, D. B., Ma, L., Pourkashanian, M. (2010c) Effect of polytetrafluoroethylene-treatment and microporous layer-coating on the in-plane permeability of gas diffusion layers used in proton exchange membrane fuel cells. *Journal of Power Sources*, 195, pp. 6619-6628.

Ismail, M. S., Ingham, D. B., Hughes, K. J., Ma, L., Pourkashanian, M. (2015) Effective diffusivity of polymer electrolyte fuel cell gas diffusion layers: An overview and numerical study. *International Journal of Hydrogen Energy*, 40, pp. 10994-11010.

Inamuddin, Cheema, T. A., Zaidi, S. M. J., Rhman, S. U. (2011) Three dimensional numerical investigations for the effects of gas diffusion layer on the PEM fuel cell performance. *Renewable Energy*, 36, pp. 529-535.

Jena, A., Gupta, K., Characterization of porosity of electrodes and separators in fuel cell industry. *Proceedings of the Annual Nagoya International battery and Power Sources Conference*, 1999. 1, pp. 105 – 114.

Jordan, L. R., Shukla, A. K., Behrsing, T., Avery, N. R., Muddle, B. C., Forsyth, M. (2000a) Diffusion layer parameters influencing optimal fuel cell performance. *Journal of Power Sources*, 86, pp. 250-254.

- Jordan, L. R., Shukla, A. K., Behrsing, T., Avery, N. R., Forsyth, M. (2000b) Effect of diffusion-layer morphology on the performance of polymer electrolyte fuel cells operating at atmospheric pressure. *Journal of Applied Electrochemistry*, 30, pp. 641-46.
- Kulikovsky, A. A., Divisek, J., Kornyshev, A. A. (1999) Modeling the cathode compartment of polymer electrolyte fuel cells: dead and active reaction zones. *Journal of The electrochemical Society*, 146, pp. 3981 – 3991.
- Koido, T., Furusawa, T., Moriyama, K. (2008) An approach to modelling two-phase transport in the gas diffusion layer of a proton exchange membrane fuel cell. *Journal of Power Sources*, 175, pp. 127 – 136.
- Kim, Y. S., Peck, D. H., Kim, S. K. Jung, D. H., Lim, S., and Kim, S. H. (2013) Effects of the microstructure and powder compositions of a micro-porous layer for the anode on the performance of high concentration methanol fuel cell. *International Journal of Hydrogen Energy*, 38, pp. 7159-68.
- Kitahara, T., Konomi, T., Nakajima, H. (2010) Microporous layer coated gas diffusion layers for enhanced performance of polymer electrolyte fuel cells. *Journal of Power Sources*, 195 (8), pp. 2202-2211.
- Ko, T. H., Kuo, W. S., Su, S. H., Lin, J. H., Chen, W. H. (2010) Effect of multi micro porous layer in proton exchange membrane fuel cell. *Exchange Membrane Fuel Cell*, pp. 1-4.
- Ladislaw, S. O., (2011). Energy and development trends: the role of rapidly emerging countries. *The Centre for Strategic and International Studies*, pp. 1 – 13.
- Litster, S., Mclean, G. (2004) PEM fuel cell electrodes. *Journal of Power Sources*, 130, pp. 61 – 76.

- Lin, G., He, W., Nguyen, T. V. (2004) Modeling liquid water effects in the gas diffusion and catalyst layers of the cathode of a PEM fuel cell. *Journal of The Electrochemical Society*, 151, p. A1999 – A2006.
- Lin, G. Nguyen, and T. V. (2005) Effect of thickness and hydrophobic polymer content of the gas diffusion layer on electrode flooding level in a PEMFC. *Journal of The Electrochemical Society*, 152 (10), pp. A1942-48.
- Lee, H. K., Park, J. H., Kim, D. Y., Lee, T. H. (2004) A study on the characteristics of the diffusion layer thickness and porosity of the PEMFC. *Journal Power Sources*, 131, pp. 200-206.
- Lim, C., Wang, C. Y. (2004) Effects of hydrophobic polymer content in GDL on power performance of a PEM fuel cell. *Electrochimica Acta*, 49, pp. 4149-4156.
- Mattick, C. S., Williams, E, Allenby, B. R. (2010). History trends in global energy consumption. *IEEE Technology and Society Magazine*, pp. 23 – 30.
- Merewether, E. A. (2003). Alternative sources of energy – an introduction to fuel cells. US. Geology Survey Bulletin 2179 [Online], [Accessed Date: 16 – 06 – 2013].<http://pubs.usgs.gov/bul/b2179>.
- Maiyalagan, T., Pasupathi, S. (2010) Components for PEM fuel cells: an overview. *Materials Science Forum*, 657. pp. 143 – 189.
- Mathias, M., Roath, J., Fleming, J. Lehnert, W. (2010) Diffusion media materials and characterisation. *Handbook of Fuel Cells*, 3, pp. 517-537.
- Mortazavi, M., Tajir, K. (2014) Effect of the PTFE content in the gas diffusion layer on water transport in polymer electrolyte fuel cells (PEFCs). *Journal of Power Sources*, 245, pp. 236-244.

Morris, D. and Scurlock, J. Bioenergy. In: G. Boyle. Renewable Energy: Power for a sustainable future, (3rd edition). UK, Oxford University Press, 2012. Chapter 4. pp. 117-126.

Moffat, R. J. (1988) Describing the uncertainties in experimental results. *Experimental Thermal and Fluid Science*, 1. pp. 3-17.

Moreira, J., Ocampo, A. L., Sebastian, P. J., Smit, M. A., Salazar, M. D., Angel, P. D., Montoya, J. A., Pérez, R., Martinez, L. (2003) Influence of the hydrophobic material content in the gas diffusion electrodes on the performance of a PEM fuel cell. *International Journal of Hydrogen Energy*, 28, pp. 625-627.

Merewether, E. A. Alternative Sources of Energy – An introduction to fuel cells [Online]. 2003.[AccessedDate: 17-0602013]. Available from: <http://pubs.usgs.gov/bul/b2179/B2179-508.pdf>.

Nguyen, T. V, Ahosseini A., Wang, X., Yarlagadda, V., Kwong, A., Weber, A. Z., Deevanhxay, P., Tsushima, S., Hirai, S. (2015) Hydrophobic gas-diffusion media for polymer-electrolyte fuel cells by direct fluorination. *Journal of The Electrochemical Society*, 162, pp. F1451-60.

Nield, D. A. and Bejan, A. (2013) *Convection in porous media*. 4th ed. London, Springer. Chapter 1. pp. 4-6.

National Institute of Standards and Technology (NIST). <https://www.nist.gov/>

National energy education development (NEED), 2016. Secondary energy infobook. <http://www.need.org/files/curriculum/guides/Secondary%20Energy%20Infobook.pdf>.

Orogbemi, O. M., Ingham, D. B., Ismail, M. S., Hughes, K. J., Ma, L., Pourkashanian, M. (2016) The effects of the composition of microporous layers on the permeability of

gas diffusion layers used in polymer electrolyte fuel cells. *International Journal of Hydrogen Energy*, 41, pp. 21345-21351.

Owejan, J. P., Trabold, T. A., Jacobson, D. L., Arif, M., Kandlikar, S. G. (2007) Effects of flow field and diffusion layer properties on water accumulation in a PEM fuel cell. *International Journal of Hydrogen Energy*, 32, pp. 4489-02.

Orogbemi, O. M., Ingham, D. B., Ismail, M. S., Hughes, K. J., Ma, L., Pourkashanian, M. (2016) Through-plane gas permeability of gas diffusion layers and microporous layer: effects of carbon loading and sintering. *International Journal of the Energy Institute*, 2016

O'Hayre, R. P., Cha, S. W., Colella, W., Prinz, F. B., Fuel cell fundamentals. John Wiley & Sons, 2006. Chapter 1. pp. 3-19.

Ong, A. L., Bottino, A., Capannelli, G., Comite, A. (2008) Effect of preparative parameters on the characteristic of poly (vinylidene fluoride)-based microporous layer for proton exchange membrane fuel cells. *Journal of Power Sources*, 183, pp. 62-68.

O'Hayre, R. P., Cha, S. W., Colella, W., Prinz, F. B., Fuel cell fundamentals. John Wiley & Sons, 2006. Chapter 6. pp. 169-204.

Orogbemi, O. M., Ingham, D. B., Ismail, M. S., Hughes, K. J., Ma, L., Pourkashanian, M. (2017) A novel method to estimate the microporous layer penetration into the polymer electrolyte fuel cell gas diffusion layer (about to publish).

Philibert, C. (2007) Technology penetration and capital stock turnover: Lessons from IEA scenario analysis. *International Energy Agency*, 4, pp. 6 – 19.

Park, S., Lee, J. W., Popov, B. N. (2006) Effect of carbon loading in microporous layer on PEM fuel cell performance. *Journal of Power Sources*, 163, p. 357-363.

- Park, S. B. Kim, S., Park, Y. I., Oh, M. H. (2009) Fabrication of GDL microporous layer using PVDF for PEMFCs. *Journal of Physics*, 165, pp. 012042-012042.
- Parikh, N., Allen, J. S., Yassar, R. S. (2012) Microstructure of gas diffusion layers for PEM fuel cells. *Fuel Cell*, 12, pp. 382-390.
- Park, S., Lee, J. W., Popov, B. N., (2012) A review of gas diffusion layer in PEM fuel cells: Materials and designs. *International Journal of Hydrogen Energy*, 37 (7), pp. 5850-5865.
- Pharoah, J. G. (2005) On the permeability of gas diffusion media used in PEM fuel cells. *Journal of Power Sources*, 144, pp. 77-82.
- Prasanna, M. Ha, H. Y. Cho, E. A., Hong, S. -A., Oh, H.-H. (2004) Influence of cathode gas diffusion media on the performance of the PEMFCs. *Journal of Power Sources*, 131 (1-2), pp. 147-154.
- Park, S., Lee, J. W., Popov, B. N., (2008) Effect of PTFE content in microporous layer on water management in PEM fuel cells. *Journal of Power Sources*, 177, pp. 457-463.
- Park, G. G., Sohn, Y. J., Yang, T. H., Yoon, Y. G., (2004) Effect of PTFE contents in the gas diffusion media on the performance of PEMFC. *Journal of Power Sources*, pp. 182-187.
- Qi, Z., and Kaufman, A. (2002) Improvement of water management by a microporous sublayer for PEM fuel cells, *Journal of Power Sources*, 109, pp. 38-46.
- Ramasamy, R. P., Kumbur, E. C., Mench, M. M., Liu, W., Moore, D., Murthy, M. (2008) Investigation of micro – and micro-porous layer interaction in polymer electrolyte fuel cells. *International Journal of Hydrogen Energy*, 33, pp. 3351-3367.

Rohendi, D. Majlan, E. H. Mohamed, A. B., Daud, W. R. W., Kadhum, A. A. H., Shyuan, L. K. (2014) Effect of PTFE content and sintering temperature on the properties of a fuel cell electrode backing layer. *Journal of Fuel Cell Science and Technology*, 11 (4), pp. 1-6.

Ramage, J. Hydroelectricity. In: G. Boyle. *Renewable for a sustainable future*, 3rd edition. UK, Oxford University Press, 2012. Chapter 5. pp. 185-190.

Robert, A. and Dietmar, G. Scanning Electron Microscopy. In: H. Wang, X. Z. Yuan, H. Li. *PEM Fuel Cells Diagnostic Tools*, London, CRC Press, 2012. Chapter 14: pp. 315-319.

Singh, D., Lu, D. M., Djilali, N., (1999) A two-dimensional analysis of mass transport in proton exchange membrane fuel cell. *International Journal of Engineering Science*, 37, pp. 431 – 452.

Sin, Y. T., Najmi W. M., W. A. (2013) Industrial and academic collaboration strategies on hydrogen fuel cell technology development in Malaysia. 6th International Conference on University Learning and Teaching (InCULT 2012). *Procedia-Social and Behavioral Sciences*, 90, pp. 879-888.

Subramanian, S., Rajaram, G., Palaniswamy, K., Jothi, V. R., (2016) Comparison of perforated and serpentine flow fields on the performance of proton exchange membrane fuel cell. *Journal of the Energy Institute*, pp. 1-9.

Schweiss, R., (2016) Benefits of membrane electrode assemblies with asymmetrical GDL configurations for PEM fuel cells. *Fuel cells*, 16, pp. 100-106.

- Su, H., Sita, C., Pasupathi, S., (2016) The effect of gas diffusion layer PTFE content on the performance of high temperature proton exchange membrane fuel cell. *International Journal of Electrochem Science*, 11, pp. 919-2926.
- Shou, D., Tang, Y., Ye, L, Fan J, Ding F. (2013) Effective permeability of gas diffusion layer in proton exchange membrane fuel cells. *International Journal of Hydrogen Energy*, 38, pp. 10519-10526.
- Sørensen, B., Hydrogen and fuel cells: Emerging technologies and applications. Elsevier Academic Press, 2004. Chapter 2. pp. 5.
- Soler, J., Hontanon, E., Daza, L. (2003) Electrode permeability and flow-field configuration: influence on the performance of a PEMFC. *Journal of Power Sources*, 118, pp. 172-178.
- Sørensen, B., A history of energy: Northern Europe from the stone age to the present day. New York (USA), Earthscan, 2012. Chapter 10. pp. 385-411.
- Tseng, C. J., and Lo, S. K. (2010) Effect of microstructure characteristics of gas diffusion layer and microporous layer on the performance of PEMFC. *Energy Conversion and Management*, 51, pp. 677-684.
- Tadbir, M. A., Hannach, M.E., Kjeang, E., Bahrami, M. (2015) An analytical relationship for calculating the effective diffusivity of micro-porous layers. *International Journal of Hydrogen Energy*, 40, pp. 10242-10250.
- Tamayol, A., McGregor, F., Bahrami, M. (2012) Single phase through-plane permeability of carbon paper gas diffusion layers. *Journal of Power Sources*, 204, pp. 94-99.
- Taylor, D. Wind Energy. In: G. Boyle. *Renewable Energy: Power for a sustainable future*, 3rd edition. UK, Oxford University Press, 2012. Chapter 7. pp. 297-299.

Uchida, M., Aoyama, Y., Eda, N., Ohta, A. (1995) Investigation of the microstructure in the Catalyst layer and effects of both Perfluorosulfonate Ionomer and PTFE-loaded carbon on the catalyst layer of polymer electrolyte fuel cells. *Journal of Electrochemical Society*, 142, pp. 4143-4149.

Vidmar, J. Costa M. D., Karim, S., Foulkes, F. R. (2009) The influence of hydrophobic polymer content in the microporous layer on the performance of proton exchange membrane fuel cell, *IEEE*, pp. 669-674.

Valayutham, G., Kaushik, J., Rajalakshmi, N, Dhathathreyan, K. S. (2007) Effect of PTFE content in gas diffusion media and microlayer on the performance of PEMFC tested under ambient pressure, *Fuel Cells*, 7, pp. 314-318.

Williams, J. C. (2006). History of Energy. *The Frankline Institute's Resources for Science learning*, pp. 2 – 8.

Williams, M. V., Begg, E., Bonville, L., Kunz, H. R., Fenton, J. M. (2004) Characterization of gas diffusion layers for PEMFC. *Journal of the Electrochemical Society*, 151 (8), pp. A1173-A1180.

Williams, M. V., Kunz, H. R. Fenton, J. M. (2004) Influence of convection through gas diffusion layers on limiting current in PEMFCs using as serpentine flow field. *Journal of the Electrochemical Society*, 151 (10), pp. A1617-A1627.

Wu, R. Liao, Q., Zhu, X. Wang, H. (2012) Liquid and oxygen transport through bilayer gas diffusion materials of proton exchange membrane fuel cells. *International Journal of Heat and Mass Transfer*, 55 (23-24), pp. 6363-6373.

- Wilde, P. M. Mändle, M. Murata, M. Berg, N. (2004) Structure and physical properties of GDL and GDL/BPP combinations and their influence on PEFC performance. *Fuel Cells*, 4 (3), pp. 180-184.
- Wang, X. L. Zhang, H. M., Zhang, J. L., Xu, H. F., Tian, Z. Q., Chen, J., Zhong, H. X., Liang, Y. M., and Yi, B. L. (2006) Micro-porous layer with composite carbon black for PEM fuel cells. *Electrochimica Acta*, 51, pp. 4909-4915.
- Wang, X., Nguyen, T. V., Hussey, D. S., Jacobson, D. L. (2010) An experimental study of relative permeability of porous media used in porous exchange membrane fuel cells. *Journal of the Electrochemical Society*, 157, pp. B1777-B1782.
- Wang, X., Zhang, H., Zhang, J., Xu, H., Zhu, X., Chen, J., Yi, B. (2006) A bi-functional micro-porous layer with composite carbon black for PEM fuel cells. *Journal of Power Sources*, 162, pp. 474-479.
- Weber, A. Z. Newman, J. (2005) Effects of microporous layers in polymer electrolyte fuel cells. *Journal of the Electrochemical Society*, 152, pp. A677- A688.
- Wang, Z. H., Wang, C. Y., Chen, K. S. (2001) Two-phase flow and transport in the air cathode of proton exchange membrane fuel cells. *Journal of Power Sources*, 94. pp.40-50.
- Wang, Y., Chen K. S., Mishler, J., Cho, S. C., Adroher, X. C. (2011) A review of polymer electrolyte membrane fuel cells: technology, applications, and needs on fundamental research. *Applied Energy*, 88. pp. 981-1007.
- Weber, A. Z., Newman, J. (2004) Transport in polymer-electrolyte membranes III. Model validation in a Simple Fuel-Cell Model. *Journal of The Electrochemical Society*, 151. pp. A326-A339.

Xie, Z., Chen, G., Yu, X., Hou, M., Shao, Z. Hong, S. Mu, C. (2015) Carbon nanotubes grown in situ on carbon paper as a microporous layer for proton exchange membrane fuel cells. *International Journal of Hydrogen Energy*, 40, pp. 8958-8965.

Xue, S., Yin, G. (2006) Methanol permeability in sulfonated poly (etheretherketone) membranes: A comparison with Nafion membranes. *European Polymer Journal*, 42, pp.776-785.

Yu, S., Li, X. Hao, J., Liu, S. Shao, Z. (2014) Preparation of microporous layer for proton exchange membrane fuel cell by suing polyvinylpyrrolidone aqueous solution. *International Journal of Hydrogen Energy*, 39 (28), pp. 15681-15686.

Ye, Q., Nguyen, T. V. (2007) Three-Dimensional Simulation of Liquid Water Distribution in a PEMFC with Experimentally Measured Capillary Functions. *Journal of the Electrochemical Society*, 154, pp. B1242-B1251.

Yu, J., Islam, M. N., Matsuura, T., Tamano, M., Hayashi, Y., Hori, M. (2005) Improving the performance of a PEMFC with Ketjenblack EC-600JD carbon black as the material of the microporous layer. *Electrochemical and Solid-State Letters*, 8 (6), pp. A320-A323.

Yuan, W., Tang, Y., Pan, M., Li, Z., Tang, B. (2010) Model prediction of effects of operating parameters on proton exchange membrane fuel cell performance. *Renewable Energy*, 35, pp. 656-666.

Zamel, N., Li, X. (2013) Effective transport properties for polymer electrolyte membrane fuel cells – with a focus on the gas diffusion layer. *Progress in Energy and Combustion Science*, 39 (1), pp. 111-146.

Zabihian, F., Fung, A. S. (2014) Performance analysis of hybrid solid oxide fuel cell and gas turbine cycle (part I): Effects of fuel composition on output power. *Journal of the Energy Institute*, 87, pp.18-27.

Zamora, H. Canizares, P., Rodrigo, M. A., Lobato, J. (2015) Improving of microporous layer based on advanced carbon materials for high temperature proton exchange membrane fuel cell electrodes. *Fuel cells*, 15. pp. 375-383.

Appendix A

Calculations of the compositions loadings for MPL ink preparation

Step 1.

Area of single sample, $A = \frac{\pi}{4} (2.54)^2 \text{ cm}^2 = 5.069 \text{ cm}^2$

Area for 6 samples, $A = (5.069 \times 6) \text{ cm}^2 = 30.414 \text{ cm}^2$

Carbon particles required, C of (i) 0.5, (ii) 1.0, (iii) 1.5, (iv) 2.0 and (v) 2.5 mg by weight is estimated as follows for loading density:

- (i) 0.5 mg/cm² of C loading: $0.5 \text{ mg/cm}^2 \times 30.414 \text{ cm}^2 = 15.207 \text{ mg}$
- (ii) 1.0 mg/cm² of C loading: $1.0 \text{ mg/cm}^2 \times 30.414 \text{ cm}^2 = 30.414 \text{ mg}$
- (iii) 1.5 mg/cm² of C loading: $1.5 \text{ mg/cm}^2 \times 30.414 \text{ cm}^2 = 45.621 \text{ mg}$
- (iv) 2.0 mg/cm² of C loading: $2.0 \text{ mg/cm}^2 \times 30.414 \text{ cm}^2 = 60.828 \text{ mg}$
- (v) 2.5 mg/cm² of C loading: $2.5 \text{ mg/cm}^2 \times 30.414 \text{ cm}^2 = 76.035 \text{ mg}$

The loss factor is assumed to be 3 then,

- (i) 0.5 mg/cm² of C loading: $15.207 \text{ mg} \times 3 = 45.621 \text{ mg}$
- (ii) 1.0 mg/cm² of C loading: $30.414 \text{ mg} \times 3 = 91.242 \text{ mg}$
- (iii) 1.5 mg/cm² of C loading: $45.621 \text{ mg} \times 3 = 136.843 \text{ mg}$
- (iv) 2.0 mg/cm² of C loading: $60.828 \text{ mg} \times 3 = 182.484 \text{ mg}$
- (v) 2.5 mg/cm² of C loading: $76.035 \text{ mg} \times 3 = 228.105 \text{ mg}$

Step 2

Adding PTFE (wt.%),

For 10 wt.% of,

$$(i) \quad 0.5 \text{ mg} = \frac{10 \text{ mg PTFE}}{90 \text{ mg C}} \times 45.621 \text{ mg}$$

$$\text{PTFE solution required, (mg)} = 5.069 \text{ mg PTFE} \times \frac{100 \text{ mgPTFE}}{62.6 \text{ mgPTFE}}$$

$$(ii) \quad 1.0 \text{ mg} = \frac{10 \text{ mg PTFE}}{90 \text{ mg C}} \times 91.242 \text{ mg}$$

$$\text{PTFE solution required, (mg)} = 10.138 \text{ mg PTFE} \times \frac{100 \text{ mgPTFE}}{62.6 \text{ mgPTFE}}$$

$$(iii) \quad 1.5 \text{ mg} = \frac{10 \text{ mg PTFE}}{90 \text{ mg C}} \times 136.843 \text{ mg}$$

$$\text{PTFE solution required, (mg)} = 15.205 \text{ mg PTFE} \times \frac{100 \text{ mgPTFE}}{62.6 \text{ mgPTFE}}$$

$$(iv) \quad 2.0 \text{ mg} = \frac{10 \text{ mg PTFE}}{90 \text{ mg C}} \times 182.484 \text{ mg}$$

$$\text{PTFE solution required, (mg)} = 20.276 \text{ mg PTFE} \times \frac{100 \text{ mgPTFE}}{62.6 \text{ mgPTFE}}$$

$$(v) \quad 2.5 \text{ mg} = \frac{10 \text{ mg PTFE}}{90 \text{ mg C}} \times 228.105 \text{ mg}$$

$$\text{PTFE solution required, (mg)} = 25.35 \text{ mg PTFE} \times \frac{100 \text{ mgPTFE}}{62.6 \text{ mgPTFE}}$$

For 20 wt.% of,

$$(i) \quad 0.5 \text{ mg} = \frac{20 \text{ mg PTFE}}{80 \text{ mg C}} \times 45.621 \text{ mg}$$

$$\text{PTFE solution required, (mg)} = 11.405 \text{ mg PTFE} \times \frac{100 \text{ mgPTFE}}{62.6 \text{ mgPTFE}}$$

$$(ii) \quad 1.0 \text{ mg} = \frac{20 \text{ mg PTFE}}{80 \text{ mg C}} \times 91.242 \text{ mg}$$

$$\text{PTFE solution required, (mg)} = 22.811 \text{ mg PTFE} \times \frac{100 \text{ mgPTFE}}{62.6 \text{ mgPTFE}}$$

$$(iii) \quad 1.5 \text{ mg} = \frac{20 \text{ mg PTFE}}{80 \text{ mg C}} \times 136.843 \text{ mg}$$

$$\text{PTFE solution required, (mg)} = 34.211 \text{ mg PTFE} \times \frac{100 \text{ mgPTFE}}{62.6 \text{ mgPTFE}}$$

$$(iv) \quad 2.0 \text{ mg} = \frac{20 \text{ mg PTFE}}{80 \text{ mg C}} \times 182.484 \text{ mg}$$

$$\text{PTFE solution required, (mg)} = 45.621 \text{ mg PTFE} \times \frac{100 \text{ mgPTFE}}{62.6 \text{ mgPTFE}}$$

$$(v) \quad 2.5 \text{ mg} = \frac{20 \text{ mg PTFE}}{80 \text{ mg C}} \times 228.105 \text{ mg}$$

$$\text{PTFE solution required, (mg)} = 57.026 \text{ mg PTFE} \times \frac{100 \text{ mgPTFE}}{62.6 \text{ mgPTFE}}$$

For 30 wt.% of,

$$(i) \quad 0.5 \text{ mg} = \frac{30 \text{ mg PTFE}}{70 \text{ mg C}} \times 45.621 \text{ mg}$$

$$\text{PTFE solution required, (mg)} = 19.552 \text{ mg PTFE} \times \frac{100 \text{ mgPTFE}}{62.6 \text{ mgPTFE}}$$

$$(ii) \quad 1.0 \text{ mg} = \frac{30 \text{ mg PTFE}}{70 \text{ mg C}} \times 91.242 \text{ mg}$$

$$\text{PTFE solution required, (mg)} = 39.104 \text{ mg PTFE} \times \frac{100 \text{ mgPTFE}}{62.60 \text{ mgPTFE}}$$

$$(iii) \quad 1.5 \text{ mg} = \frac{30 \text{ mg PTFE}}{70 \text{ mg C}} \times 136.843 \text{ mg}$$

$$\text{PTFE solution required, (mg)} = 58.647 \text{ mg PTFE} \times \frac{100 \text{ mgPTFE}}{62.6 \text{ mgPTFE}}$$

$$(iv) \quad 2.0 \text{ mg} = \frac{30 \text{ mg PTFE}}{70 \text{ mg C}} \times 182.484 \text{ mg}$$

$$\text{PTFE solution required, (mg)} = 78.207 \text{ mg PTFE} \times \frac{100 \text{ mgPTFE}}{62.6 \text{ mgPTFE}}$$

$$(v) \quad 2.5 \text{ mg} = \frac{30 \text{ mg PTFE}}{70 \text{ mg C}} \times 228.105 \text{ mg}$$

$$\text{PTFE solution required, (mg)} = 97.759 \text{ mg PTFE} \times \frac{100 \text{ mgPTFE}}{62.6 \text{ mgPTFE}}$$

For 40 wt.% of,

$$(i) \quad 0.5 \text{ mg} = \frac{40 \text{ mg PTFE}}{60 \text{ mg C}} \times 45.621 \text{ mg}$$

$$\text{PTFE solution required, (mg)} = 30.414 \text{ mg PTFE} \times \frac{100 \text{ mgPTFE}}{62.6 \text{ mgPTFE}}$$

$$(ii) \quad 1.0 \text{ mg} = \frac{40 \text{ mg PTFE}}{60 \text{ mg C}} \times 91.242 \text{ mg}$$

$$\text{PTFE solution required, (mg)} = 60.828 \text{ mg PTFE} \times \frac{100 \text{ mgPTFE}}{62.6 \text{ mgPTFE}}$$

$$(iii) \quad 1.5 \text{ mg} = \frac{40 \text{ mg PTFE}}{60 \text{ mg C}} \times 136.843 \text{ mg}$$

$$\text{PTFE solution required, (mg)} = 91.229 \text{ mg PTFE} \times \frac{100 \text{ mgPTFE}}{62.6 \text{ mgPTFE}}$$

$$(iv) \quad 2.0 \text{ mg} = \frac{40 \text{ mg PTFE}}{60 \text{ mg C}} \times 182.484 \text{ mg}$$

$$\text{PTFE solution required, (mg)} = 121.656 \text{ mg PTFE} \times \frac{100 \text{ mgPTFE}}{62.6 \text{ mgPTFE}}$$

$$(v) \quad 2.5 \text{ mg} = \frac{40 \text{ mg PTFE}}{60 \text{ mg C}} \times 228.105 \text{ mg}$$

$$\text{PTFE solution required, (mg)} = 152.07 \text{ mg PTFE} \times \frac{100 \text{ mgPTFE}}{62.6 \text{ mgPTFE}}$$

For 50 wt.% of,

$$(i) \quad 0.5 \text{ mg} = \frac{50 \text{ mg PTFE}}{50 \text{ mg C}} \times 45.621 \text{ mg}$$

$$\text{PTFE solution required, (mg)} = 45.621 \text{ mg PTFE} \times \frac{100 \text{ mgPTFE}}{62.6 \text{ mgPTFE}}$$

$$(ii) \quad 1.0 \text{ mg} = \frac{50 \text{ mg PTFE}}{50 \text{ mg C}} \times 91.242 \text{ mg}$$

$$\text{PTFE solution required, (mg)} = 91.242 \text{ mg PTFE} \times \frac{100 \text{ mgPTFE}}{62.6 \text{ mgPTFE}}$$

$$(iii) \quad 1.5 \text{ mg} = \frac{50 \text{ mg PTFE}}{50 \text{ mg C}} \times 136.843 \text{ mg}$$

$$\text{PTFE solution required, (mg)} = 136.843 \text{ mg PTFE} \times \frac{100 \text{ mgPTFE}}{62.6 \text{ mgPTFE}}$$

$$(iv) \quad 2.0 \text{ mg} = \frac{50 \text{ mg PTFE}}{50 \text{ mg C}} \times 182.484 \text{ mg}$$

$$\text{PTFE solution required, (mg)} = 182.484 \text{ mg PTFE} \times \frac{100 \text{ mgPTFE}}{62.6 \text{ mgPTFE}}$$

$$(v) \quad 2.5 \text{ mg} = \frac{50 \text{ mg PTFE}}{50 \text{ mg C}} \times 228.105 \text{ mg}$$

$$\text{PTFE solution required, (mg)} = 228.105 \text{ mg PTFE} \times \frac{100 \text{ mgPTFE}}{62.6 \text{ mgPTFE}}$$

Step 3

Table 3.3 summarised the individual loadings for carbon black and PTFE solution as required materials of the prepare MPL mixture.

Step 4

Amounts of carbon black particles, C and PTFE solution required to add together.

Recall, area of sample, $A = 5.069 \text{ cm}^2$,

1. For carbon black particles loading, C;

$$(i) \quad 0.5 \text{ mg/cm}^2 \text{ of C loading: } 0.5 \text{ mg/cm}^2 \times 5.069 \text{ cm}^2 = 2.535 \text{ mg}$$

$$(ii) \quad 1.0 \text{ mg/cm}^2 \text{ of C loading: } 1.0 \text{ mg/cm}^2 \times 5.069 \text{ cm}^2 = 5.069 \text{ mg}$$

$$(iii) \quad 1.5 \text{ mg/cm}^2 \text{ of C loading: } 1.5 \text{ mg/cm}^2 \times 5.069 \text{ cm}^2 = 7.604 \text{ mg}$$

$$(iv) \quad 2.0 \text{ mg/cm}^2 \text{ of C loading: } 2.0 \text{ mg/cm}^2 \times 5.069 \text{ cm}^2 = 10.138 \text{ mg}$$

$$(v) \quad 2.5 \text{ mg/cm}^2 \text{ of C loading: } 2.5 \text{ mg/cm}^2 \times 5.069 \text{ cm}^2 = 12.673 \text{ mg}$$

2. For PTFE solution required, PTFE;

(i) 0.5 mg C

$$(a) \quad 10 \text{ wt. \%} = \frac{10 \text{ mgPTFE}}{90 \text{ mg C}} \times 2.535 \text{ mg C} = 0.282 \text{ wt. \%}$$

$$(b) \quad 20 \text{ wt. \%} = \frac{20 \text{ mgPTFE}}{80 \text{ mg C}} \times 2.535 \text{ mg C} = 0.634 \text{ wt. \%}$$

$$(c) \quad 30 \text{ wt. \%} = \frac{30 \text{ mgPTFE}}{70 \text{ mg C}} \times 2.535 \text{ mg C} = 1.086 \text{ wt. \%}$$

$$(d) 40 \text{ wt.}\% = \frac{40 \text{ mgPTFE}}{60 \text{ mg C}} \times 2.535 \text{ mg C} = 1.690 \text{ wt.}\%$$

$$(e) 50 \text{ wt.}\% = \frac{50 \text{ mgPTFE}}{50 \text{ mg C}} \times 2.535 \text{ mg C} = 2.535 \text{ wt.}\%$$

(ii) 1.0 mg C

$$(a) 10 \text{ wt.}\% = \frac{10 \text{ mgPTFE}}{90 \text{ mg C}} \times 5.069 \text{ mg C} = 0.563 \text{ wt.}\%$$

$$(b) 20 \text{ wt.}\% = \frac{20 \text{ mgPTFE}}{80 \text{ mg C}} \times 5.069 \text{ mg C} = 1.267 \text{ wt.}\%$$

$$(c) 30 \text{ wt.}\% = \frac{30 \text{ mgPTFE}}{70 \text{ mg C}} \times 5.069 \text{ mg C} = 2.172 \text{ wt.}\%$$

$$(d) 40 \text{ wt.}\% = \frac{40 \text{ mgPTFE}}{60 \text{ mg C}} \times 5.069 \text{ mg C} = 3.379 \text{ wt.}\%$$

$$(e) 50 \text{ wt.}\% = \frac{50 \text{ mgPTFE}}{50 \text{ mg C}} \times 5.069 \text{ mg C} = 5.069 \text{ wt.}\%$$

(iii) 1.5 mg C

$$(a) 10 \text{ wt.}\% = \frac{10 \text{ mgPTFE}}{90 \text{ mg C}} \times 7.604 \text{ mg C} = 0.845 \text{ wt.}\%$$

$$(b) 20 \text{ wt.}\% = \frac{20 \text{ mgPTFE}}{80 \text{ mg C}} \times 7.604 \text{ mg C} = 1.901 \text{ wt.}\%$$

$$(c) 30 \text{ wt.}\% = \frac{30 \text{ mgPTFE}}{70 \text{ mg C}} \times 7.604 \text{ mg C} = 3.259 \text{ wt.}\%$$

$$(d) 40 \text{ wt.}\% = \frac{40 \text{ mgPTFE}}{60 \text{ mg C}} \times 7.604 \text{ mg C} = 5.069 \text{ wt.}\%$$

$$(e) 50 \text{ wt.}\% = \frac{50 \text{ mgPTFE}}{50 \text{ mg C}} \times 7.604 \text{ mg C} = 7.604 \text{ wt.}\%$$

(iv) 2.0 mg C

$$(a) 10 \text{ wt.}\% = \frac{10 \text{ mgPTFE}}{90 \text{ mg C}} \times 10.138 \text{ mg C} = 1.126 \text{ wt.}\%$$

$$(b) 20 \text{ wt.}\% = \frac{20 \text{ mgPTFE}}{80 \text{ mg C}} \times 10.138 \text{ mg C} = 2.535 \text{ wt.}\%$$

$$(c) 30 \text{ wt.}\% = \frac{30 \text{ mgPTFE}}{70 \text{ mg C}} \times 10.138 \text{ mg C} = 4.345 \text{ wt.}\%$$

$$(d) 40 \text{ wt.}\% = \frac{40 \text{ mgPTFE}}{60 \text{ mg C}} \times 10.138 \text{ mg C} = 6.759 \text{ wt.}\%$$

$$(e) 50 \text{ wt.}\% = \frac{50 \text{ mgPTFE}}{50 \text{ mg C}} \times 10.138 \text{ mg C} = 10.138 \text{ wt.}\%$$

(v) 2.5 mg C

$$(a) 10 \text{ wt.}\% = \frac{10 \text{ mgPTFE}}{90 \text{ mg C}} \times 12.673 \text{ mg C} = 1.408 \text{ wt.}\%$$

$$(b) 20 \text{ wt.}\% = \frac{20 \text{ mgPTFE}}{80 \text{ mg C}} \times 12.673 \text{ mg C} = 3.168 \text{ wt.}\%$$

$$(c) 30 \text{ wt.}\% = \frac{30 \text{ mgPTFE}}{70 \text{ mg C}} \times 12.673 \text{ mg C} = 5.431 \text{ wt.}\%$$

$$(d) 40 \text{ wt.}\% = \frac{40 \text{ mgPTFE}}{60 \text{ mg C}} \times 12.673 \text{ mg C} = 8.449 \text{ wt.}\%$$

$$(e) 50 \text{ wt.}\% = \frac{50 \text{ mgPTFE}}{50 \text{ mg C}} \times 12.673 \text{ mg C} = 12.673 \text{ wt.}\%$$

Therefore, add carbon black, C and PTFE together (C+PTFE) by weight, see Table 3.4.

Step 5

Carbon black particles and PTFE required per a single sample, (C + PTFE);

(i) 0.5 mg C

$$(a) 10 \text{ wt.}\% \text{ PTFE} = \frac{2.535+0.282}{5.069} = 0.556 \text{ wt.}\%$$

$$(b) 20 \text{ wt.}\% \text{ PTFE} = \frac{2.535+0.634}{5.069} = 0.625 \text{ wt.}\%$$

$$(c) 30 \text{ wt.}\% \text{ PTFE} = \frac{2.535+0.429}{5.069} = 2.964 \text{ wt.}\%$$

$$(d) 40 \text{ wt.}\% \text{ PTFE} = \frac{2.535+0.600}{5.069} = 0.619 \text{ wt.}\%$$

$$(e) 50 \text{ wt.}\% \text{ PTFE} = \frac{2.535+1.00}{5.069} = 0.697 \text{ wt.}\%$$

(ii) 1.0 mg C

$$(a) 10 \text{ wt.}\% \text{ PTFE} = \frac{5.069 + 0.563}{5.069} = 1.111 \text{ wt.}\%$$

$$(b) 20 \text{ wt.}\% \text{ PTFE} = \frac{5.069+1.267}{5.069} = 1.250 \text{ wt.}\%$$

$$(c) 30 \text{ wt.}\% \text{ PTFE} = \frac{5.069+2.172}{5.069} = 1.423 \text{ wt.}\%$$

$$(d) 40 \text{ wt.}\% \text{ PTFE} = \frac{5.069+3.379}{5.069} = 1.667 \text{ wt.}\%$$

$$(e) 50 \text{ wt.}\% \text{ PTFE} = \frac{5.069+5.069}{5.069} = 2.00 \text{ wt.}\%$$

(iii) 1.5 mg C

$$(a) 10 \text{ wt.}\% \text{ PTFE} = \frac{7.604+0.845}{5.069} = 1.667 \text{ wt.}\%$$

$$(b) 20 \text{ wt.}\% \text{ PTFE} = \frac{7.604+1.901}{5.069} = 1.875 \text{ wt.}\%$$

$$(c) 30 \text{ wt.}\% \text{ PTFE} = \frac{7.604+3.259}{5.069} = 2.143 \text{ wt.}\%$$

$$(d) 40 \text{ wt.}\% \text{ PTFE} = \frac{7.604+ 5.069}{5.069} = 2.500 \text{ wt.}\%$$

$$(e) 50 \text{ wt.}\% \text{ PTFE} = \frac{7.604+7.604}{5.069} = 3.000 \text{ wt.}\%$$

(iv) 2.0 mg C

$$(a) 10 \text{ wt.}\% \text{ PTFE} = \frac{10.138+1.126}{5.069} = 2.222 \text{ wt.}\%$$

$$(b) 20 \text{ wt.}\% \text{ PTFE} = \frac{10.138+2.535}{5.069} = 2.500 \text{ wt.}\%$$

$$(c) \text{ 30 wt.\% PTFE} = \frac{10.138+4.345}{5.069} = 2.857 \text{ wt.\%}$$

$$(d) \text{ 40 wt.\% PTFE} = \frac{10.138+6.759}{5.069} = 3.333 \text{ wt.\%}$$

$$(e) \text{ 50 wt.\% PTFE} = \frac{10.138+10.138}{5.069} = 4.000 \text{ wt.\%}$$

(v) 2.5 mg C

$$(a) \text{ 10 wt.\% PTFE} = \frac{12.673+1.408}{5.069} = 2.778 \text{ wt.\%}$$

$$(b) \text{ 20 wt.\% PTFE} = \frac{12.673+3.168}{5.069} = 3.125 \text{ wt.\%}$$

$$(c) \text{ 30 wt.\% PTFE} = \frac{12.673+5.431}{5.069} = 3.572 \text{ wt.\%}$$

$$(d) \text{ 40 wt.\% PTFE} = \frac{12.673+8.449}{5.069} = 4.167 \text{ wt.\%}$$

$$(e) \text{ 50 wt.\% PTFE} = \frac{12.673+12.673}{5.069} = 5.000 \text{ wt.\%}$$

The amount of carbon black particles and PTFE loadings required by a sample summarised in Table 3.5. However, specific amounts of carbon particles and PTFE from the values above are determined as follows:

For carbon black loading per sample is,

$$\frac{\text{C (mg)} + \text{PTFE (mg)}}{5.069} \times \text{C \% (by weight)}$$

Example, 0.5 mg/cm² of 20 wt.% PTFE is

$$\frac{2.535+0.634}{5.069} \times \frac{80}{100} = 0.500 \text{ mg/cm}^2 \text{ carbon black}$$

The total amount MPL slurry coated is 0.625 mg/cm², and amount of carbon in the MPL coated is 0.50 mg/cm², then the amount of PTFE loading per sample is 0.125 mg/cm² (i.e., 0.625 – 0.500) mg/cm².

Appendix B

Estimation value for MPL-coated GDLs thickness with Ketjenblack and Vulcan carbon black loading

Table B-1: MPL-coated GDL thickness with 0.5 mg/cm² Ketjenblack carbon black and PTFE loading.

C-0%	Mean μm	95% Conf. Int.	C-30%	Mean μm	95% Conf. Int.
445	432	±15.77	385	403	±17.86
438			393		
420			403		
420			393		
453			408		
418			433		
C-10%	Mean μm	95% Conf. Int.	C-40%	Mean μm	95% Conf. Int.
410	401	±31.27	423	419	±11.93
383			420		
388			413		
385			425		
458			433		
382			400		
C-20%	Mean μm	95% Conf. Int.	C-50%	Mean μm	95% Conf. Int.
418	419	±25.60	463	453	±12.29
408			453		
423			460		
465			430		
400			455		
400			455		

Table B-2: MPL-coated GDL thickness with 1.0 mg/cm² Ketjenblack carbon black and PTFE loading.

C-0%	Mean μm	95% Conf. Int.	C-30%	Mean μm	95% Conf. Int.
485	467	±20.30	408	415	±6.79
440			425		
458			415		
455			408		
475			413		
490			418		
C-10%	Mean μm	95% Conf. Int.	C-40%	Mean μm	95% Conf. Int.
428	428	±3.84	413	416	±8.30
425			428		
428			420		
428			408		
425			420		
435			408		
C-20%	Mean μm	95% Conf. Int.	C-50%	Mean μm	95% Conf. Int.
520	473	±39.92	535	481	±33.43
513			475		
468			483		
465			493		
450			458		
420			443		

Table B-3: MPL-coated GDL thickness with 1.5 mg/cm² Ketjenblack carbon black and PTFE loading.

C-0%	Mean μm	95% Conf. Int.	C-30%	Mean μm	95% Conf. Int.
488	515	±18.77	470	464	±16.56
520			470		
543			480		
513			438		
518			453		
508			475		
C-10%	Mean μm	95% Conf. Int.	C-40%	Mean μm	95% Conf. Int.
435	462	±17.63	478	464	±20.16
450			460		
468			483		
475			473		
480			458		
465			430		
C-20%	Mean μm	95% Conf. Int.	C-50%	Mean μm	95% Conf. Int.
465	438	±20.17	513	509	±12.99
428			520		
453			508		
410			485		
438			515		
435			513		

Table B-4: MPL-coated GDL thickness with 2.0 mg/cm² Ketjenblack carbon black and PTFE loading.

C-0%	Mean μm	95% Conf. Int.	C-30%	Mean μm	95% Conf. Int.
510	520	±6.63	465	464	±26.01
523			480		
523			490		
513			420		
525			455		
523			475		
C-10%	Mean μm	95% Conf. Int.	C-40%	Mean μm	95% Conf. Int.
548	565	±14.49	450	477	±16.48
570			470		
580			478		
575			488		
570			480		
548			495		
C-20%	Mean μm	95% Conf. Int.	C-50%	Mean μm	95% Conf. Int.
515	484	±29.46	588	565	±24.87
488			590		
468			578		
488			535		
438			555		
508			543		

Table B-5: MPL-coated GDL thickness with 2.5 mg/cm² Ketjenblack carbon black and PTFE loading.

C-0%	Mean μm	95% conf. Int.	C-30%	Mean μm	95% Conf. Int.
578	559	±19.78	533	525	±16.05
578			533		
560			548		
545			510		
530			513		
563			513		
C-10%	Mean μm	95% Conf. Int.	C-40%	Mean μm	95% Conf. Int.
535	530	±16.19	540	547	±42.01
518			580		
533			603		
538			515		
548			495		
505			550		
C-20%	Mean μm	95% Conf. Int.	C-50%	Mean μm	95% Conf. Int.
550	522	±23.09	650	626	±23.56
513			600		
535			600		
525			650		
525			625		
485			630		

Table B-6: MPL-coated GDL thickness with 0.5 mg/cm² Vulcan carbon black and PTFE loading.

C-0%	Mean μm	95% Conf. Int.	C-30%	Mean μm	95% Conf. Int.
445	432	±15.77	450	432	±23.15
438			455		
420			448		
420			418		
453			403		
418			415		
C-10%	Mean μm	95% Conf. Int.	C-40%	Mean μm	95% Conf. Int.
470	435	±21.17	413	430	±27.31
418			418		
438			405		
415			468		
428			420		
443			458		
C-20%	Mean μm	95% Conf. Int.	C-50%	Mean μm	95% Conf. Int.
505	491	±41.92	488	439	±31.04
548			458		
518			415		
468			420		
465			438		
440			413		

Table B-7: MPL-coated GDL thickness with 1.0 mg/cm² Vulcan carbon black and PTFE loading.

C-0%	Mean μm	95% Conf. Int.	C-30%	Mean μm	95% Conf. Int.
415	433	±16.64	393	410	±23.90
418			425		
440			400		
438			445		
430			415		
458			383		
C-10%	Mean μm	95% Conf. Int.	C-40%	Mean μm	95% Conf. Int.
410	403	±15.89	390	409	±23.07
403			405		
418			388		
418			400		
385			443		
385			428		
C-20%	Mean μm	95% Conf. Int.	C-50%	Mean μm	95% Conf. Int.
520	473	±39.92	445	393	±29.81
513			375		
468			373		
465			373		
450			405		
420			385		

Table B-8: MPL-coated GDL thickness with 1.5 mg/cm² Vulcan carbon black and PTFE loading.

C-0%	Mean μm	95% Conf. Int.	C-30%	Mean μm	95% Conf. Int.
483	462	±24.58	468	447	±18.91
460			440		
480			428		
418			440		
468			433		
460			470		
C-10%	Mean μm	95% Conf. Int.	C-40%	Mean μm	95% Conf. Int.
420	439	±30.29	428	427	±14.15
410			450		
468			430		
468			418		
460			410		
410			428		
C-20%	Mean μm	95% Conf. Int.	C-50%	Mean μm	95% Conf. Int.
513	490	±55.29	420	427	±7.56
473			433		
463			438		
460			420		
587			425		
445			428		

Table B-9: MPL-coated GDL thickness with 2.0 mg/cm² Vulcan carbon black and PTFE loading.

C-0%	Mean μm	95% Conf. Int.	C-30%	Mean μm	95% Conf. Int.
485	476	±8.30	438	460	±19.63
478			458		
475			443		
463			463		
473			468		
483			490		
C-10%	Mean μm	95% Conf. Int.	C-40%	Mean μm	95 Conf. Int.
428	446	±18.10	448	465	±11.66
475			473		
435			475		
455			473		
435			465		
445			455		
C-20%	Mean μm	95% Conf. Int.	C-50%	Mean μm	95% Conf. Int.
483	507	±25.76	425	437	±21.11
515			433		
515			410		
548			440		
495			443		
485			470		

Table B-10: MPL-coated GDL thickness with 2.5 mg/cm² Vulcan carbon black and PTFE loading.

C-0%	Mean μm	95% Conf. Int.	C-30%	Mean μm	95% Conf. Int.
418	448	±24.15	485	507	±43.75
435			570		
465			470		
440			523		
448			533		
483			463		
C-10%	Mean μm	95% Conf. Int.	C-40%	Mean μm	95% Conf. Int.
488	459	±30.62	510	466	±36.92
465			450		
468			505		
408			460		
443			420		
480			448		
C-20%	Mean μm	95% Conf. Int.	C-50%	Mean μm	95% Conf. Int.
510	504	±10.55	473	485	±19.14
518			500		
500			455		
488			498		
505			485		
505			500		

Appendix C

Estimation values for carbon-PTFE loaded onto GDL samples

Table C-1: 0.5 mg Vulcan carbon black and PTFE loading.

C-0 %	mean mg/cm²	95 % Conf. Int.	C-30%	mean mg/cm²	95 % Conf. Int.
0.94	0.76	±0.16	0.89	0.97	±0.07
0.96			0.99		
0.74			1.04		
0.68			1.02		
0.65			0.98		
0.61			0.9		
C-10%	mean mg/cm²	95 % Conf. Int.	C-40%	mean mg/cm²	95 % Conf. Int.
0.9	0.85	±0.07	1.34	1.43	±0.06
0.92			1.38		
0.82			1.41		
0.75			1.5		
0.8			1.46		
0.91			1.47		
C-20%	mean mg/cm²	95 % Conf. Int.	C-50%	mean mg/cm²	95 % Conf. Int.
0.56	0.90	±0.18	1.03	0.95	±0.06
0.99			1.01		
1.01			0.93		
0.97			0.91		
0.93			0.93		
0.95			0.9		

Table C-2: 1.0 mg Vulcan carbon black loading.

C-0%	mean mg/cm²	95% Conf. Int.	C-30%	mean mg/cm²	95% Conf. Int.
1.1	1.32	±0.29	1.88	1.84	±0.13
1.43			2.07		
1.28			1.81		
1.14			1.77		
1.13			1.78		
1.83			1.75		
C-10%	mean mg/cm²	95% Conf. Int.	C-40%	mean mg/cm²	95% Conf. Int.
1.19	1.29	±0.08	2.25	2.41	±0.28
1.25			2.43		
1.38			2.19		
1.25			2.23		
1.28			2.44		
1.37			2.91		
C-20%	mean mg/cm²	95% Conf. Int.	C-50%	mean mg/cm²	95% Conf. Int.
3.58	1.96	±0.83	2.39	2.39	±0.16
1.58			2.55		
1.62			2.43		
1.65			2.11		
1.69			2.38		
1.64			2.45		

Table C-3: 1.5 mg Vulcan carbon black loading.

C-0%	mean mg/cm²	95% Conf. Int.	C-30%	mean mg/cm²	95% Conf. Int.
1.94	1.79	±0.13	1.88	1.84	±0.13
1.86			2.07		
1.67			1.81		
1.62			1.77		
1.77			1.78		
1.87			1.75		
C-10%	mean mg/cm²	95% Conf. Int.	C-40%	mean mg/cm²	95% Conf. Int.
1.87	1.74	±0.13	2.25	2.41	±0.28
1.67			2.43		
1.63			2.19		
1.61			2.23		
1.73			2.44		
1.91			2.91		
C-20%	mean mg/cm²	95% Conf. Int.	C-50%	mean mg/cm²	95% Conf. Int.
1.87	2.29	±0.25	2.39	2.39	±0.16
2.28			2.55		
2.61			2.43		
2.4			2.11		
2.25			2.38		
2.3			2.45		

Table C-4: 2.0 mg Vulcan carbon black loading.

C-0%	mean mg/cm²	95% Conf. Int.	C-30%	mean mg/cm²	95% Conf. Int.
2.42	2.64	±0.14	2.74	3.22	±0.31
2.71			3.49		
2.78			3.11		
2.71			3.1		
2.54			3.36		
2.69			3.5		
C-10%	mean mg/cm²	95% Conf. Int.	C-40%	mean mg/cm²	95% Conf. Int.
3.09	3.45	±0.21	2.59	2.61	±0.13
3.59			2.62		
3.54			2.55		
3.57			2.65		
3.33			2.82		
3.57			2.45		
C-20%	mean mg/cm²	95% Conf. Int.	C-50%	mean mg/cm²	95% Conf. Int.
2.54	2.75	±0.29	3.75	3.65	±0.26
2.86			3.96		
2.98			3.58		
3.11			3.23		
2.55			3.59		
2.44			3.78		

Table C-5: 2.5 mg Vulcan carbon black loading.

C-0%	mean mg/cm²	95% Conf. Int.	C-30%	mean mg/cm²	95% Conf. Int.
2.51	2.69	±0.27	4.69	4.58	±0.50
2.38			5.42		
2.93			4.58		
2.59			4.49		
2.69			4.1		
3.04			4.18		
C-10%	mean mg/cm²	95% Conf. Int.	C-40%	mean mg/cm²	95% Conf. Int.
3.44	3.58	±0.24	6.34	5.21	±0.99
3.98			6.44		
3.47			4.79		
3.38			4.58		
3.46			4.22		
3.72			4.89		
C-20%	mean mg/cm²	95% Conf. Int.	C-50%	mean mg/cm²	95% Conf. Int.
3.71	3.53	±0.17	5.43	5.19	±0.61
3.47			6.09		
3.66			5.32		
3.62			4.55		
3.38			4.57		
3.33			5.15		

Table C-6: 0.5 mg Ketjenblack carbon black and PTFE loading.

C-0%	mean mg/cm²	95% Conf. Int.	C-30%	mean mg/cm²	95% Conf. Int.
0.41	0.46	±0.05	0.74	0.85	±0.14
0.5			0.81		
0.5			0.76		
0.48			0.86		
0.45			1.1		
0.4			0.83		
C-10%	mean mg/cm²	95% Conf. Int.	C-40%	mean mg/cm²	95% Conf. Int.
0.73	0.81	±0.37	0.89	1.02	±0.17
1.03			1.18		
0.34			1.05		
1.38			1.11		
0.75			1.11		
0.64			0.76		
C-20%	mean mg/cm²	95% Conf. Int.	C-50%	mean mg/cm²	95% Conf. Int.
0.56	0.63	±0.08	1.1	1.04	±0.05
0.68			1.07		
0.72			1.02		
0.68			1.01		
0.62			1.06		
0.53			0.97		

Table C-7: 1.0 mg Ketjenblack carbon black and PTFE loading.

C-0%	Mean mg/cm²	95% Conf. Int.	C-30%	Mean mg/cm²	95% Conf. Int.
1.47	1.11	±0.19	1.73	1.67	±0.12
0.99			1.81		
1.01			1.52		
1.05			1.63		
1.05			1.57		
1.09			1.77		
C-10%	Mean mg/cm²	95% Conf. Int.	C-40%	Mean mg/cm²	95% Conf. Int.
1.1	1.29	±0.10	1.98	1.86	±0.11
1.29			1.79		
1.32			1.97		
1.37			1.71		
1.31			1.86		
1.34			1.83		
C-20%	mean mg/cm²	95% Conf. Int.	C-50%	mean mg/cm²	95% Conf. Int.
1.27	1.24	±0.28	2.18	2.53	±0.27
1.37			2.69		
0.71			2.67		
1.42			2.72		
1.28			2.7		
1.37			2.22		

Table C-8: 1.5 mg Ketjenblack carbon black and PTFE loading.

C-0%	Mean mg/cm²	95% Conf. Int.	C-30%	Mean mg/cm²	95% Conf. Int.
1.55	1.74	0.16	2.32	2.34	0.16
1.75			2.23		
1.98			2.62		
1.8			2.28		
1.74			2.38		
1.61			2.2		
C-10%	Mean mg/cm²	95% Conf. Int.	C-40%	Mean mg/cm²	95% Conf. Int.
1.56	1.82	0.18	2.69	3.03	0.40
1.81			2.82		
1.9			3.53		
2.03			3.14		
1.94			3.37		
1.69			2.61		
C-20%	Mean mg/cm²	95% Conf. Int.	C-50%	Mean mg/cm²	95% Conf. Int.
2.6	2.47	0.29	3.14	3.12	0.09
2.63			3.01		
2.6			3.26		
2.63			3.12		
2.46			3.14		
1.92			3.07		

Table C-9: 2.0 mg Ketjenblack carbon black and PTFE loading.

C-0%	Mean mg/cm²	95% Conf. Int.	C-30%	Mean mg/cm²	95% Conf. Int.
2.01	2.02	0.02	3.01	3.44	0.43
2.02			3.38		
2.02			3.53		
2.06			4.02		
2.02			3.72		
2.01			2.96		
C-10%	Mean mg/cm²	95% Conf. Int.	C-40%	Mean mg/cm²	95% Conf. Int.
2.21	2.28	0.07	3.47	3.62	0.50
2.29			4.03		
2.21			3.23		
2.37			3.09		
2.23			3.59		
2.34			4.33		
C-20%	Mean mg/cm²	95% Conf. Int.	C-50%	Mean mg/cm²	95% Conf. Int.
2.47	2.43	0.10	4.01	4.16	0.16
2.29			4.08		
2.39			4.44		
2.57			4.11		
2.41			4.24		
2.44			4.08		

Table C-10: 2.5 mg Ketjenblack carbon black and PTFE loading.

C-0%	Mean mg/cm²	95% Conf. Int.	C-30%	Mean mg/cm²	95% Conf. Int.
2.58	2.71	0.15	3.68	3.79	0.18
2.89			3.97		
2.62			3.91		
2.79			3.89		
2.82			3.51		
2.55			3.75		
C-10%	Mean mg/cm²	95% Conf. Int.	C-40%	Mean mg/cm²	95% Conf. Int.
2.82	2.98	0.17	3.99	4.21	0.88
2.99			5.59		
2.96			4.84		
3.2			3.78		
3.11			3.52		
2.78			3.52		
C-20%	Mean mg/cm²	95% Conf. Int.	C-50%	Mean mg/cm²	95% Conf. Int.
3.23	3.32	0.42	5.37	5.32	0.09
3.08			5.36		
3.26			5.38		
4.11			5.2		
3.19			5.23		
3.02			5.4		

Appendix D

The Measurement of Error Bars of 95% Confidence Interval for Gas Permeability of MPL-coated GDLs with Ketjenblack and Vulcan carbon blacks

D-1: MPL-coated GDL with Ketjenblack carbon black loading for gas permeability for each of 6 tested samples with various PTFE loadings in the MPLs.

For 0.5 mg Ketjenblack loading

Wt.% PTFE	1	2	3	4	5	6
0	1.56×10^{-11} $\pm 2.36 \times 10^{-12}$	1.17×10^{-11} $\pm 8.07 \times 10^{-13}$	1.65×10^{-11} $\pm 2.22 \times 10^{-12}$	1.53×10^{-11} $\pm 2.44 \times 10^{-12}$	1.46×10^{-11} $\pm 2.68 \times 10^{-12}$	1.76×10^{-11} $\pm 1.76 \times 10^{-12}$
10	9.15×10^{-12} $\pm 8.87 \times 10^{-14}$	9.46×10^{-12} $\pm 9.34 \times 10^{-13}$	1.11×10^{-11} $\pm 1.15 \times 10^{-13}$	9.86×10^{-12} $\pm 7.76 \times 10^{-13}$	1.05×10^{-11} $\pm 4.11 \times 10^{-13}$	1.25×10^{-11} $\pm 1.45 \times 10^{-13}$
20	5.85×10^{-12} $\pm 2.59 \times 10^{-13}$	5.15×10^{-12} $\pm 1.32 \times 10^{-13}$	5.93×10^{-12} $\pm 2.33 \times 10^{-13}$	6.19×10^{-12} $\pm 9.83 \times 10^{-14}$	5.21×10^{-12} $\pm 2.07 \times 10^{-14}$	5.83×10^{-12} $\pm 1.72 \times 10^{-13}$
30	8.65×10^{-12} $\pm 4.24 \times 10^{-13}$	6.86×10^{-12} $\pm 2.34 \times 10^{-13}$	9.69×10^{-12} $\pm 7.85 \times 10^{-14}$	5.89×10^{-12} $\pm 1.52 \times 10^{-13}$	3.21×10^{-12} $\pm 6.47 \times 10^{-14}$	7.35×10^{-12} $\pm 7.30 \times 10^{-14}$
40	8.44×10^{-12} $\pm 1.19 \times 10^{-13}$	6.60×10^{-12} $\pm 3.30 \times 10^{-14}$	7.75×10^{-12} $\pm 6.11 \times 10^{-14}$	6.47×10^{-12} $\pm 1.45 \times 10^{-13}$	5.64×10^{-12} $\pm 7.64 \times 10^{-14}$	8.87×10^{-12} $\pm 2.43 \times 10^{-13}$
50	1.10×10^{-11} $\pm 8.86 \times 10^{-13}$	1.10×10^{-11} $\pm 8.86 \times 10^{-13}$	1.06×10^{-11} $\pm 9.95 \times 10^{-13}$	9.64×10^{-12} $\pm 2.04 \times 10^{-13}$	8.02×10^{-12} $\pm 6.10 \times 10^{-13}$	9.64×10^{-12} $\pm 2.04 \times 10^{-13}$

For 1.0 mg Ketjenblack loading

Wt.% PTFE	1	2	3	4	5	6
0	6.40×10^{-12} $\pm 1.00 \times 10^{-13}$	2.71×10^{-12} $\pm 2.36 \times 10^{-14}$	2.17×10^{-12} $\pm 7.22 \times 10^{-14}$	7.08×10^{-12} $\pm 2.24 \times 10^{-13}$	5.53×10^{-12} $\pm 8.04 \times 10^{-14}$	3.16×10^{-12} $\pm 4.28 \times 10^{-14}$
10	4.34×10^{-12} $\pm 1.41 \times 10^{-13}$	1.52×10^{-12} $\pm 1.53 \times 10^{-14}$	3.04×10^{-12} $\pm 3.85 \times 10^{-14}$	1.52×10^{-12} $\pm 2.92 \times 10^{-14}$	2.47×10^{-12} $\pm 2.00 \times 10^{-14}$	3.13×10^{-12} $\pm 3.37 \times 10^{-14}$
20	2.07×10^{-12} $\pm 7.30 \times 10^{-14}$	1.37×10^{-12} $\pm 1.04 \times 10^{-14}$	2.21×10^{-12} $\pm 1.52 \times 10^{-13}$	1.64×10^{-12} $\pm 2.68 \times 10^{-14}$	2.01×10^{-12} $\pm 4.68 \times 10^{-14}$	1.33×10^{-12} $\pm 1.31 \times 10^{-14}$
30	2.75×10^{-12} $\pm 1.74 \times 10^{-14}$	2.24×10^{-12} $\pm 2.10 \times 10^{-14}$	3.49×10^{-12} $\pm 6.18 \times 10^{-14}$	2.35×10^{-12} $\pm 1.93 \times 10^{-14}$	2.29×10^{-12} $\pm 2.67 \times 10^{-14}$	1.44×10^{-12} $\pm 1.37 \times 10^{-14}$
40	2.02×10^{-12} $\pm 3.79 \times 10^{-14}$	3.05×10^{-12} $\pm 2.54 \times 10^{-14}$	2.17×10^{-12} $\pm 3.12 \times 10^{-14}$	2.68×10^{-12} $\pm 3.05 \times 10^{-14}$	1.58×10^{-12} $\pm 1.14 \times 10^{-14}$	2.48×10^{-12} $\pm 3.59 \times 10^{-14}$
50	4.73×10^{-12} $\pm 6.35 \times 10^{-14}$	2.95×10^{-12} $\pm 9.52 \times 10^{-14}$	1.79×10^{-12} $\pm 1.86 \times 10^{-14}$	3.13×10^{-12} $\pm 4.73 \times 10^{-14}$	2.00×10^{-12} $\pm 2.77 \times 10^{-14}$	3.42×10^{-12} $\pm 6.14 \times 10^{-14}$

For 1.5 mg Ketjenblack loading

Wt.% PTFE	1	2	3	4	5	6
0	2.48×10^{-12} $\pm 3.23 \times 10^{-14}$	2.22×10^{-12} $\pm 3.38 \times 10^{-14}$	1.26×10^{-12} $\pm 186 \times 10^{-14}$	1.46×10^{-12} $\pm 1.22 \times 10^{-14}$	1.24×10^{-12} $\pm 7.33 \times 10^{-14}$	1.38×10^{-12} $\pm 1.04 \times 10^{-14}$
10	3.48×10^{-12} $\pm 8.04 \times 10^{-14}$	2.32×10^{-12} $\pm 4.45 \times 10^{-14}$	2.24×10^{-12} $\pm 1.46 \times 10^{-14}$	2.38×10^{-12} $\pm 2.77 \times 10^{-14}$	2.70×10^{-12} $\pm 3.88 \times 10^{-14}$	2.36×10^{-12} $\pm 2.71 \times 10^{-14}$
20	1.49×10^{-12} $\pm 3.79 \times 10^{-14}$	1.29×10^{-12} $\pm 1.13 \times 10^{-14}$	1.69×10^{-12} $\pm 2.31 \times 10^{-14}$	1.21×10^{-12} $\pm 7.58 \times 10^{-15}$	8.94×10^{-13} $\pm 2.62 \times 10^{-14}$	7.65×10^{-13} $\pm 2.01 \times 10^{-14}$
30	1.66×10^{-12} $\pm 1.04 \times 10^{-14}$	1.83×10^{-12} $\pm 8.51 \times 10^{-15}$	1.05×10^{-12} $\pm 2.34 \times 10^{-14}$	2.45×10^{-12} $\pm 1.88 \times 10^{-14}$	9.99×10^{-13} $\pm 2.67 \times 10^{-15}$	1.07×10^{-12} $\pm 1.32 \times 10^{-14}$
40	1.80×10^{-12} $\pm 1.85 \times 10^{-14}$	1.25×10^{-12} $\pm 1.83 \times 10^{-14}$	7.62×10^{-13} $\pm 1.84 \times 10^{-14}$	9.86×10^{-13} $\pm 9.63 \times 10^{-15}$	5.98×10^{-13} $\pm 3.27 \times 10^{-14}$	7.45×10^{-13} $\pm 3.10 \times 10^{-14}$
50	2.10×10^{-12} $\pm 4.28 \times 10^{-14}$	1.89×10^{-12} $\pm 2.72 \times 10^{-14}$	1.71×10^{-12} $\pm 1.60 \times 10^{-14}$	1.46×10^{-12} $\pm 1.02 \times 10^{-14}$	1.23×10^{-12} $\pm 6.30 \times 10^{-15}$	2.30×10^{-12} $\pm 2.54 \times 10^{-14}$

For 2.0 mg Ketjenblack loading

Wt.% PTFE	1	2	3	4	5	6
0	1.22×10^{-12} $\pm 1.06 \times 10^{-14}$	1.90×10^{-12} $\pm 2.21 \times 10^{-13}$	7.37×10^{-13} $\pm 6.67 \times 10^{-14}$	1.44×10^{-12} $\pm 2.84 \times 10^{-14}$	1.08×10^{-12} $\pm 1.20 \times 10^{-14}$	9.05×10^{-13} $\pm 2.87 \times 10^{-14}$
10	3.40×10^{-12} $\pm 1.34 \times 10^{-13}$	3.51×10^{-12} $\pm 2.74 \times 10^{-14}$	3.33×10^{-12} $\pm 5.38 \times 10^{-14}$	3.28×10^{-12} $\pm 6.90 \times 10^{-14}$	2.23×10^{-12} $\pm 4.57 \times 10^{-14}$	1.84×10^{-12} $\pm 1.80 \times 10^{-14}$
20	2.19×10^{-12} $\pm 2.15 \times 10^{-14}$	1.86×10^{-12} $\pm 1.93 \times 10^{-14}$	2.19×10^{-12} $\pm 3.24 \times 10^{-14}$	2.53×10^{-12} $\pm 1.50 \times 10^{-14}$	1.44×10^{-12} $\pm 1.51 \times 10^{-14}$	1.13×10^{-13} $\pm 2.62 \times 10^{-14}$
30	1.30×10^{-12} $\pm 8.49 \times 10^{-15}$	9.35×10^{-13} $\pm 2.64 \times 10^{-14}$	5.08×10^{-13} $\pm 5.94 \times 10^{-15}$	6.06×10^{-13} $\pm 3.07 \times 10^{-14}$	6.62×10^{-13} $\pm 1.70 \times 10^{-14}$	2.34×10^{-12} $\pm 2.95 \times 10^{-14}$
40	1.78×10^{-12} $\pm 2.90 \times 10^{-14}$	2.02×10^{-12} $\pm 1.81 \times 10^{-14}$	1.20×10^{-12} $\pm 2.84 \times 10^{-14}$	2.01×10^{-12} $\pm 3.36 \times 10^{-14}$	1.06×10^{-12} $\pm 2.63 \times 10^{-14}$	1.10×10^{-12} $\pm 2.07 \times 10^{-14}$
50	6.68×10^{-13} $\pm 2.44 \times 10^{-14}$	1.87×10^{-12} $\pm 8.71 \times 10^{-15}$	7.37×10^{-13} $\pm 2.17 \times 10^{-14}$	9.29×10^{-13} $\pm 3.75 \times 10^{-14}$	9.58×10^{-13} $\pm 1.63 \times 10^{-14}$	1.19×10^{-12} $\pm 2.18 \times 10^{-14}$

For 2.5 mg Ketjenblack loading

Wt.% PTFE	1	2	3	4	5	6
0	1.15×10^{-12} $\pm 3.52 \times 10^{-14}$	9.58×10^{-13} $\pm 2.37 \times 10^{-14}$	1.56×10^{-13} $\pm 1.01 \times 10^{-14}$	1.60×10^{-12} $\pm 2.30 \times 10^{-14}$	1.82×10^{-12} $\pm 1.16 \times 10^{-14}$	7.87×10^{-13} $\pm 2.43 \times 10^{-14}$
10	2.39×10^{-12} $\pm 3.20 \times 10^{-14}$	1.46×10^{-12} $\pm 1.61 \times 10^{-14}$	1.62×10^{-12} $\pm 8.45 \times 10^{-15}$	1.60×10^{-12} $\pm 1.70 \times 10^{-14}$	1.58×10^{-12} $\pm 8.52 \times 10^{-15}$	1.02×10^{-12} $\pm 3.89 \times 10^{-14}$
20	2.46×10^{-12} $\pm 5.08 \times 10^{-14}$	1.76×10^{-12} $\pm 2.06 \times 10^{-14}$	2.17×10^{-12} $\pm 1.36 \times 10^{-14}$	2.22×10^{-12} $\pm 1.43 \times 10^{-14}$	1.94×10^{-12} $\pm 1.69 \times 10^{-14}$	1.14×10^{-12} $\pm 5.72 \times 10^{-15}$
30	9.00×10^{-13} $\pm 4.48 \times 10^{-14}$	7.65×10^{-13} $\pm 4.27 \times 10^{-14}$	6.12×10^{-13} $\pm 2.51 \times 10^{-14}$	8.72×10^{-13} $\pm 2.75 \times 10^{-14}$	7.85×10^{-13} $\pm 4.45 \times 10^{-14}$	8.89×10^{-13} $\pm 1.58 \times 10^{-14}$
40	1.71×10^{-12} $\pm 4.98 \times 10^{-14}$	8.16×10^{-13} $\pm 6.22 \times 10^{-14}$	7.28×10^{-13} $\pm 9.57 \times 10^{-15}$	1.28×10^{-12} $\pm 2.41 \times 10^{-14}$	8.50×10^{-13} $\pm 4.80 \times 10^{-14}$	6.09×10^{-13} $\pm 5.05 \times 10^{-14}$
50	6.98×10^{-13} $\pm 5.97 \times 10^{-14}$	4.48×10^{-13} $\pm 1.73 \times 10^{-14}$	1.56×10^{-12} $\pm 1.01 \times 10^{-14}$	1.60×10^{-12} $\pm 2.30 \times 10^{-14}$	1.82×10^{-12} $\pm 1.16 \times 10^{-14}$	7.87×10^{-13} $\pm 2.43 \times 10^{-14}$

D-2: MPL-coated GDL with Vulcan black loading for gas permeability for each of 6 tested samples with various PTFE loadings in the MPLs.

For 0.5 mg Vulcan loading

Wt.% PTFE	1	2	3	4	5	6
0	1.65×10^{-11} $\pm 7.20 \times 10^{-13}$	1.46×10^{-11} $\pm 2.63 \times 10^{-13}$	1.78×10^{-11} $\pm 6.83 \times 10^{-13}$	2.22×10^{-11} $\pm 6.27 \times 10^{-13}$	2.02×10^{-11} $\pm 4.45 \times 10^{-13}$	1.97×10^{-11} $\pm 9.27 \times 10^{-13}$
10	1.52×10^{-11} $\pm 3.26 \times 10^{-13}$	1.53×10^{-11} $\pm 5.57 \times 10^{-13}$	1.42×10^{-11} $\pm 3.99 \times 10^{-13}$	1.77×10^{-11} $\pm 3.25 \times 10^{-13}$	1.31×10^{-11} $\pm 6.11 \times 10^{-13}$	1.27×10^{-11} $\pm 4.62 \times 10^{-13}$
20	1.64×10^{-11} $\pm 2.66 \times 10^{-13}$	1.71×10^{-11} $\pm 1.41 \times 10^{-12}$	1.69×10^{-11} $\pm 1.42 \times 10^{-12}$	1.97×10^{-11} $\pm 2.10 \times 10^{-12}$	1.69×10^{-11} $\pm 1.44 \times 10^{-12}$	1.20×10^{-11} $\pm 5.45 \times 10^{-13}$
30	1.40×10^{-11} $\pm 4.17 \times 10^{-13}$	1.67×10^{-11} $\pm 6.25 \times 10^{-13}$	1.42×10^{-11} $\pm 3.31 \times 10^{-13}$	1.93×10^{-11} $\pm 1.01 \times 10^{-12}$	1.92×10^{-11} $\pm 3.78 \times 10^{-13}$	1.62×10^{-11} $\pm 2.09 \times 10^{-12}$
40	1.18×10^{-11} $\pm 4.28 \times 10^{-13}$	9.37×10^{-12} $\pm 3.58 \times 10^{-13}$	9.94×10^{-12} $\pm 5.54 \times 10^{-13}$	1.10×10^{-11} $\pm 3.14 \times 10^{-13}$	9.05×10^{-12} $\pm 5.79 \times 10^{-13}$	1.02×10^{-11} $\pm 1.92 \times 10^{-13}$
50	1.46×10^{-11} $\pm 8.20 \times 10^{-13}$	2.40×10^{-11} $\pm 8.20 \times 10^{-12}$	2.12×10^{-11} $\pm 5.33 \times 10^{-13}$	1.51×10^{-11} $\pm 3.57 \times 10^{-13}$	2.09×10^{-11} $\pm 1.73 \times 10^{-12}$	1.61×10^{-11} $\pm 1.73 \times 10^{-12}$

For 1.0 mg Vulcan loading

Wt.% PTFE	1	2	3	4	5	6
0	1.22×10^{-11} $\pm 3.73 \times 10^{-13}$	7.38×10^{-12} $\pm 2.89 \times 10^{-13}$	1.05×10^{-11} $\pm 2.11 \times 10^{-13}$	1.42×10^{-11} $\pm 5.24 \times 10^{-13}$	1.28×10^{-11} $\pm 5.11 \times 10^{-13}$	1.42×10^{-11} $\pm 7.81 \times 10^{-13}$
10	5.41×10^{-12} $\pm 1.47 \times 10^{-13}$	9.13×10^{-12} $\pm 2.65 \times 10^{-13}$	4.88×10^{-12} $\pm 4.18 \times 10^{-13}$	8.95×10^{-12} $\pm 4.18 \times 10^{-13}$	5.85×10^{-12} $\pm 1.29 \times 10^{-13}$	7.02×10^{-12} $\pm 2.74 \times 10^{-13}$
20	1.11×10^{-11} $\pm 5.00 \times 10^{-13}$	9.69×10^{-12} $\pm 4.16 \times 10^{-13}$	5.95×10^{-12} $\pm 1.00 \times 10^{-13}$	8.23×10^{-12} $\pm 2.70 \times 10^{-13}$	6.18×10^{-12} $\pm 1.81 \times 10^{-13}$	8.45×10^{-12} $\pm 8.45 \times 10^{-13}$
30	6.75×10^{-12} $\pm 2.04 \times 10^{-13}$	6.40×10^{-12} $\pm 1.72 \times 10^{-13}$	9.10×10^{-12} $\pm 5.3 \times 10^{-13}$	7.93×10^{-12} $\pm 2.95 \times 10^{-13}$	9.20×10^{-12} $\pm 3.97 \times 10^{-13}$	7.74×10^{-12} $\pm 2.92 \times 10^{-13}$
40	1.07×10^{-11} $\pm 6.78 \times 10^{-13}$	6.93×10^{-12} $\pm 2.43 \times 10^{-13}$	8.72×10^{-12} $\pm 4.71 \times 10^{-13}$	7.33×10^{-12} $\pm 4.20 \times 10^{-13}$	7.59×10^{-12} $\pm 3.72 \times 10^{-13}$	7.18×10^{-12} $\pm 2.75 \times 10^{-13}$
50	8.07×10^{-12} $\pm 2.44 \times 10^{-13}$	1.03×10^{-11} $\pm 4.98 \times 10^{-13}$	1.43×10^{-11} $\pm 4.62 \times 10^{-13}$	1.12×10^{-11} $\pm 6.54 \times 10^{-13}$	9.42×10^{-12} $\pm 4.37 \times 10^{-13}$	1.19×10^{-11} $\pm 7.95 \times 10^{-13}$

For 1.5 mg Vulcan loading

Wt.% PTFE	1	2	3	4	5	6
0	3.47×10^{-12} $\pm 5.94 \times 10^{-14}$	3.04×10^{-12} $\pm 6.89 \times 10^{-14}$	4.70×10^{-12} $\pm 1.18 \times 10^{-13}$	4.77×10^{-12} $\pm 5.29 \times 10^{-14}$	3.58×10^{-12} $\pm 7.02 \times 10^{-14}$	3.31×10^{-12} $\pm 7.39 \times 10^{-14}$
10	5.44×10^{-12} $\pm 4.86 \times 10^{-14}$	5.09×10^{-12} $\pm 4.87 \times 10^{-14}$	6.30×10^{-12} $\pm 7.02 \times 10^{-14}$	4.49×10^{-12} $\pm 7.51 \times 10^{-14}$	5.85×10^{-12} $\pm 6.55 \times 10^{-14}$	2.79×10^{-12} $\pm 5.25 \times 10^{-14}$
20	2.18×10^{-12} $\pm 3.28 \times 10^{-14}$	1.28×10^{-12} $\pm 1.22 \times 10^{-14}$	2.26×10^{-12} $\pm 3.62 \times 10^{-14}$	1.88×10^{-12} $\pm 1.09 \times 10^{-14}$	3.27×10^{-12} $\pm 6.61 \times 10^{-14}$	1.39×10^{-12} $\pm 2.06 \times 10^{-14}$
30	3.54×10^{-12} $\pm 9.27 \times 10^{-14}$	4.39×10^{-12} $\pm 6.49 \times 10^{-14}$	4.89×10^{-12} $\pm 1.25 \times 10^{-13}$	4.89×10^{-12} $\pm 4.74 \times 10^{-14}$	7.86×10^{-12} $\pm 2.61 \times 10^{-13}$	6.80×10^{-12} $\pm 2.44 \times 10^{-13}$
40	6.22×10^{-12} $\pm 9.45 \times 10^{-14}$	5.52×10^{-12} $\pm 1.27 \times 10^{-13}$	7.88×10^{-12} $\pm 2.24 \times 10^{-13}$	6.15×10^{-12} $\pm 1.60 \times 10^{-13}$	5.68×10^{-12} $\pm 1.87 \times 10^{-13}$	3.46×10^{-12} $\pm 6.92 \times 10^{-14}$
50	4.93×10^{-12} $\pm 1.52 \times 10^{-13}$	4.34×10^{-12} $\pm 3.45 \times 10^{-14}$	4.48×10^{-12} $\pm 1.10 \times 10^{-13}$	6.60×10^{-12} $\pm 1.30 \times 10^{-13}$	8.07×10^{-12} $\pm 2.87 \times 10^{-13}$	6.89×10^{-12} $\pm 3.45 \times 10^{-13}$

For 2.0 mg Vulcan loading

Wt.% PTFE	1	2	3	4	5	6
0	4.85×10^{-13} $\pm 6.03 \times 10^{-14}$	6.88×10^{-13} $\pm 1.05 \times 10^{-14}$	4.57×10^{-13} $\pm 4.57 \times 10^{-14}$	1.30×10^{-12} $\pm 1.84 \times 10^{-14}$	1.22×10^{-12} $\pm 4.68 \times 10^{-14}$	4.10×10^{-13} $\pm 2.26 \times 10^{-14}$
10	4.62×10^{-13} $\pm 6.22 \times 10^{-14}$	4.12×10^{-13} $\pm 5.78 \times 10^{-14}$	3.81×10^{-13} $\pm 1.02 \times 10^{-14}$	4.39×10^{-13} $\pm 2.20 \times 10^{-14}$	4.54×10^{-13} $\pm 1.04 \times 10^{-13}$	3.86×10^{-13} $\pm 2.11 \times 10^{-14}$
20	2.58×10^{-12} $\pm 1.76 \times 10^{-14}$	2.49×10^{-12} $\pm 4.58 \times 10^{-14}$	4.47×10^{-12} $\pm 3.53 \times 10^{-14}$	4.26×10^{-12} $\pm 5.58 \times 10^{-14}$	4.50×10^{-12} $\pm 4.83 \times 10^{-14}$	5.28×10^{-12} $\pm 8.00 \times 10^{-14}$
30	1.46×10^{-12} $\pm 1.25 \times 10^{-14}$	7.52×10^{-13} $\pm 9.95 \times 10^{-15}$	8.11×10^{-13} $\pm 1.86 \times 10^{-14}$	1.55×10^{-12} $\pm 1.45 \times 10^{-14}$	7.52×10^{-13} $\pm 9.95 \times 10^{-15}$	7.61×10^{-13} $\pm 1.58 \times 10^{-14}$
40	2.26×10^{-12} $\pm 4.26 \times 10^{-14}$	2.26×10^{-12} $\pm 2.19 \times 10^{-14}$	4.08×10^{-13} $\pm 4.28 \times 10^{-14}$	3.80×10^{-12} $\pm 3.90 \times 10^{-13}$	2.33×10^{-12} $\pm 2.96 \times 10^{-14}$	3.69×10^{-12} $\pm 4.08 \times 10^{-14}$
50	1.25×10^{-12} $\pm 2.23 \times 10^{-14}$	6.32×10^{-12} $\pm 1.74 \times 10^{-14}$	4.08×10^{-13} $\pm 2.43 \times 10^{-14}$	1.63×10^{-12} $\pm 2.43 \times 10^{-14}$	2.55×10^{-12} $\pm 2.43 \times 10^{-14}$	1.67×10^{-12} $\pm 2.13 \times 10^{-14}$

For 2.5 mg Vulcan loading

Wt.% PTFE	1	2	3	4	5	6
0	2.05×10^{-12} $\pm 2.40 \times 10^{-14}$	2.14×10^{-12} $\pm 2.31 \times 10^{-14}$	1.95×10^{-12} $\pm 2.50 \times 10^{-14}$	2.18×10^{-12} $\pm 1.38 \times 10^{-14}$	1.72×10^{-12} $\pm 3.22 \times 10^{-14}$	1.56×10^{-12} $\pm 2.23 \times 10^{-14}$
10	1.45×10^{-13} $\pm 1.90 \times 10^{-14}$	8.55×10^{-13} $\pm 1.31 \times 10^{-14}$	4.84×10^{-13} $\pm 1.12 \times 10^{-14}$	7.44×10^{-13} $\pm 2.89 \times 10^{-14}$	1.33×10^{-12} $\pm 2.99 \times 10^{-14}$	1.60×10^{-12} $\pm 1.71 \times 10^{-14}$
20	8.36×10^{-13} $\pm 1.11 \times 10^{-14}$	4.77×10^{-13} $\pm 1.11 \times 10^{-14}$	6.60×10^{-13} $\pm 4.01 \times 10^{-15}$	3.55×10^{-13} $\pm 1.82 \times 10^{-14}$	3.96×10^{-13} $\pm 1.82 \times 10^{-14}$	4.88×10^{-13} $\pm 5.84 \times 10^{-15}$
30	2.11×10^{-12} $\pm 4.84 \times 10^{-14}$	2.00×10^{-12} $\pm 2.64 \times 10^{-14}$	8.98×10^{-13} $\pm 2.10 \times 10^{-14}$	2.34×10^{-12} $\pm 4.35 \times 10^{-14}$	9.21×10^{-13} $\pm 2.97 \times 10^{-14}$	8.44×10^{-13} $\pm 4.89 \times 10^{-14}$
40	2.45×10^{-12} $\pm 6.39 \times 10^{-14}$	3.59×10^{-12} $\pm 1.27 \times 10^{-13}$	3.98×10^{-12} $\pm 6.13 \times 10^{-14}$	1.11×10^{-12} $\pm 1.82 \times 10^{-14}$	2.41×10^{-12} $\pm 3.29 \times 10^{-14}$	5.06×10^{-13} $\pm 2.17 \times 10^{-14}$
50	1.60×10^{-12} $\pm 2.88 \times 10^{-14}$	6.25×10^{-13} $\pm 1.28 \times 10^{-14}$	1.13×10^{-12} $\pm 1.13 \times 10^{-14}$	5.05×10^{-12} $\pm 1.42 \times 10^{-13}$	3.07×10^{-12} $\pm 3.48 \times 10^{-14}$	2.45×10^{-12} $\pm 2.45 \times 10^{-14}$